The Two-Photon Excitation Fluorescence (TPEF) Enhancement of Dipolar Organic Chromophores in Y Zeolites

by

Pankaj Subedi

Submitted in partial fulfillment of the requirements for

the degree of Master of Science

at

Dalhousie University

Halifax, Nova Scotia

March 2016

Dedicated to my parents and my late grandmother.

My High School Chemistry Teacher (Mr. John Ramsden).

My A-level Biology teacher (Liz Lucas).

Table of Contents

List of Tables

List of Figures

List of Schemes

Abstract

Two-Photon Absorption (TPA) is a non-linear optical (NLO) process that involves simultaneous absorption of two photons. Efficiency of two photon absorption by organic compounds is influenced by many different factors, including the nature of the surrounding environment (e.g. polarity). In the present work, the influence of the constricting and highly polar environment of zeolites on two-photon absorption of incorporated nitrobenzoxadiazole (NBD) derivatives is investigated.

Six different analogues of NBD chromophores consisting of unsubstituted, *N*-alkylated and *N,N*-dialkylated amines were investigated. All showed strong single photon fluorescence (either conventional or laser induced), and easily detected femtosecond laser two-photon induced fluorescence, both in solution and in zeolites. The results show that the efficiency of two-photon induced fluorescence remained largely unaffected by solvent polarity for all of the NBD derivatives examined. However, the efficiency of two-photon induced fluorescence was substantially influenced by the zeolite environment, with some NBD derivatives showing almost a 10-fold increase.

List of Abbreviations and Symbols Used

Compound Abbreviations

NBD- Cl	4-Chloro-7-nitrobenzofurazan
NBD-NH_2	7-Nitro-2,1,3-benzoxadiazol-4-amine
NBD-methylamine (MA)	*N*-Methyl-7-nitro-2,1,3-benzoxadiazol-4-Amine
NBD-ethylamine (EA)	*N*-Ethyl-7-nitro-2,1,3-benzoxadiazol-4-amine
NBD-DMA	*N,N*-dimethyl-7-nitro-2,1,3-benzoxadiazol-4-amine
NBD-ethylmethylamine (EMA)	*N*-ethyl-*N*-methyl-7-nitro-2,1,3-benzoxadiazol-4-amine
NBD-DEA	*N,N*-diethyl-7-nitro-2,1,3-benzoxadiazol-4-amine

Other Abbreviations and Symbols

A	Zeolite A
A_g	Rotational Symmetry
APCI-MS	Atmospheric pressure chemical ionisation mass spectrometry
ArCO-	ArylCarbonyl
Ar	Aromatic
As	Absorbance of the standard
Ax	Absorbance of the unknown
BBU	Basic Building Units
BDBAS	4-4'-bis(di-*n*-butylamino)stilbene
BDPAS	4-4'-bis(diphenylamino)stilbene
BLA	Bond length alteration
BODIPY	Boron-dipyrromethane
br	Broad
$CaF_2:Eu^{2+}$	Europium doped Calcium Fluoride
CBU	Composite Building Units

DMABN	(Dimethylamine) benzonitrile
D-π-A	Donor-π-Acceptor (π also refers to electrons)
d	Doublet
ESI MS	Electron spray ionisation mass spectrometry
Fs	Area under the emission curve/ number of photons for standard
Fx	Area under the emission curve/ number of photons for unknown
GM	Göppert-Mayer
GW	Gaussian Width
HPLC	High Performance Liquid Chromatography
HOMO	Highest Occupied Molecular Orbital
hν	Photon
ICT	Intramolecular Charge Transfer
I_0	Pulse Radiation
k	Rate Constant
L	Sample Thickness
LUMO	Lowest Occupied Molecular Orbital
M	Monovalent counterbalancing cations
MAS NMR	Magnetic angle spinning nuclear magnetic resonance
N	Normality
N	Number of Molecules per cm^3
NBD-	Nitrobenzoxadiazole
n_{cavity}	Number of moles of zeolite cavities
NIR	Near Infra-red
NLO	Non-linear Optical
ppm	Parts per million
p	Pentet
q	Quartet
R	Reflectance

s	Singlet
<S>	Loading Level
S_0	Ground State
S_1	First excited state
S_2	Second excited state
Si/Al	Silicon to aluminium ratio
SPA	Single-Photon Absorption
SPE	Single Photon Excitation
SPEF	Single Photon Excited Fluorescence
t	Triplet
T	Transmittance
T	Tetrahedral
THF	Tetrahydrofuran
TICT	Twisted intramolecular charge transfer
TMS	Tetramethylsiane
TPA	Two-Photon Absorption
TPE	Two-Photon Excitation
TPEF	Two-Photon Excited Fluorescence
UV	Ultraviolet
X	Faujasite- type zeolite X
Y	Faujasite- type zeolite Y
z_0	Rayleigh length
z	Sample Position
ZSM-5	Zeolite ZSM-5
σ	Two-Photon Absorption Cross Section
λ	Wavelength
ε	Molar Extinction Coefficient
β	TPA Coefficient

Φ	Quantum Yield
δ	Chemical Shift
n	Refractive index.
2P:1P	Ratio of two photon: one photon

Acknowledgements

I would like to start by acknowledging my research supervisor Dr. Fran Cozens, I will be forever grateful for the opportunity provided to work in her research lab. All the progress and improvements that I have made in the last few years as a chemistry student would not have been possible without the immense faith and the support that I received from Dr. Fran Cozens. Thank you for believing in my abilities. I would also like to express my gratitude towards Dr. Norman Schepp, who has also shown faith and support and has contributed significantly towards my development as a chemistry student. Thank you for always finding time to answer my questions and helping me when needed. Using all the equipment to prepare the zeolite samples was a challenging experience and even more challenging experience was the use of the femtosecond laser and Dr. Norman Schepp, provided me with all the assistance on how to use these equipment. This work would not have been possible with the help and assistance of Dr. Norman Schepp.

I would like to thank Dr. Jean Burnell, for all his help and advice during my time as an undergraduate and a graduate student. Finally, I would like to thank the rest of my Defense Committee, Dr. Alex Speed and Dr. Robert White.

This work would also not have been possible without the help and assistance of many people in the department of chemistry. I would like to thank Dr. Mike Lumsden for all the assistance with the NMR, particularly the temperature control experiments, Xiao Feng (mass spectrometer technologist), Courtney Calahoo from Dr. Josef W. Zwanziger research group (diffuse reflectance spectra), Dr. Reinaldo Moya-Barrios (melting point, his advice regarding zeolite preparation were also very useful), Mike Boutilier (Machinist), Todd Carter (scientific glass blower) Cathy Ryan (chemistry stores). I would also like to thank Giselle Andrews for all the help and support.

Finally I would like to thank all the current and past members of the Schepp and Cozens group.

Introduction

The concept of two-photon absorption (TPA) was first proposed in 1931 by Maria Göppert-Mayer in her doctoral dissertation, in which she predicted the theory of two-photon quantum transitions in atoms.[1-3] According to Göppert-Mayer, an atom or a molecule may absorb two photons simultaneously in the same quantum event.[1-3] The two-photon absorption cross section (σ) measures the ability of a chromophore to undergo two-photon absorption and the unit for TPA cross section (σ) is GM, which is named after Göppert-Mayer.[2] Experimental confirmation of two-photon absorption (TPA) was only observed 30 years later in 1961, and this work was enabled by the development of highly intense pulsed laser.[2-4] W. Kaiser and C.G.B Garett demonstrated the concept of TPA experimentally in 1961 by generating a blue fluorescent light at λ = 425 nm, by illuminating $CaF_2:Eu^{2+}$ crystals with a red light at λ = 694 nm with a ruby beam laser.[5] They were also able to experimentally demonstrate the two-photon excitation fluorescence of organic dyes.[3] The concept of two-photon absorption has become easier to investigate with the increasing availability of highly intense femtosecond and picosecond pulsed lasers.[2-5] In addition, there have been increasing demands for organic dyes that exhibit enhanced two-photon absorption properties, because of their use in various applications, such as fluorescence microscopy,[6-7] 3D-optical data storage,[8] 3D-microfabrication,[9] and drug-delivery[10] along with other applications. As a result, research in the area of two-photon absorption has been gathering significant momentum.

Scope of the Thesis.

The work presented in this thesis involves investigating the effect of the zeolite environment on two-photon excitation properties of small organic compounds, with the goal being to determine whether or not the polar and restrictive environment within zeolite cavities can enhance two photon absorption relative to that in solution.

The rest of this chapter is devoted to a description of the concept of two photon absorption (TPA). This chapter focusses on two-photon absorption from an organic chemistry perspective and as a result, the structure-property relationship of organic compounds, which makes them an efficient two-photon absorption chromophore will be discussed. A segment of this chapter also describes the one- and two-photon chemistry of 4-amino-7-nitrobenz-2,1,3-oxadiazol derivatives used in this work as the two-photon chromophore.

Zeolites are explored as a solid-state media that may have an effect on the efficiency of two-photon excitation of incorporated chromophores. A detailed discussion regarding the structure and the properties of zeolites will be provided in Chapter 2.

The experimental procedures for the work presented will be discussed in Chapter 3. The procedures for the synthesis of the organic chromophores along with the methodology used for the incorporation of the chromophores in zeolites will be discussed. In addition, a description of the laser system and the methods used to record single-photon excitation fluorescence (SPEF) and two-photon excitation fluorescence (TPEF) spectra will be provided. All the relevant results along with discussion and conclusions obtained from the work will be given in Chapter 4.

Single photon and two-photon absorption

The first of the two laws of photochemistry was proposed in 1817 by Theodor Grotthuss, and independently in 1842 by John William Draper.[11] The first law of photochemistry states that an organic compound or an organic dye must be able to absorb light at a given frequency in order to undergo any photochemical change.[11] The second law of photochemistry was proposed by Johannes Stark in 1908, and independently in 1913 by Albert Einstein, which is jointly known as Stark-Einstein law.[11] According to the second law of photochemistry, a single chemical change will occur for every photon absorbed by a photo-reactive compound, known as chromophore.[11] The chain of various photophysical events that can occur upon absorption of light can be summarised by a Jablonski diagram shown in Figure 1.1.[12]

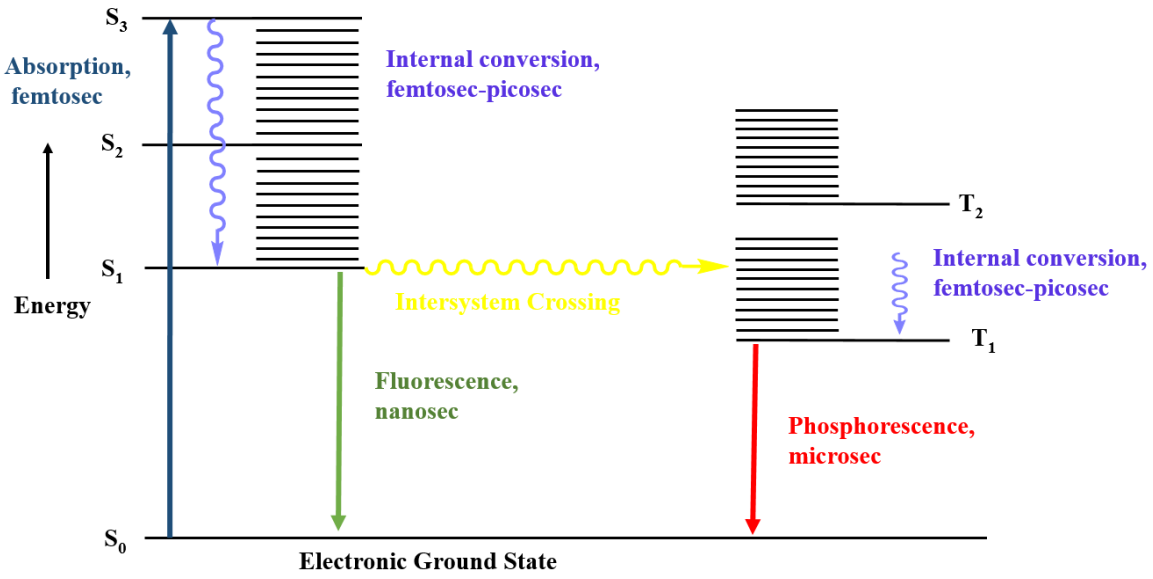

Figure 1.1. Jablonski diagram showing various different events that can occur upon absorption of light. The singlet state is represented by the letter S and the triplet state by T. (Drawn based on information in Reference 12).

Some of the events that may occur upon absorption of light are fluorescence, internal conversion or vibrational conversion, intersystem crossing from a singlet state to a triplet state, and phosphorescence.[12] The lifetime of each event is usually very short and can vary from microseconds to femtoseconds.[12] The concepts initially put forward only focussed on single-photon absorption (SPA) but with time and with the development of femtosecond and picosecond lasers, the concepts were also explored through two-photon absorption (TPA).

The concept of two-photon absorption (TPA) is lesser known compared to single-photon absorption (SPA). The understanding of TPA can start with a comparison with the more familiar single-photon absorption (SPA). For single-photon absorption, an electron in the ground state undergoes a transition to an excited state when it absorbs a single photon with an energy hv.[2-3,13,14] For single-photon absorption (SPA) of a small organic chromophore, the photons needed are usually relatively high in energy and typically require a wavelength in the ultraviolet (UV) region, or around the blue region of the electromagnetic spectrum, where the wavelengths are usually equal to or less than 400 nm.[3,11,13,14] Organic chromophores undergo fluorescence when the electron in the singlet excited state relaxes back to the ground state by releasing radiation in the form of visible, ultraviolet or infrared light.[3,13-14] This process is known as single-photon excitation fluorescence (SPEF).

As shown in Equation 1.1, the rate of single-photon absorption (SPA) is a first order process and depends linearly on the light intensity.[2] There are various different sources for single-photon excitation such as sunlight, UV-lamp, light bulb, laser, etc.[11]

$$\text{Rate of absorption} = k\,[\text{light intensity}] \qquad (1.1)$$

In contrast, two-photon absorption (TPA) is a non-linear optical (NLO) process, in which an electron undergoes a transition to the excited state through simultaneous absorption of two photons.[1-5] Upon absorption of the first photon ($h\nu_1$), the electron undergoes a transition to a state known as a virtual excited state.[2,3] This is a very short-lived state, and promotion of the electron to the fully excited state requires absorption of the second photon ($h\nu_2$) to be "simultaneous" with absorption of the first photon.[2,3] A comparison between single-photon absorption and two-photon absorption is provided in Figure 1.2. Organic chromophores that undergo two-photon excitation can also fluoresce when the excited state relaxes back to the ground state. This phenomenon is known as two-photon excitation fluorescence (TPEF).[2,3]

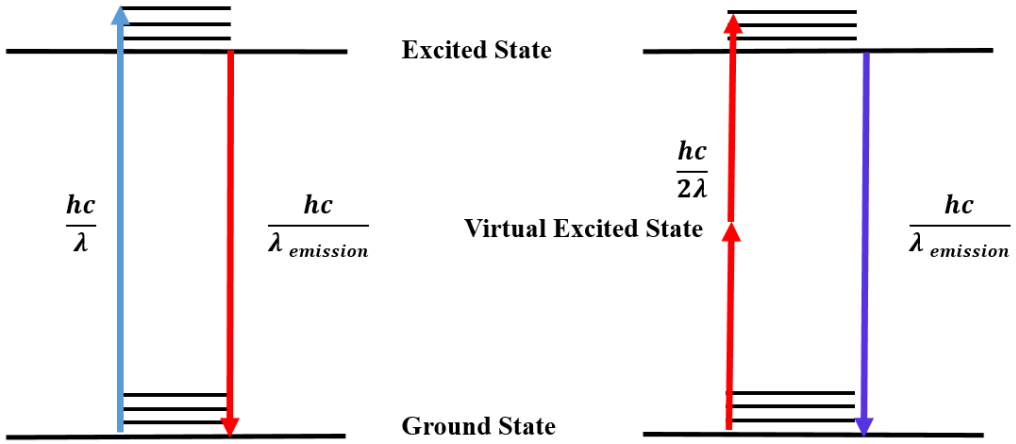

Figure 1.2. Comparison between single-photon absorption (SPA) and two-photon absorption (TPA). (Drawn based on information in Reference 3).

The significance of two-photon absorption (TPA) is that, in this process, electrons undergo transition to an excited state using photons of half the energy (twice the wavelength) compared to single-photon excitation.[2,3] The photons often lie in the near-infrared (NIR) region, around 800 nm. Since TPA involves two photons, the process depends on the square of light intensity.[2,3]

$$\text{Rate of absorption} = k\,[\text{light intensity}]^2 \tag{1.2}$$

For simultaneous two-photon absorption (TPA), where the two photons have the same energy and wavelength, a single source of excitation is needed. However, the intensity of the light must be very high in order to increase the probability of simultaneous absorption of two-photons. This kind of intensity is only found in femtosecond and sometimes picosecond pulsed lasers that have extremely high peak intensities. Hence, picosecond and femtosecond lasers are needed for efficient TPA.[2-6]

For single-photon absorption (SPA), molar extinction coefficient (ε) measures the ability of a chromophore to undergo single-photon absorption (SPA). Likewise, the two-photon absorption cross section (σ) measures the ability of a chromophore to undergo two-photon absorption (TPA).[2] The unit for two-photon absorption is Göppert-Mayer (GM), named after Maria Göppert-Mayer, who initially proposed the theory. The exact units for two-photon excitation have been provided in Equation 1.3.[14]

$$1\ \text{GM} = 10^{-50}\text{cm}^4\ \text{s photon}^{-1} \tag{1.3}$$

The non-linear optical (NLO) property of two-photon absorption (TPA) means that the determination of the two-photon absorption cross-section (σ) is more complicated in comparison with the determination of the molar extinction coefficient (ε). There are generally two different techniques associated with the determination of TPA cross-sections. The first technique is known as the Z-scan technique.[15-16] The basic experimental setup for the Z-scan technique is provided in Figure 1.3.[2]

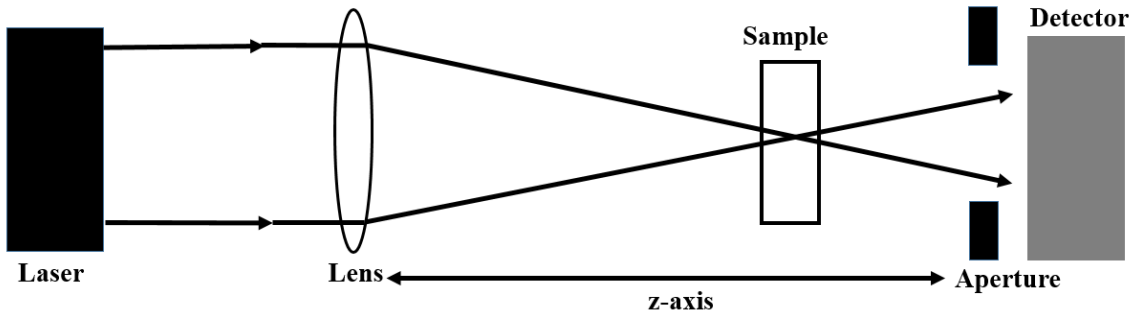

Figure 1.3. Experimental setup for the Z-scan technique. (Drawn based on information in Reference 2).

The Z-scan technique involves varying the position of the sample through the focal point of the laser beam along the z-axis, while keeping the incident energy of the laser beam constant.[2] The resulting transmittance that arises from the sample is then monitored and recorded as a function of the z-axis. A typical result obtained from a Z-scan experiment is shown in Figure 1.4.[17]

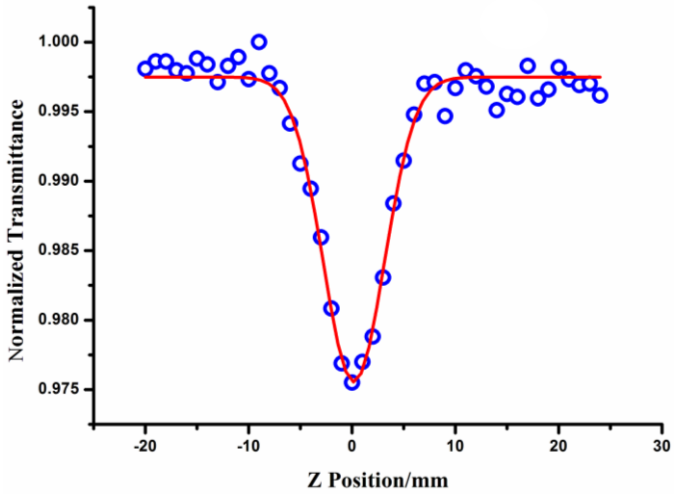

Figure 1.4. A typical Z-scan technique graph.[17]

The transmittance value (at z=0) along with complex mathematics, Equations 1.4-1.6 are then needed to determine the two-photon cross section (σ). A Gaussian pulse equation can be used to calculate the TPA coefficient (β) first.[15-18]

$$T(z)=\frac{1}{\sqrt{\pi}q_0\,(z,0)}\int_{-\infty}^{\infty}\ln\left[1+q_0\,(z,0)e^{-\tau^2}\right]dt \qquad (1.4)$$

Where,

$$q_0=\beta I_0(t)L\left(\frac{1+z^2}{z_0{}^2}\right)^{-1} \qquad (1.5)$$

In Equation 1.4, τ is Gaussian pulse width, usually measured in femtoseconds and picoseconds. In Equation 1.5, L is the sample thickness usually measured in millimetres (mm), z_0 is the Rayleigh length equal to $n\pi w_0^2/\lambda$, where n is the refractive index, w_0 is Gaussian beam spot radius at focus, z is the sample position with respect to focal position and I_0 is the pulse radiance at the focus (at z=0), with an unit of $GW^{2/}cm$. The TPA coefficient (β) can be determined through Equations 1.4 and 1.5. The relationship between the TPA coefficient (β) and TPA cross section (σ) has been provided in Equation 1.6. [15-18]

$$\sigma=\frac{h\nu\beta}{N} \qquad (1.6)$$

In Equation 1.6, hν is the exciton photon energy and N is the number of molecules per cm^3. The unit of TPA coefficient (β) is GW/cm.

A second technique associated with the determination of TPA cross-section (σ) is known as the two-photon excitation fluorescence (TPEF) technique.[2,19] This is a referencing method in which the two-photon excitation fluorescence (TPEF) spectra of reference compounds with known

TPA cross-sections (σ) are recorded using a femtosecond pulsed laser.[2] A total of four reference compounds were used to determine the TPA cross-section in the work provided in Chapter 4. Using this method, fluorescence intensities of the reference compounds are measured at given concentrations. A calibration plot is then generated of fluorescence intensity at those concentration vs the TPA cross section (σ). Fluorescence intensity measured under the same experimental conditions (concentration and laser power) for a compound with an unknown TPA cross section (σ) can be then used with the calibration plot to determine the TPA cross section (σ).

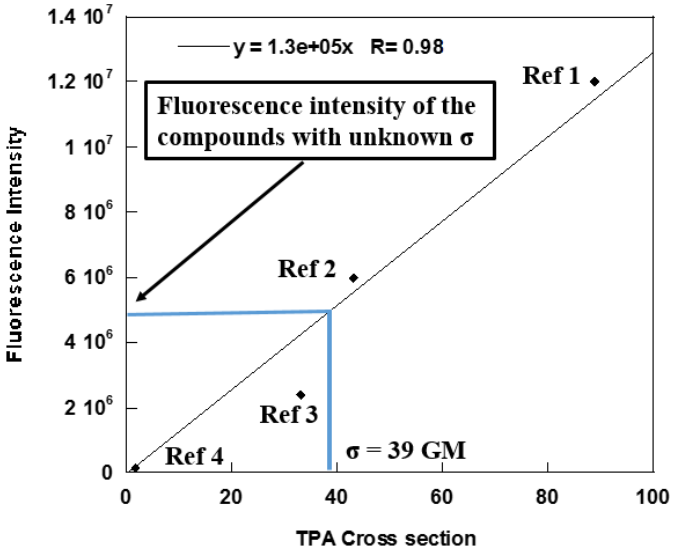

Figure 1.5. A TPA calibration curve for the determination of TPA cross section (σ) at a given concentration.

Finally, the TPA cross-section (σ) values obtained through this method has to be corrected for quantum yield of fluorescence using Equation 1.7.[2]

$$\frac{\sigma\ observed}{\phi} = \sigma\ actual \qquad (1.7)$$

The Z-scan technique requires special equipment not available in our lab, so the TPEF method was used. The errors in the determination of TPA cross-section (σ) are generally greater than 10% even under the best experimental conditions of Z-scan technique and the TPEF method. Hence, the TPA cross-sections (σ) are usually reported to two significant figures.[2] Some of the commonly used TPA reference compounds are rhodamine B, fluorescein, coumarin 307, anthracene and BODIPY.[2,20]

1.1 Advantages of Two-Photon Absorption.

Two-photon excitation initiates the absorption of chromophores using half the energy compared to single-photon excitation, through the use of red light, which lies in the near infrared (NIR) region of the electromagnetic spectrum (700-900 nm).[2,3,14,21-22] As a result, there are many advantages of TPA particularly for microscopy and other biological applications.[2-3,21-22] TPA is usually an inefficient process and very few biological cells are strong absorbers of TPA in comparison to SPA.[21] As a result, the use of TPA with highly absorbing chromophores as probe molecules may be more compatible with the biological system because they are likely to result in less photo damage within the biological system.[21] As shown in Equation 1.2, the process of TPA depends linearly on the square of the light intensity. This feature allows the excitation source to be restricted around the focal point of the source, usually a laser, which reduces the scattering of light.[2-3,14,21-22] The scattered light from the TPA source often do not have enough energy to initiate background excitation away from the focus point. Reduced scattering allows greater tissue penetration with two-photon excitation, usually two-to-three fold higher, compared to single-photon excitation.[2-3,14,21-22] Studies have shown that a one-photon fluorescence probe is limited to a depth around 100-200 μm, limited to the surface of the tissue, but two-photon fluorescence probes have shown to provide a depth of greater than 500 μm and thus allowing the imaging of

cells within the tissue.[23] The various different applications associated with two-photon absorption means that there is a greater demand for organic chromophores that exhibit high TPA properties. The TPA properties of the organic chromophore can be directly related to the structure- property relationship, which will be discussed in the next section.

1.2 Factors that Influence the Two-Photon Absorption (TPA) Properties of Organic Chromophore

Marder, Perry and co-workers in 1997 were one of the first groups to explore the structure-property relationship of organic chromophores. In 1997, they examined the presence of terminal donor groups on *trans*-stilbene and the direct effect on the TPA cross section (σ) of the substituted *trans*-stilbene.[24] A series of symmetrical stilbenes bearing various electron donor groups were examined. Upon examination of various different stilbene chromophores, it was found that 4,4'-bis(di-*N*-butylamino)stilbene (BDBAS) and 4,4'-bis(diphenylamino)stilbene (BDPAS), Figure 1.6, showed greater two-photon absorptivity.[24]

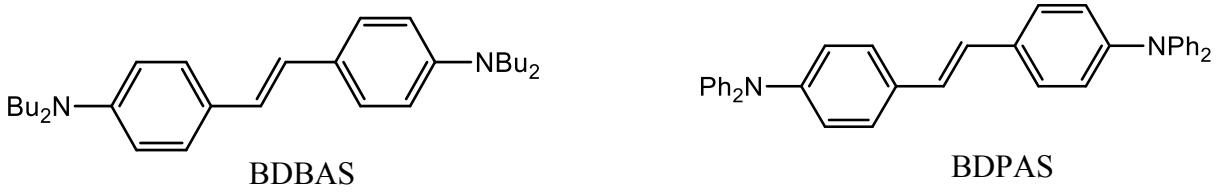

Figure 1.6. Structures of 4,4'-bis(di-*N*-butylamino)stilbene (BDBAS) and 4,4'-bis(diphenylamino)stilbene (BDPAS).

The TPA cross section (σ) for *trans*-stilbene has been reported to be 12 GM at 610 nm,[2,24] and introduction of strongly electron-donating *N*-butylamino groups resulted in the increase of the TPA cross section (σ) to 110 GM at 620 nm.[2,24] The introduction of the strong donor groups resulted in the increase of the TPA cross section (σ) by approximately a factor of 10. The

introduction of diphenylamine at both terminal groups increased the TPA cross section (σ) to 340 GM.[24] For *trans*-stilbene and its derivatives, two-photon transition is usually from the ground state (S_0, $1A_g$) to the lowest excited state A_g symmetry (S_2, $2A_g$).[25] Upon introduction of the donor group, there is an increase in the transition dipole moment of S_0 to S_1 and S_1 to S_2 transitions, respectively, which directly results in the increase of the TPA cross-section (σ) of the derivatives.[25] The electronic redistribution of the π-electronic density is also correlated with the increase in electron delocalisation in the first excited state, which results in substantial increase in S_1 to S_2 transition dipole moment and thus resulting in greater TPA cross section (σ).[25] The higher TPA cross section of BDPAS in comparison to BDBAS can be correlated to the fact that the two-photon state gets selectively stabilized by the diphenylamino group because of a greater electron delocalisation.[2,24,25]

Overall, the enhancement in the TPA cross section (σ) was directly related to the symmetrical charge transfer from the donor nitrogen atom of the amine groups, to the central conjugated bridge. Introducing various different donor substituents that enhance the intramolecular charge transfer (ICT) within the molecule is therefore one strategy in developing efficient TPA chromophores.[2,14,24-25]

Another way of enhancing intramolecular charge transfer (ICT) would be through the introduction of an electron-withdrawing substituent or an acceptor group within the organic chromophore.[26] An example has been provided in Figure 1.7.

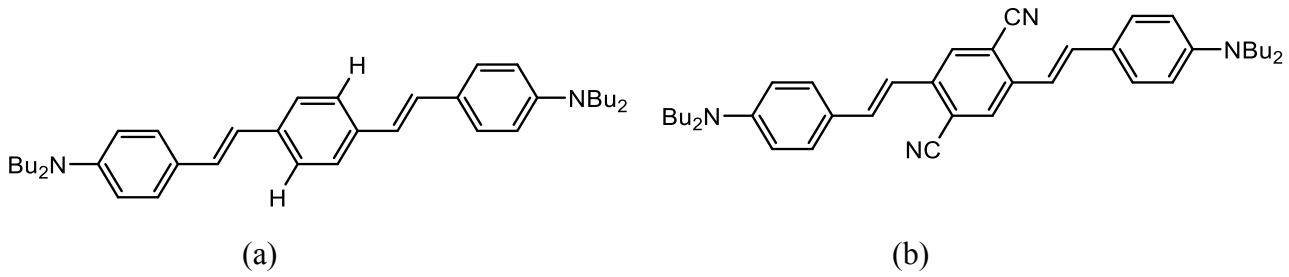

(a) (b)

Figure 1.7. Structure of (a) 4,4'-[1,4-phenylenedi(*E*)-2,1-ethenediyl]bis(*N*,*N*-dibutylaniline) (b) 2,5-dicyano-1,4-bis[2-(4-(di-*n*-butylamino)phenyl)vinyl]benzene.

The TPA cross section (σ) for the compound (a) in Figure 1.7 is 640 GM at 725 nm.[2,26] Upon introduction of the two electron-withdrawing cyano groups to the compound in (b), the TPA cross section (σ) increases to 1700 GM at 825 nm.[2,26] The presence of two electron-withdrawing substituents significantly increases the TPA cross section (σ) of the chromophore by a factor of approximately 3. The presence of the acceptor groups within the chromophore means that the donor group and the acceptor group are capable of interacting with each other through the π-bridge, which increases ICT within the molecule resulting in the increase of the TPA cross section (σ).[2,14,26]

Overall, it can be concluded that there are three essential components that need to be considered when designing an efficient TPA chromophore. An ideal TPA chromophore requires (1) an electron rich substituent (π-donor) and (2) an electron-withdrawing substituent (π-acceptor) that interact with each other through (3) a strong polarizable π-system through a Donor-π-Acceptor interaction.[2,14,24-26]

In terms of π-acceptors, or the electron-withdrawing substituents, the most commonly used groups are nitro-, cyano-, sulfonyl-, triflyl (CF_3SO_2-), arylcarbonyl (ArCO-), aldehyde and phosphonate groups.[2,14] The most commonly used π-donor substituents are disubstituted amines,

usually dialkyl and diaryl amines.[2,14] The disubstituted amines are preferred because they are capable of acting as a strong terminal donor and also possess higher oxidative stability.[14] Along with a strong donor and acceptor group, an efficient π-conjugated system is required to facilitate an efficient ICT. Phenylene-vinylene, ethynyl/phenethynyl and fluorenyl bridges are the most commonly used hydrocarbon based π-conjugated bridge in a TPA chromophore.[2,14]

1.3 Classification of Two-Photon Absorption (TPA) Chromophores

Typically TPA chromophores can be classified into three different types. The first type of TPA chromophores were first proposed in 1998 by Reinhardt, Prasad and co-workers, Figure 1.8.[14,27]

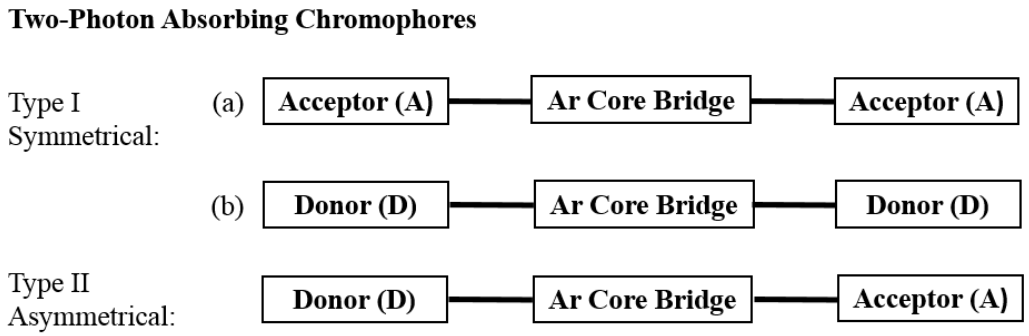

Figure 1.8. Molecular-structure design for dipolar organic chromophores, Ar = Aromatic building block. (Drawn based on information in Reference 14).

Reinhardt, Prasad and co-workers classified the chromophores into two different types, Type I and Type II. The Type I chromophores are usually symmetrical in nature, and the interaction in these type of chromophores are of either Donor-π-Donor or Acceptor-π-Acceptor interactions. The lack of either a donor or an acceptor group in these chromophores means that ICT within the molecule may not be as efficient, which may lead to poor TPA properties.[14,27] The Type II chromophores are usually asymmetrical, and the nature of interaction in these chromophores are

usually Donor-π-Acceptor interactions. The presence of a donor and an acceptor group within the molecule means that unsymmetrical Type II chromophores are also commonly known as dipolar chromophores.[14,27] The interaction between the donor and acceptor groups present at either end of the conjugated π-system leads to an increase in displacement of charge during the transition from highest occupied molecular orbital (HOMO) to lowest unoccupied molecular orbital (LUMO).[14,27] As a result, there is an enhancement in the transition dipole moment, which defines the transition of the electrons from the ground state to an excited state. The enhancement of the transition dipole leads to enhanced TPA properties in chromophores with D-π-A interactions. As a result, the asymmetric Type II chromophores have shown to be effective and efficient TPA chromophores compared to the symmetric Type I chromophores.[14,27]

The second type of organic chromophores are the quadrupolar centrosymmetric organic chromophores.[2,14,26] The concept was first proposed in 1998 by Marder, Perry and co-workers and follows similar concept as the Type I (a) and Type I (b) chromophores.[2,14] In this type of molecule, the donor group and the acceptor group interact with each other through alternating vinyl and 1,4-arylene bridges.[2,14] The compound shown in Figure 1.7 (b) is a typical example of centrosymmetric chromophore. The donor groups are usually located in the terminal position and during ICT the charge flows from the terminal position to the centre of the molecule where an acceptor group is usually located.[2,14] The nature of interactions in these types of molecules are usually Donor-π-Acceptor-π-Donor interactions. The ICT causes reorganization of dipoles within the molecule, which allows the energy required to make a transition from the ground state to the excited state much more accessible and as a result both the SPA and TPA properties are enhanced.[2,14] Centrosymmetric chromophores containing acceptor groups in the terminal position and donor group in the central position have also shown to be TPA active.[2] However, these

chromophores are less effective and less efficient in comparison to the centrosymmetric chromophore that contain acceptor group in the terminal position.[2,14] The centrosymmetric chromophores usually show enhanced TPA properties in comparison to the dipolar chromophores, because in dipolar molecules the Donor-π-Acceptor interactions are usually polarised in only one direction. In comparison, for the centrosymmetric molecule, the interaction is of Donor-π-Acceptor-π-Donor, which means that the charges flow from both ends of the chromophore.[2,14]

Based on the comparison between the dipolar and the quadrupolar chromophores, it is evident that the multibranched chromophores are likely to possess more enhanced TPA properties resulting from the increased amount of charge redistribution.[14] The third type of TPA chromophores are the octupolar chromophores and just like the quadrupolar chromophores, these chromophores can be centrosymmetric.[14] Reinhardt, Prasad and co-workers named the octupolar chromophores as Type III chromophores, where two or more dipolar chromophores are combined together in order to increase the π-conjugation system and overall donor and acceptor strength.[14] Amongst the three different chromophores that have been discussed, octupolar chromophores show the greatest TPA response.[14] The octupolar chromophores are further classified based on their molecular symmetry.

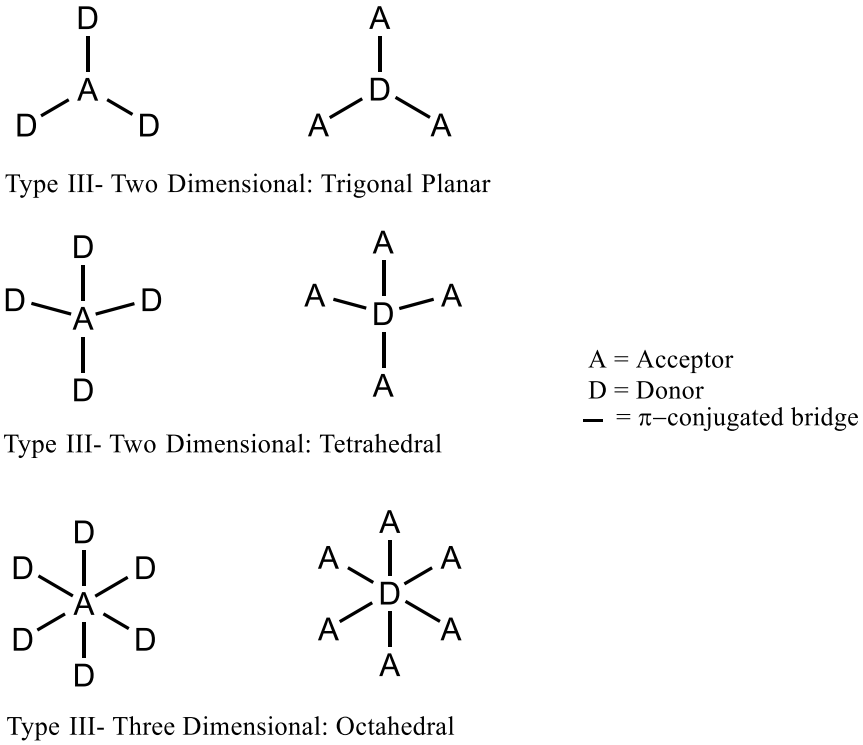

Figure 1.9. The donor-acceptor interactions in an octupolar chromophore. (Drawn based on information in Reference 14).

As shown in Figure 1.9, the octupolar chromophores with trigonal planar and tetrahedral symmetry are generally classified as Type III two dimensional chromophores and the chromophores with octahedral symmetry are known as Type III three dimensional chromophores.[14] For all the octupolar chromophores the electrons can either flow from the branches to the core or vice versa.[14]

The chromophore of interest in the work presented herein is a Type II dipolar chromophore with Donor-π-Acceptor interactions. The structure and property of this chromophore will be discussed in the next section.

1.4.Chromophore Used in this Work.

The structure of the chromophores used in this work is given in Figure 1.10.

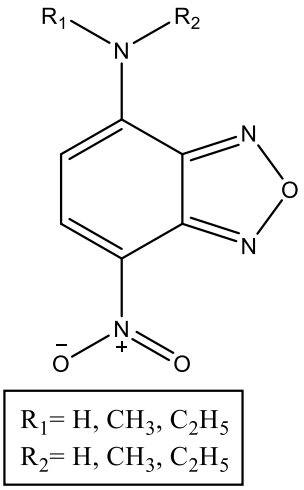

Figure 1.10. Structural motif of the chromophore used in the work.

As shown in Figure 1.10, the π-acceptor substituent in the molecule is the nitro group, one of the most commonly used electron-withdrawing substituents in TPA chromophores.[14] There are essentially two different donor groups interacting with the nitro group through the π-conjugated system. The first π-donor group is the oxadiazole group attached to the benzene ring and the second π-donor group is the amine located in the para- position to the nitro group. No variation will be provided to the oxadiazole in the present work, whereas various mono- and di-substituted amines will be introduced within the chromophore. The variation is provided through the introduction of different alkyl groups in the amine.

Dipolar molecules such as acedan (2-acetyl-6-(dimethylamino)naphthalene), coumarins and naphthalamides shown in Figure 1.11 have been widely used as molecular probes and biological tags because of their high emission properties.[28] Dialkyl amino groups are the commonly used donor species but as mentioned before, unsubstituted and *N*-alkylsubstituted amines will also be used as donor substituents in the work presented.

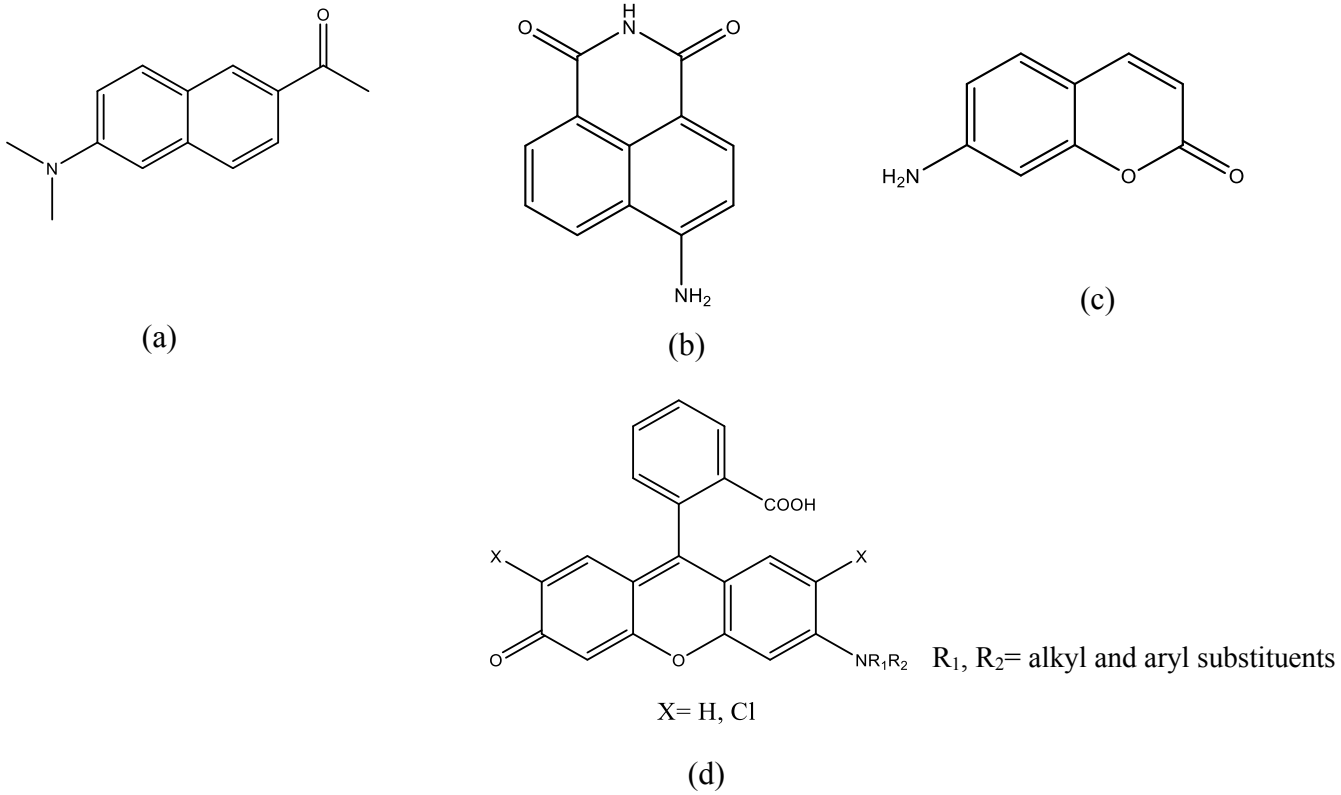

Figure 1.11. Structure of (a) 2-acetyl-6-(dimethylamino)naphthalene (b) 4-amino-1,8-naphthalimide (c) 7-aminocoumarin and (d) rhodol derivative.

A recently published article in 2015 by Joo *et al.* has shown that *N,N*-dialkylamino groups possess superior donating ability compared to *N*-alkyl substituted amines.[28] As a result, greater ICT can be expected for NBD chromophores consisting of *N,N*-dialkylamino as the donor species.[28] The two-photon absorption cross sections (σ) of the NBD chromophores have yet to be reported in the literature. The TPA cross sections (σ) of the NBD chromophores are determined in the work provided through TPEF method.

The substitution pattern of the amine is also likely to dictate the emission properties of the NBD-chromophores. A sterically hindered amine substituent is likely to undergo slow internal rotation in the excited state, which minimises non-radiative decays and thus results in enhanced fluorescence.[28] Disubstituted amines are more sterically hindered compared to the mono- and

unsubstituted amines. As a result, an enhanced emission property might be expected for *N,N*-dialkylamine derivatives. However, results reported in the literature have suggested otherwise.[28,29] For example, Yang *et al.* in 2009 reported the fluorescence behaviour of rhodol derivatives, Figure 1.11 (d) and established that the fluorescent behaviour of rhodol was influenced by the *N*-substituents present within the chromophore.[29] Absorption and emission bands of rhodol derivatives with *N,N*-dialkylamines as the donor groups occurred at longer wavelengths compared to rhodol with *N*-alkylsubstituted and unsubstituted amines.[29] This was attributed to the enhanced ICT because of the superior donating abilities of *N,N*-dialkylamines compared to to *N*-alkylated and unsubstituted amines. However, rhodol consisting of unsubstituted and *N*-alkylsubstituted amine were observed to be more fluorescent than the rhodol with *N,N*-dialkylsubstituted amine.[29] Likewise, Joo *et al.* noticed that acedan with *N*-alkylsubstitued amine also emitted superior fluorescence intensities compared to acedan consisting of *N,N*-dialkylsubstituted amine.[28] Joo *et al.* also briefly discussed the fluorescence behaviour of NBD chromophores containing *N,N*-dialkylamines as the donor. A detailed discussion regarding the fluorescent behaviour of NBD chromophores consisting of unsubstituted, *N*-alkylsubstituted amine and *N,N*-dialkylamines as the donor substituents have yet to be extensively discussed in the literature.

1.4.1. Twisted Intramolecular Charge Transfer (TICT) and Allylic 1,3-Strain

Grabowski *et al.* in 1973 based on the results obtained from (dimethylamino)benzonitrile (DMABN) proposed a hypothesis known as the twisted intramolecular charge transfer (TICT) hypothesis.[30] According to the hypothesis, in polar solvents an excited DMABN molecule undergoes a rotation of the dimethylamino group about the amino-phenyl bond to achieve a perpendicular geometry with respect to the aromatic ring.[30] The perpendicular rotation results in increased transition dipole moment and leads to a greater charge separation known as twisted

intramolecular charge transfer (TICT).[30] The twisted charge separated is greatly stabilised under polar solvents which results in dual fluorescence consisting of a UV component and a red-shifted emission band.[30] The dual fluorescence also appears because of the rapid equilibration between the twisted and planar state in the more polar solvent. The TICT is more prevalent in a polar solvent. The concept of TICT has since been extended to many other classes of molecules including dipolar chromophores such as acedan, where a donor and an acceptor species are interacting with each other through an aromatic system.[28,30,31]

Allylic 1,3-strain is one of the types of torsional strain that arises when two substituents are held in a close 1,3-proximity on a rigid allylic or benzylic skeleton.[32] The potential allylic 1,3-strain that could exist in the NBD chromophores is shown in Scheme 1.1, where the proton in the 1 position and the alkyl substituent bonded to nitrogen amine in the 3 position are likely to cause the allylic 1,3-strain.[28,32]

Scheme 1-1

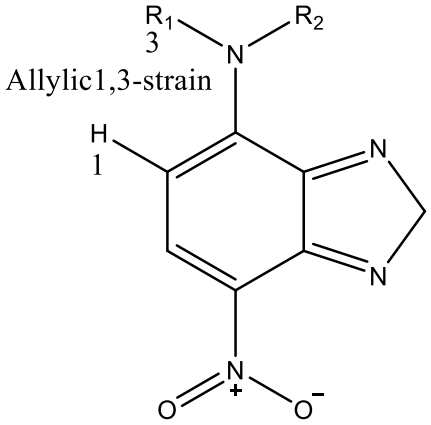

Joo *et al.* suggested that the allylic 1,3-strain results in the formation of TICT excited states that compete with fluorescence by the non-radiative decay of the excited states resulting in poor

emission properties.[28] Yang *et al.* suggested that the greater the steric hindrance in the nitrogen of the amine, the greater formation of the TICT excitation states.[29] Whether the allylic 1,3-strain in NBD chromophores resulting from more sterically substituted amines results in poor emission properties remains to be seen.

1.5.The Effect of Solvatochromism on Two-Photon Absorption (TPA)

An efficient TPA organic chromophore needs to have a strong donor group interacting with a strong acceptor group through a π-conjugated system resulting in Donor-π-Acceptor interactions.[2,14,24-27] Chromophores with Donor-π-Acceptor interactions are also known as push-pull chromophores or dipolar chromophores.[2,14] Such TPA compounds are said to have large ground state dipole moments. The enhanced ICT within the molecule leads to an intense (π to π*) transition in the UV-vis spectrum. A change in intensity, frequency and wavelength for the π to π* transition is observed for solvents with different polarities. Studies have shown that the environment, such as solvent polarity, has a strong influence towards ICT.[2,34-36] In 2000, Luo *et al.* studied the solvent effect on the TPA properties of $NO_2(C_2H_2)_2NH_2$ and found that the TPA cross section (σ) is strongly influenced by the geometrical changes brought about by the solvent polarity.[34] They found that a polar solvent increases the degree of bond length alteration (BLA), which is the average difference in length between single and double bonds in a π-conjugated system. An increase in BLA leads to an increase in ICT and any effects on the ICT of an organic chromophore subsequently has a direct impact on the TPA cross section (σ).[34] In 2003, Wang *et al.* studied the solvent effect on a TPA chromophore with Donor-π-Acceptor interaction and concluded that polar solvents are capable of inducing a change in the electronic structure of an organic chromophore, and thus influencing TPA properties of organic chromophores.[35,36]

Chapter 2: Zeolites

Introduction

Zeolites are naturally occurring minerals that have been mined for more than 1000 years for use in cement and building stones.[37] Usually found in specific types of sedimentary rocks in the form of small crystals, zeolites were first isolated and studied in 1756 by a Swedish scientist A. F. Cronstedt while heating stilbite in a blowpipe flame. Zeolites are named after a Greek word, the word "*zeo*" means boil and "*lithos*" means stone.[38,39] Up until early 1950s it was believed that zeolites were found only inside the volcanic cavities but in the late 1950s and early 1960s zeolites were discovered in tuffs, a type of igneous rock formed by the consolidation of volcanic ash ejected from a vent during explosive volcanic eruptions.[37] These volcanic tuffs were initially located mainly in western United States, Japan and Italy. Similar deposits have since been discovered all over the world including Cuba, Hungary and New Zealand.[37] The crystal structure of zeolites allows them to act as molecular sieves and host-guest molecules within its framework.[37-39]

There are approximately 40 naturally occurring and 150 synthesized zeolites.[40] The most common naturally occurring zeolites are analcime, chabazite, erionite, ferrierite, laumontite, mordenite, and phillipsite. The most commonly synthesized zeolites are zeolites A, X, Y and ZMS-5.[40] Naturally occurring zeolites are used in applications such as pet litter, horticultural applications and waste water treatment.[40] Synthesized zeolites are used as catalysts for petroleum cracking, water-softening agents in laundry detergents and molecular sieves.[40]

An understanding of the structure and the properties of zeolites is essential in order to understand the chemistry of encapsulated organic chromophores within a zeolite framework. This chapter explores the properties and the chemistry within zeolites.

2.1 The Structure and Geometry of Zeolites

Zeolites are crystalline aluminosilicates that are constructed from repeating tetrahedron units of TO_4, where T represents a tetrahedral Si or Al atom.[41] Each of the various different naturally occurring and synthesized zeolites has an unique structure and topology but they are initially composed of common building blocks of TO_4. These common building blocks are referred to as basic building units (BBU).[41-42] As shown in Figure 2.1 (a), the tetrahedral atoms in zeolites are usually located in the central position, with oxygen occupying the corners. Zeolites are called tecto-aluminosilicates because as shown in Figure 2.1 (b), the apical oxygen atom bridges two tetrahedral atoms.[41,42]

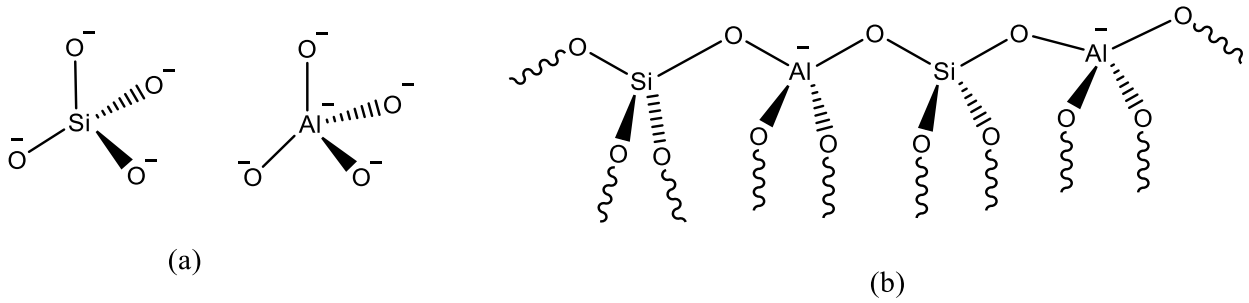

Figure 2.1. (a) Tetrahedral structure with aluminium and silicon atom as the central atom. (b) The tecto-aluminosilicate framework of zeolites. (Drawn based on information in Reference 39).

Silicon is tetravalent in nature and prefers forming bonds with four neighbouring atoms, which means that the silicate part of zeolite is neutral and does not carry any formal charge. In comparison, aluminium ends up bearing a formal charge of -1 when bonded to four oxygen atoms. The aluminosilicates therefore carry an overall negative framework charge and positively charged counter ions are required to achieve a neutral state within the framework.[39] Only aluminosilicates are considered to be zeolites and molecular frameworks with T atoms other than aluminium and

silicates are not considered to be zeolites.[39] Solid frameworks containing Ga, Ge and P as the T atoms were considered to be zeolites in the past, but they are now commonly known as metallosilicates.[39]

The tetrahedra within the zeolite framework are very rigid and the O-T-O angle is close to the ideal value for a tetrahedral shape of 109° 28'. In contrast, the T-O-T angle within the zeolite framework is flexible at an angle of approximately 140-165°.[42] The flexibility of the T-O-T is considered to be very important as it is this flexibility that allows the formation of a diverse variety of zeolite frameworks without much thermodynamic penalty.[42] The flexibility of the T-O-T angle also allows formation of various different rings and other complex building units within the zeolite framework.[42]

The single tetrahedral unit or the basic building unit (BBU) can be further linked together *via* bridging oxygens, which results in the formation of rings of tetrahedra of various different sizes. The most common rings contain 4, 5, 6, 8, 10 or 12 units of tetrahedra bridged together by oxygens, as shown in Figure 2.2 (a).[42] These rings are commonly referred to as the composite building units (CBU) and are more complex compared to BBU.[42] The n-rings can further combine to form even more complex and diverse three-dimensional arrays of tetrahedral aluminosilicate substructures such as the polyhedral units of chains and cages.[42]

Cages are polyhedral units with narrow rings that only allow the passage of molecules smaller than water.[42] Sodalite cages shown in Figure 2.2 (b) are one of the common examples of cages, which contain simple arrangements of truncated octahedra.[42] The tetrahedra are arranged at corners of the truncated octahedron with eight hexagonal faces, six square faces, 24 vertices and 36 edges.[42]

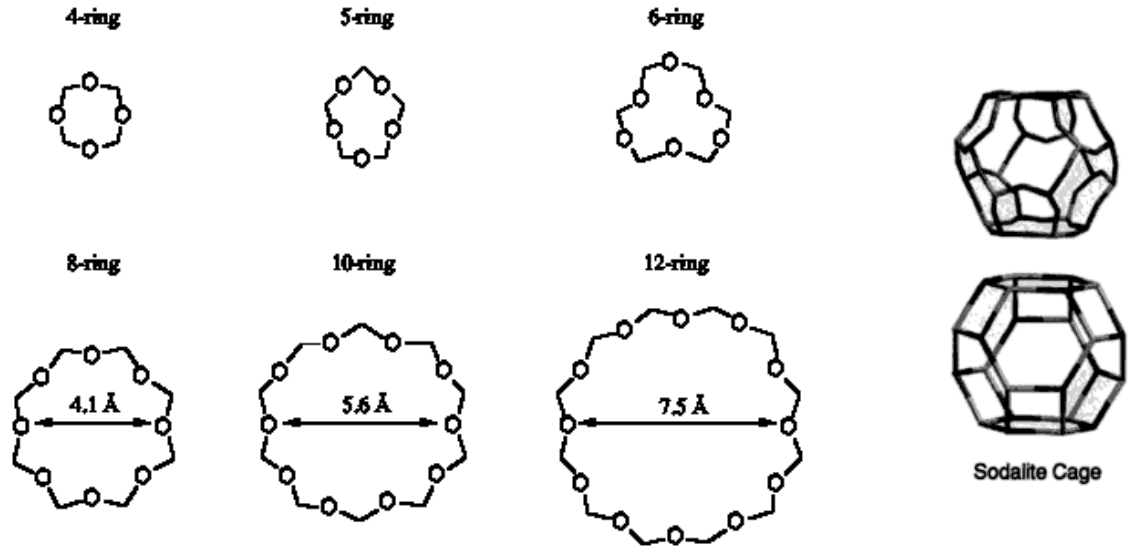

(a) (b)

Figure 2.2. (a) Relative sizes of the n-rings commonly found within the zeolite framework. (b) The three-dimensional structure of the sodalite cage which is formed through the combination of 4- and 6-rings. (Based on information in Reference 42).

Other polyhedral units present within the zeolite framework are cavities, channels and pores. Cavities are a larger CBU compared to cages that are capable of allowing the passage of larger molecules in and out of the zeolite.[42] A typical example of a cavity is the "supercage" found X and Y zeolites. The cavity within the supercage has tetrahedral symmetry with four 12-rings within its structure, which enables the passage of larger molecules.[42] Neopentane and trimethylbenzene are some of the compounds that can pass through the supercages of the Y zeolite.[42] The NBD chromophores discussed in Chapter 1 are also expected to pass through the cavities of Y zeolite. The size of the molecule usually determines whether it can enter a pore of a certain diameter. Similarly, the diameter of the cage determines how many molecules can occupy the cage or the channel.[42]

A channel is a pore that is extended in at least one dimension with a minimum amount of n-rings that allows the guest molecules to diffuse along the pores.[42] In many zeolites, the channels

intersect, forming a two- and three-dimensional channel system. The dimension and size of the pores of the zeolite is one of the most important features of the zeolite as this determines the maximum size of molecules that can enter the micropores of the zeolite.[42] The size or the dimensions of the channels is determined by the size of the n-rings. Structures with 8-ring, 10-ring and 12-ring are known as small, medium and large pores, respectively. The previously mentioned zeolite "supercages" consist of 12-rings.[42]

In addition to n-rings, a free diameter is also used to measure the size of the pores within zeolites.[42] The free diameter identifies the approximate size of the molecules that can penetrate the channels within zeolites. The free diameter is usually determined by subtracting 2.7 Å from the crystallographic distance between the oxygen atoms on the opposite sides of the pore (an ionic radius of 1.35 Å is assumed for oxygen). Channels with 8-rings, 10-rings, and 12-rings have an approximate free diameter of 4.0 Å, 5.6 Å and 7.6 Å, respectively.[42] The actual dimensions of the molecules that can enter the channels within the zeolite are also influenced by the structure and composition of the zeolites. For example, the size of the counterbalancing cations might influence the entry of molecules within the channels of the zeolites as larger counterions certainly occupy a much larger space.[42]

2.2 Chemical Composition of Zeolites

The composition of the single unit of zeolite can be represented by the following empirical formula:

$$M^{n+}_{x/n}[(AlO_2)_x\ (SiO_2)_y]^*\ mH_2O$$

In the given formula, M represents counterbalancing metal cation, whereas x, y and n are integers with $y > x$.[43] Usually, the counter ions are protons, or cations of alkali metals such as Li^+, Na^+, K^+,

Rb^+ and Cs^+.[43] The counterbalancing cations are not covalently bonded to the zeolite framework and can be replaced with other cations. The presence of balancing counterions leads to the formation of electrostatic forces within the zeolite, which create a hygroscopic environment within the zeolite framework.[43] The hygroscopic environment means that the positively charged counter ions are capable of interacting with water molecules and other guest molecules encapsulated within the framework. The water molecules can be adsorbed into the zeolite framework in three different ways, as summarised in Figure 2.3.[44]

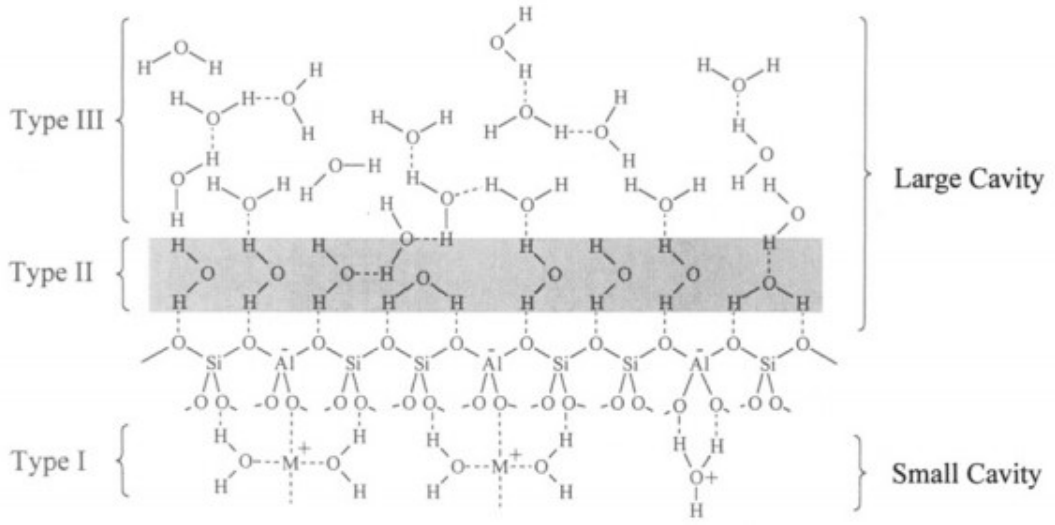

Figure 2.3. The different ways in which water molecules can be adsorbed within a zeolite cavity.[44]

As shown in Figure 2.3, in a Type I interaction, the water molecules are co-ordinated to the metal cation and are usually located in small cavities such as a single unit of sodalite cage. These Type I water molecules can be removed by heating at 300ºC or higher.[44] Type II and Type III molecules are usually found in the larger cavities. Type II water molecules are bound to the oxygen that is bridging or coordinating the aluminium and the silicon atoms. Type II water molecules can be removed by mildly heating the zeolites at 100ºC.[44] The Type III water molecules are not necessarily interacting with any species present within the zeolite cavities; instead they are

clustered together within the cavity. The lack of interaction of the Type III water molecules means that they are relatively easy to remove compared to to the Type I and Type II water molecules. The Type III cations can usually be removed in ambient temperatures through gentle evacuations.[44]

2.2.1 The Silicon to Aluminium Ratio in Zeolites.

The ratio of silicon and aluminium atoms can vary with different types of zeolites. The proportion of silicon atoms in zeolites is always higher than the proportion of aluminium atoms, leading to an overall Si/Al ratio greater than 1 on every occasion.[42] In naturally occurring zeolites, the Si/Al ratio is usually less than 5, with mordenite having a Si/Al ratio of exactly 5.[41,45] The Si/Al ratio follows the Loewenstein rule, also commonly known as the aluminium avoidance rule.[46] Aluminium can replace only up to 50% of the silicon, as the presence of more than 50% of aluminium would mean that two negatively charged aluminium atoms would be adjacent to each other and bridged by an oxygen atom, which would destabilize the zeolites.[39,42,46] The bond length of Al-O is approximately 1.70-1.73 Å, whereas the bond length of Si-O is 1.58-1.64 Å, which means that the Al-O bonds are longer and weaker than Si-O.[42] The Si/Al ratio for X zeolite and Y zeolite are 1.23 and 2.43 respectively.[47]

2.3 The Faujasite of X and Y Zeolites

Two of the most commonly used zeolites for host guest studies are X and Y zeolites and the work presented in this thesis focuses on Y zeolites. X and Y zeolites are synthetic analogues of naturally occurring faujasite zeolites constructed from three different CBUs: the double 6-ring, the sodalite cage and large cavities known as supercages.[42] As shown in Figure 2.2 (b), the sodalite cage has a diameter of 6.6 Å and an entry aperture of 2.2 Å. Molecules larger than water and ammonia cannot pass into the sodalite cages. The second CBU is a double 6-membered oxygen

ring that connects the sodalite cages resulting in formation of the large cavities known as supercages.[42]

A diagram showing the structure of a supercage has been provided in Figure 2.4.[48] As mentioned previously, the supercages are constructed with 12-rings and have a diameter of approximately 13.1 Å, which allows the passage of molecules larger than water. A single unit of faujasite is made up of 8 supercages, 8 sodalite cages and 16 double 6-rings.[42] Typical unit cell compositions of X and Y zeolites are summarised below where M is a monovalent counterbalancing cation present within the zeolite.[49]

X zeolite: $M_{86}\ (AlO_2)_{86}\ (SiO_2)_{106}$ *264 H_2O

Y zeolite: $M_{56}\ (AlO_2)_{56}\ (SiO_2)_{136}$ *253 H_2O

The counterbalancing cations are known to occupy three different positions in X and Y zeolites, predominantly in and around the cavity where the oxygen atoms are coordinated or where the guest molecules are located. The interaction with the cations is one of the main reasons why compounds are able to be adsorbed within zeolites.[50] The counterbalancing cations interact with adsorbed molecules containing alkenes and aromatic group through metal-π-cation interactions.[48-50]

As shown in Figure 2.4, there are three different cations, Type I, II and III. There are 16 Type I cations per unit cell for both the X and Y zeolites, often located in the centre of the hexagonal prism between the sodalite cages. There are 32 Type II cations per unit cells for both the X and Y zeolites and these cations are located on the six-membered unjoined open hexagonal faces in the faujasites. There are 38 Type III cations for the X zeolite and 8 for the Y zeolite and these cations are located in the walls of the channels adjacent to the four-membered oxygen rings.

The location of the different types of cations within faujasites means that only Type II and Type III cations are readily available for interaction with the encapsulated guest molecules.[45,48,49]

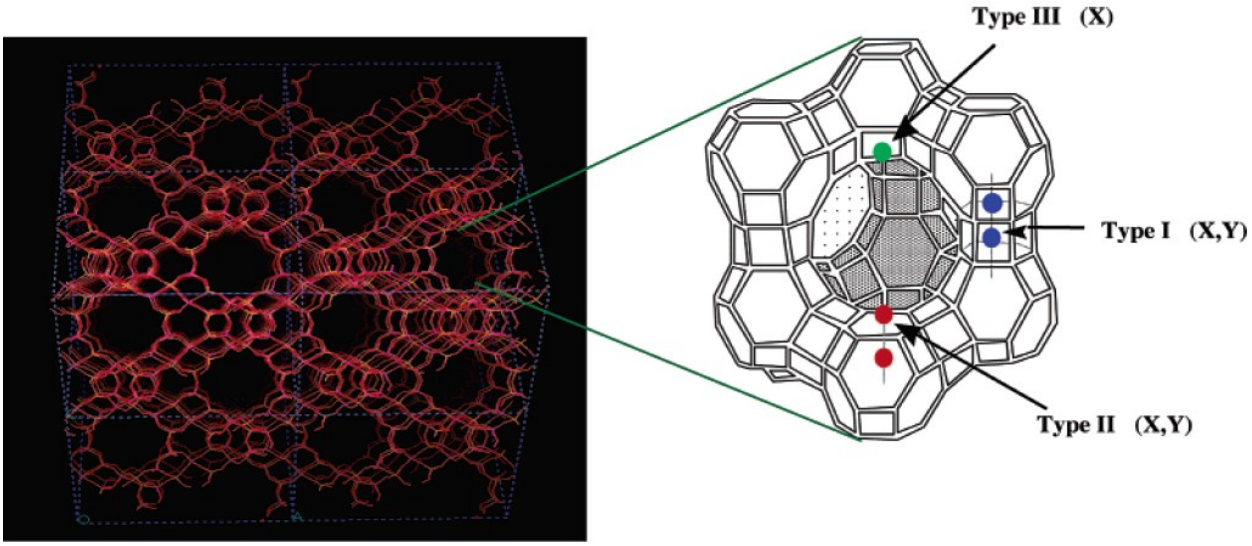

Figure 2.4. Structure of the faujasite (left) and zeolite supercage (right) with the locations of Type I, II and III cations identified.[48]

2.4 The Superpolar Nature of the Zeolite Supercages.

In a dry zeolite, one side of the Type II and III cations is shielded, whereas the side that is exposed to the centre of the supercage remains unshielded, resulting in only partial shielding of the anionic aluminosilicate framework, which leads to the generation of large electric fields extending into the supercage. Following the incorporation into the zeolite framework, the guest molecules are polarised in such a way that the negative end is stabilized by the cation and the positive end is stabilized by the anionic framework. In qualitative terms, this process of stabilization is considered to be similar to when a reactant molecule is dissolved in a highly polar salt solution.[51] In addition to the polarity, the guest molecules are also influenced by the electric

field generated by the cations present within the zeolite framework. In theory, polarity is defined as the ability of a solvent to polarize solute and given the solid state nature of zeolites, the environment within the zeolite cavities is commonly known as micropolar.[51] A study carried out by V. Ramamurthy *et al.* discovered that the micropolarity of a zeolite supercage is far higher than any organic solvent, and the authors concluded that zeolite cavities are "superpolar". The superpolar nature of the zeolites means that compounds encapsulated within the zeolite framework might show extra features and properties in comparison to when dissolved in solvents.[51]

In order to maintain the "superpolarity" within the zeolite cavity, the zeolite has to be completely dry, ensuring no water molecules or any organic solvents are present. The presence of water molecules or organic solvents within the zeolite framework would eliminate the contribution of cations, which in turn would reduce the micropolarity or the superpolarity within the zeolite cavity. The water molecules in Y zeolites in the present work provided were removed by heating zeolites at 450^{o} C.[51]

The counterbalancing cations are not covalently bound to the zeolite framework and can be replaced by other cations.[52,53] In addition to helping create a superpolar environment within the supercages, the cations also dictate the size and the number of molecules that can enter the supercage.[52] The vacant space available within the cavity of the zeolite is influenced by the size of the cations, as the larger the cations, the less space is available for guest molecules. Alkali metals are commonly used as counterbalancing cations, and Table 2.1 highlights the effect of the presence of cations of various different sizes.[52]

Table 2.1 Table showing the relationship between the radius of the cation and the space available within the zeolite framework. (Based on information in Reference 52)

Cation	Radius of the cation (Å)	Vacant Space within the supercage ($Å^3$) X zeolite	Vacant Space within the supercage ($Å^3$) Y zeolite	Electrostatic Field within the cage (V/Å)
Li^+	0.76	873	834	2.1
Na^+	1.02	852	827	1.3
K^+	1.38	800	807	1.0
Rb^+	1.52	770	796	1.8
Cs^+	1.67	732	781	0.6

As the radius of the alkali earth metal cation increases from Li^+ to Cs^+, the vacant space available within the zeolite is reduced, which may restrict the size and the number of molecules entering the supercage. Another important observation from Table 2.1 is that the electrostatic field generated within the supercages is reduced as the size of the cation increases. The reduction of the electrostatic field generated has a direct effect towards the micropolarity of the zeolites. As a result, the polarity within the supercages decreases as the size of the counterbalancing cation increases. The order of polarity of the alkali metal cations within the zeolite framework, particularly for the X and Y zeolites, is $Li^+ > Na^+ > K^+ > Rb^+ > Cs^+$.[52]

2.5 The Amphoteric Supercages of Zeolites.

The presence of the counterbalancing cations allows the supercages to possess an amphoteric property, enabling zeolites to act as both acids and bases.[53,54] The acidity within the zeolite supercages can be categorised into two different types: Lewis acidity and Brønsted acidity.

Brønsted acidity is less common and only exists when protons are used as counterbalancing cations. The protons in acidic zeolites are covalently bonded to oxygen atoms that are in turn bonded to aluminium atoms, Figure 2.5, resulting in the formation of oxonium species.[54] The Si-OH---Al groups are usually referred to as the Brønsted acid sites. One Brønsted acid for every 116 aluminium atoms is found for alkali metal cation-exchanged Y zeolites, accounting for less than 1% of the cations. The Brønsted acidity can almost be ignored in pure X and Y zeolites.[54]

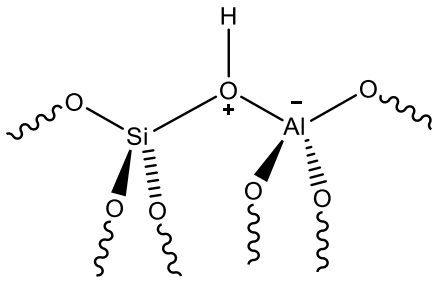

Figure 2.5. Formation of an oxonium species through bonding of a proton with an oxygen. (Drawn based on information in Reference 54).

Basic sites within the zeolite framework can result from the presence of basic hydroxyl groups OH^- (Brønsted base). However, in aluminosilicate zeolites, the framework basic hydroxyl groups (OH^-) do not occur. The hydroxyl groups may instead behave as ligands and coordinate to the charge-balancing multivalent cations.[55]

Zeolites are also capable of acting as Lewis acids. Initially, the Lewis acidity within the zeolite framework was attributed to the tricoordinated aluminium. However, ^{27}Al MAS NMR was unable to detect this type of tricoordinated aluminium. Instead the Lewis acidity is now partly attributed to the octahedrally coordinated Al centres generated during calcination or steaming of hydrated zeolites.[56] The counterbalancing cations are also known to possess Lewis acidity. As far as alkali metal cations are concerned, the Lewis acidity decreases with increasing atomic radius of

the cation, $Li^+ > Na^+ > K^+ > Rb^+ > Cs^+$. The Lewis acidity within the zeolite framework allows zeolites to possess electron-accepting ability. The Lewis acid strength of the zeolite increases with an increase in Si/Al ratio.[47]

The Lewis basicity within the zeolite framework is also thought to depend on the average negative charge on oxygen.[47] The oxygen atoms adjacent to aluminium atoms are considered to be more basic as these oxygen atoms bear more partial negative charge. In contrast to the Lewis acidity, the Lewis basicity increases with increasing atomic radius and follows the pattern of $Cs^+ > Rb^+ > K^+ > Na^+ > Li^+$. The basicity of oxygen increases with the decreasing Si/Al ratio, as the increase in the aluminium atoms is likely to increase the overall negative charge on oxygen.[47] The ability of zeolites to act as Lewis bases allows zeolites to possess electron-donating ability. Overall, the amphoteric property of zeolites allows them to act as both electron donors and electron acceptors.[47,55]

2.6. The Ability of Zeolites to Act as a Host.

The structural framework and the supercages enable zeolites to act as hosts to guest molecules of various sizes. The presence of counterbalancing alkali ions and their interactions with the guest molecules through cation-π interactions plays an important role in the adsorption of organic molecules.[57,58] Usually for aromatic compounds such as benzene, the cation-π interactions occur in the centre of the molecule.[59,60] When the benzene group is substituted with a polar group such as a nitro group or a carbonyl group, the counterbalancing alkali cations interact with the oxygen of the polar group through alkali ion-dipolar interactions.[48,57,58] In context of the NBD chromophores, alkali ion-dipolar interaction can be predicted to exist between the oxygen of the nitro group and the cations.

The cations can also form an interaction with the lone pair present in the nitrogen of the amine. For example, studies have shown that when the aromatic compound is pyridine, an interaction likely exists between the lone pair of nitrogen and the cation through alkali ion-nitrogen lone pair interaction.[60,61] The alkali ion-nitrogen lone pair interaction in the zeolite framework means that the free movement of the compounds within zeolite framework is restricted and they are confined within zeolite cavity.[48] Previously reported studies in the literature of lone pair containing nitrogen compounds, such as phenylalanine, within zeolites has shown that the nitrogen lone pair-alkali ion interaction restricts the conformation mobility of the compounds.[48,62] Once again in the context of NBD-chromophores, alkali ion-nitrogen lone pair interaction is likely to exist between the amine of the NBD-chromophore and the counterbalancing metal cations in zeolites. In addition to cation-π, alkali ion-dipolar and alkali ion-nitrogen lone pair interactions, the guest molecules may experience other interactions such as weak van der Waals forces and electrostatic forces.[48] Whether the ability of the counterbalancing cations in zeolites to interact with both the donor and acceptor group of the NBD-chromophore has any influence on its two-photon properties remains to be seen.

Zeolites exhibit very solvent-like properties but in terms of interaction, when a molecule interacts with a solvent, more often than not a homogenous solution is formed where the fluid solutions allow reacting molecules to experience an average microenvironment by the virtue of fast relaxation time and the high mobility of the reactant molecules.[63] When using solvents, it is easy to establish trends of various different properties with respect to varying concentration. On the other hand, due to the solid state nature of zeolites, the rate of diffusion and the mobility of the guest molecules within the framework might not be as efficient resulting in a heterogeneous

environment. As a result the molecules adsorbed in zeolites are unlikely to face the same average microenvironment.[63]

The word *occupancy* is used to describe the aggregate encapsulation of the guest molecules within the zeolite framework. Supercages are the primary site of occupancy for guest molecules, and the occupancy depends on the size and the number of the guest molecules.[64] The heterogeneous environment in zeolite means that the molecules may not be able to occupy the supercages uniformly, instead they might be distributed on a random basis. It might be easier for the smaller molecules to occupy the supercages uniformly. With the increasing size of the molecules, it is more than likely that the random distribution of guest molecules within the zeolite supercages also increases.[63,64]

2.6.1. Loading Level

When a molecule is dissolved in various solvents, the homogenous solution that is formed is quantified in terms concentration. The occupancy of the guest molecules within the zeolite supercages can be quantified through loading level. The term loading level which is also known as average occupancy defines the number of guest molecules incorporated or encapsulated within the available zeolite supercages.[63] Loading levels are usually represented by <S>, and the loading level numbers are usually represented in decimals.[63] For example, a loading level <S> of 0.1 means that, averaged over all of the supercages, one would expect to find one guest molecule in every 10 supercages. As described in the experimental section, the process of calculating the loading level is fairly simple, but, due to the heterogeneous microenvironment within the zeolite framework, it is difficult to predict the actual distribution of molecules within the zeolite framework. For example, consider a loading level of <S> = 0.4, which means there is an average of 2 molecules in every 5 supercages. This loading level does not necessarily mean that the 2 of every 5 supercages

are actually occupied, since there is some probability that the two molecules will occupy the same supercage, leaving 4 empty supercages.[63]

2.7. Zeolites and Two-Photon Absorption

The two-photon absorption (TPA) or two-photon excitation (TPE) efficiency of dipolar organic chromophores is influenced by intramolecular charge transfer (ICT) through Donor-π-Acceptor interactions. Following the discussion of the structure and properties of zeolites, there are three features in particular that may be of interest with respect to TPE. The TPE properties of organic dipolar chromophores are likely to be enhanced in more polar solvents because of the enhanced ICT caused by the more polar solvent. The supercages of zeolites are "superpolar" in nature; thus if polarity is one of the major factors for TPE enhancement, then enhancements in TFE efficiency would be expected to be observed for the NBD-chromophores in Y zeolites.

The aluminosilicate framework of zeolites has a rigid structure, and the rigidity is maintained during the adsorption of guest molecules. In contrast, the distribution of the counterbalancing cations is much more variable and depends on the nature of the incorporated guest molecule.[58] Kirschhock *et al.* in 1996 suggested that cations tend to assume positions whereby they can coordinate to the oxygen located either in the zeolite framework or in the incorporated guest molecules. Kirschhock *et al.* also suggested that nitro groups are strongly polarised and prefer interacting with the cations instead of the framework. In the same study it was discovered that the cations tend to assume positions where greater interactions are likely to take place between the cations and the oxygen of the nitro group.[58] The nitro group is the acceptor substituent in the NBD-chromophore and the charge balancing cations are likely to interact with the polar oxygen of the nitro group.

In addition to the interaction with the polar nitro groups, interactions between the lone pair of the amine and the cation through alkali ion-nitrogen lone pair interactions have also been previously mentioned in the literature.[48,60-62] Overall, the alkali metal cations are known to interact with both donor and acceptor substituents of the NBD-chromophore which may influence or enhance the charge redistribution between the donor and the acceptor substituents of the NBD-chromophores within the zeolite framework. Any influence on the charge redistribution will have a direct effect on the TPA properties of the NBD- chromophores.

Chapter 3: Experimental

3.1 General Techniques

Proton nuclear magnetic resonance (^{1}H-NMR) spectra were obtained using a Bruker AV-500 spectrometer in automation mode. Temperature controlled proton (^{1}H) NMR spectra were obtained using a Bruker AV-300 spectrometer. Chemical shifts (δ) are reported in parts per million (ppm) relative to tetramethylsilane (TMS) as the internal standard (0.00 ppm). The multiplicities are as follows: s= singlet, d=doublet, t= triplet, q=quartet, p=pentet, br=broad. Coupling constants of the ^{1}H-NMR peaks are reported in hertz (Hz). The ESI mass spectra (MS) were obtained from a Bruker microTOF Focus mass spectrometer. The mass spectrometer samples were prepared in HPLC-grade acetonitrile. Melting points were determined using a IA9000 series digital melting point apparatus. Fluorescence spectra were obtained using a PTI fluorimeter. The ultraviolet visible (UV-vis) absorption spectra were obtained using a Varian Cary 100 Bio spectrophotometer. The diffuse reflectance spectra were also obtained using a Varian Cary 100 Bio spectrophotometer. The diffuse reflectance spectra were obtained as %Reflectance as a function of wavelength. The %Reflectance was converted to absorbance using the Kubelka-Munk equation shown in Equation 3.1., where R= reflectance.[65]

$$f\,(R) = \frac{(1-R)^2}{2R} \tag{3.1}$$

3.2 Materials

The main precursor for the compounds used in this work, 4-chloro-7-nitrobenzofurazan (NBD-Cl, 98% purity), along with other reactants ammonia (7 N in methanol), methylamine (2.0 M in methanol), dimethylamine (2.0 M in methanol), ethylamine (2.0 M in methanol), *N*-ethylmethylamine (97% purity) and diethylamine (99.5% purity) were commercially available from Sigma Aldrich and used as received. Additionally, the two-photon absorption (TPA) reference compounds, perylene (sublimed grade, ≥ 99.5% purity), coumarin 153 (99% purity), fluorescein sodium salt (99% purity) and rhodamine B (99% purity) were also commercially available from Sigma Aldrich and were used as received. Tetrahydrofuran (THF) (Class 1B) was commercially available from Fisher Scientific and was used as received. $CDCl_3$ (99.8% purity with 0.05% TMS as internal standard) was obtained from Cambridge Isotopic Laboratories Inc and CD_3CN (99.8 atom % D) was obtained from Sigma Aldrich. Chromasolv® HPLC dichloromethane (99.8% purity), Chromasolv® LC-MS acetonitrile (99.9% purity) and Chromasolv® HPLC methanol (99.9% purity) were all commercially available from Sigma Aldrich and were used as received. Absolute ethanol was used as received from the chemistry stores at Dalhousie University. Zeolite NaY (molecular sieve, Si/Al= 2.4) was also commercially available from Sigma Aldrich and used as received. The alkali metal cation exchanged zeolites of LiY, KY, RbY and CsY were previously prepared by others in the lab and were available for use. A typical degree of cation exchange in Y zeolites is 49% for LiY, 85% for KY, 73% for RbY and 62% for CsY.[66]

3.2.1 Synthesis of the Organic Chromophores.

The reaction scheme for the synthesis of the organic compounds used in this work is summarised in Scheme 3.1 below:

Scheme 3-1

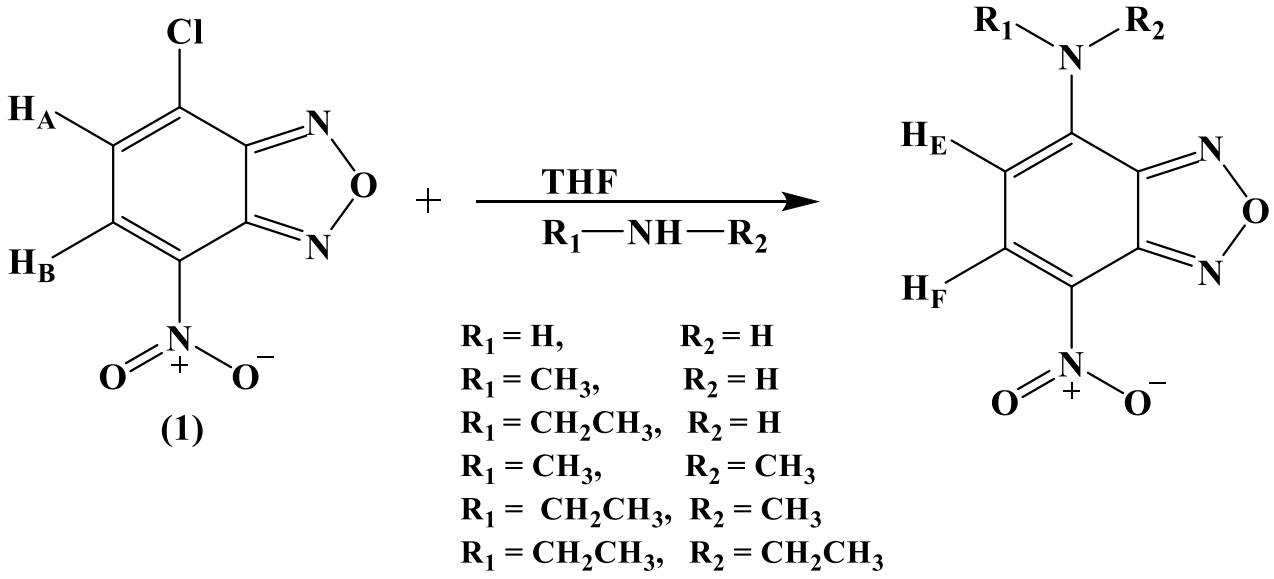

Synthesis of the compounds followed the same literature procedure in all cases.[67,68] Approximately 0.4 g (2 mmol) of NBD-Cl (**1**) was dissolved in 5 mL of tetrahydrofuran (THF), and a 1.5 to 3 fold excess of the appropriate amine dissolved in methanol was added. The reaction mixture was stirred at room temperature for 16 hours. Solvent was removed under reduced pressure, and the product was purified by recrystallization or column chromatography.

7-Nitro-2,1,3-benzoxadiazol-4-amine (NBD-NH_2, $R_1 = R_2 = H$): 4-Chloro-7-nitrobenzofurazan (0.408 g, 2 mmol) in 5 mL of tetrahydrofuran (THF) and 0.7 mL of 7N ammonia in methanol followed by the purification on silica gel using ethyl acetate: hexane (3:1), resulted in brownish green powder (0.179 g, 48% yield). The melting point of the product was determined to be 235-

238° C (literature 237° C).[69] ^{1}H NMR (CD_3CN, AV-500 spectrometer): δ 8.55 (d, J = 9 Hz, 1H, proton H_F), 6.82 (s, br 2H), 6.50 (H_C, d, J = 9 Hz, 1H, proton H_E). The NMR data are consistent with the literature.[68] ESI-MS [$C_6H_4N_4O_3Na^+$] 203.00.

***N*-Methyl-7-nitro-2,1,3-benzoxadiazol-4-amine (NBD-Methylamine, R_1 = H, R_2 = CH_3)**: 4-Chloro-7-nitrobenzofurazan (0.407 g, 2 mmol) in 5 mL of THF and 0.8 mL of 2M methylamine in methanol after recrystallization from absolute ethanol resulted in dark green powder (0.124 g, 40% yield). The melting point was determined to be in the range of 254-256° C (literature 259-261° C).[70] ^{1}H NMR (CD_3CN, AV-500 spectrometer): δ 8.57 (d, J = 9 Hz, 1H, proton H_F), 6.29 (d, J = 9 Hz, 1H, proton H_E), 3.15 (s, 3H). APCI-MS [$C_7H_5N_4O_3^-$] 193.00. The NMR and mass spectrometer data are consistent with the literature.[70]

***N,N*-Dimethyl-7-nitro-2,1,3-benzoxadiazol-4-amine (NBD-DMA, R_1 = R_2 = CH_3)**: 4-Chloro-7-nitrobenzofurazan (0.361 g, 2 mmol) in 5 mL of THF and 0.8 mL of 2M dimethyl amine in methanol resulted in bright orange powder (0.180 g, 37% yield). The melting point was determined to be 220-221° C (literature 224-225° C).[67] ^{1}H NMR (CD_3CN, AV-500): δ 8.54 (d, J = 9 Hz, 1H, proton H_F), 7.47 (s, 1H) 6.28 (d, J = 9 Hz, 1H, proton H_E), 3.13 (br s, 6H). ESI-MS [$C_8H_8N_4O_3Na^+$] 231.20. The spectral data are consistent with the literature.[28]

***N,N*-Diethyl-7-nitro-2,1,3-benzoxadiazol-4-amine (NBD-DEA, R_1 = R_2 = C_2H_5)**: 4-Chloro-7-nitrobenzofurazan (0.432 g, 2 mmol) in 5 mL of THF and 0.8 mL of 99.5% diethylamine resulted in a bright orange powder. (0.247 g, 48% yield). The melting point was determined to be 136-137°C (literature 138-139.5°C).[67] ^{1}H NMR ($CDCl_3$, AV-300, Room Temperature): δ 8.48 (d, J = 9 Hz, 1H, proton H_F), 6.16 (d, J = 9 Hz, 1H, proton H_E), 3.96 (d, J = 8 Hz, 4H), 1.42 (t, J = 7 Hz, 6H). ^{1}H NMR ($CDCl_3$, AV-300, 288 K): δ 8.48 (d, J = 9 Hz, 1H, proton H_F), 6.16 (d, J = 9 Hz, 1H, proton H_E), 3.96 (br s, 4H), 1.42 (t, J = 7 Hz, 6H) ^{1}H NMR ($CDCl_3$, AV-300, 320 K) δ 8.48

(d, J = 9 Hz, 1H, proton H_F), 6.16 (d, J = 9 Hz, 1H, proton H_E), 3.96 (q, J = 7 Hz, 4H), 1.42 (t, J = 7 Hz, 6H). There are no NMR data available for NBD-DEA in the literature. ESI-MS [$C_{10}H_{12}N_4O_3Na^+$] 259.10.

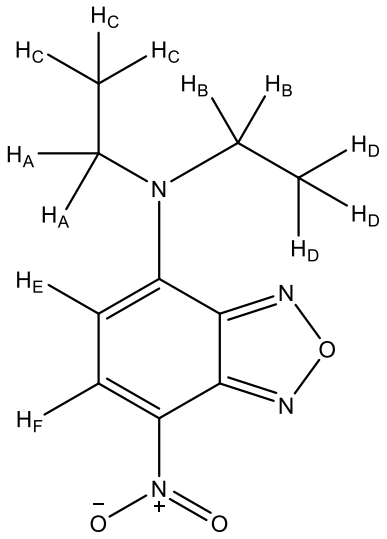

Figure 3.1. Structure of *N,N*-diethyl-7-nitro-2,1,3-benzoxadiazol-4-amine.

The splitting pattern, based on the number of neighbouring protons, of the peak at 3.96 ppm for H_A and H_B is expected to be a quartet. Instead the peak at 3.96 ppm demonstrates unusual splitting pattern and instead of being a quartet, the multiplicity of H_A and H_D resembles a doublet.

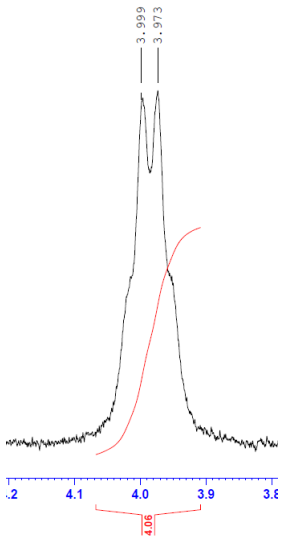

Figure 3.2. Splitting pattern observed at 3.96 ppm for NBD-DEA from AV-300 spectrometer at room temperature.

This can be attributed to restricted rotation about the *N,N*-substituted amine attached to the aromatic ring, with this restricted rotation causing the 2 alkyl- groups to exist in slightly different environments. To examine this possibility, ^{1}H-NMR of NBD-DEA was obtained at lower temperature (288 K) and higher temperature (330 K).[71,72]

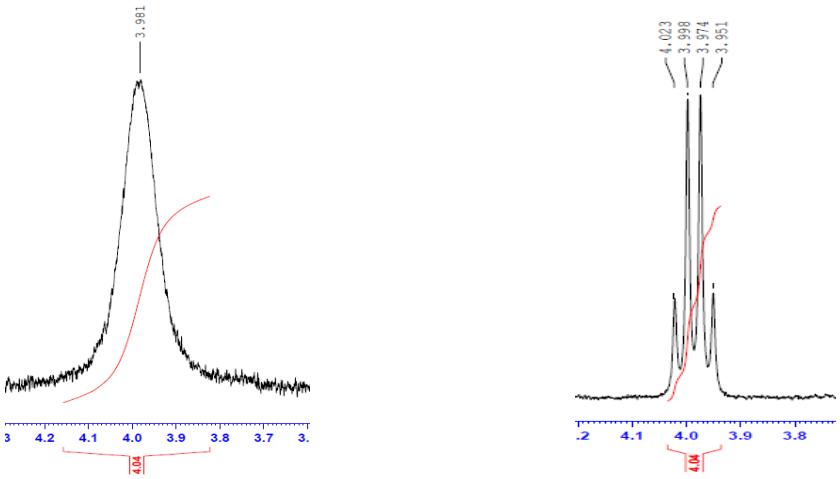

(a) (b)

Figure 3.3. Peak observed for H_A and H_D protons of NBD-diethylamine at 3.96 ppm, obtained from AV-300 NMR spectrometer at (a) 288 K (b) 330 K.

As expected, when the temperature was increased to 330 K, a distinct quartet with an integration of 4 was observed, which suggests faster rotation at higher temperature. Interestingly, at lower temperature of 288 K, the peak at 3.96 ppm was observed to further coalesce to a broad singlet, as the rotation became slower.

***N*-Ethyl-7-nitro-2,1,3-benzoxadiazol-4-amine (NBD-Ethylamine, R_1 = H, R_2 = C_2H_5)**: 4-Chloro-7-nitrobenzofurazan (0.416 g, 2 mmol) in 5 mL of THF and 0.8 mL of 2.0 M ethylamine in methanol followed by recrystallization in absolute ethanol resulted in a dark green powder (0.107 g, 29% yield). The melting point of the compound was determined to be 155-157^{o}C (literature 164^{o}C).[73] ^{1}H NMR (CD_3CN, AV-500 spectrometer): δ 8.54 (d, J = 9 Hz, 1H, proton H_F), 7.30 (s, 1H, proton H_D), 6.32 (d, J = 9 Hz, 1H, proton H_E), 3.59 (broad s, 2H, protons H_A), 1.38 (t, J = 7 Hz, 3H, protons H_C). ^{1}H NMR (CD_3CN, AV-300 spectrometer at 330 K): δ 8.54 (d, J = 9 Hz, 1H, proton H_F), 7.30 (s, 1H, proton H_D), 6.34 (d, J = 9 Hz, 1H, proton H_E) 3.59 (p, J = 7 Hz, 2H, protons H_A), 1.35 (t, J = 7 Hz, 3H, protons H_C) ESI-MS [$C_8H_8N_4O_3Na^+$] 231.1. The NMR data obtained are consistent with the literature. However, the literature only mentions the chemical shifts of the signals. The multiplicities of the signals are missing.[73]

The expected splitting pattern, based on the number of neighbouring protons, of the peak that appears at 3.59 ppm for H_A is a quartet as the adjacent carbon contains 3 H_C protons. If the proton H_D attached to nitrogen is also to be taken into consideration, the expected splitting would be doublet of quartets.

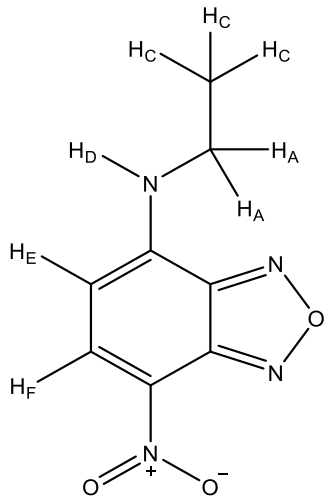

Figure 3.4. Structure of *N*-ethyl-7-nitro-2,1,3-benzoxadiazol-4-amine.

The signal for H_A obtained from AV-500 and AV-300 NMR spectrometer at room temperature is shown in Figure 3.5.

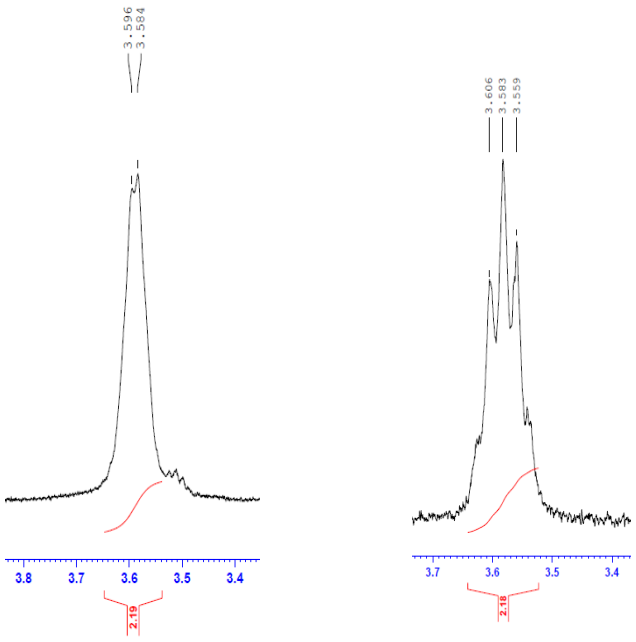

(a) (b)

Figure 3.5. Signal observed for H_A protons of NBD-Ethylamine obtained (a) from AV-500 NMR spectrometer (b) AV-300 spectrometer.

The peak at 3.59 ppm that was expected to appear as either a quartet or a doublet of quartets resembles a broad singlet using AV-500 spectrometer and a triplet using the AV-300 spectrometer. In terms of frequency, switching to a higher frequency is equivalent to cooling down the NMR sample and switching to lower frequency is equivalent to heating up a sample.[71] During the NMR timescale experiment for NBD-DEA, it was established that the observed NMR signal for NBD-DEA at 3.96 ppm coalesces at lower temperature and the peaks are more distinct at higher temperature. This phenomenon can be used to relate to the different multiplicities observed in 300 MHz and 500 MHz NMR for the same proton (H_A). [71-72]

The ^{1}H-NMR spectrum of *N*-ethyl-7-nitro-2,1,3-benzoxadiazol-4-amine was also obtained at 330 K using AV-300 NMR. The peak obtained for H_A and H_D protons of NBD-Ethylamine is shown in Figure 3.6.

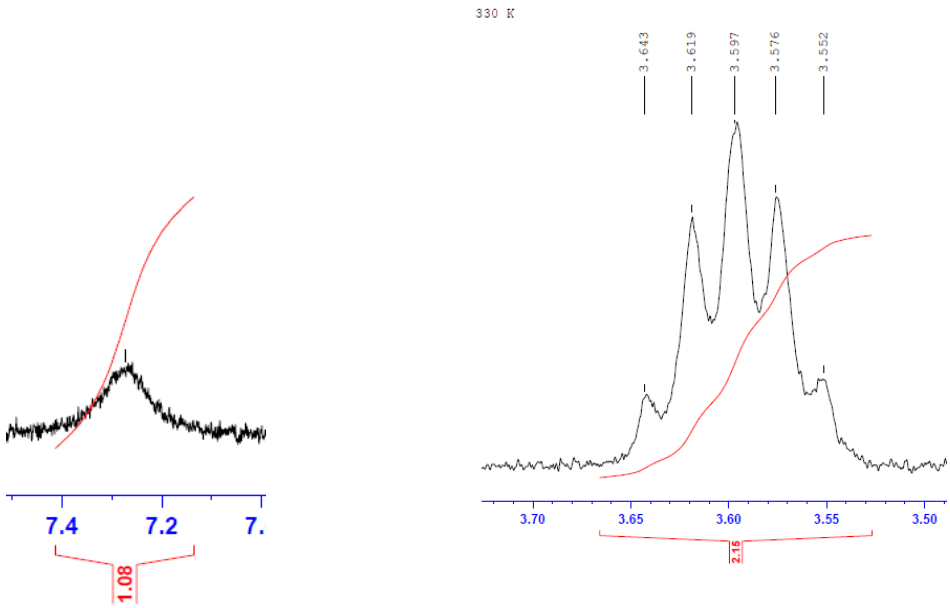

(a) (b)

Figure 3.6. Peaks observed for (a) H_D (amine proton, see Figure 3.4) and (b) H_A of NBD-ethylamine at 330 K using AV-300 NMR.

As shown in Figure 3.6, the splitting pattern for proton H_A at 3.59 ppm at 330 K now resembles a pentet. The appearance of a pentet can be attributed to similar ^3J coupling between H_A and H_C, and H_C and H_D.

***N*-Ethyl-*N*-methyl-7-nitro-2,1,3-benzoxadiazol-4-amine (NBD-Ethylmethylamine, $R_1 = CH_3$, $R_2 = C_2H_5$)**: 4-Chloro-7-nitrobenzofurazan (0.415 g, 2 mmol) in 5 mL of THF and 0.8 mL of 97% *N*-ethylmethylamine gave a bright orange powder (0.270 g, 55% yield). The melting point was determined to be 172-173° C (literature 172-174°C).[67] ^{1}H NMR ($CDCl_3$, AV-500): δ 8.43 (d, J = 9 Hz, 1H, proton H_F), 7.26 (s, 1H), 6.10 (d, J = 9 Hz, 1H, proton H_E), 4.11(s, 2H), 3.49 (broad s, 3H), 1.40 (t, J = 7 Hz, 3H). ESI-MS [$C_9H_{10}N_4O_3Na^+$] 245.10. There were no spectral data available in the literature for NBD-ethylmethylamine.

3.3 Zeolite Sample Preparation

As mentioned before, NaY was commercially available and used as received. The alkali metal cation exchanged zeolites LiY, KY, RbY, CsY were already prepared and ready to use.[66] A typical degree of cation exchange in Y zeolites is 49% for LiY, 85% for KY, 73% for RbY and 62% for CsY.[66]

3.3.1 Incorporation of the organic chromophores in zeolites

Incorporation of the organic chromophore in zeolites was carried out as described below

Day 1: The zeolites were accurately weighed in a crucible and heated in an oven to 450° C for at least 24 hours to remove water. There are 8 supercages per unit framework of Y zeolites and the main target was to incorporate the compounds into 1.5 x 10^{-4} mol of zeolite supercages. The molar masses of the hydrated alkali metal cation zeolites calculated using the formula below are provided in Table 3.1.[66]

Zeolite Y: M_{56} $(AlO_2)_{56}$ $(SiO_2)_{136}$ *253 H_2O

Table 3.1. Typical unit cell molar mass of alkali-metal cation faujasites and mass required for 1.5 x 10^{-4} mole of zeolite supercages within the zeolite framework.

Zeolite	MW/mol unit cell	Mass (mg)
LiY	16421.44	313
NaY	17320.80	330
KY	18222.34	347
RbY	20819.06	397
CsY	23475.14	447

Day 2: Following the removal of water molecules from zeolites, the zeolites were then placed in a clean, oven-dried centrifuge tubes containing an oven-dried stir bar. After approximately 30 seconds of cooling at room temperature, 20 mL of Chromasolv® HPLC dichloromethane was added to the centrifuge tube. The centrifuge tubes were then sealed with septa to avoid contamination, especially absorption of water from the air, during stirring.

The next step was to inject a measured volume of a stock solution of the chromophore (in dichloromethane or acetonitrile) to meet the intended loading level <S>. The concentration of the stock solution prepared usually ranged from 0.01 to 0.05 M.

The formulae used to determine loading level are provided in Equations 3.2 and 3.3.

$$< S > = \frac{\text{n compound}}{\text{n cavity}} \qquad (3.2)$$

$$n\ cavity = \frac{mass\ of\ zeolite}{MW\ per\ unit\ cell} X\ 8 \qquad (3.3)$$

In the equation 3.2, <S> represents the intended loading level, *n compound* represents the number of moles of the compounds to be incorporated and *n cavity* represents the number of moles of zeolite cavities. For example, assume a stock solution of 0.01 M of a certain compound is prepared with an intention of incorporating the compound in 0.330 g NaY at a loading level <S> = 1/20 or 0.05 molecule/supercage.

Using Equation 3.3:

$$ncavity = \frac{0.300\ g\ NaY}{17320.8\ (\frac{g}{mol\ unit\ cell})} X\ \frac{8\ supercages}{mol\ unit\ cell} = 1.52X10^{-4}\ mol\ supercages$$

Using Equation 3.2:

$$< S > = \frac{n\ compound}{1.52X10^{-4}\ mol\ supercages}$$

$$0.05\frac{molecule}{supercage} = \frac{n\ compound}{1.52X10^{-4} mol\ supercage}$$

$$n\ compound = (0.05 * 1.52X10^{-4} mol)$$

$$Volume\ Required = \frac{7.62X10^{-6}\ mol}{0.01\ (\frac{mol}{L})} = 762\ \mu L$$

Once the appropriate amount of volume of compound was injected, the zeolite slurry was stirred for 4 hours at room temperature. The tube was then centrifuged and the supernatant liquid

was quickly decanted to a clean Erlenmeyer flask. The septum was removed prior to decanting but quickly replaced after the addition of fresh 20 mL of dichloromethane. The zeolite samples were further stirred for 20 more minutes in order to remove any material remaining on the surface of the zeolites. After 20 minutes the tube was centrifuged and the second supernatant was combined with the first supernatant to give a 40 mL volume that was later analyzed to determine the actual loading level. The zeolites were then dried in a desiccator under vacuum for 12 hours.

Day 3: The zeolite samples were now ready to be transferred into a 3 X 7 mm^2 laser cell. The desiccator along with all the other necessary apparatus were transferred to a glovebag filled with nitrogen in order to avoid any possible adsorption of water and moisture into the zeolite framework. The zeolites were transferred to the laser cell and then connected to a vacuum line, and the zeolites were further dried under reduced pressure (1 - 2 mTorr) for 12-16 hours.

3.3.1.1 Determination of the Actual Loading Level

Some compounds undergo 100% incorporation within the zeolite framework, but for compounds that are not fully incorporated within the zeolite framework, the actual loading level has to be determined. The method used to determine the actual loading level has been described in a stepwise process:

1. The first step in determining the actual loading level of the compound was to prepare an absorbance vs concentration calibration curve of the compound in dichloromethane. The calibration curve provides an equation for the line of best fit using the Beer-Lambert equation, $A= \varepsilon l c$, where $l = 1$ cm, ε is the extinction coefficient at the wavelength used, and c is the molar concentration.

2. The next step was to record the UV-vis spectrum of the 40 mL of the decanted supernatant that was collected after the two zeolite washes.
3. From this UV-Vis spectrum and the appropriate calibration curve, the concentration of the compound in the supernatant can be calculated. This can be converted into number of moles, which corresponds to the moles of compound that did NOT get incorporated into the zeolites, or the "mol out".
4. Once “mol out” was calculated, the actual moles of the compound can be calculated using equation 3.4, where "mol in" is the number of moles of compound originally placed in to the centrifuge tube.

$$Actual\ mol\ in = mol\ in - molout \tag{3.4}$$

5. Actual loading level was then calculated using Equation 3.5.

$$Actual\ Loading\ Level = \frac{Actual\ mol\ in}{mol\ supercages} \tag{3.5}$$

3.4 Laser Experiments

The single-photon excitation fluorescence (SPEF) and two-photon excitation fluorescence (TPEF) spectra for solution and for zeolites were obtained using the set-up described in the schematic provided in Figure 3.7.

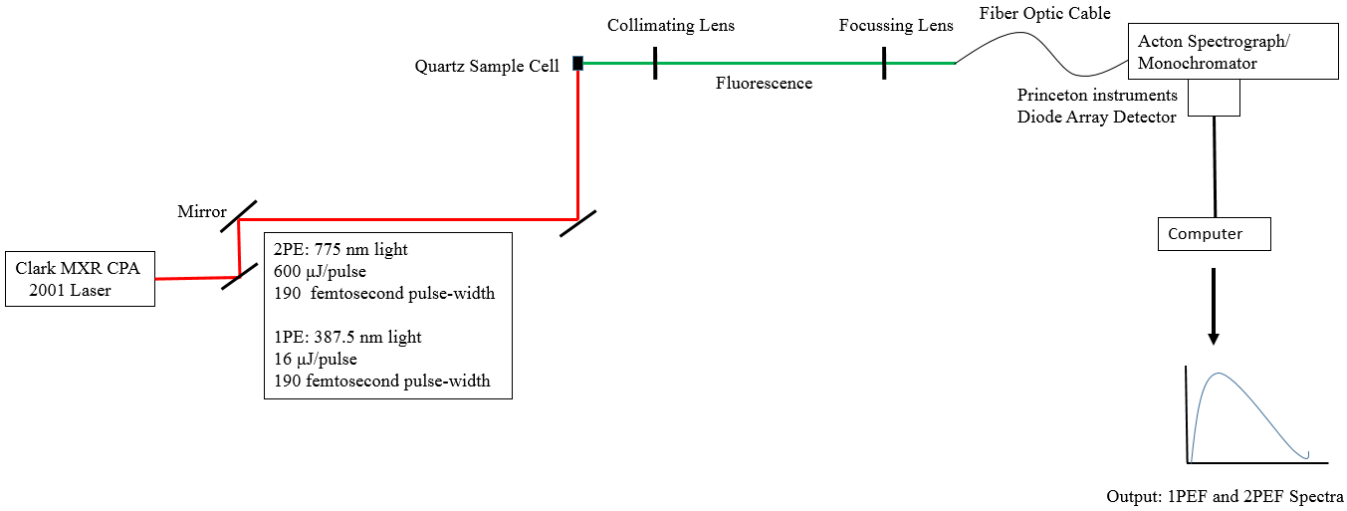

Figure 3.7. Schematic diagram of one- and two-photon induced fluorescence set-up.

The excitation source was a Clark-MXR laser which can be set to emit either 387.5 nm light for single-photon excitation (SPE) or 775 nm light for two-photon excitation (TPE). The pulse-width for both SPE and TPE was 190 femtoseconds and the intensity of the pulse used for SPE was approximately 16 μJ/ pulse and 600 μJ/pulse for TPE. Actual laser power were measured with a Power Max meter. Solution samples were placed in a 1 cm quartz fluorescence cuvette, the concentrations of the chromophore used to obtain SPEF spectra ranged from 10^{-6} M to 10^{-4} M, whereas the concentration in the range from 10^{-4} to 10^{-3} was used to obtain TPEF spectra. The zeolites samples were placed in 3 X 7 mm^2 quartz cells.

Fluorescence is emitted when a sample containing organic chromophore in either the cuvette or a laser cell is placed in a laser beam path. The fluorescence emitted by the sample is collected by the collimating lens and focussed on to the fiber optic cable through the focussing lens. The fiber optic cable directs the fluorescence towards the monochromator, where the fluorescence gets separated into a frequency spectrum. The frequency-separated fluorescence is then directed

towards the diode array detector where the fluorescence intensity is recorded as a function of wavelength. The fluorescence spectrum is transferred to an Apple PowerMac computer for processing. The experimental data can be processed in a programme called Labview, and the data can be transferred to either Kaleidagraph or Microsoft Excel for further processing.

Four readings were recorded for the zeolites samples that were sealed into the laser cell, two readings per each side of the laser cell. During the experiments, the sample cell was moved and/or shaken between each recordings to make sure that a fresh region of the zeolite surface was accessible for each recording. An average value from the four readings for both SPEF and TPEF was used to analyse the results also taking any anomalous results into consideration.

3.4.1 Analysis of the Results from Laser Experiments

Using the fluorescence intensity from SPEF and TPEF spectra obtained from solution and the zeolite samples, the following ratios were determined.

$$\text{Ratio}_{\text{solution}} = \frac{\text{Fl}_{\text{2PE solution}}}{\text{Fl}_{\text{1PE Solution}}} \qquad \text{Ratio}_{\text{zeolite}} = \frac{Fl_{\text{2PEzeolites}}}{Fl_{\text{1PE zeolites}}} \tag{3.6}$$

The same singlet excited state is formed with single-photon and two-photon excitation. As a result, any differences in the absolute efficiency of single-photon excitation (SPE) caused by differences in excited state lifetimes in solution and in zeolites will also be reflected in the absolute efficiency of two-photon excitation (TPE). In order to determine the effect of the zeolite environment on the two-photon excitation (TPE) efficiency within the zeolite framework a ratio of ratios can be thus obtained, using Equation 3.7.

$$\text{Ratio of Ratios} = \frac{\text{Ratio zeolite}}{\text{Ratio solution}} = \text{Effect of zeolite on TPEF} \qquad (3.7)$$

If the value obtained through Equation 3.7 is greater than 1, this implies that there is a two-photon excitation efficiency enhancement within the zeolite framework for the incorporated organic chromophores. If the value obtained is approximately equal to 1, the zeolite framework has no effect on the two-photon excitation efficiency of the incorporated organic chromophore. Finally, if the value is smaller than 1, this implies that the two-photon excitation efficiency of the organic chromophore is reduced within the zeolite framework.

3.5. Determination of the Two-Photon Absorption (TPA) cross-section (σ) and the Quantum Yield (ф) of the NBD- chromophores.

The structures of four TPA reference compounds fluorescein, rhodamine B, perylene and coumarin 153 used in the determination of the TPA cross section (σ) are shown in Figure 3.8.

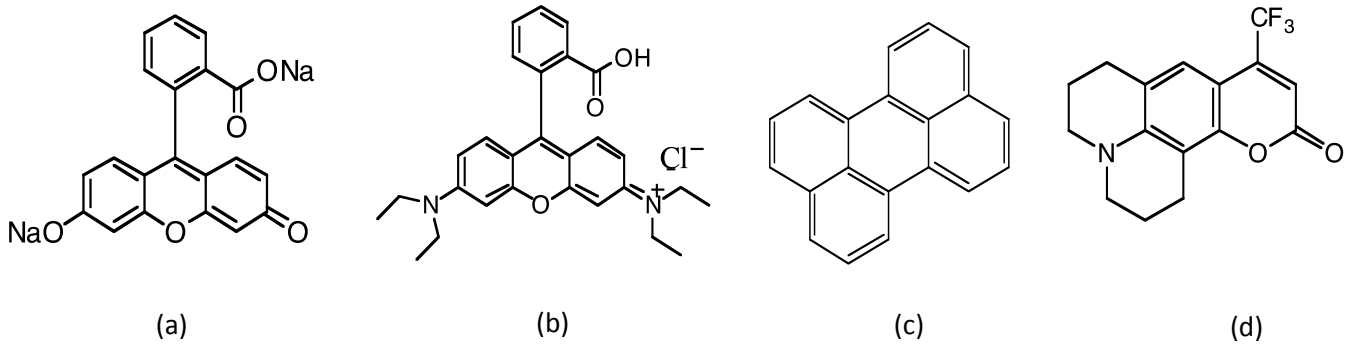

Figure 3.8. Chemical structures of the four standard dyes: (a) fluorescein, (b) rhodamine b, (c) perylene, (d) coumarin 153.

The TPEF spectra of the four standard dyes at various different concentrations were obtained. The TPEF intensities of the standards were then used to plot a calibration plot of

fluorescence intensity vs concentration, and the slope was obtained. The slope for each standard dye was used to extrapolate the TPEF intensities to a concentration of 0.006 M. A second calibration plot of TPEF intensities vs cross section (σ) was obtained using the extrapolated TPEF intensities for the respective compounds at 0.006 M. The TPEF spectra of 0.006 M NBD-chromophores were obtained and the intensities of the spectra and the second calibration plot was used to determine the initial TPA cross section (σ)

The TPA cross section (σ) values have to be corrected for quantum yield (ϕ), which was determined by using Equation 3.8.[74]

$$\phi_F(X) = \left(\frac{A_s}{A_x}\right)\left(\frac{F_x}{F_s}\right)\left(\frac{n_x}{n_s}\right)^2 \phi_F(s) \qquad (3.8)$$

In Equation 3.8, ϕ_F is the fluorescence quantum yield, A is the absorbance at the excitation wavelength, F is the area under the emission curve and n refers to the refractive index. Subscripts s and x refers to the standard and unknown, respectively.[74]

In terms of selection of the standard, it is useful to select a standard that exhibits similar absorption and emission properties as the compound of interest. Fluorescein was the chosen standard as it demonstrated similar absorption properties as the NBD- chromophores. The quantum yield of fluorescein is 0.93.[75] The same excitation wavelength has to be used when obtaining the emission spectra of the standard and the unknown. The excitation wavelength was the λ_{max} of absorbance for the respective NBD-chromophores. The ideal absorbance for fluorescence is between 0.04 and 0.05. When the absorbance is below 0.04, impurities may influence the result whereas, when the absorbance is above 0.05, the emission intensity can no longer be assumed to be proportional to analyte. Finally, the experimental setup for both standard and the unknown

compound has to be similar when determining both the quantum yield (ϕ) and the TPA cross section (σ).

Chapter 4: Results and Discussion

4.1 Synthetic Pathway Followed by the Reaction Precursor.

Six benzoxadiazole derivatives were examined for the study of two-photon excitation fluorescence (TPEF) efficiency enhancement within the zeolite framework. The mechanism for the reaction is summarised in Scheme 4.1.

Scheme 4-1.

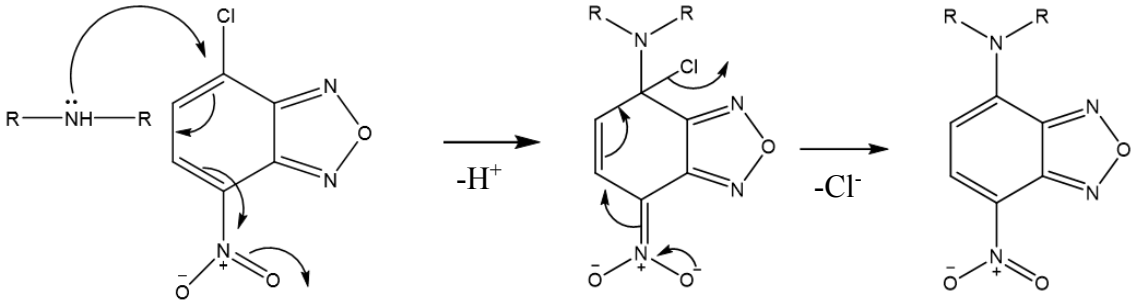

Meisenheimer Complex

The Cl in NBD-Cl is a good leaving group and is located at the 4-position or the para position relative to the nitro group, a strong electron-withdrawing substituent. This provides a highly favourable environment for a nucleophilic addition-elimination reaction, which allows a good nucleophile such as amine to attack the halogen-containing aromatic carbon, resulting in the formation of a zwitterionic Meisenheimer complex and loss of aromaticity. The loss of chloride restores the aromaticity and results in the formation of the final product.[67]

4.2 Single-Photon and Two-Photon Properties of 7-Nitro-2,1,3-benzoxadiazol-4-amine (NBD-NH_2)

Ultraviolet-visible (UV-vis) and fluorescence spectra of NBD-NH_2 were obtained in solvents with different polarity, Figure 4.1. Absorption maxima, fluorescence maxima and extinction coefficients are summarized in Table 4.1.

Table 4.1. Summary of some optical properties of NBD-NH_2 in various solvents.

Solvent	Polarity (Dielectric Constant)[76]	λ_{max} absorbance (nm)	λ_{max} fluorescence (nm)	Molar extinction coefficient (ε) (L $mol^{-1}cm^{-1}$)
Dichloromethane	8.93	442	517	994
Acetonitrile	37.5	447	523	1055
Methanol	32.7	455	528	1108
Ethanol	24.5	455	535	1039
50% Methanol 50% H_2O	---	460	540	1182
H_2O	80.1	465	548	1275

From the data summarized in Table 4.1, it is evident that the chromophores are sensitive to solvent polarity as, generally speaking, the λ_{max} for both absorbance and fluorescence undergoes a red-shift (i.e., moves to higher wavelength) with increasing solvent polarity. The red-shift, also known as the bathochromic shift, is observed because of a greater stabilization of the excited state relative to the ground state in more polar solvents that results in a greater charge redistribution (ICT) between the donor and the acceptor substituents upon excitation.[17] It is worth noting that a larger red-shift in λ_{max} for absorbance and emission is observed in methanol and ethanol in comparison to the more polar acetonitrile. The observations can be related to an article by Wang *et al.* which proposes that a relatively large red-shift in methanol and ethanol can be attributed to

a hydrogen bonding interaction between the OH- group of the solvent and the chromophore.[17] The molar extinction co-efficient (ε) for NBD-NH_2, which measures the ability of the compound to undergo single-photon absorption, is also shown to increase with increasing solvent polarity.

An increase in ICT between donor and acceptor substituents can also influence the two-photon excitation (TPE) properties of organic chromophores, which was discussed at a greater length in Chapter 1.[2,4,24,25] As a result, the next step was to investigate whether the two-photon excitation (TPE) efficiency of NBD-NH_2 is enhanced in strongly polar solvents compared to weakly polar solvents. Laser induced single-photon excitation fluorescence (SPEF) and two-photon excitation fluorescence (TPEF) spectra were obtained using a femtosecond pulsed laser for various different concentrations of NBD-NH_2 in the same solvents listed in Table 4.1. Typical SPEF and TPEF spectra obtained for NBD-NH_2 are shown in Figure 4.2. The rest of the spectra are provided in the appendix. The SPEF and TPEF intensities of NBD-NH_2 vary from one solvent to another, with the highest SPEF and TPEF intensities being observed in dichloromethane, the least polar of the solvents used and the lowest intensities are observed in water, the most polar solvent. An article in 2015 by Joo *et al.* provides a rationale for why lower emission intensities might be observed in polar aqueous environment.[28] According to their suggestion, a hydrogen bonding interaction between water and the nitrogen of the amine exists that can suppress and restrict the charge transfer between the donor and the acceptor substitutents, Scheme 4.2.

Scheme 4-2

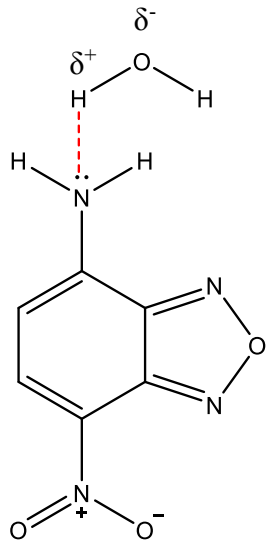

In dipolar compounds such as NBD- chromophores, reduction or suppression of charge redistribution can lead to a reduction in the transition dipole moment, which then results in poor emission properties of the organic chromophore.[28] In addition, hydrogen bonding between the chromophore and the water molecules also offers a major non-radiative deactivation pathway.[28] As a result, dipolar compounds with Donor-π-Acceptor interactions, show good emission properties in organic solvents but not in an aqueous environment which is evident in Figure 4.2.[28] Amongst the solvents used, dichloromethane is the solvent that is least capable of interacting with the nitrogen of the amine through hydrogen bonding interactions, thus allowing NBD-NH_2 to possess superior emission properties, which perhaps results from enhanced charge redistribution between donor and acceptor species.

Although Joo *et al.* did not mention hydrogen bonding interactions involving other solvents such as methanol and ethanol, it is reasonable to conclude, particularly from the observations made

by Wang *et al*. that the lower SPEF and TPEF intensities observed in these solvents is also due to the hydrogen bonding effects.[17]

As shown in Figure 4.3 (blue circles), the fluorescence intensity for NBD-NH_2 in acetonitrile in the SPEF experiments initially increases with respect to increasing concentration at low concentrations, but at about 2 x 10^{-4} M the fluorescence intensity begins to level off and then eventually declines at even higher concentrations. In the fluorescence set-up used in this work, excited chromophores near the centre of the sample cuvette are the ones whose fluorescence is successfully emitted through a pin hole in the cuvette holder and directed towards the detector. If the excitation beam is significantly attenuated on the way to the centre of the cuvette, the detected fluorescence will decrease, since less chromophores near the centre of the sample cuvette will be excited. Thus, in the present work, the observed levelling off at concentrations above 1 x 10^{-4} M is likely due to the strongly absorbing NBD-NH_2 no longer allowing all of the excitation beam to reach the center of the cuvette. As a result, the observed fluorescence intensity at these higher concentrations is less than what the actual fluorescence would be in the absence of the attenuation effect. This trend is also evident in other solvents.

Since TPEF is much less efficient than SPEF, little TPEF was observed at concentrations of NBD-NH_2 below 1 x 10^{-4} M. Significant fluorescence was observed at higher concentrations, Figure 4.3 (red circles), with a linear increase in fluorescence intensity being observed with respect to increasing concentrations. Note that a levelling effect at these higher concentrations is not observed in the TPEF experiments, since NBD-NH_2 does not efficiently absorb the 775 nm excitation beam, which is always able to reach the centre of the cuvette largely unattenuated.

As discussed in Chapter 3, one of the main goals of the work provided was to obtain a ratio of two photon to one photon (2P:1P) induced fluorescence intensity under the conditions of the

experiment, with the ratio in solution being used as a reference for determining if zeolites have an effect on two photon efficiency. The ratio of the slope of the TPEF data, and the slope of the linear region of the SPEF data can be used to determine this ratio. As shown in Figure 4.3, the slope of the data obtained using TPEF is 5.8 x 10^7 M^{-1}, while that for the linear portion of the SPEF is 1.8 x 10^9 M^{-1}. Dividing the slope for the TPEF by the slope for the SPEF, gives a ratio of 0.032. Thus, for a given concentration of NBD-NH_2, excitation with 775 nm light with an intensity of 22 μJ will lead to fluorescence emission that 0.032 times that for the emission obtained from the same compound at the same concentration using 387.5 nm light with an intensity of 620 μJ. A graph similar to acetonitrile was created for all the solvents and has been provided in the appendix, with the observed results summarised in Table 4.2.

Table 4.2. Summary of the ratio of the slope of TPEF:SPEF intensities for NBD-NH_2 in solvents of varying polarity. (Power of the laser recorded during the experiment included)

Solvent	Power of the laser for SPEF (μJ/pulse)	Power of the laser for TPEF (μJ/pulse)	Slope SPEF M^{-1}	Slope TPEF M^{-1}	Ratio 2P:1P
Dichloromethane	23	530	3.83 x 10^9	6.74 x 10^7	0.018
Acetonitrile	22	620	1.84 x 10^9	5.81 x 10^7	0.032
Methanol	20	540	1.23 x10^9	1.55 x 10^7	0.013
Ethanol	23	631	1.38 x 10^9	1.64 x10^7	0.012
50% H_2O 50% Methanol	21	600	2.98 x 10^8	4.92 x 10^6	0.016
H_2O	20	641	8.07 x 10^7	2.33 x 10^6	0.030

Unlike the earlier observation that NBD-NH_2 exhibits different SPEF and TPEF intensities in solvents with different polarity, the ratio of two photon: one photon induced fluorescence (2P:1P) obtained for NBD-NH_2 in all the solvents are about the same, ranging from 0.012 to 0.032. The similar ratios obtained in all solvents suggest that the factors that influence the SPEF

properties in solution also directly influence the TPEF properties. Most importantly, the similar ratios indicate that there is no direct evidence suggesting a two-photon excitation fluorescence (TPEF) efficiency enhancement in more polar solvents. Instead, both the SPEF and TPEF intensities are much lower in polar solvents compared to the less polar solvents.

4.2.1 Single-Photon and Two-Photon Properties of 7-Nitro-2,1,3-benzoxadiazol-4-amine (NBD-NH_2) in Y zeolites

Diffuse reflectance and fluorescence spectra of NBD-NH_2 incorporated in various different alkali cation exchanged zeolites, at an experimental loading level of, <S> =1/50, are provided in Figure 4.4 and the results have been summarised in Table 4.3.

Table 4.3. Summary of single-photon optical properties of NBD-NH_2 in alkali cation exchanged Y zeolites.

Zeolites	λ_{max} Reflectance (nm)	λ_{max} Fluorescence (nm)
LiY	464	514
NaY	465	521
KY	467	529
RbY	470	531
CsY	474	546

In Chapter 2, it was discussed that the order of polarity in alkali cation exchanged zeolites is LiY> NaY> KY> RbY> CsY, with the polarity within the zeolite decreasing as the size of the cation increases. The results shown in Figure 4.4 and summarised in Table 4.3 show that the λ_{max} for the reflectance and fluorescence for NBD-NH_2 in alkali metal cation exchanged zeolite is red-shifted as the size of the cation increases. The red-shifting of the λ_{max} implies that the ICT between

donor and acceptor substituent of NBD-NH_2 in Y zeolite increases as the size of the cation increases, which is opposite to what is expected based on polarity, and indicates that some parameter other than polarity is influencing the photophysics of this system.

NBD-NH_2 was incorporated in NaY at various different loading levels, and the SPEF and TPEF spectra were obtained using a femtosecond laser as the excitation source. Typical SPEF and TPEF spectra of NBD-NH_2 in NaY are provided in Figure 4.5, and the rest have been included in the appendix. It was highlighted in Chapter 2 that, when a compound is dissolved in a solvent, a homogenous mixture is formed where the fluid solutions allow reacting molecules to experience an average microenvironment by the virtue of a fast relaxation time. In contrast, the incorporated compounds within the zeolite framework are more likely to experience a heterogeneous environment because the molecules within the zeolite cavities are likely to be distributed on a random basis. As a result, the method used to determine the ratio of 2P:1P in solution (Table 4.2) may not be suitable for NaY or any other zeolites.[63] While one method to determine the ratio of two photon: one photon (2P:1P) in NaY would be to just divide the TPEF intensities by the SPEF intensities using Equation 3.6, an alternate and more efficient method would to be to generate a plot of *TPEF intensity vs SPEF intensity* using the respective intensities of SPEF and TPEF spectra of NBD-NH_2 in NaY at various different loading level <S>, Figure 4.6. The slope of the plot 0.036, is effectively the 2P:1P ratio in NaY, averaged over all loading levels <S>. A detailed table summarising the SPEF and TPEF intensities and the ratios obtained has been provided in the appendix.

The ratio of 2P:1P in solution and in NaY can be used to determine the ratio of ratios using Equation 3.7, which would help determine if there is any two-photon excitation fluorescence (TPEF) enhancement caused by increased efficiency of two-photon absorption for NBD-NH_2 in

NaY. A calculation has been provided below, using an average value of 0.020 for the 2P:1P ratio determined in the various solvents listed in Table 4.2.

Average 2P:1P ratio in solution = 0.020

Average 2P:1P ratio in NaY = 0.036

$$Ratio\ of\ Ratios = \frac{Ratio\ Zeolites}{Ratio\ Solution} = \frac{0.036}{0.020} = 1.75\ \approx 2$$

The ratio of ratios obtained from the calculation above is about 2, suggesting that there is only a small two-photon excitation fluorescence (TPEF) efficiency enhancement for NBD-NH_2 in NaY relative to solution. It is worth nothing that the ratio of 0.036 obtained in NaY for NBD-NH_2 is similar to the ratio obtained for NBD-NH_2 in acetonitrile and water (Table 4.2).

A possible two-photon excitation fluorescence (TPEF) efficiency enhancement was also explored amongst the rest of the alkali metal cation exchanged zeolites. SPEF and TPEF spectra for NBD-NH_2 in LiY, KY, RbY and CsY have been provided in Figure 4.8. The summary of results has been provided in Table 4.4.

Table 4.4. Summary of SPEF and TPEF properties of NBD-NH_2 incorporated in alkali earth metal cation exchanged zeolites at an experimental loading level of <S> = 1/20.

Zeolites	**Experimental Loading Level <S>**	**Actual Loading Level <S>**	**SPEF 16 µJ/pulse**	**TPEF 600 µJ/pulse**	**2P:1P**	**Enhancement Factor**
LiY	1/40	1/240	5.27×10^5	1.77×10^4	0.034	2
KY	1/40	1/44	2.86×10^5	1.51×10^4	0.053	2
RbY	1/40	1/52	1.97×10^5	1.29×10^4	0.066	3
CsY	1/40	1/94	2.36×10^5	1.53×10^4	0.065	3

The ratio of ratios obtained for the alkali cation exchanged zeolite (LiY, KY, RbY, CsY) are similar to the ratio obtained for NaY, which suggests a small TPEF enhancement. A slightly larger enhancement is observed for RbY and CsY.

Overall, it can be concluded that there is only a small two-photon excitation fluorescence (TPEF) efficiency enhancement for NBD-NH_2 in zeolites compared to in solution, and that the zeolites provide only a small increase in two-photon absorption efficiency for this chromophore.

4.3 Single-Photon and Two-Photon Properties of N,N-Dimethyl-7-nitro-2,1,3-benzoxadiazol-4-amine (NBD-DMA)

NBD-DMA consists of *N,N*-dimethyl substituted amine as the donor substituent. UV-vis and fluorescence spectra of NBD-DMA were obtained in solvents with different polarity shown in Figure 4.9. The information obtained from the UV-vis and fluorescence spectra is summarised in Table 4.5.

Table 4.5. Summary of one-photon optical properties of NBD-DMA in solvents with different polarity.

Solvent	λ_{max} absorbance (nm)	λ_{max} fluorescence (nm)	Molar extinction coefficient (ε) $LMol^{-1}cm^{-1}$
Dichloromethane	473	526	12100
Acetonitrile	478	530	13400
Methanol	477	533	13900
Ethanol	475	536	13700
50% Methanol 50% H_2O	494	550	16400
H_2O	497	555	19400

The presence of the two methyl substituents on the amine results in a red-shift of the λ_{max} for both absorbance and fluorescence of NBD-DMA compared to NBD-NH_2 (Table 4.1). For example, the λ_{max} for absorbance and fluorescence of NBD-DMA in acetonitrile occurs at 478 nm and 530 nm, respectively, which are red-shifted by 31 nm and 7 nm, respectively, compared to NBD-NH_2 in acetonitrile. A red-shift in the π to π^* transition of the chromophore is usually attributed to an increase in charge redistribution between the donor and acceptor species within the molecule upon excitation, which suggests that the donating ability of the amine of NBD-chromophore strengthens upon introduction of of *N,N*-methyl substituents to the amine.[17,28,29] The observation is consistent with the discussion in Chapter 1 and literature where it was suggested that the donating ability of the amine increases as it becomes more substituted.[17,28,29]

An increase in molar extinction coefficient (ε) is also observed for NBD-DMA compared to NBD-NH_2. NBD-DMA follows similar trends as NBD-NH_2, where the λ_{max} for absorbance and fluorescence is red-shifted with increasing polarity.

SPEF and TPEF spectra of NBD-DMA in solvents with different polarity were obtained to examine the effect of polarity on the emission properties of NBD-DMA. Typical SPEF and TPEF spectra are shown in Figure 4.10. Using the similar approach as for NBD-NH_2 in Table 4.2, a ratio of the slope of TPEF data and linear region the SPEF data was determined, Figure 4.11. The results obtained are summarised in Table 4.6.

Table 4.6. Summary of the ratio of the slope of TPEF:SPEF intensities for NBD-DMA in solvents with different polarity. (Power of the laser recorded during the experiment included)

Solvent	Power of the laser for SPEF (μJ/pulse)	Power of the laser for TPEF (μJ/pulse)	SPEF Slope	TPEF Slope	Average of 2P:1P
Dichloromethane	16	520	8.91×10^7	1.66×10^6	0.019
Acetonitrile	18	510	4.82×10^7	1.10×10^6	0.023
Methanol	22.1	636	6.66×10^7	1.45×10^6	0.022
Ethanol	23.5	580	8.54×10^7	1.75×10^6	0.021
50% H_2O 50% MeOH	17	580	3.19×10^7	1.75×10^6	0.055
100% Water	16.5	551	3.11×10^7	8.57×10^5	0.028
				Average	**0.028 (+/-) 0.007**

When comparing the SPEF and TPEF spectra of NBD-DMA in Figure 4.10 with NBD-NH_2 in Figure 4.2, the SPEF and TPEF intensities for NBD-DMA are more than 10 fold lower than NBD-NH_2. The poor emission properties of NBD-chromophore consisting of *N,N*-dialkylated amine can be related to allylic 1,3-strain which was discussed in Chapter 1, and which results in the formation of twisted intramolecular charge transfer (TICT) excited states that compete with the fluorescence generation by non-radiative decay of the excited state.[28,29] Overall, the optical properties of the two NBD-analogues are consistent with the optical properties of acedan and rhodol that were discussed in Chapter 1.

Despite being less fluorescent compared to NBD-NH_2, emission intensities of NBD-DMA in different solvents follow a similar trend as NBD-NH_2 in solution. The highest SPEF and TPEF

intensities for NBD-DMA were once again observed in dichloromethane, the solvent of lowest polarity and the lowest SPEF and TPEF intensities were observed in water, the most polar solvent, which can once again be related to Scheme 4.2, where a hydrogen bonding interaction between the solvent and the nitrogen amine restricts the ICT between the donor and the acceptor substituents.

Finally, the 2P:1P ratios determined for NBD-DMA in solvents with different polarity are in the range of 0.02- 0.03, Table 4.6, with the 2P:1P ratio of 0.055 in 50% MeOH and 50% H_2O considered to be an outlier. The ratio of 2P:1P obtained in solution for NBD-DMA provides further evidence that the factors that influence the TPE properties directly influence the SPE properties in solution.

4.3.1 Single-Photon and Two-Photon Properties of N,N-Dimethyl-7-nitro-2,1,3-benzoxadiazol-4-amine (NBD-DMA) in Y zeolites.

Diffuse reflectance and fluorescence spectra were obtained for NBD-DMA incorporated in various different alkali metal cation exchanged zeolites at a loading level of <S> = 1/20, in Figure 4.12. The information is summarised in Table 4.7.

Table 4.7. Summary of single-photon optical properties of NBD-DMA in alkali earth metal cation exchanged Y zeolites.

Zeolites	λ_{max} Reflectance (nm)	λ_{max} Fluorescence (nm)
LiY	497	531
NaY	497	542
KY	499	542
RbY	500	545
CsY	502	543

As was the case in solution, the λ_{max} for the diffuse reflectance and fluorescence spectra of NBD-DMA in zeolites is red-shifted compared to NBD-NH_2 shown earlier (Figure 4.17 and Table 4.3). For example, the λ_{max} for the diffuse reflectance for NBD-DMA in NaY occurs at 497 nm in comparison to NBD-NH_2 in NaY, which occurs at 465 nm. Similarly, the λ_{max} for the diffuse reflectance of NBD-DMA in alkali metal cation exchanged zeolite is red-shifted with the increasing size of the metal cations.

Typical SPEF and TPEF spectra of NBD-DMA are shown in Figure 4.13 and appendix. Plots of SPEF and TPEF intensity vs loading level are given in Fig 4.14. As was the case with NBD-NH_2, no obvious trend is observed. A plot of TPEF intensity vs SPEF intensity at different loading levels <S> of NBD-DMA is shown in Figure 4.15. The data in the plot are scattered but the slope, 0.17 ± 0.01, can still be used to determine the average 2P:1P in NaY at all loading levels. A summary of SPEF and TPEF intensities are provided in the appendix.

The calculation for the determination of the ratio of ratios for NBD-DMA has been provided below,

Average 2P:1P NBD-DMA in solution= 0.028

Average 2P:1P for NBD-DMA in NaY= 0.17 (+/-) 0.01

Using Equation 3.7,

$$Ratio\ of\ Ratios = \frac{(Ratio\ zeolites)}{(Ratio\ solution)} = \frac{0.17}{0.028} = 6.0$$

This result suggests that there is a two-photon excitation fluorescence (TPEF) efficiency enhancement by factor of 6 for NBD-DMA within the cavities of NaY compared to solution, which

means that the zeolite environment provides a significant six-fold increase in efficiency of two-photon absorption.

TPEF efficiency enhancement for NBD-DMA in the rest of alkali metal cation exchanged zeolites was also investigated. NBD-DMA was incorporated in LiY, KY, RbY and CsY. The SPEF and TPEF spectra for NBD-DMA in cation-exchanged zeolites have been provided in Figure 4.16 and appendix and the results obtained are summarized in Table 4.8.

Table 4.8. Summary of TPEF enhancement observed for NBD-DMA in various different alkali metal cation exchanged Y zeolites.

Zeolites	Average (2P:1P)	Enhancement Factor
LiY	0.19	7
NaY	0.17	6
KY	0.25	9
RbY	0.25	9
CsY	0.10	4

The ratio of ratios obtained for NBD-DMA in alkali metal cation exchanged zeolites summarised in Table 4.8 also show a TPEF enhancement in each of the five zeolites examined. The enhancement factor amongst the five exchange zeolites is about the same, although the ratio seems to increase slightly with the increasing size of the cations, which was also evident for NBD-NH_2 in Table 4.4. The enhancement factor is shown to be greatest in KY and RbY compared to the other zeolites. A small enhancement by a factor of 4 is however observed in CsY. Overall, the results summarised in Table 4.8 provide further evidence of increased two-photon absorption efficiency for NBD-DMA in Y zeolites.

In all of the experiments described so far, the zeolite samples were dehydrated (heated at 450^{o} C) prior to incorporation of the NBD-DMA. To examine the effect of water, experiments were carried out where NaY and the NBD-DMA were stirred without first drying the zeolite sample. SPEF and TPEF spectra for one of the loading levels have been provided in Figure 4.17, and the rest of the spectra have been provided in the appendix. 2P:1P ratios and zeolite enhancement values determined at several different loading levels are summarised in Table 4.9. Under these conditions, all of the zeolite enhancements values are close to one, indicating that hydrated NaY is much less effective than dry NaY in enhancing the two-photon absorbing abilities of the incorporated NBD-DMA samples. In order words, the presence of water within the zeolite cavities seem to inhibit the ability of the NaY environment to cause the two-photon absorbing enhancement observed within the dry zeolite samples.

Table 4.9. Summary of SPEF and TPEF intensities obtained from the respective spectra for NBD-DMA in non-dehydrated NaY.

Experimental Loading Level <S>	**Actual Loading Level <S>**	**SPEF 16 µJ/pulse**	**TPEF 620 µJ/pulse**	**2P:1P**	**Enhancement Factor**
1/15	1/36	5.03×10^{4}	1.41×10^{3}	0.028	1
1/20	1/34	6.96×10^{4}	2.20×10^{3}	0.032	1
1/30	1/63	4.44×10^{4}	1.03×10^{3}	0.023	1
1/40	1/100	3.89×10^{4}	1.14×10^{3}	0.029	1

4.4. Conclusion from the Initial Studies of 7-Nitro-2,1,3-benzoxadiazol-4-amine (NBD-NH_2) and N,N-Dimethyl-7-nitro-2,1,3-benzoxadiazol-4-amine (NBD-DMA)

It is evident from these studies that the photophysical properties of the dipolar NBD-chromophores in solution and in zeolites are influenced by factors such as polarity, hydrogen bonding and the *N*-substitution pattern of the amines. The emission properties of both NBD-NH_2 and NBD-DMA are significantly influenced by the *N*-substitution pattern of the amine, with superior SPEF and TPEF intensities emitted by the NBD-NH_2 chromophore with the unsubstituted amine. Likewise, superior fluorescence is emitted for both NBD-chromophores in the solvent that is least polar, as more polar solvents are likely to form hydrogen bonding interactions with the lone pair of the amine that inhibit fluorescence.[28] Regardless of the magnitude of intensities of SPEF and TPEF emitted by the two NBD-chromophores in solvents with varying polarity, similar 2P:1P ratios in the range of 0.01-0.03 are observed for both in solution.

A 2P:1P ratio of 0.035 is observed for NBD-NH_2 in NaY resulting in a small TPEF enhancement in NaY compared to solution. A similar trend is also observed for NBD-NH_2 in the rest of alkali metal cation exchanged zeolites. On the other hand, a ratio of 0.17 is observed for NBD-DMA in NaY, resulting in a significant TPEF enhancement by a factor of 6. Similar or higher enhancements have been observed for NBD-DMA in rest of the alkali metal cation exchanged zeolites.

A major difference between NBD-DMA and NBD-NH_2 in terms of structure is the nature of substitution of the donor amine. NBD-NH_2 consists of an unsubstituted amine as the donor group, whereas NBD-DMA consists of *N,N*-dimethyl substituted amine as the donor substitutent. Since the presence or absence of alkyl groups on the amine have a large effect, four more analogues of NBD-chromophores consisting of *N*-alkyl and *N,N*-dialkyl substituted amines were synthesized

in order to investigate the influence of *N*-substituents on the SPEF and TPEF properties of NBD-chromophores in solution and in zeolites.

4.5 Single-Photon and Two-Photon Optical Properties of the Analogues of NBD-chromophores consisting of N-alkyl and N,N-dialkylsubstituted amine in solution.

UV-vis and fluorescence spectra of different analogues of NBD-chromophores containing *N*-alkyl and *N,N*-dialkylsubstituted amine were obtained in acetonitrile, Figures 4.18-4.19. Relevant data from these spectra are summarised in Table 4.10.

Table 4.10. Summary of the single-photon optical properties of different NBD-chromophores with *N*-alkyl and *N,N*-dialkyl substituted amines.

Amine type	λ_{max} Absorbance (nm)	λ_{max} Fluorescence (nm)
H-N-H	447	523
H-N-CH_3	460	521
H-N-C_2H_5	461	521
CH_3-N-CH_3	478	530
CH_3-N-C_2H_5	480	534
C_2H_5-N-C_2H_5	484	536

Taking the results from Table 4.1, 4.5 and 4.10 into consideration, it can be concluded that the λ_{max} for both absorption and emission is red-shifted as the amine becomes more substituted. For example, NBD-methylamine has a λ_{max} for absorption at λ= 460 nm, which is red-shifted in comparison to NBD-NH_2 (447 nm) and blue-shifted (occur at a lower wavelength) in comparison to NBD-DMA (478 nm).

Elongation in the chain length seems to have a minimal impact as the λ_{max} for absorbance for NBD-ethylamine, λ_{max} = 461 nm, is red-shifted by only 1 nm compared to NBD-methylamine, λ_{max} = 460 nm, while the λ_{max} for fluorescence remains unchanged. Similar results are also observed for analogues of NBD-chromophores containing *N,N*-dialkylsubstituted amine.

SPEF and TPEF spectra of the NBD-analogues were obtained in solution, Figure 4.20. SPEF and TPEF from NBD-analogues consisting of *N*-alkyl substituted amine were relatively intense, and quite similar to SPEF and TPEF of NBD-NH_2, Figure 4.2. NBD-analogues with *N,N*-dialkylsubstituted showed SPEF and TPEF intensities similar to that from NBD-DMA in Figure 4.10. In addition, The SPEF and TPEF intensities of the NBD-analogues consisting of *N,N*-dialkylsubstituted amine were observed to get weaker with increasing chain length of the *N*-substituent. The observed emission properties could be because of the increase in allylic 1,3-strain with the increasing chain length of the *N*-substituents, thus resulting in an increase in the formation of the TICT excited states that compete with the fluorescence generation by the non-radiative decay of the excited state.[28,29]

The weak emission properties of NBD-analogues with the *N,N*-dialkyl substituted amine meant that it was only possible to obtain SPEF and TPEF spectra of these NBD-analogues in dichloromethane. The SPEF and TPEF spectra of NBD-methylamine was obtained in acetonitrile and the remaining three chromophores in dichloromethane. The ratio of the slope of intensities of TPEF and the slope of the linear region of the SPEF was determined as shown in Figure 4.21 and the results have been summarised in Table 4.11.

Table 4.11. Summary of the ratio of the slope of TPEF:SPEF intensities for analogues of NBD-chromophore consisting of *N*-alkyl and *N,N*-dialkyl substituted amines. (16 μJ/pulse for 387.5 nm and 600 μJ/pulse for 775 nm)

Compound	Slope SPEF (linear)	Slope TPEF	Ratio (2P:1P)
[1]NBD-NH_2	1.84×10^9	5.81×10^7	0.032
[1]NBD-Methylamine	1.18×10^9	3.96×10^7	0.033
[2]NBD-Ethylamine	1.34×10^9	2.58×10^7	0.019
[2]NBD-Ethylmethylamine	1.01×10^8	2.09×10^6	0.020
[2]NBD-Dimethylamine	8.91×10^7	1.66×10^6	0.019
[2]NBD-Diethylamine	1.81×10^7	8.10×10^5	0.045

1= spectra obtained in acetonitrile, 2 in dichloromethane

Once again, the ratio of the slope of 2P:1P in solution are relatively similar and in the range of 0.019 to 0.045. The 2P:1P ratio are slightly higher for NBD-NH_2, NBD-methylamine and NBD-diethylamine in comparison to the rest which suggests of a small enhancement for these three NBD-analogues. The enhancement is relatively small in comparison to what was observed for NBD-DMA in Y zeolites. Overall, the *N*-substitution pattern of the amines seems to equally influence the SPEF and TPEF properties of NBD-chromophores.

4.5.1 Single-Photon and Two-Photon Optical Properties of the Analogues of NBD-chromophores consisting of N-alkyl and N,N-dialkylsubstituted amine in Y zeolites.

The NBD-analogues were incorporated in NaY at various different loading levels <S> and the SPEF and TPEF spectra obtained. The spectra are provided in Figure 4.22 and in the appendix. Higher SPEF and TPEF intensities were also emitted in NaY by NBD-analogues consisting of *N*-alkyl substituted amines that were relatively similar to the fluorescence emitted by the parent NBD-NH_2 analogue.

Plots of intensities of TPEF vs SPEF at different loading levels are given in Figure 4.23. Reasonably good correlations are observed for NBD-MA, NBD-EA and NBD-EMA, but the correlation for data obtained with NMD-DEA was quite poor. The poor quality of the NBD-DEA data may be due to the poor intensity of its emission under both single and two photon excitation. Nonetheless, slopes for all four plots were calculated into order to obtain an average 2P:1P ratio for all loading levels used, and the values of these slopes are shown in Table 4.12.

Table 4.12. Summary of the ratio of TPEF:SPEF and ratio of ratios observed for different NBD-analogues of NBD-chromophore consisting of *N*-alkyl and *N,N*-dialkyl substituted amines. (16 μJ/pulse for 387.5 nm and 600 μJ/pulse for 775 nm)

Compound	λ_{max} (nm)	Ratio (2P:1P) Solution	Ratio (2P:1P) NaY	Ratio of Ratios (Enhancement Factor)
NBD-NH_2	447	0.020	0.036 ±0.003	2
NBD-Methylamine	460	0.033	0.12±0.01	3
NBD-Ethylamine	461	0.019	0.10±0.01	5
NBD-Dimethylamine	478	0.028	0.017 ±0.01	6
NBD-Ethylmethylamine	480	0.020	0.17±0.01	8
NBD-Diethylamine	484	0.045	0.22±0.03	5

In contrast to the 2P:1P ratios obtained in solution that vary only slightly as a function of the number of alkyl groups on the amine, the 2P:1P ratios in NaY are observed to vary more considerably with respect to the *N*-substitution pattern of amines. Initially, the ratio in NaY for NBD-NH_2 was determined to be 0.036 and upon introduction of one *N*-methyl group to the NBD-chromophore, the 2P:1P ratio increases almost four-fold to 0.12. Elongation of the chain length from *N*-methyl to *N*-ethyl results has little effect, but the 2P:1P ratio is further increased upon the

introduction of *N,N*-dialkyl substituted amines to the NBD-chromophore, as a 2P:1P ratio of 0.17 was observed for NBD-DMA. The largest ratio of 0.22 has been observed for NBD-DEA, the most substituted and more sterically hindered amine.

The data in Table 4.14 clearly show that the significant enhancement are observed for all of the NBD derivatives, and that the value of the enhancement is affected by the nature of the alkyl substitution. In particular, except for NBD-DEA, which may be an outlier due to weak emission, enhancement seems to increase as the number and size of alkyl groups on amine increases, starting from a low of 2 for NBD-NH_2 up to a high of 8 for NBD-EMA. This suggests that size plays a key role in determining whether or not the zeolite can have a positive influence on the ability of incorporated chromophores to undergo two-photon absorption.

It is worth noting from the data in Table 4.12 that the increase of 2P:1P and hence the two-photon enhancement factor for the NBD-chromophores with *N*-alkyl groups in NaY is consistent with the red-shifting of the λ_{max} of the absorbance of the NBD-chromophores shown in Table 4.10. The red-shift in λ_{max} of absorption can usually be attributed to enhanced charge redistribution between donor and acceptor substituents upon excitation.[17,18,29] Since two-photon absorption efficiencies also tend to increase with enhanced charge redistribution, the observation that the enhancement factors follow the same trend as the absorption maxima suggests that zeolites are enhancing two-photon absorption efficiency by increasing charge redistribution. The mechanism by which the zeolites effect this increased charge distribution cannot be determined by the results in the present work.[58,60,61]

The TPEF efficiency enhancement for three of the four NBD-analogues was also explored in the other alkali metal cation exchanged zeolites. The SPEF and TPEF spectra are provided in Figure 4.24 and in the appendix, with the results summarised in Table 4.13.

Table 4.13. Summary of the ratio of TPEF:SPEF observed for different analogues of NBD-chromophore consisting of *N*-alkyl and *N,N*-dialkylsubstituted amines incorporated in metal cation exchanged Y zeolites. Enhancement factor relative to solution provided in the bracket. (16 μJ/pulse for 387.5 nm and 600 μJ/pulse for 775 nm)

		2P:1P Ratio (enhancement factor)				
Compound	**2P:1P (solution)**	**LiY**	**NaY**	**KY**	**RbY**	**CsY**
NBD-Methylamine	0.033	0.077 (2)	0.12 (3)	0.19 (6)	0.20 (6)	0.19 (6)
NBD-Ethylamine	0.019	0.080 (4)	0.10 (5)	0.12 (6)	0.36 (19)	0.16 (8)
NBD-Ethylmethylamine	0.020	0.26 (13)	0.17 (8)	0.32 (16)	0.14 (7)	0.10 (5)

The data in the first two rows of Table 4.13 suggest a trend whereby the relative two-photon absorption efficiency of NMD-MA and NBD-EA increase as the cation size increases. Conversely, an opposite trend is observed for NBD-EMA, and for NBD-NH_2 and NBD-DMA, no distinct trends are observed. Thus, we can only conclude at this time that cations have no effect on the ability of the zeolite to influence the two-photon photochemistry of these chromophores.

4.6. Determination of the Two-Photon Absorption (TPA) cross-section (σ) of the analogues of NBD- chromophores.

The two techniques used to determine the TPA cross-section (σ) of TPA active chromophores were discussed in Chapter 1. The TPA cross-sections (σ) of the six NBD-chromophores used in this work were determined through two-photon excitation fluorescence (TPEF) method. The four standard compounds used for this experiment are rhodamine B, fluorescein, perylene and coumarin 153.

TPEF spectra of various different concentrations of perylene and coumarin 153 were obtained in dichloromethane, and rhodamine B and fluorescein were obtained in methanol. The spectra have been provided in Figure 4.25 and the appendix. The TPEF intensities were used to generate a calibration plot of TPEF intensitiy vs concentration and the slope was determined for each standard compound, Figure 4.26. The slope of the calibration curve allows extrapolation of TPEF intensity of the standard compounds to the concentrations at which the TPEF spectra of the six NBD-chromophores were obtained, which is at 0.006 M. The TPEF spectra of NBD-NH_2 and NBD-methylamine were obtained in acetonitrile and the rest in dichloromethane.

Once the TPEF intensity at 0.006 M for the four standard compounds was determined, a second calibration plot of fluorescence intensity (at 0.006 M) vs TPA cross-section was generated, Figure 4.27, and the slope was determined to be 1.3×10^5. The results obtained for the four reference compounds are summarised in Table 4.14.

Table 4.14. Summary of Quantum yield (ϕ), TPA cross-section (σ) and observed TPEF intensities of reference compounds. [20,28,75-78]

Reference Compound	Quantum Yield (ϕ)[74,75]	Literature TPA cross-section (GM)[20]	Power of the laser for TPEF (μJ/pulse)	TPEF slope	Predicted TPEF intensity at 0.006 M
Coumarin 153	0.54	33	620	4.04×10^8	2.40×10^6
Fluorescein	0.93	43	600	1.40×10^9	6.00×10^6
Perylene	0.91	1.6	615	2.19×10^7	1.20×10^5
Rhodamine B	0.71	89	623	1.83×10^9	1.20×10^7

Using similar experimental conditions as for the standard compounds, the TPEF spectra of 0.006 M NBD-chromophores were obtained (see appendix). The TPEF intensity of 0.006 M NBD-

chromophores and the slope of the second calibration plot in Figure 4.27 were then used to determine the TPA cross-section of the NBD-chromophores. Actual values for the two-photon cross-section (σ) require a correction for quantum yield (Φ), Equation 1.7.

The quantum yield (Φ) for the NBD-chromophores can be calculated using Equation 3.8. The standard used in the quantum yield determination is fluorescein as it exhibits similar optical properties in the UV-vis spectrum as the NBD-chromophores. The quantum yield of fluorescein is 0.93 (see Table 4.14). Absorption and fluorescence spectra for fluorescein and NBD compounds used to determine the quantum yield have been provided in Figures 4.28 and 4.29, and the results are summarised in Table 4.15

Table 4.15. Summary of experimental parameters used to determine the quantum yield of the NBD-chromophores.

Compound	**(A_s/ A_x)**	**F_x**	**F_s**	**F_x/ F_s**	**$(n_x/n_s)^2$**	**Quantum Yield (ϕ)**
NBD-Amine	0.91	7.15×10^6	1.17×10^6	0.61	1.00	0.53
NBD-Methylamine	1.04	7.99×10^6	1.31×10^6	0.64	1.00	0.59
NBD-Ethylamine	0.98	7.89×10^6	1.25×10^6	0.61	1.00	0.58
NBD-Dimethylamine	1.07	7.50×10^6	1.45×10^6	0.52	1.15	0.59
NBD-Ethylmethylamine	1.03	3.41×10^6	1.17×10^6	0.29	1.15	0.32
NBD-Diethylamine	1.31	2.26×10^6	1.22×10^6	0.18	1.15	0.22

Once the quantum yields of the NBD-chromophores were obtained, the corrected TPA cross-section (σ) was determined using Equation 1.7. The results have been summarised in Table 4.16. The power of the laser is included to show that similar experimental conditions were used to obtain the TPEF spectra of standard compounds and the NBD-chromophores. The entire

experiment was run over the course of two days. The error in the TPA cross-section for the standard compounds was +/- 15% and similar error percentage can be assumed for the NBD-chromophores.[20]

Table 4.16. Table summarising the parameters used to determine the TPA cross-section (σ) of the NBD-chromophores.

Compound	Quantum Yield (ϕ)	Power of the laser for TPEF (μJ/pulse)	TPEF intensities for 0.006 M	Observed σ (GM)	Corrected σ (GM)
NBD-Amine	0.53	646	9.45×10^4	0.73	1.40
NBD-Methylamine	0.59	646	9.22×10^4	0.71	1.20
NBD-Ethylamine	0.58	600	7.05×10^4	0.54	0.94
NBD-Dimethylamine	0.59	630	3.54×10^4	0.27	0.46
NBD-Ethylmethylamine	0.32	630	1.45×10^4	0.11	0.35
NBD-Diethylamine	0.22	630	6.65×10^3	0.05	0.23

Overall, the TPA cross-section (σ) of the NBD-chromophores are relatively low and are observed to decrease as the donor amine in the NBD-chromophore becomes more substituted and sterically hindered.

The observed reduction of the TPA cross-section (σ) can possibly be related to allylic1,3-strain, which places the amine group in an orientation that has a reduced interaction with the nitro group, thus reducing the charge transfer phenomena that seems to be needed for efficient two photon absorption. A more detailed explanation requires some computational work that is outside the scope of this thesis.

It is evident from the work provided that enhanced charge redistribution between donor and acceptor does not necessarily result in enhanced TPA cross-section as tuning the emission properties and the selection of the *N*-substituents are equally important.

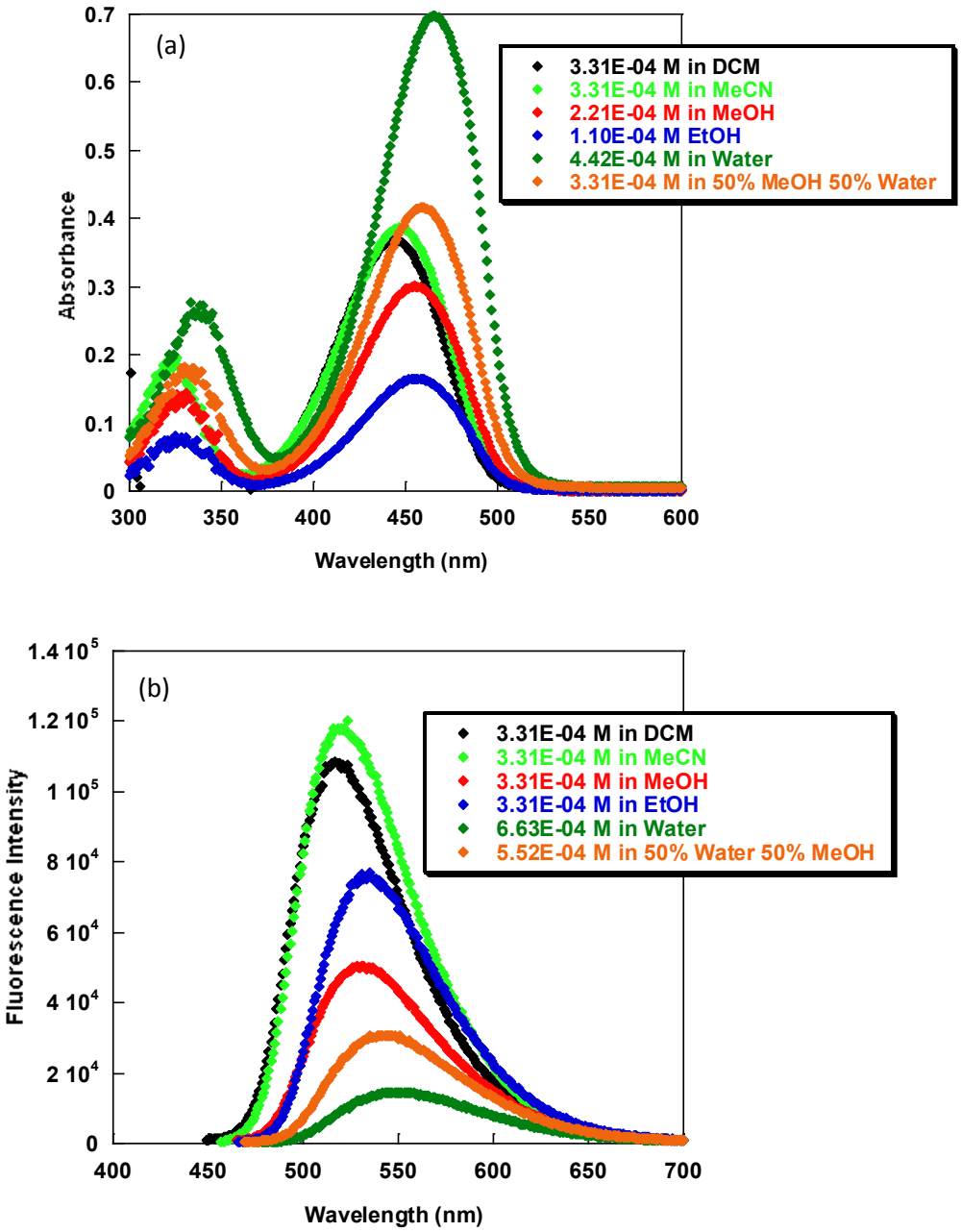

Figure 4.1 (a) UV-vis absorption spectra and (b) fluorescence spectra of NBD-NH_2 in solvents with different polarity. Fluorescence spectra were obtained using the observed λ_{max} of absorption as the excitation wavelength for the respective solvent (Table 4.1).

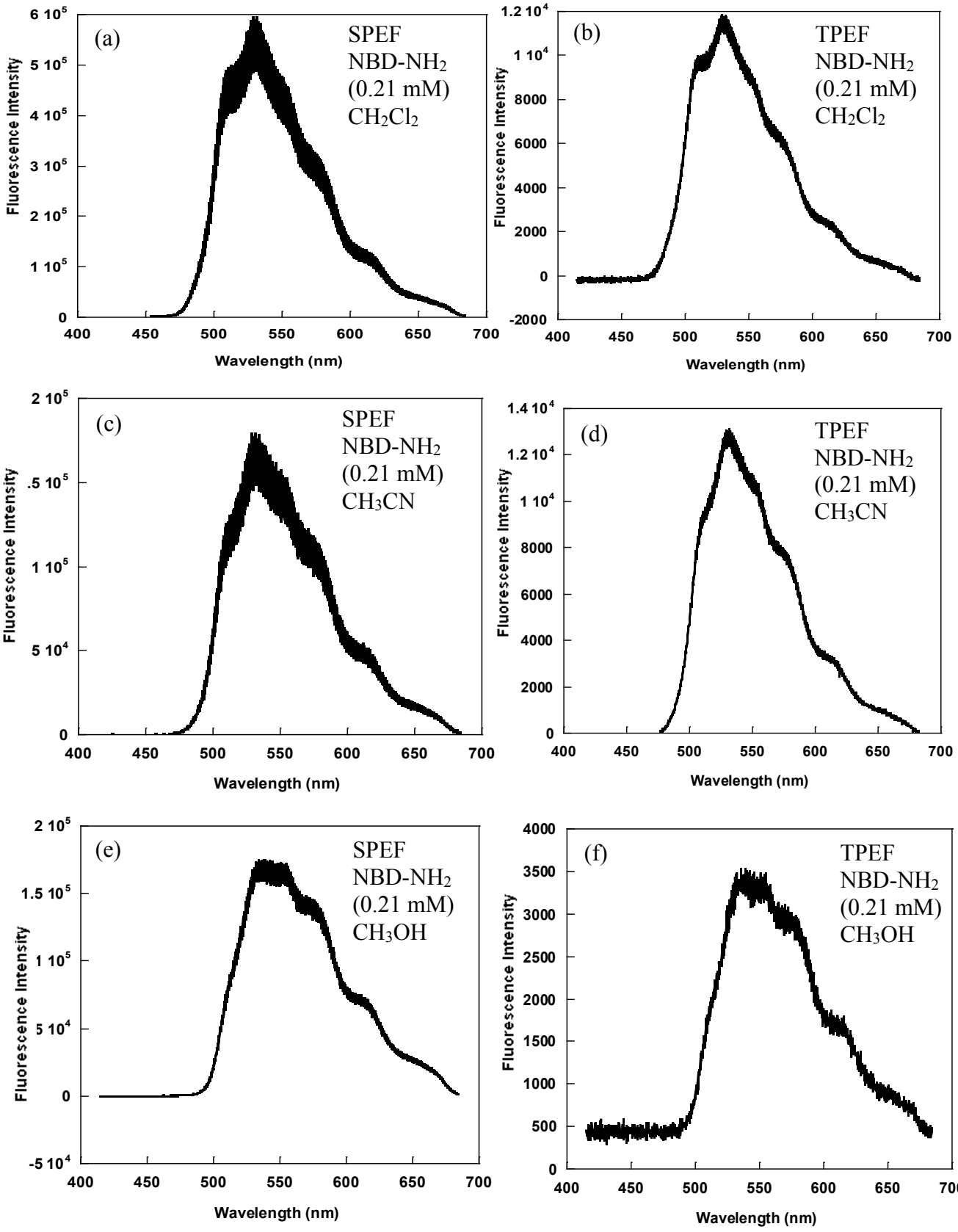
(a)
SPEF
NBD-NH2
(0.21 mM)
CH2Cl2
(b)
TPEF
NBD-NH2
(0.21 mM)
CH2Cl2
(c)
SPEF
NBD-NH2
(0.21 mM)
CH3CN
(d)
TPEF
NBD-NH2
(0.21 mM)
CH3CN
(e)
SPEF
NBD-NH2
(0.21 mM)
CH3OH
(f)
TPEF
NBD-NH2
(0.21 mM)
CH3OH
Fluorescence Intensity
Wavelength (nm)

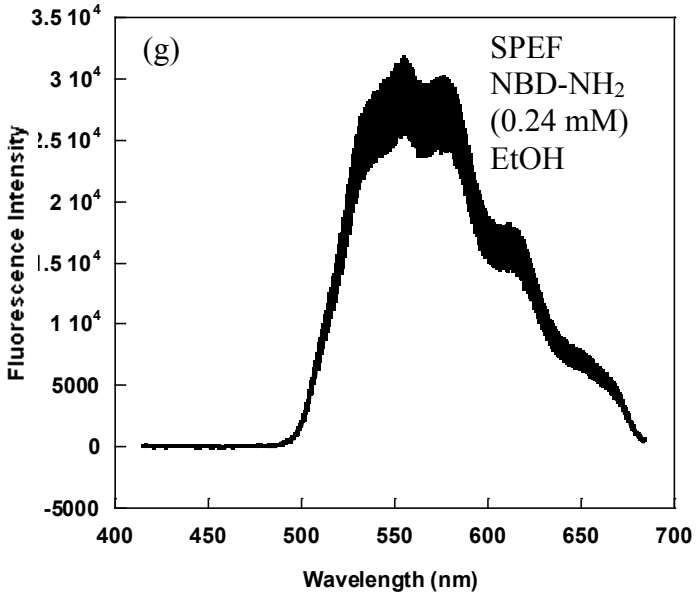
(g)
SPEF
NBD-NH2
(0.24 mM)
EtOH
Fluorescence Intensity
Wavelength (nm)
3.5 10^4
3 10^4
2.5 10^4
2 10^4
1.5 10^4
1 10^4
5000
0
-5000
400
450
500
550
600
650
700

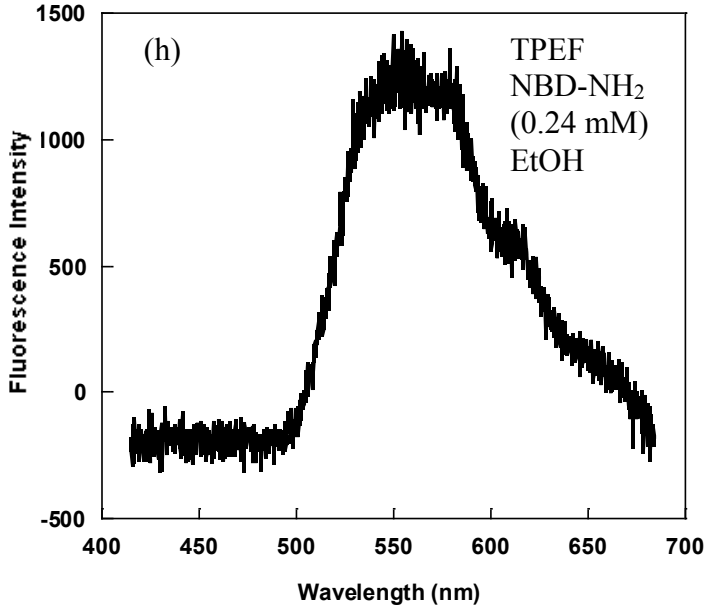
(h)
TPEF
NBD-NH2
(0.24 mM)
EtOH
Fluorescence Intensity
Wavelength (nm)
1500
1000
500
0
-500
400
450
500
550
600
650
700

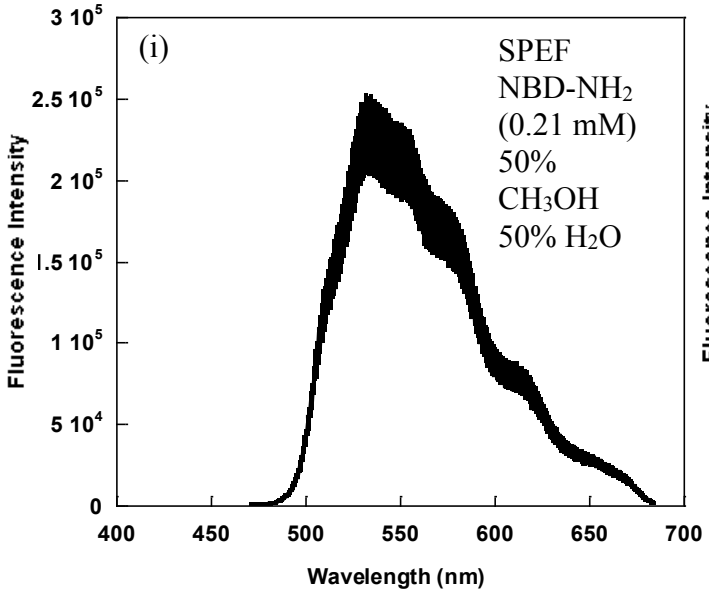
(i)
SPEF
NBD-NH2
(0.21 mM)
50%
CH3OH
50% H2O
Fluorescence Intensity
Wavelength (nm)
3 10^5
2.5 10^5
2 10^5
1.5 10^5
1 10^5
5 10^4
0
400
450
500
550
600
650
700

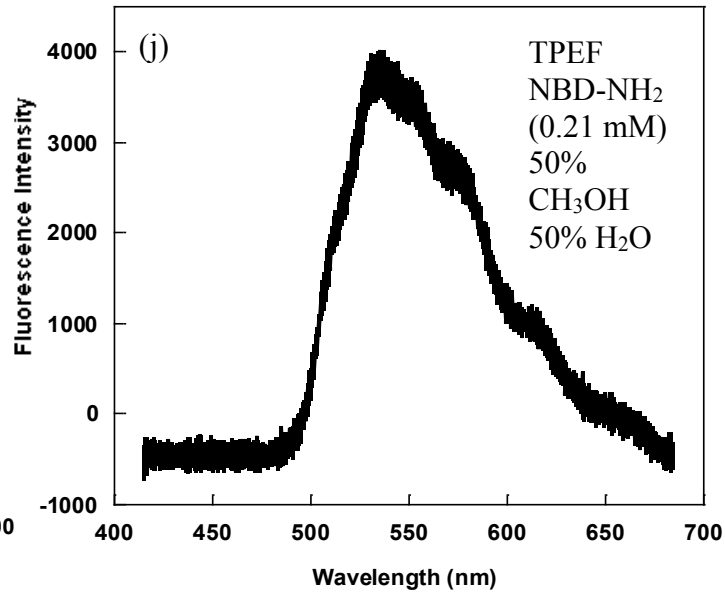
(j)
TPEF
NBD-NH2
(0.21 mM)
50%
CH3OH
50% H2O
Fluorescence Intensity
Wavelength (nm)
4000
3000
2000
1000
0
-1000
400
450
500
550
600
650
700

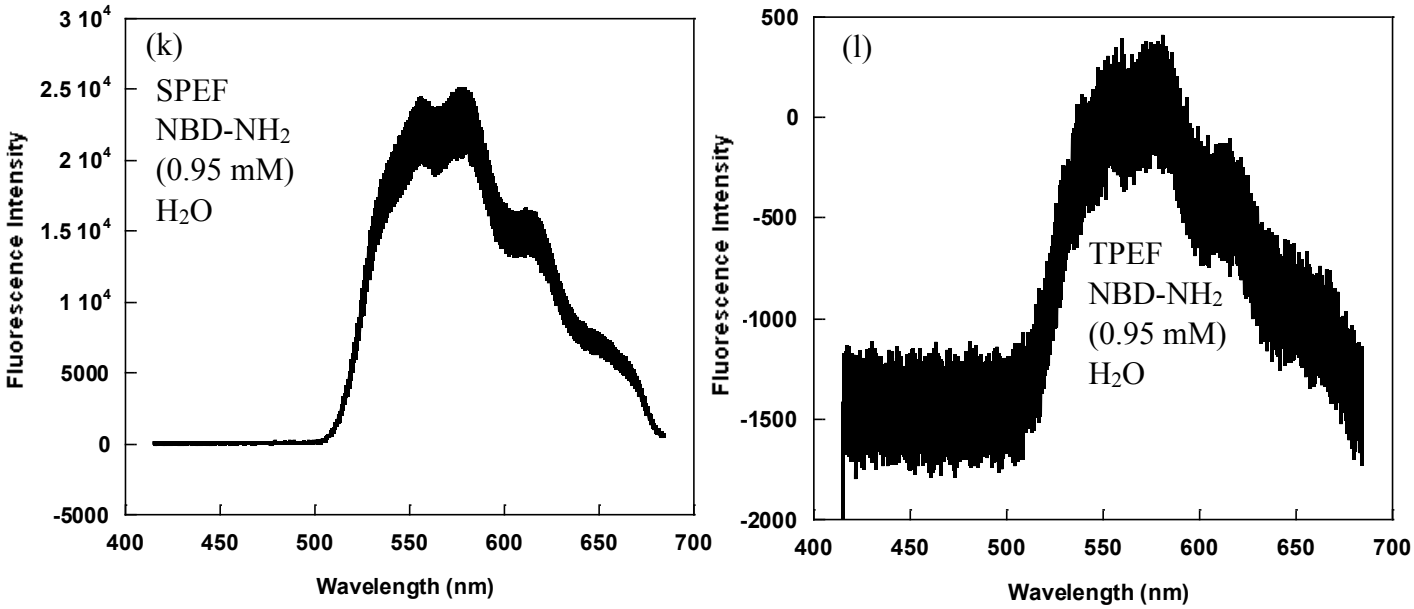

Figure 4.2. (a) SPEF and (b) TPEF spectra of 2.07 x10^{-4} M NBD-NH_2 in dichloromethane. (c) SPEF and (d) TPEF spectrum of 2.07 x 10^{-4} M NBD-NH_2 in acetonitrile. (e) SPEF and (f) TPEF spectra of 2.21 x 10^{-4} M NBD-NH_2 in methanol. (g) SPEF and (h) TPEF spectra of 2.42 x 10^{-4} M NBD-NH_2 in ethanol. (i) SPEF and (j) TPEF spectra of 2.07 x 10^{-4} M NBD-NH_2 in 50% H_2O:50% MeOH. (k) SPEF and (l) TPEF spectra of 9.50 x 10^{-4} M NBD-NH_2 100% H_2O. SPEF and TPEF spectra obtained upon excitation at λ = 387.5 and 775 nm, respectively.

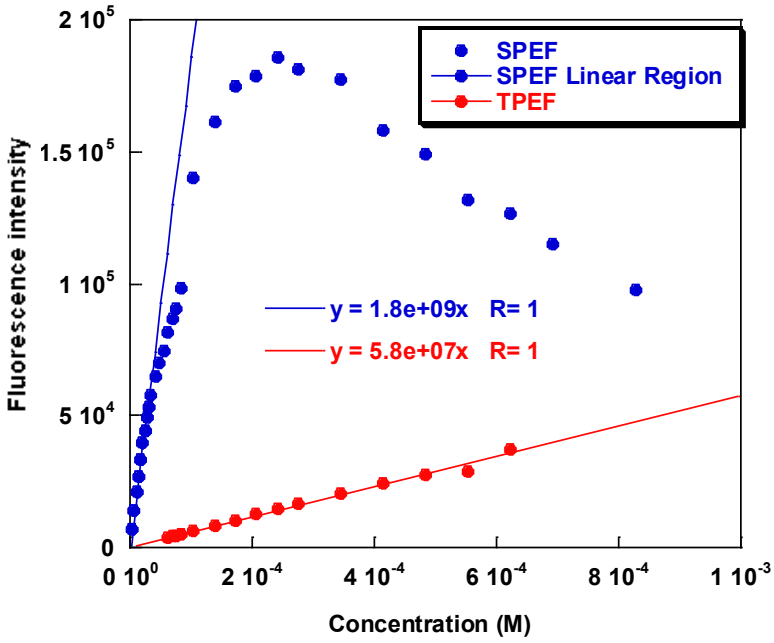

Figure 4.3. Relationship between fluorescence intensity and concentration of NBD-NH_2 upon (blue circles) single photon excitation (387.5 nm) and (red circles) two photon excitation (775 nm) in 100% acetonitrile as the solvent.

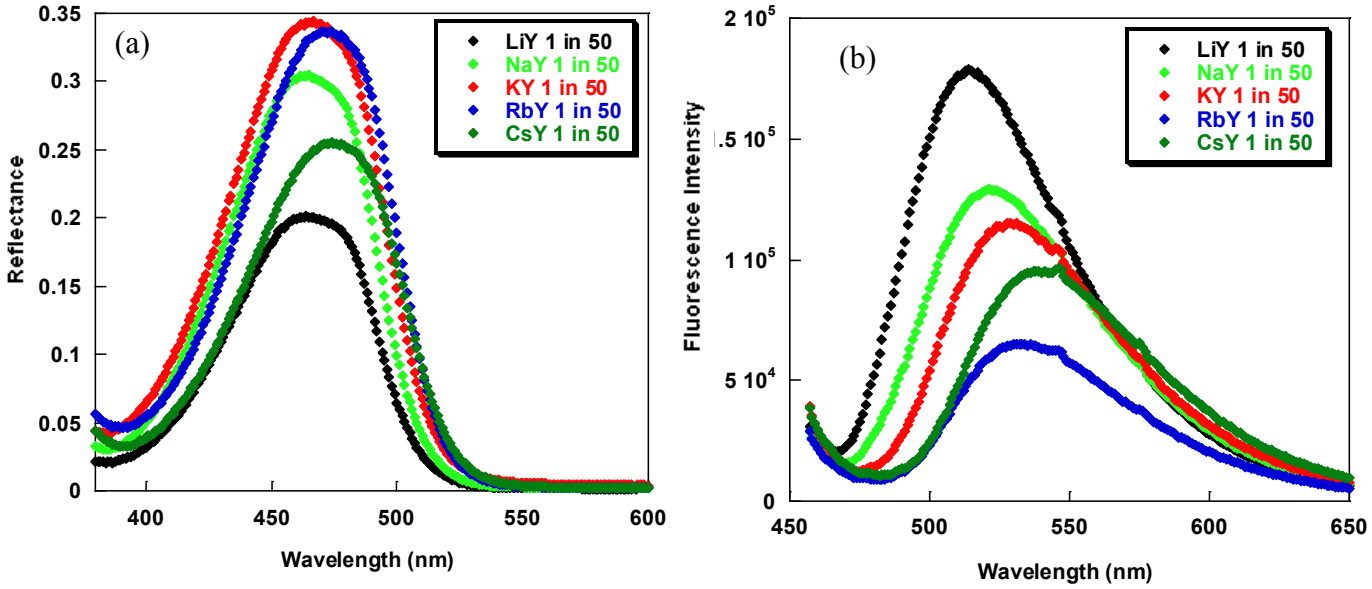

Figure 4.4. (a) Diffuse Reflectance Spectra and (b) fluorescence spectra of NBD-NH_2 incorporated in various different alkali earth metal cation exchanged Y zeolites at an experimental loading level of <S> = 1/50. Excitation wavelength for fluorescence spectrum at λ= 447 nm**.**

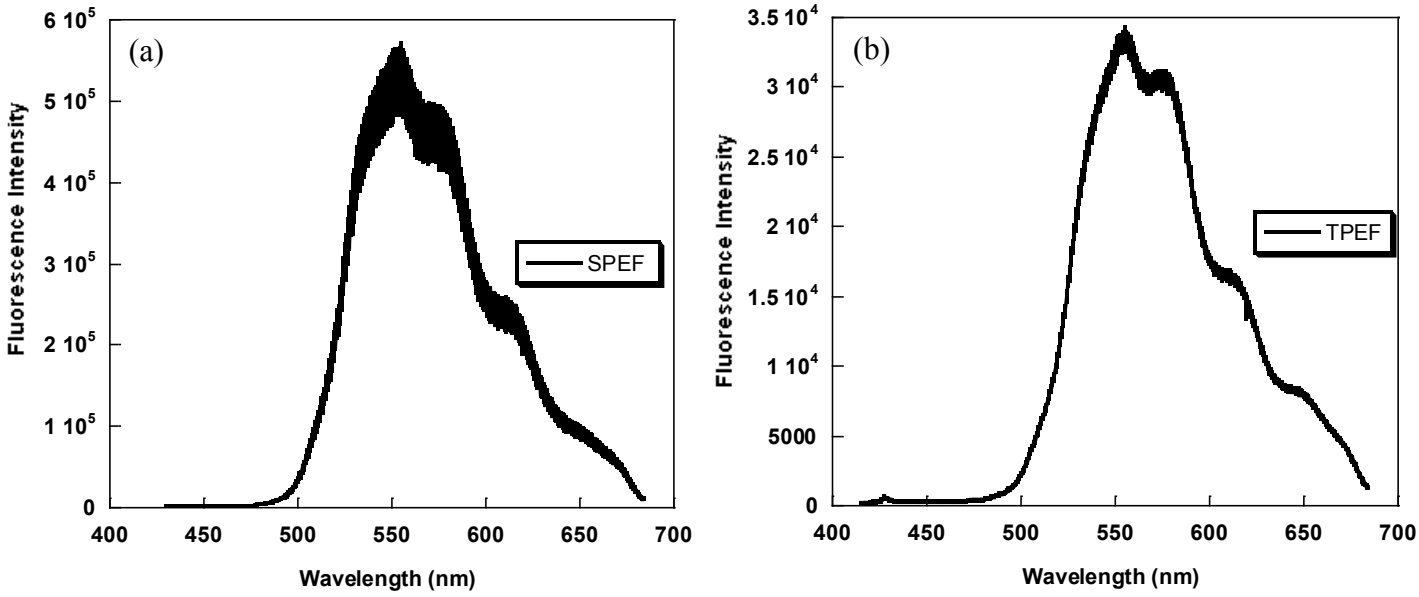

Figure 4.5 (a) SPEF and (b) TPEF spectra of NBD-NH_2 incorporated in NaY at a loading level of <S> = 1/17. SPEF and TPEF spectra obtained upon excitation at λ = 387.5 and 775 nm, respectively.

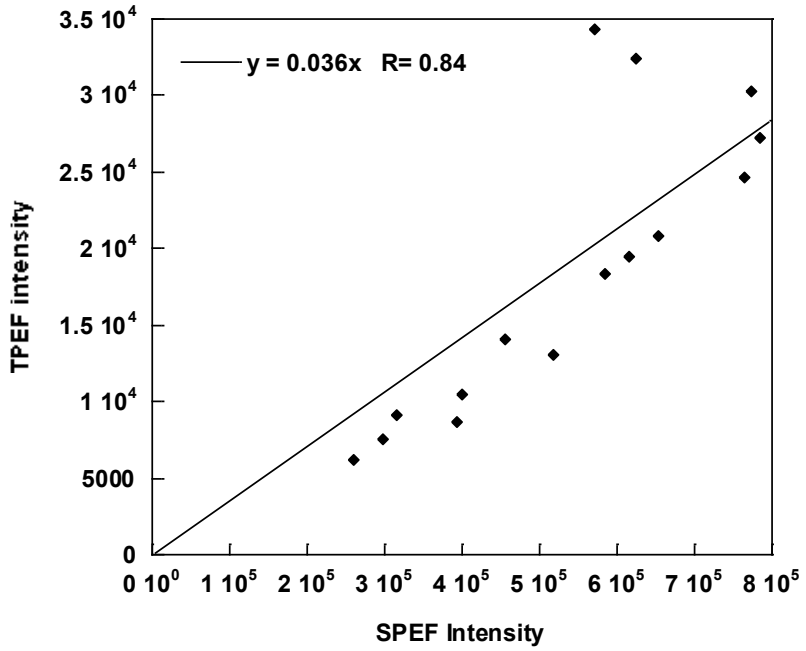

Figure 4.6. A plot of TPEF intensities vs SPEF intensities obtained from the respective SPEF and TPEF spectra of NBD-NH_2 incorporated in NaY at various different loading level <S>. SPEF spectra obtained upon excitation at 387.5 nm and SPEF spectra obtained upon excitation at 775 nm. The slope is the ratio of 2P:1P in NaY.

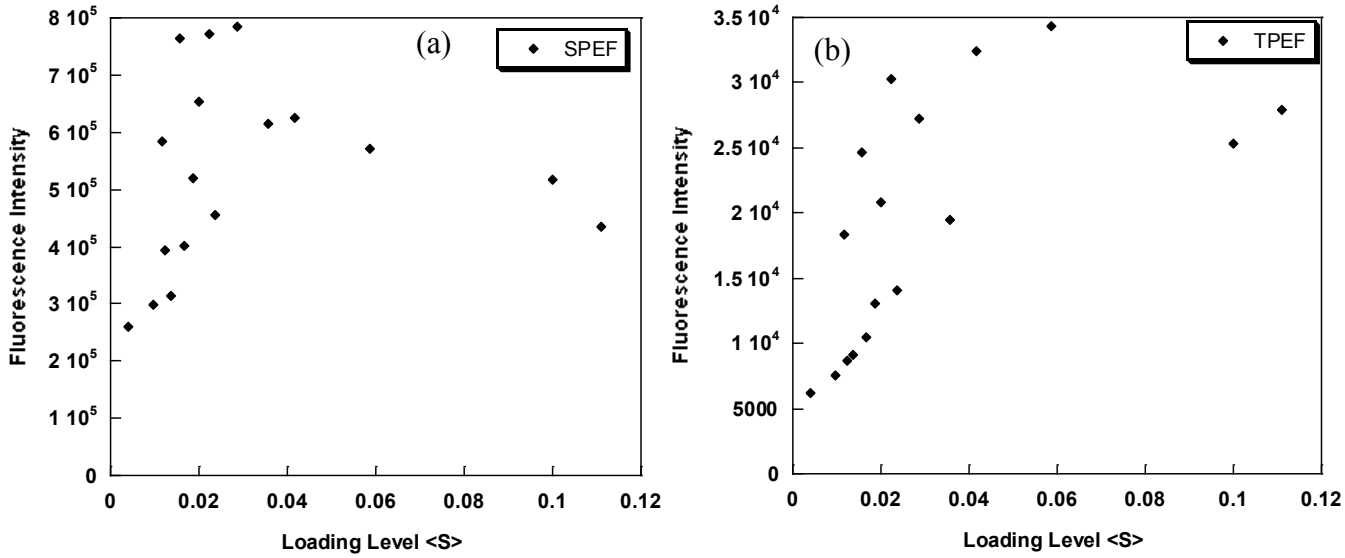

Figure 4.7. A plot summarising the relationship between fluorescence intensity and loading level of NBD-NH_2 <S> in NaY, upon (a) single photon excitation (λ= 387.5 nm) and (b) two photon excitation (λ = 775 nm).

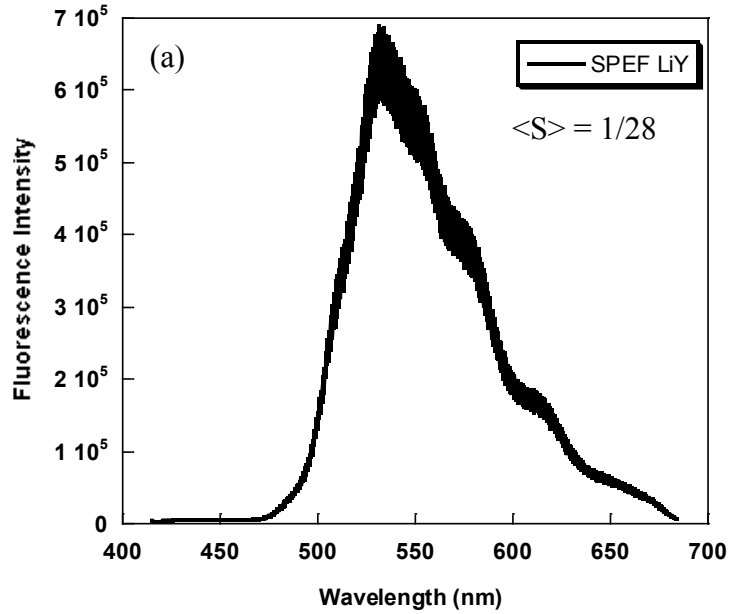
(a)
SPEF LiY
<S> = 1/28
Fluorescence Intensity
Wavelength (nm)

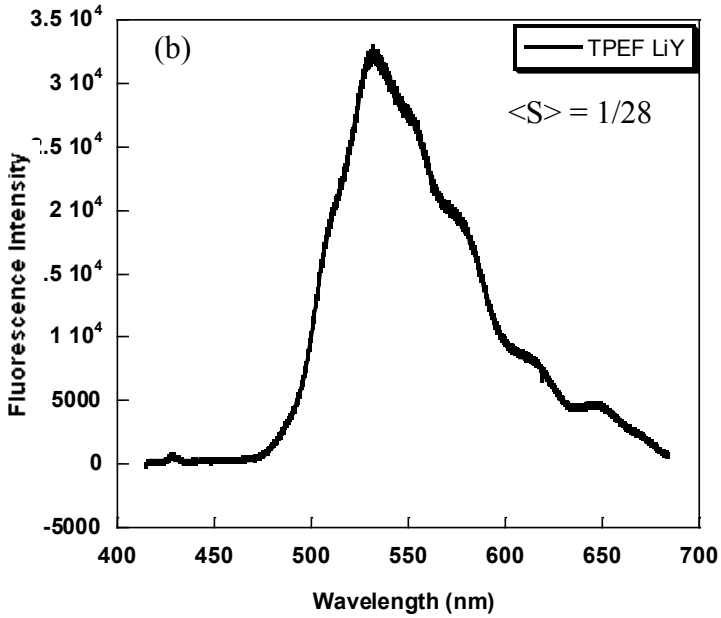
(b)
TPEF LiY
<S> = 1/28
Fluorescence Intensity
Wavelength (nm)

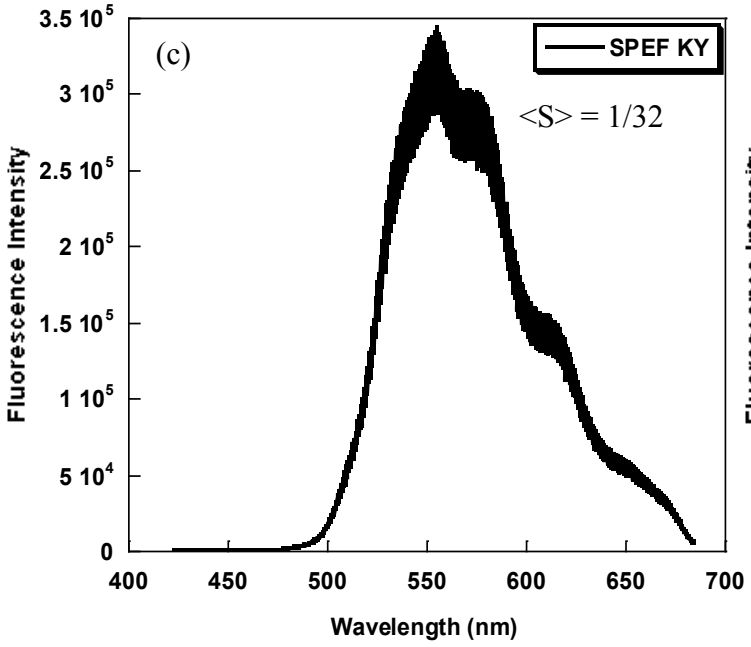
(c)
SPEF KY
<S> = 1/32
Fluorescence Intensity
Wavelength (nm)

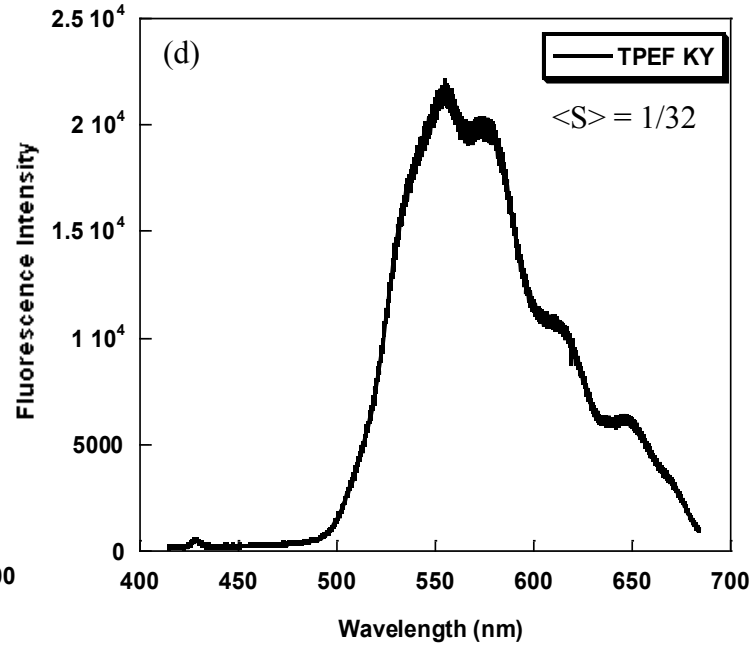
(d)
TPEF KY
<S> = 1/32
Fluorescence Intensity
Wavelength (nm)

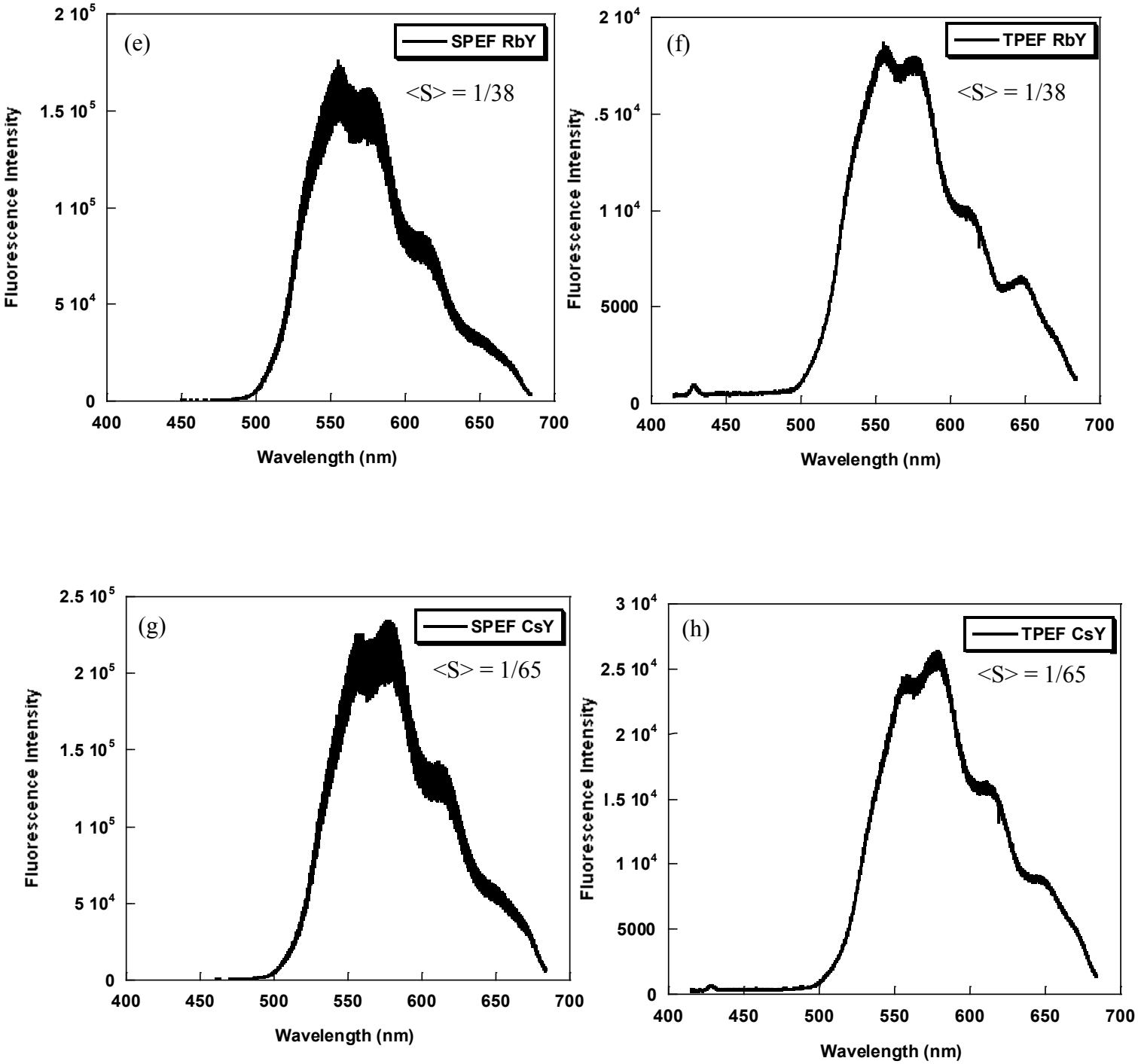

Figure 4.8. (a) SPEF and (b) TPEF spectra of NBD-NH_2 incorporated in LiY at a loading level of <S>= 1/28. (c) SPEF and (b) TPEF spectra of NBD-NH_2 in KY at a loading level <S> = 1/32. (e) SPEF and (f) TPEF spectra of NBD-NH_2 in RbY at a loading level <S>= 1/38. (g) SPEF and (h) TPEF spectra of NBD-NH_2 in CsY at a loading level of <S>= 1/65. SPEF and TPEF spectra obtained upon excitation at λ = 387.5 and 775 nm, respectively.

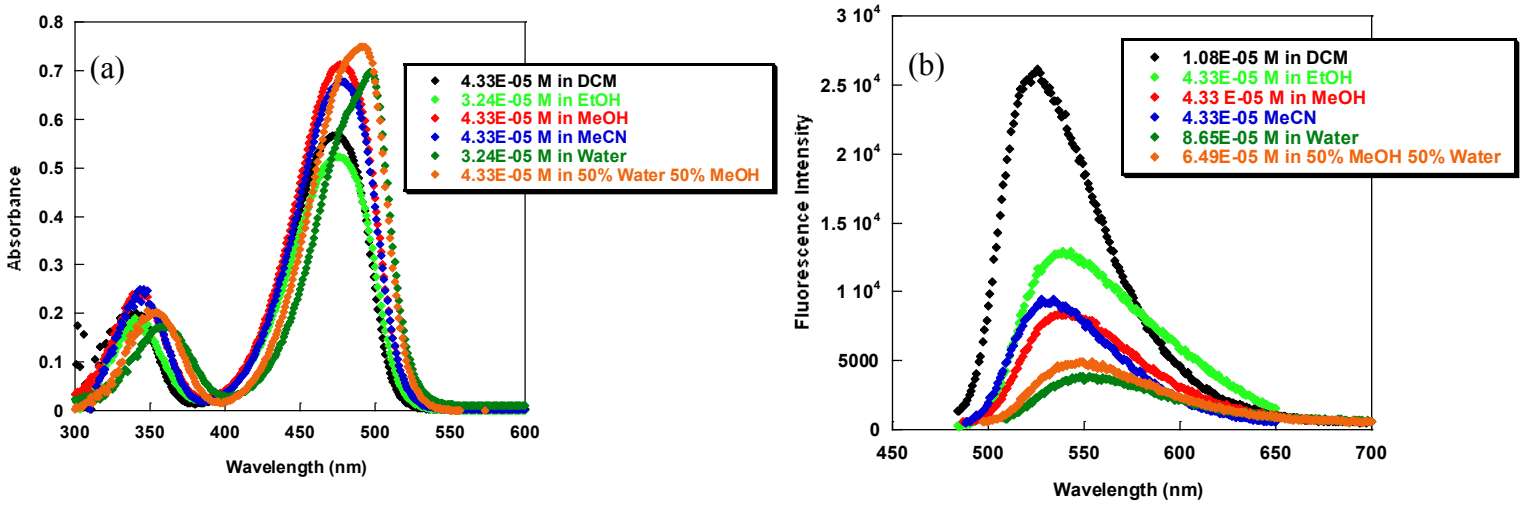

Figure 4.9. (a) UV-vis absorption spectra and (b) fluorescence spectra of NBD-DMA in solvents with different polarity. Fluorescence spectra were obtained using the observed λ_{max} of absorption as the excitation wavelength in respective solvent (Table 4.5).

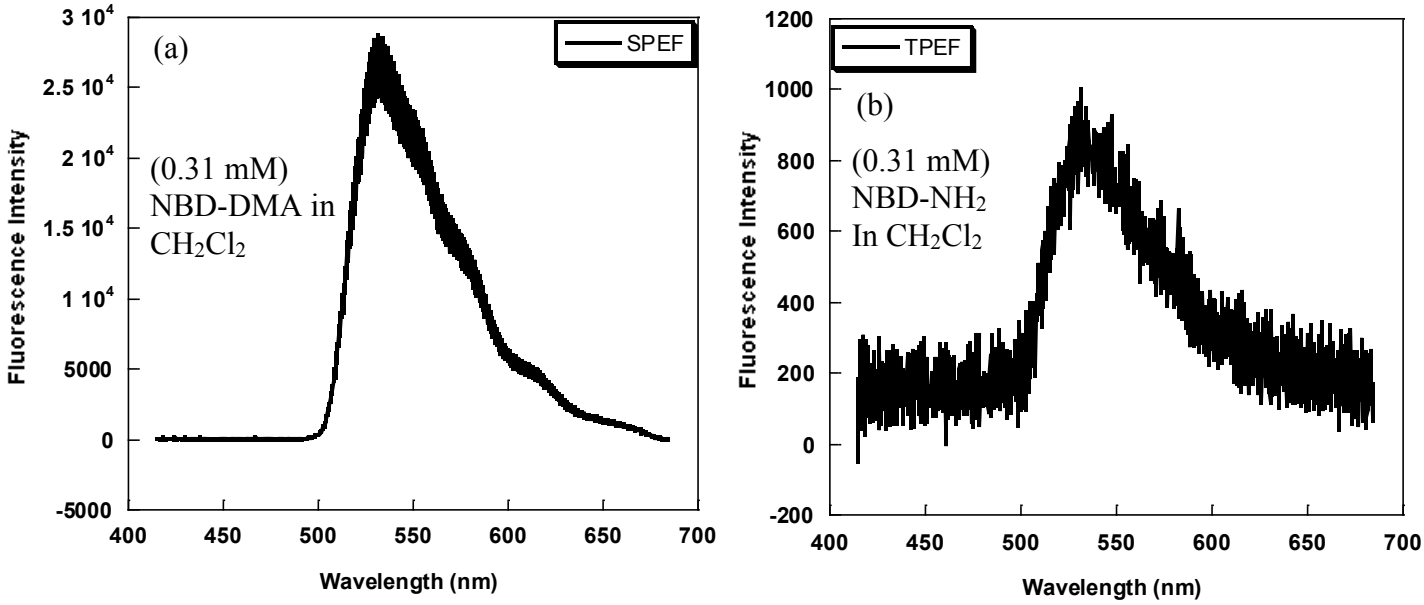

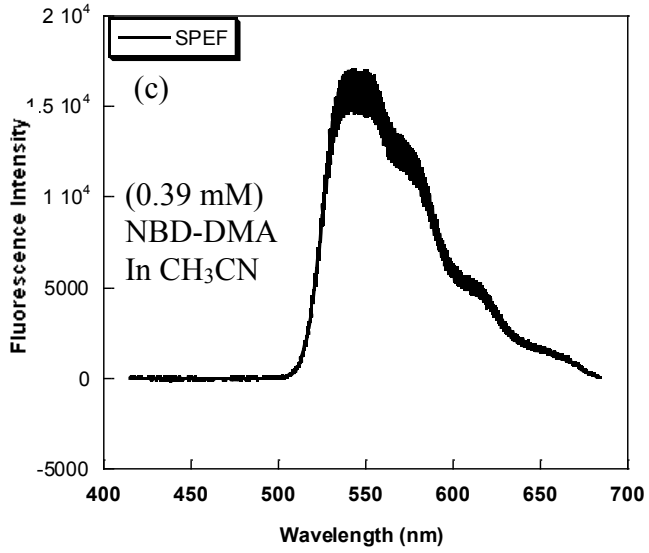
SPEF
(c)
(0.39 mM)
NBD-DMA
In CH3CN
Fluorescence Intensity
Wavelength (nm)

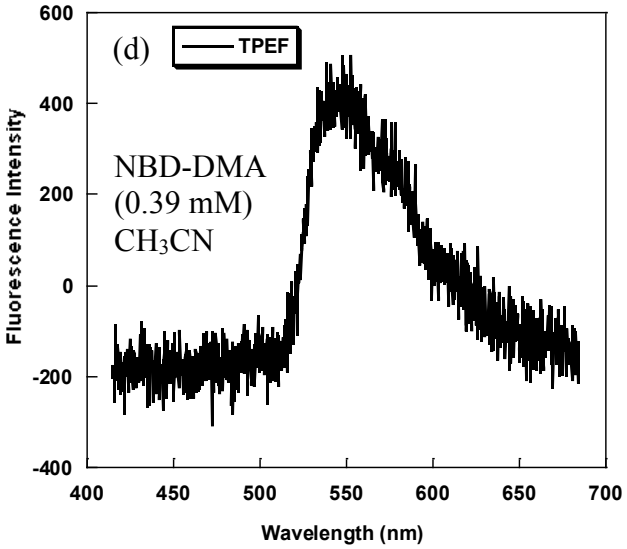
TPEF
(d)
NBD-DMA
(0.39 mM)
CH3CN
Fluorescence Intensity
Wavelength (nm)

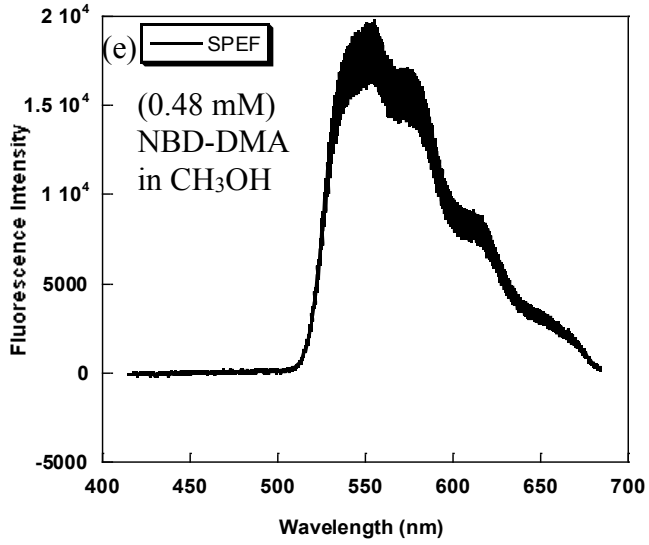
SPEF
(e)
(0.48 mM)
NBD-DMA
in CH3OH
Fluorescence Intensity
Wavelength (nm)

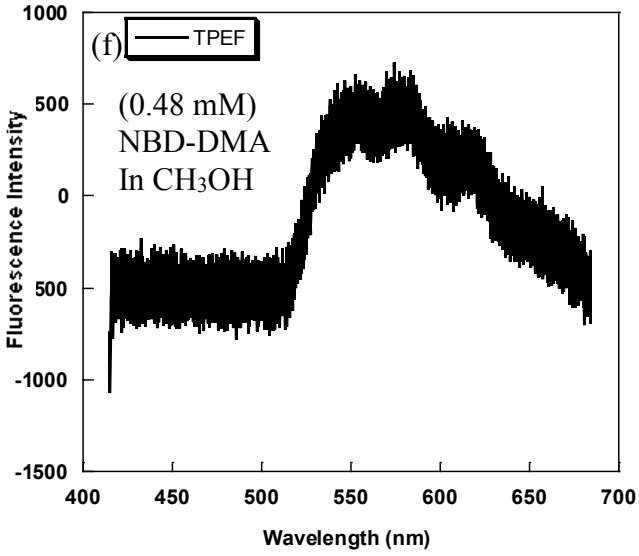
TPEF
(f)
(0.48 mM)
NBD-DMA
In CH3OH
Fluorescence Intensity
Wavelength (nm)

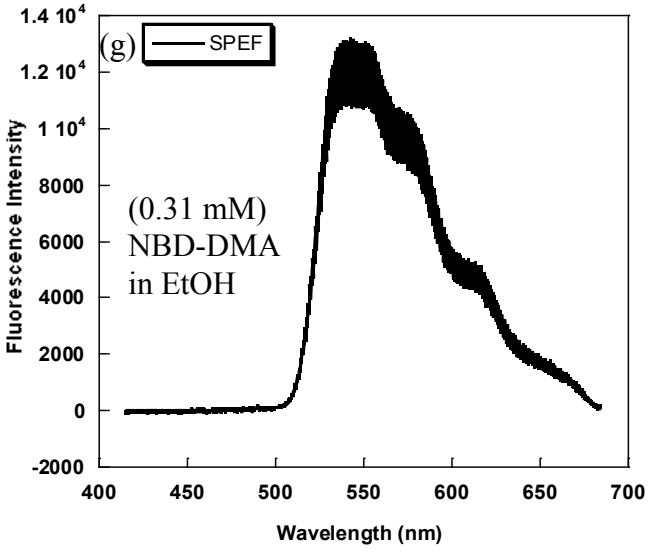
SPEF
(g)
(0.31 mM)
NBD-DMA
in EtOH
Fluorescence Intensity
Wavelength (nm)

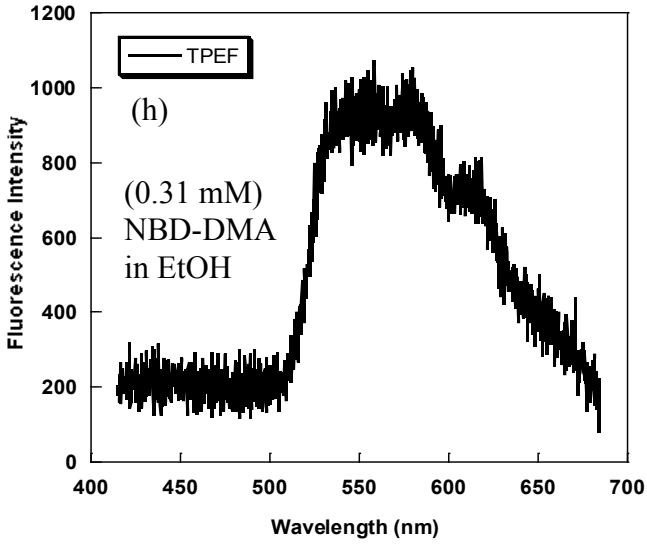
TPEF
(h)
(0.31 mM)
NBD-DMA
in EtOH
Fluorescence Intensity
Wavelength (nm)

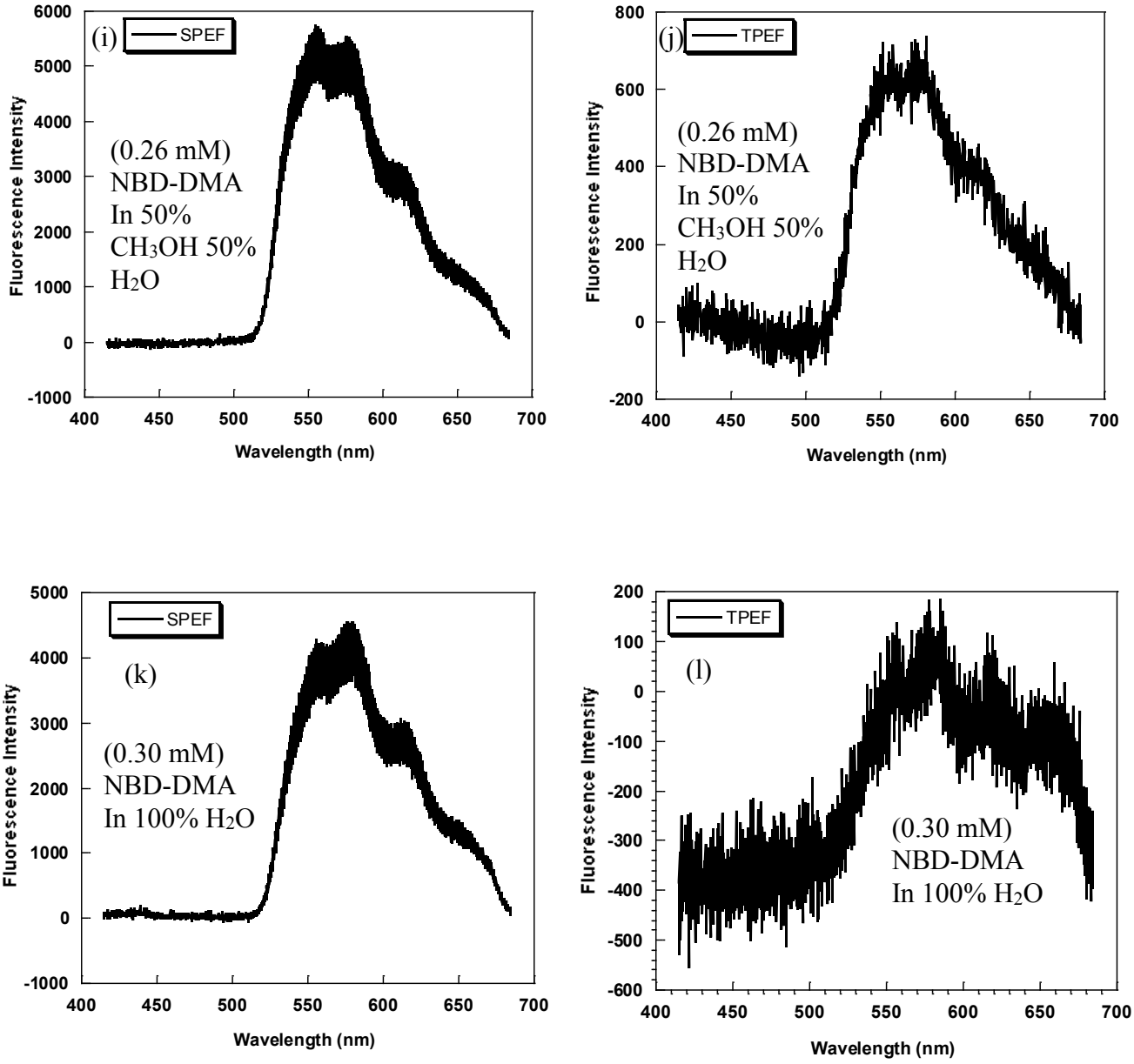

Figure 4.10. (a) SPEF and (b) TPEF spectra of 3.12 x 10^{-4} M NBD-DMA in dichloromethane. (c) SPEF of 3.87 x 10^{-4} M and (d) TPEF spectra of 5.05 x 10^{-4} M NBD-DMA in acetonitrile. (e) SPEF and (f) TPEF spectra of 4.81 x 10^{-4} M NBD-DMA in methanol. (g) SPEF and (h) TPEF spectra of 3.06 x 10^{-4} M NBD-DMA in ethanol. (i) SPEF and (j) TPEF spectra of 2.64 x 10^{-4} M NBD-DMA in 50% methanol 50% H_2O. (k) SPEF and (l) TPEF spectra of 3.00 x 10^{-4} NBD-DMA in 100% H_2O. SPEF and TPEF spectra obtained upon excitation at λ = 387.5 and 775 nm, respectively.

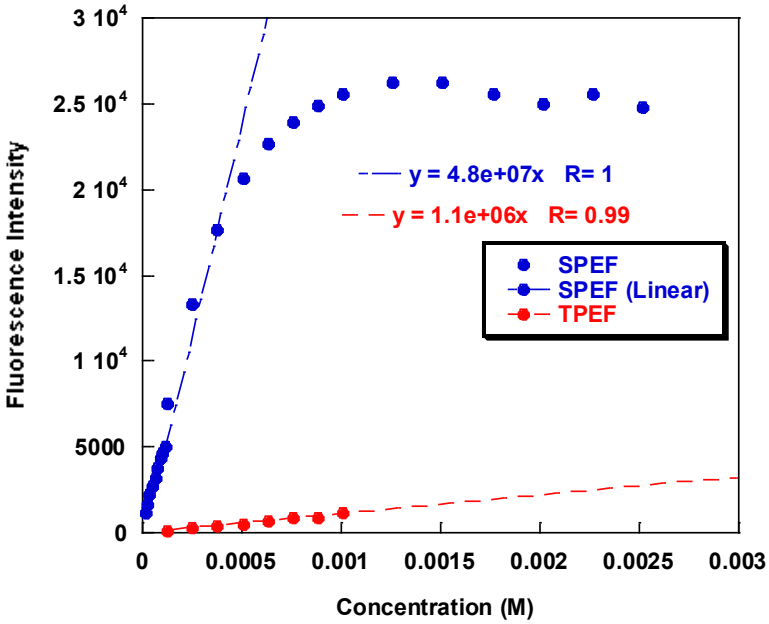

Figure 4.11. Relationship between fluorescence intensity and concentration of NBD-DMA upon (blue circle) single photon excitation (387.5 nm) and (red circle) two photon excitation (775 nm) in 100% acetonitrile as the solvent.

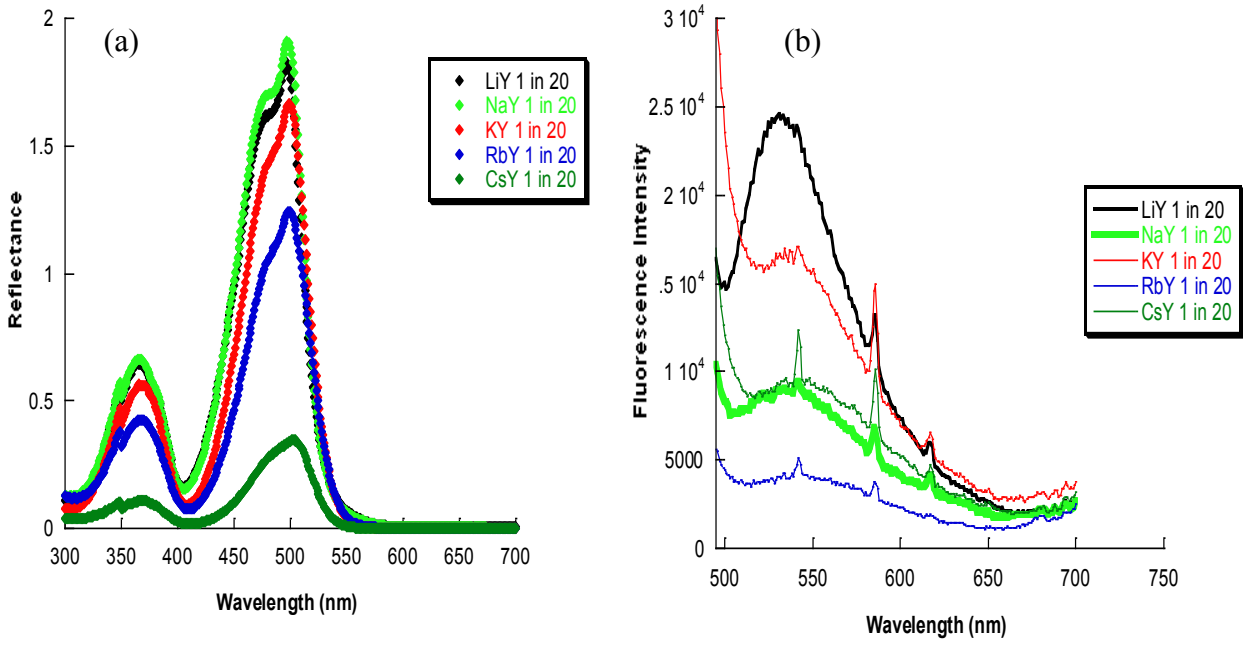

Figure 4.12. (a) Diffuse reflectance and (b) fluorescence spectra of NBD-DMA incorporated in various different alkali earth metal cation exchanged Y zeolites at an experiment loading level of <S> = 1/20. Excitation wavelength for the fluorescence spectra at λ= 478 nm.

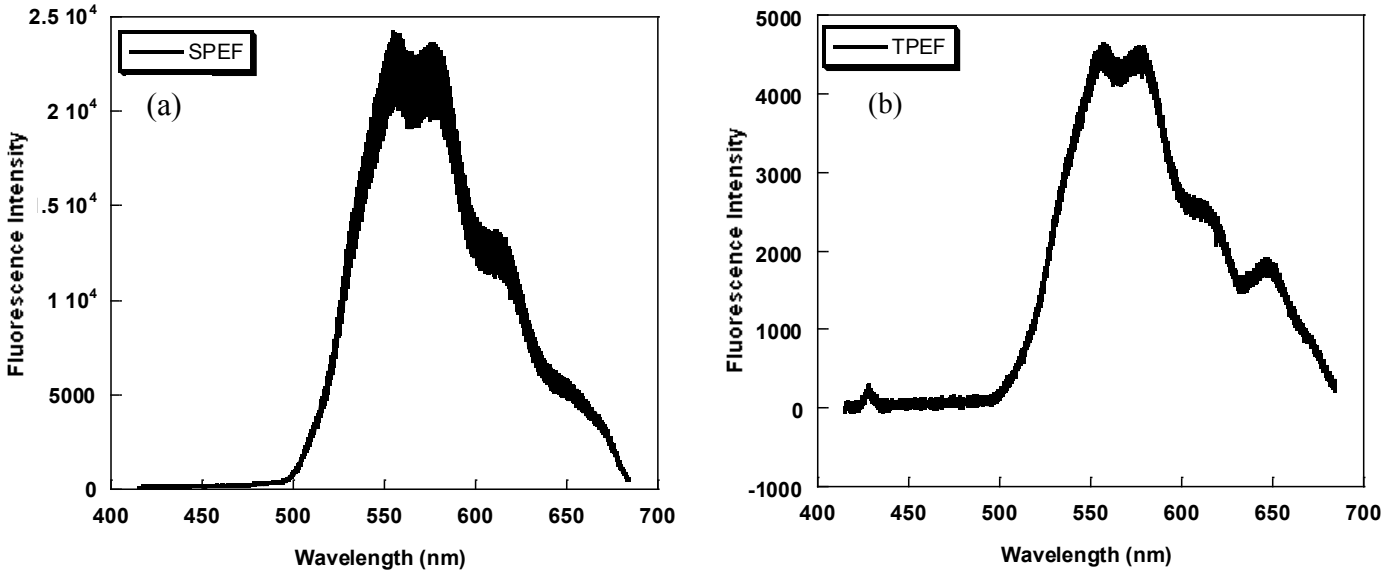

Figure 4.13. (a) SPEF and (b) TPEF spectra of NBD-DMA incorporated in NaY at a loading level of <S> = 1/25. SPEF and TPEF spectra obtained upon excitation at λ = 387.5 and 775 nm, respectively.

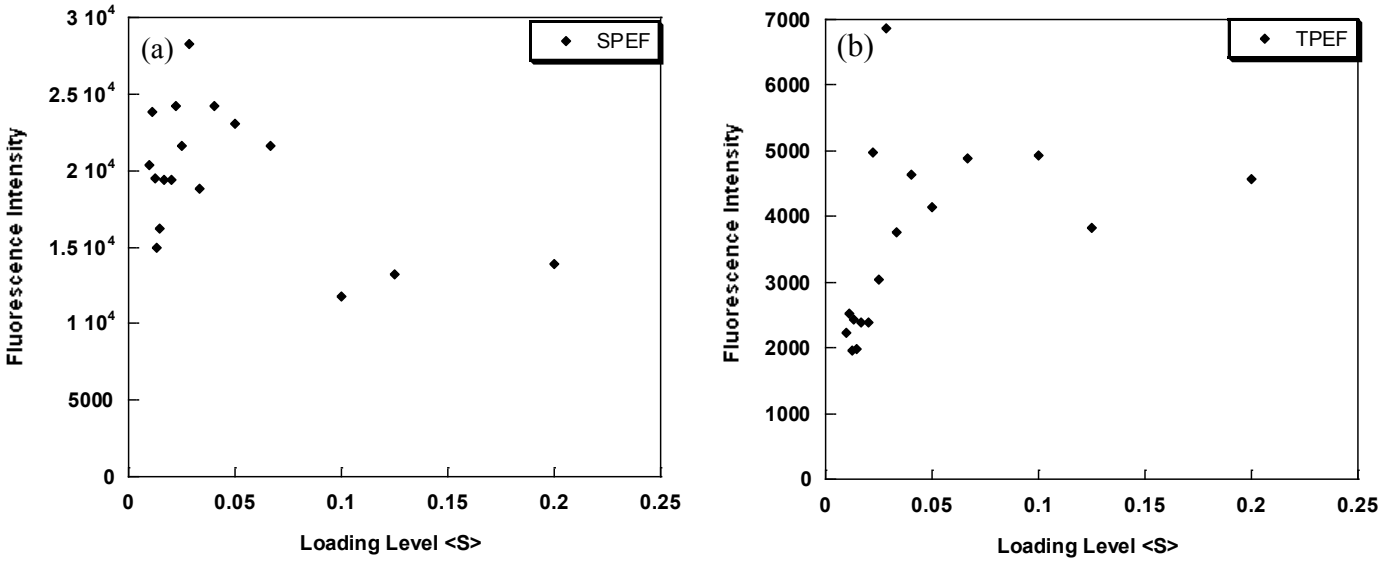

Figure 4.14. A plot summarising the relationship between fluorescence intensity and loading level of NBD-DMA, <S> in NaY, upon (a) single photon excitation (λ= 387.5 nm) and (b) two photon excitation (λ = 775 nm).

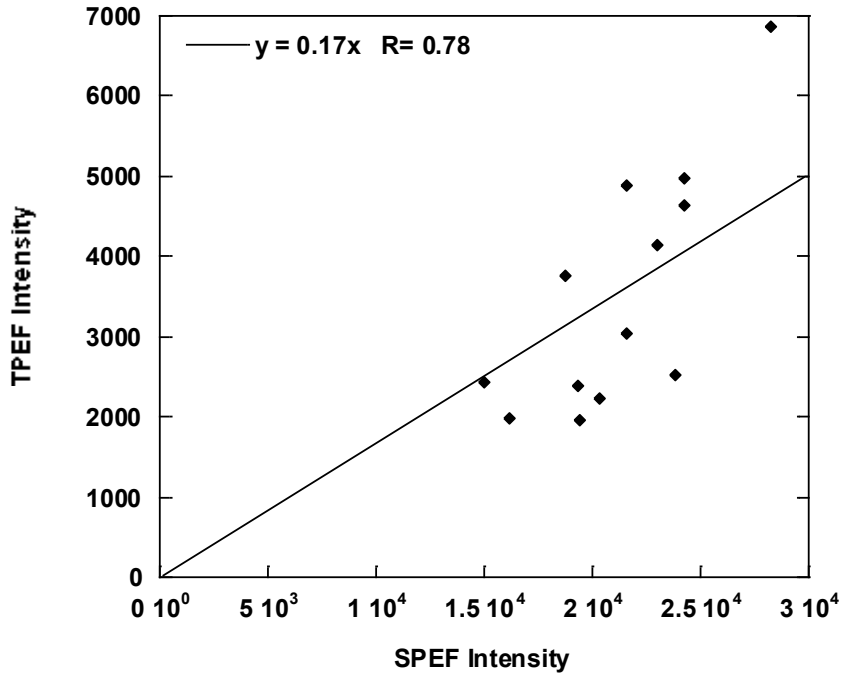

Figure 4.15. A plot of TPEF intensities vs SPEF intensities obtained from the respective SPEF and TPEF spectra for NBD-DMA incorporated in NaY at various loading level <S>. SPEF spectra obtained upon excitation at 387.5 nm and SPEF spectra obtained upon excitation at 775 nm. The slope is the ratio of 2P:1P in NaY.

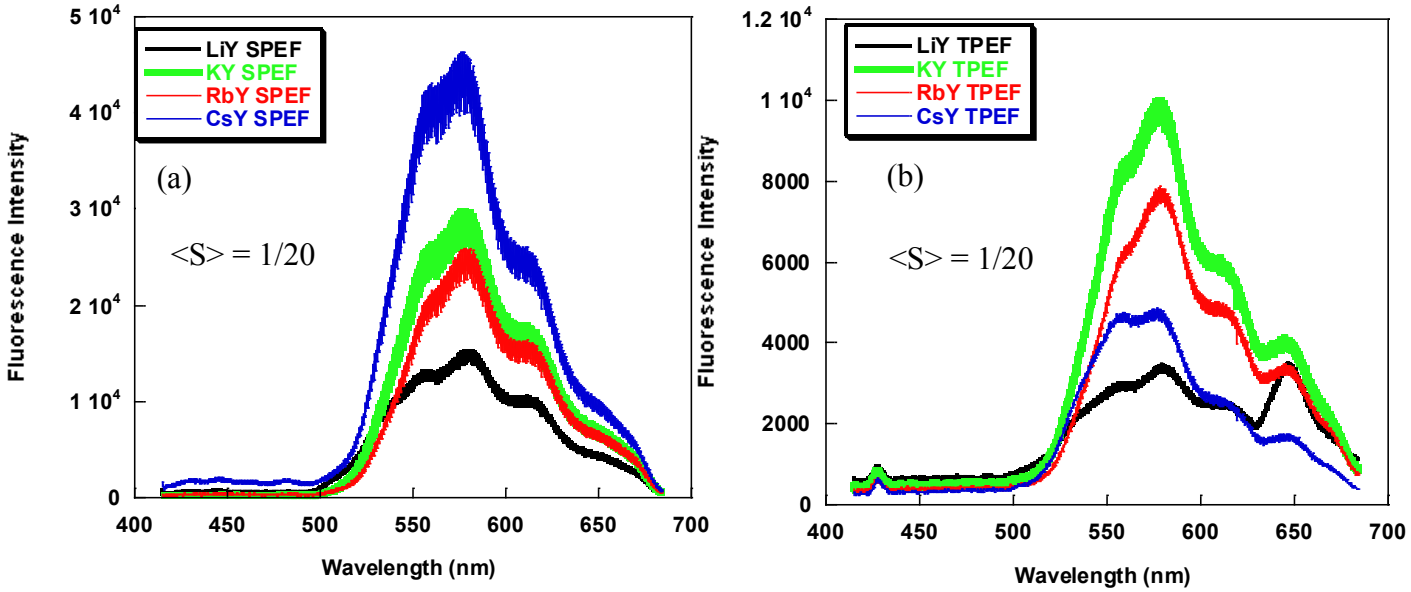

Figure 4.16. (a) SPEF and (b) TPEF spectra of NBD-DMA in LiY (black line), KY (green line), RbY (red line) and CsY (blue line) at an experimental loading level of <S> = 1/20. SPEF and TPEF spectra obtained upon excitation at λ = 387.5 and 775 nm, respectively.

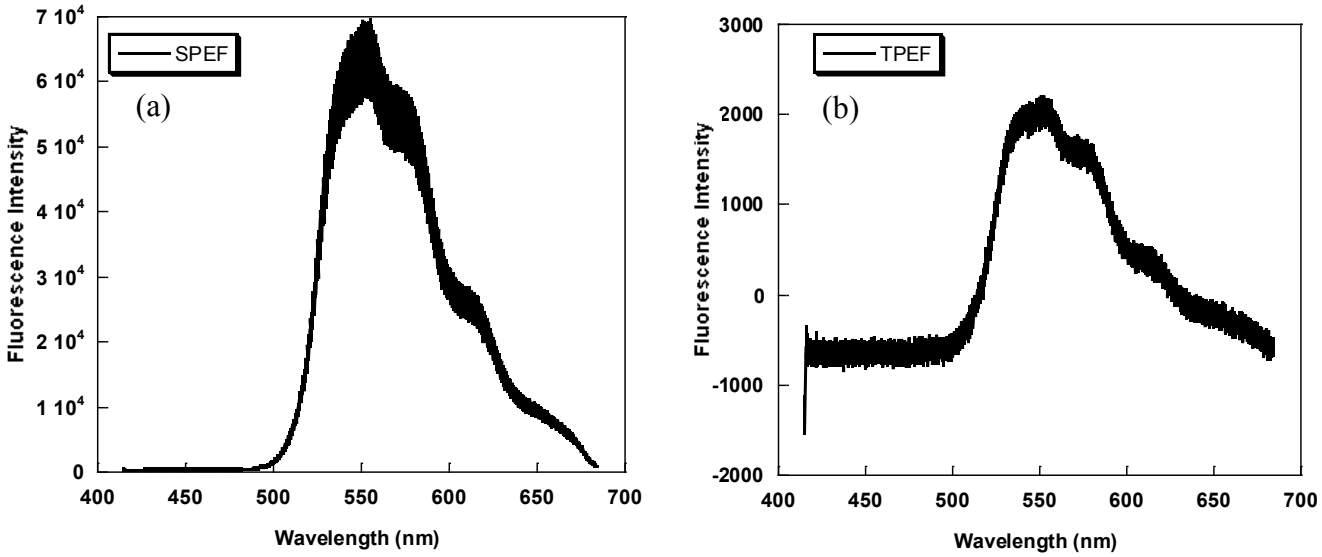

Figure 4.17. (a) SPEF (b) TPEF spectra of NBD-DMA incorporated in a non-dehydrated zeolite at an experimental loading level of <S> = 1/ 34. Sample transferred directly to laser cell in open atmosphere without being placed in a dessicator under vacuum. Water and dichloromethane present in the zeolite sample.

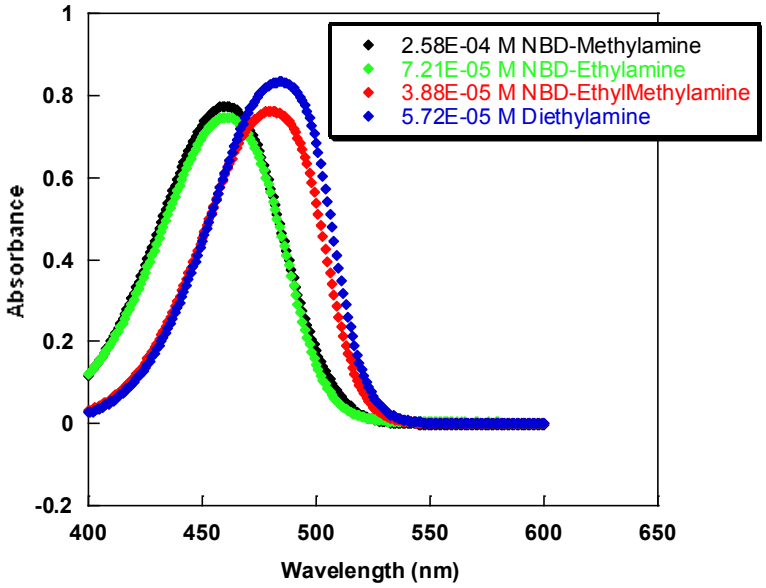

Figure 4.18. UV-vis spectrum of 2.58 x 10^{-4} M NBD-methylamine (black line, λ_{max} = 460 nm), 7.21 x 10^{-5} M NBD-ethylamine (green line, λ_{max} = 461 nm), 3.88 x10^{-5} M NBD-ethylmethylamine (red line, λ_{max} = 480 nm) and 5.72 x 10^{-4} M diethylamine (blue line, λ_{max} = 484 nm) obtained in acetonitrile.

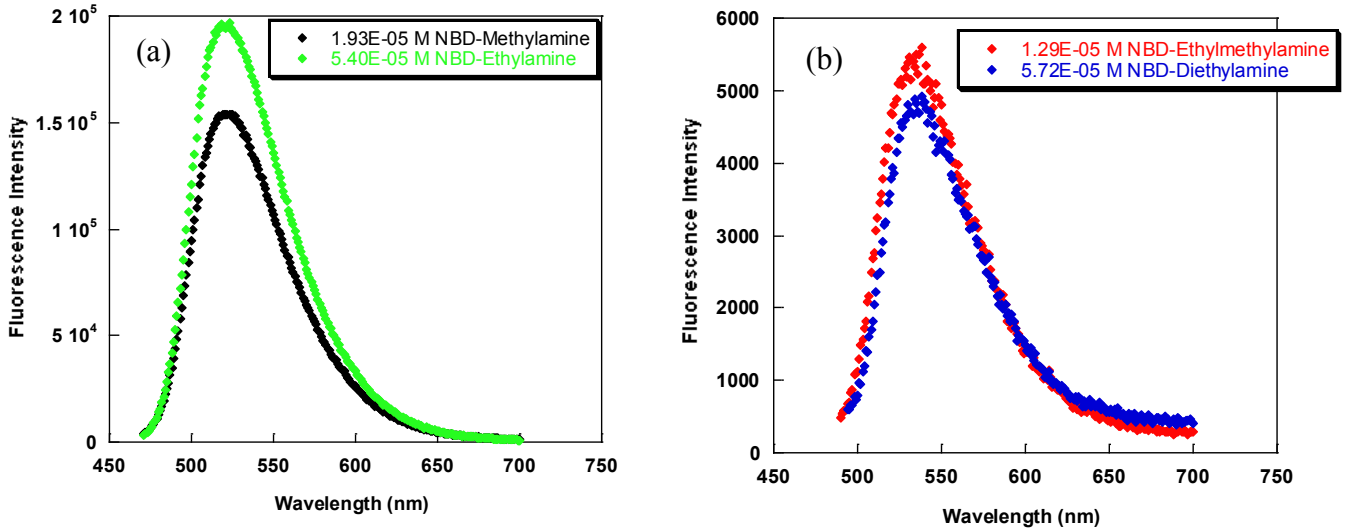

Figure 4.19. Fluorescence spectra of (a) 1.93 x 10^{-5} M NBD-methylamine (excitation wavelength at λ = 460 nm, black line) and 5.40 x 10^{-5} M NBD-ethylamine (excitation wavelength at λ = 461 nm, green line) in acetonitrile. (b) 1.29 x 10^{-5} M NBD-ethylmethylamine (excitation wavelength at λ = 480 nm, red line) and 5.72 x 10^{-5} NBD-diethylamine (excitation wavelength at λ = 484 nm, blue line) in acetonitrile. Fluorescence spectra were obtained by using the λ_{max} of absorption as the excitation wavelength for the respective compounds.

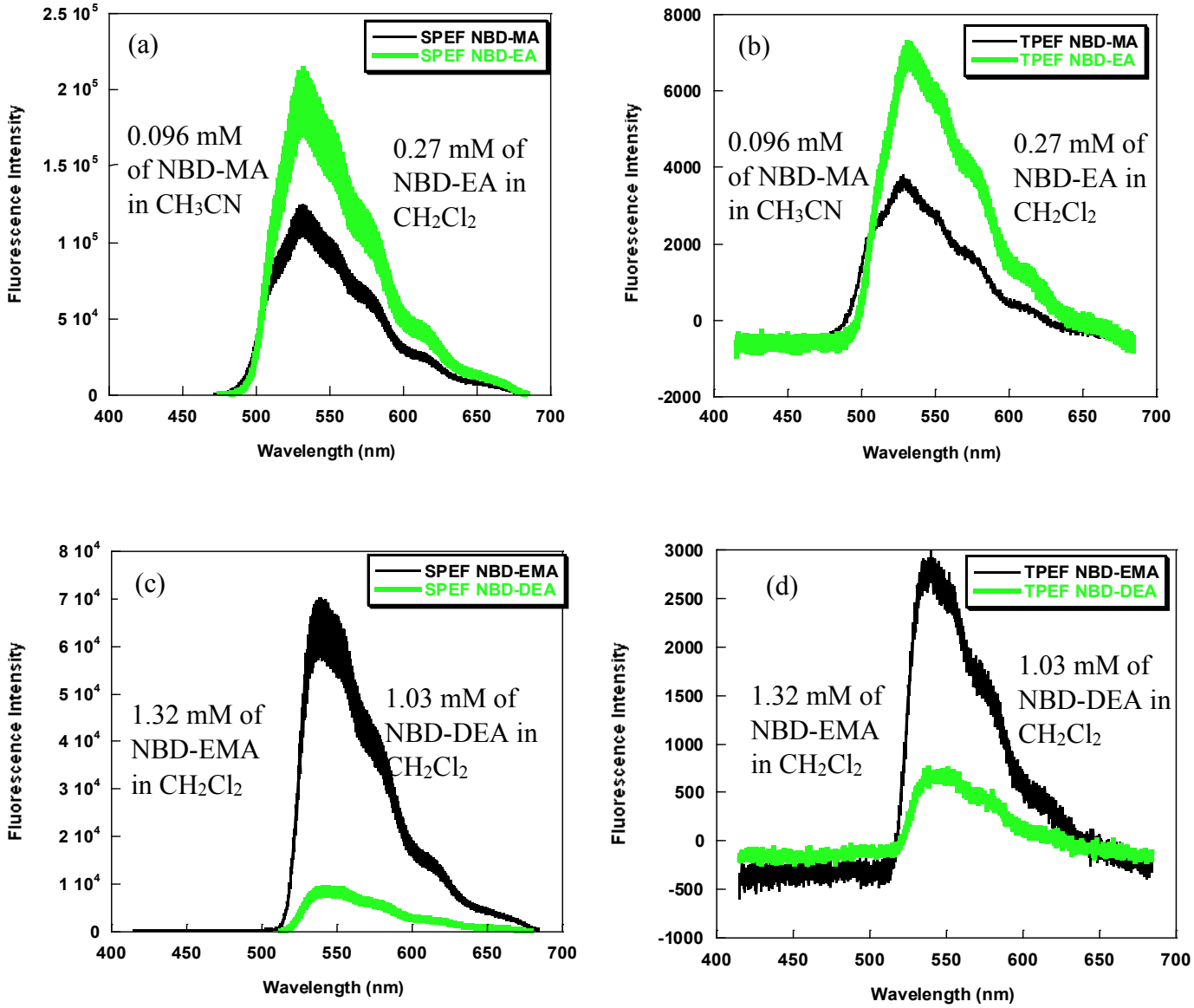

Figure 4.20. (a) SPEF and (b) TPEF spectra of 9.66 x 10^{-5} M NBD-methylamine (black line) in acetonitrile and 2.70 x 10^{-4} M NBD-ethylamine (green line) in dichloromethane, (c) SPEF and (d) TPEF spectra of 1.32 x 10^{-3} M NBD-ethylmethylamine (black spectrum) spectrum of 1.03 x 10^{-3} M NBD-diethylamine (green spectrum) in dichloromethane. SPEF and TPEF spectra obtained upon excitation at λ = 387.5 and 775 nm, respectively.

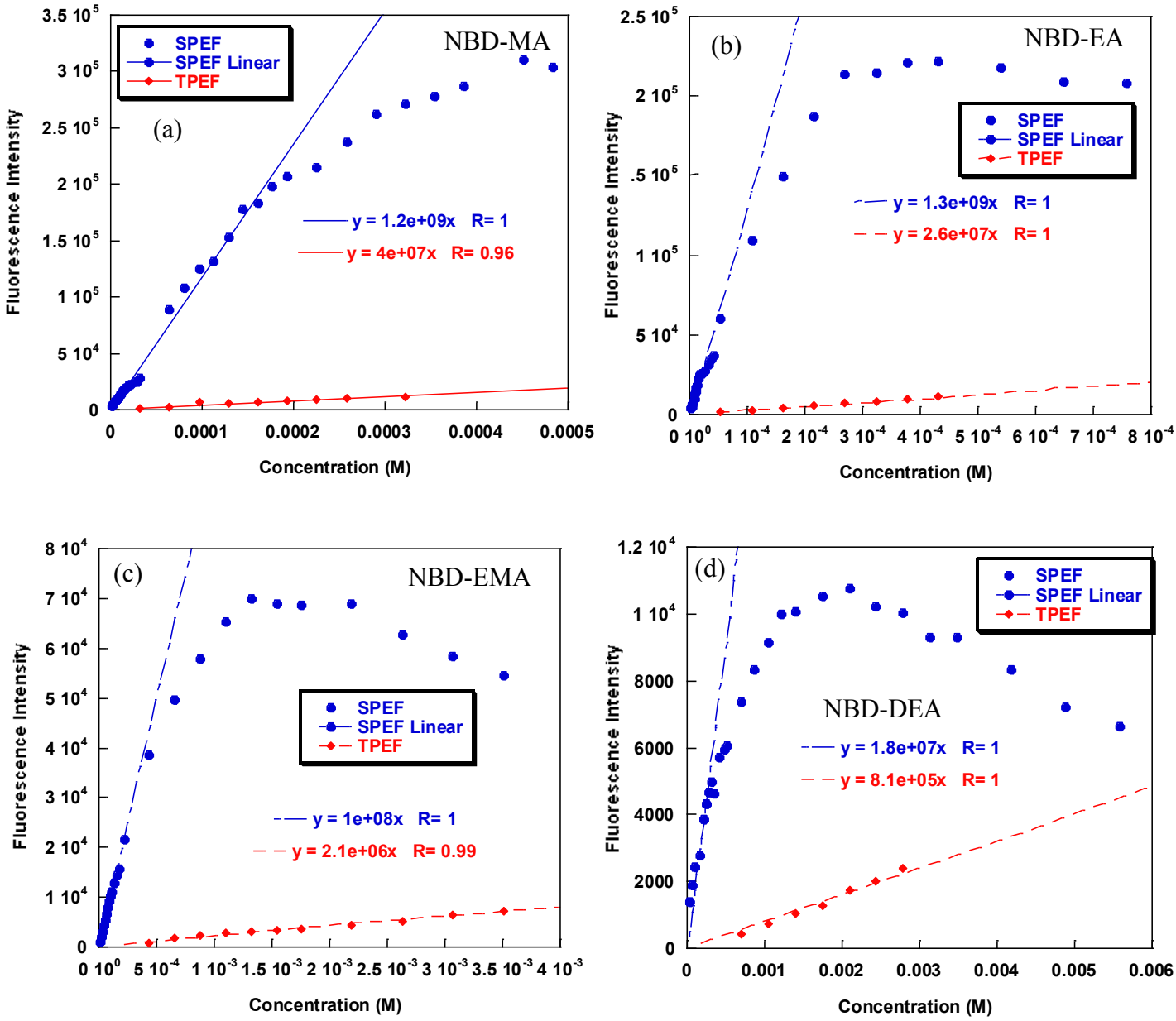

Figure 4.21. Relationship between fluorescence intensity and concentration of (a) NBD-methylamine in acetonitrile, (b) NBD-ethylamine in dichloromethane, (c) NBD-ethylmethylamine in dichloromethane and (d) NBD-diethylamine in dichloromethane, upon (blue circles) single photon excitation (387.5 nm) and (red circles) two photon excitation (775 nm) in 100% acetonitrile as the solvent.

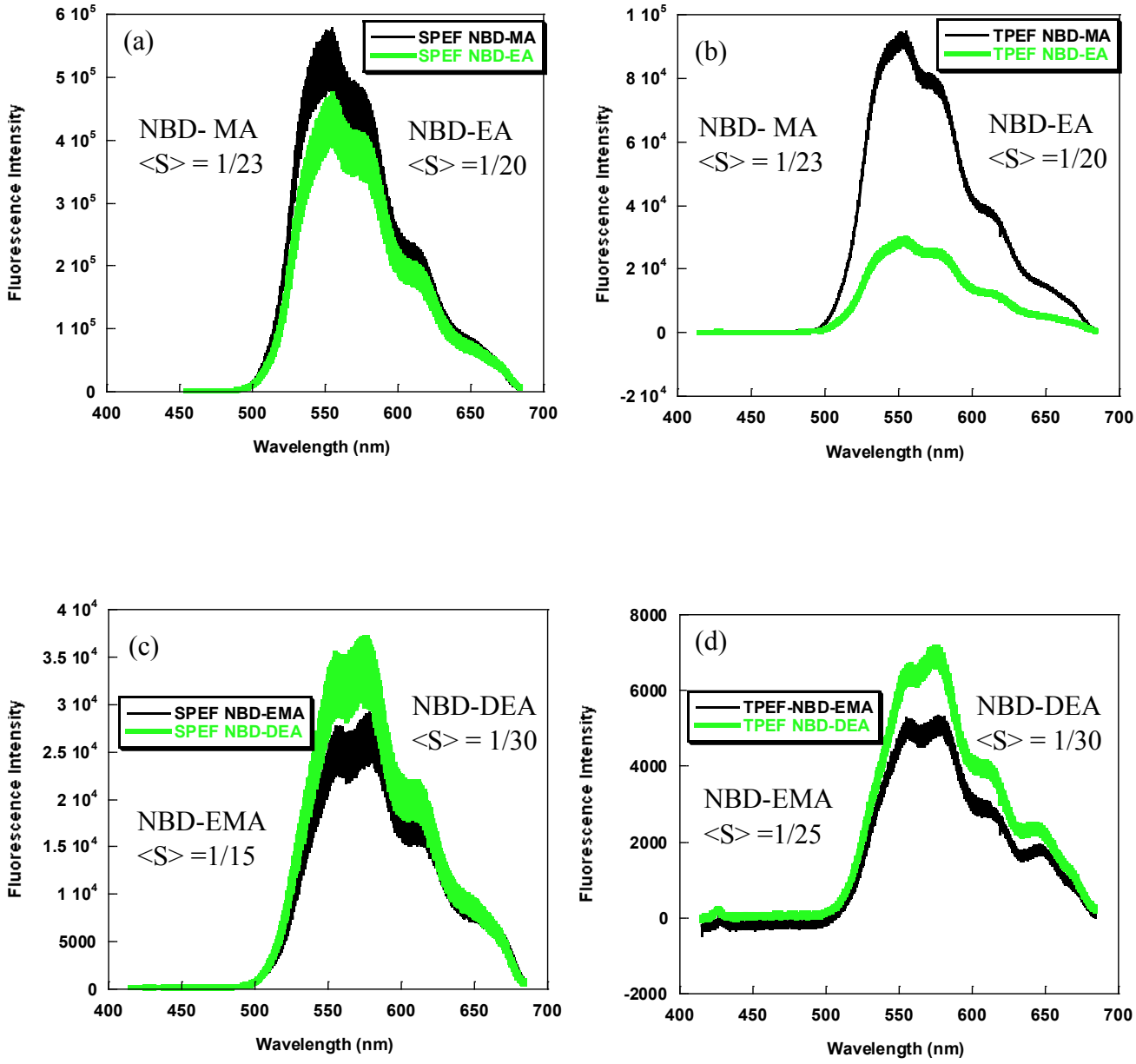

Figure 4.22 (a) SPEF and (b) TPEF spectra of NBD-methylamine (black line) and NBD-ethylamine (green line) incorporated in NaY at a loading level of, <S> = 1/23 and <S> = 1/20 respectively. (c) SPEF and (c) TPEF of NBD-ethylmethylamine (black line) and NBD-diethylamine (green line) in NaY, <S> = 1/15 and 1/30 respectively. (Note: TPEF spectra of NBD-ethymethylamine obtained at <S> = 1/25) SPEF and TPEF spectra obtained upon excitation at λ = 387.5 and 775 nm, respectively.

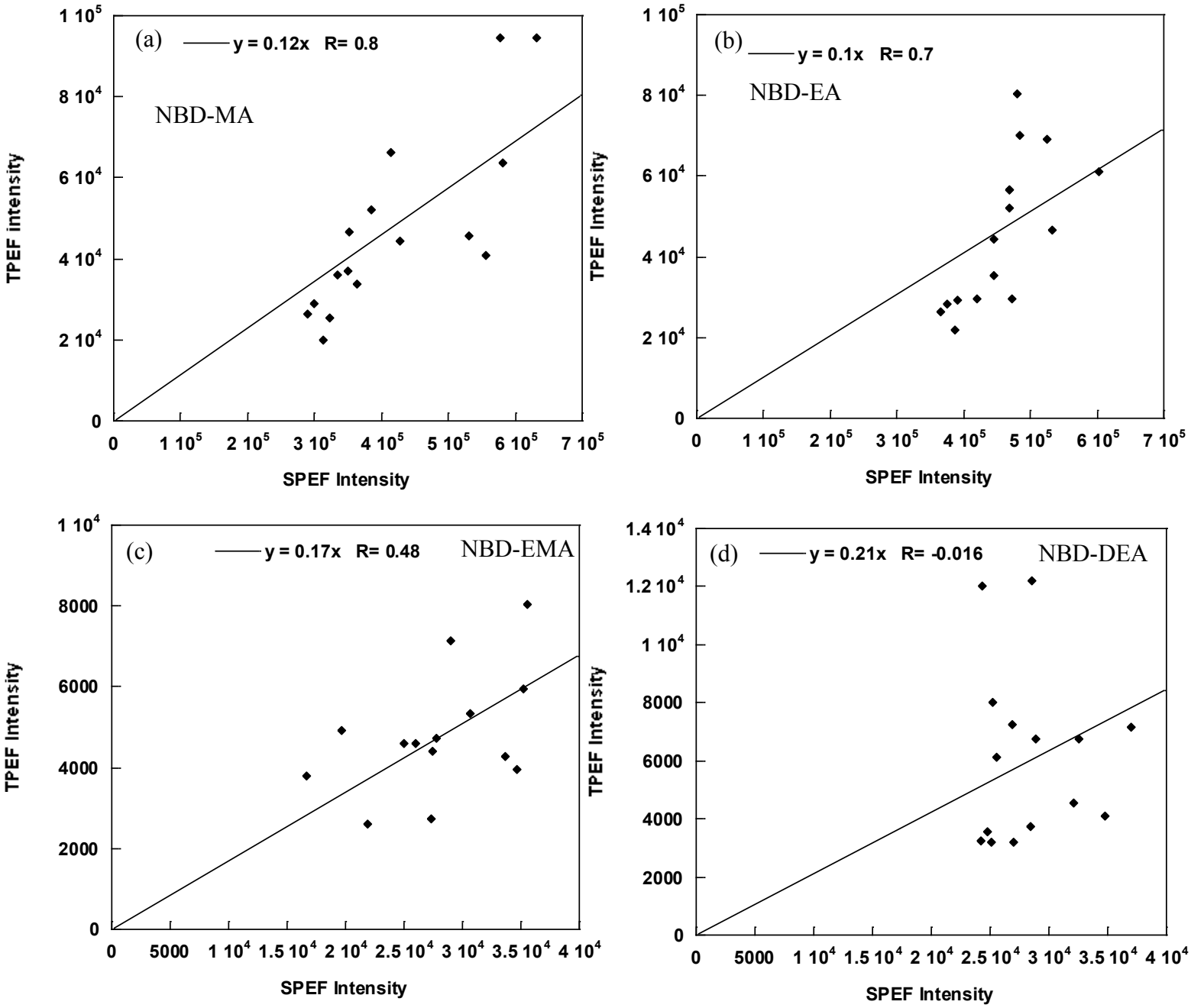

Figure 4.23. A plot of TPEF intensities vs SPEF intensities of (a) NBD-methylamine, (b) NBD-ethylamine, (c) NBD-ethylmethylamine and (d) NBD-diethylamine obtained from their respective spectra, in NaY at various loading levels <S>. SPEF spectra obtained upon excitation at 387.5 nm and TPEF spectra obtained upon excitation at 775 nm. The slope is the ratio of two photon: one photon.

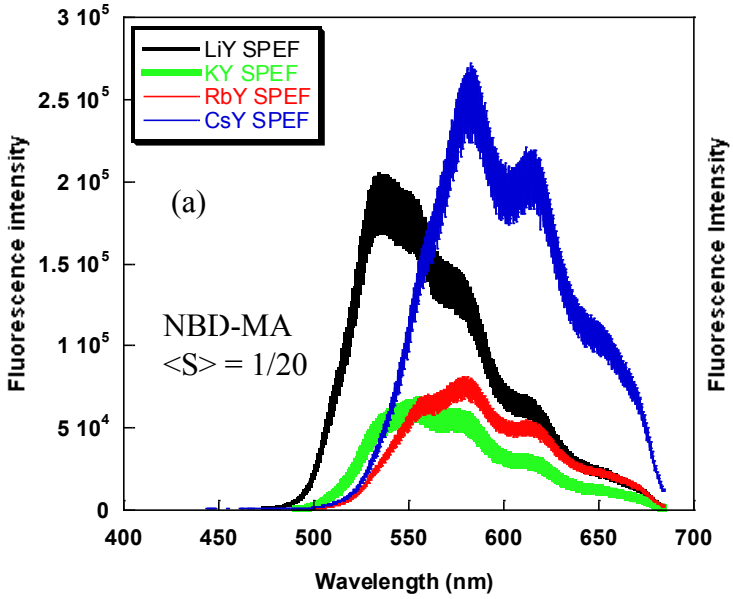
LiY SPEF
KY SPEF
RbY SPEF
CsY SPEF
(a)
NBD-MA
<S> = 1/20
Fluorescence intensity
Wavelength (nm)

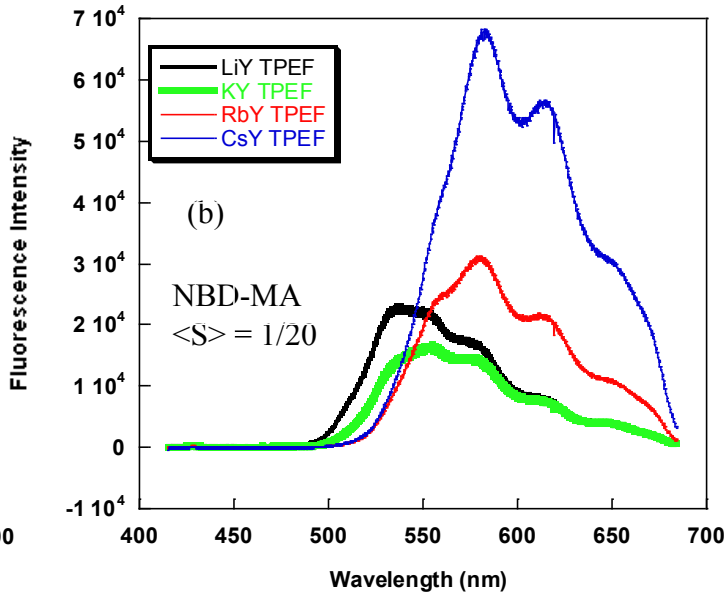
LiY TPEF
KY TPEF
RbY TPEF
CsY TPEF
(b)
NBD-MA
<S> = 1/20
Fluorescence Intensity
Wavelength (nm)

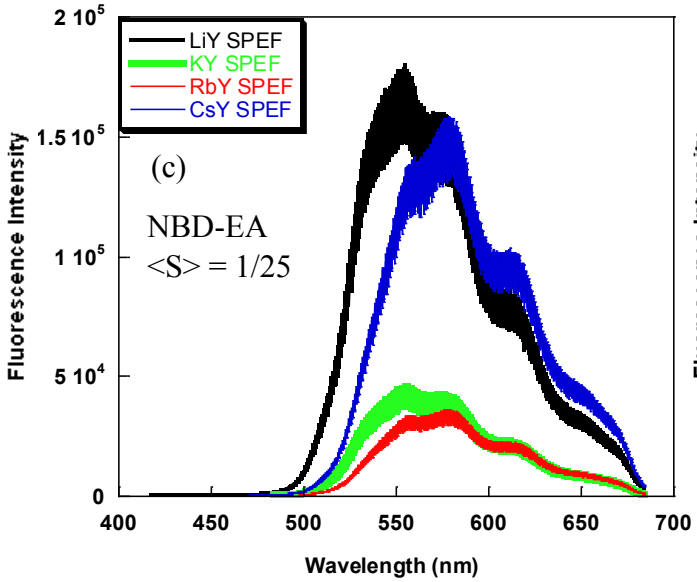
LiY SPEF
KY SPEF
RbY SPEF
CsY SPEF
(c)
NBD-EA
<S> = 1/25
Fluorescence Intensity
Wavelength (nm)

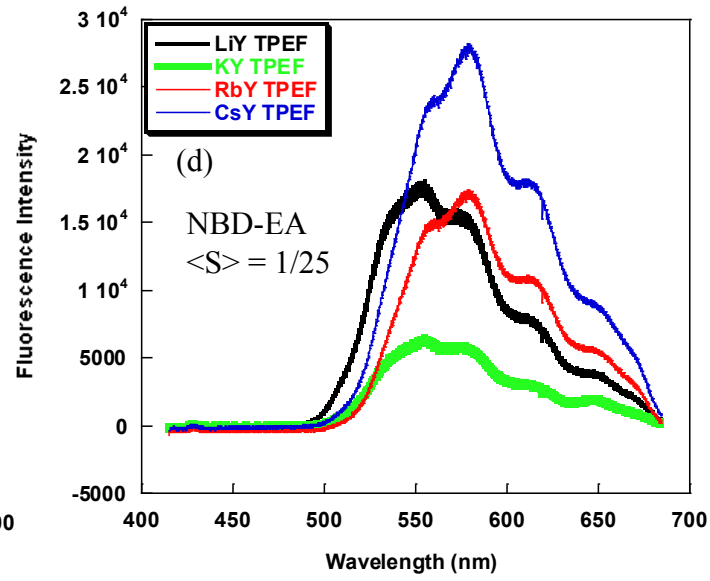
LiY TPEF
KY TPEF
RbY TPEF
CsY TPEF
(d)
NBD-EA
<S> = 1/25
Fluorescence Intensity
Wavelength (nm)

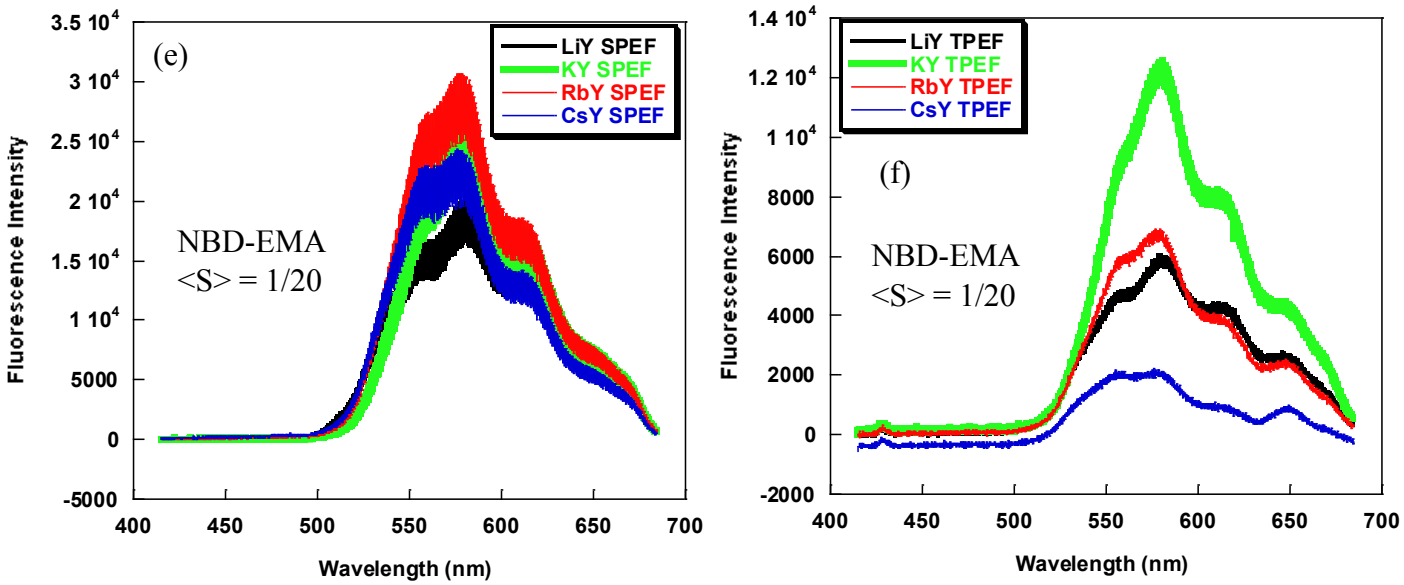

Figure 4.24. (a) SPEF and (b) TPEF spectra of NBD-methylamine incorporated in LiY (black line), KY (green line), RbY (red line) and CsY (blue line) at an experimental loading level of <S> = 1/20 for all zeolites. (c) SPEF and (d) TPEF spectra of NBD-ethylamine in LiY (black line), KY (green line), RbY (red line) and CsY (blue line), <S> = 1/25 for all zeolites. (e) SPEF and (f) TPEF spectra of NBD-ethylmethylamine in LiY (black line), KY (green line), RbY (red line) and CsY (blue line), <S> = 1/20 for all zeolites. SPEF and TPEF spectra obtained upon excitation at λ = 387.5 and 775 nm, respectively.

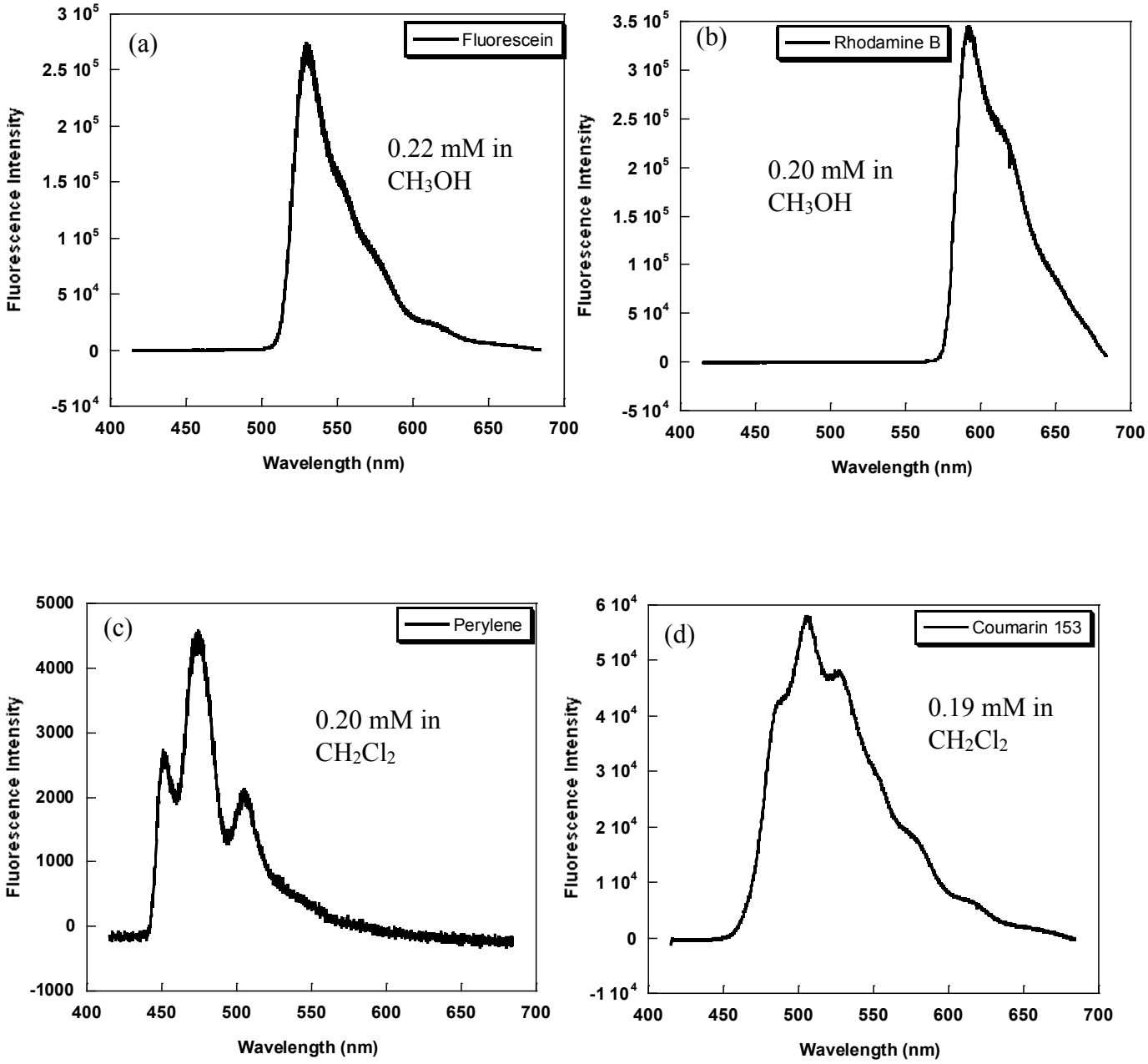

Figure 4.25. TPEF spectra of (a) 2.19 x 10^{-4} M fluorescein (b) 1.98 x 10^{-4} rhodamine B in methanol. (c) 2.04 x 10^{-4} M perylene and (d) 1.89 x 10^{-4} M coumarin 153 in dichloromethane. TPEF spectra obtained upon excitation at $\lambda = 775$ nm.

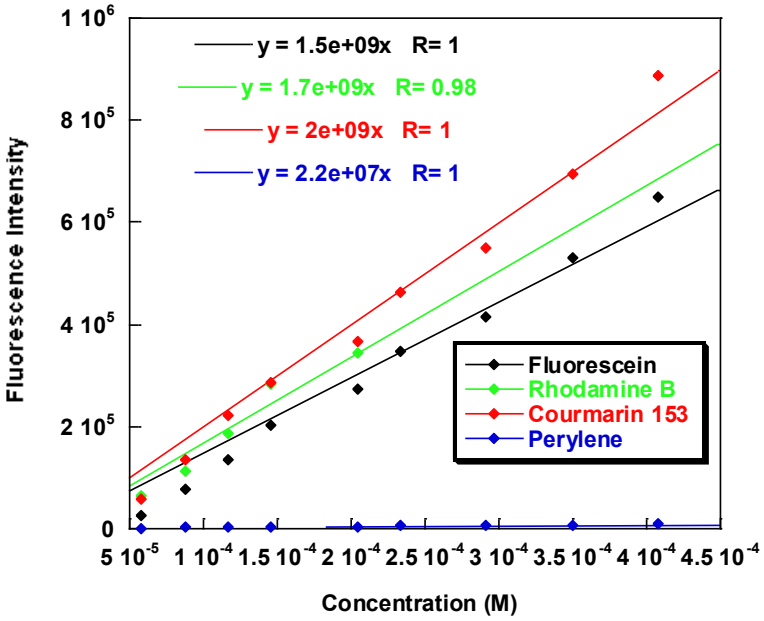

Figure 4.26. A TPEF calibration plot showing the relationship between fluorescence intensity and concentration of fluorescein (black line), rhodamine b (green line) in methanol, coumarin 153 (red line) and perylene (blue line) in dichloromethane. TPEF spectra obtained upon excitation at λ = 775 nm.

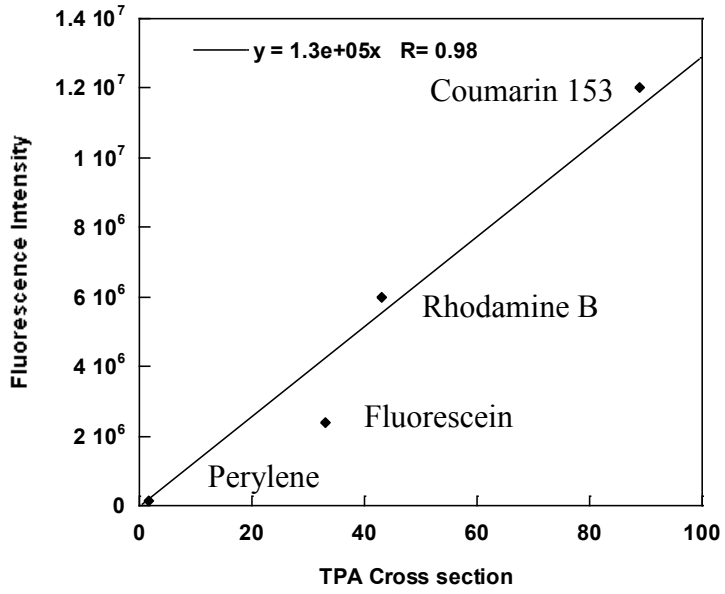

Figure 4.27. A TPEF calibration plot showing the relationship between fluorescence intensity and TPA cross-section (σ) of the four reference compounds at 0.006 M (perylene and fluorescein in dichloromethane, and fluorescein and rhodamine B in methanol) . The TPEF intensities is obtained at 0.006 M using the slope generated from the respective plot in Figure 4.26.

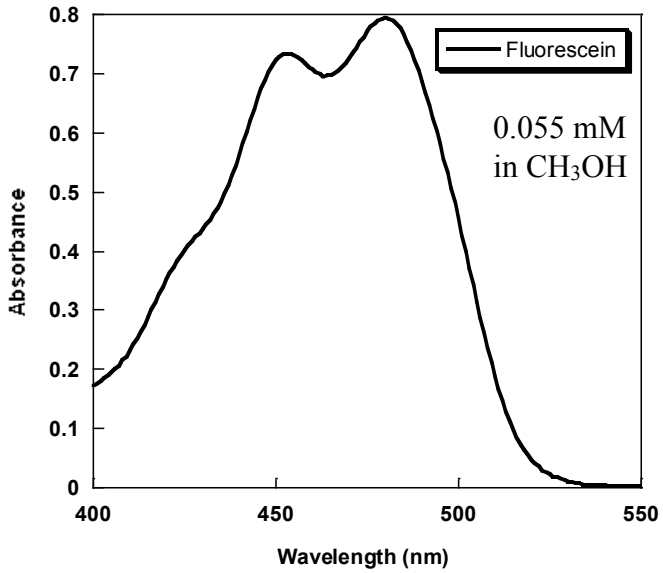

Figure 4.28. UV-vis spectrum of 5.48 x 10^{-5} M fluorescein in methanol.

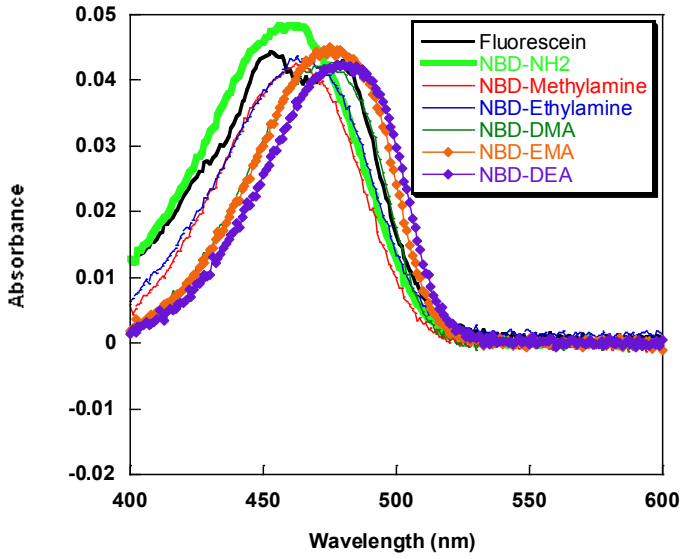

Figure 4.29. UV-vis spectra of 4.07 x 10^{-7} M fluorescein (black line), 3.86 x 10^{-6} M NBD-NH2 (bright green line), 4.52 x 10^{-6} M NBD- methylamine (red line) and 4.27 x10^{-6} M NBD-ethylamine (blue line) in methanol , 3.37 x10^{-6} M NBD-dimethylamine (light green line), 1.20x10^{-4} M NBD-ethylmethylamine (orange square) and 1.17 x 10^{-4} M NBD-diethylamine in dichloromethane. The absorbance of all 7 compounds between 0.04 -0.05 for the purpose of quantum yield determination.

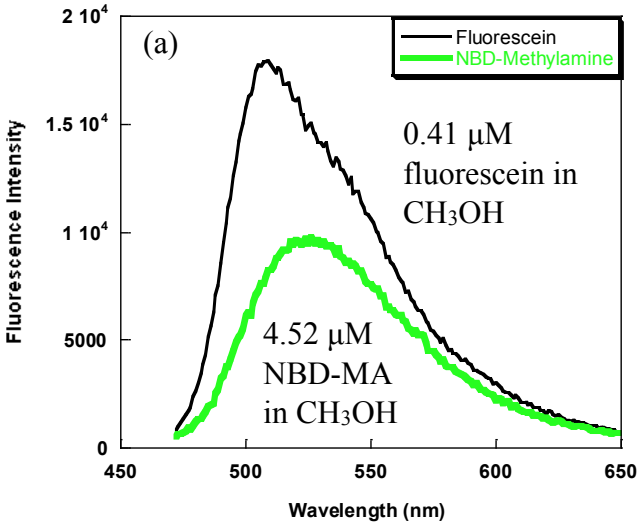
(a)
Fluorescein
NBD-Methylamine
0.41 µM
fluorescein in
CH3OH
4.52 µM
NBD-MA
in CH3OH
Fluorescence Intensity
Wavelength (nm)
2 10^4
1.5 10^4
1 10^4
5000
0
450
500
550
600
650

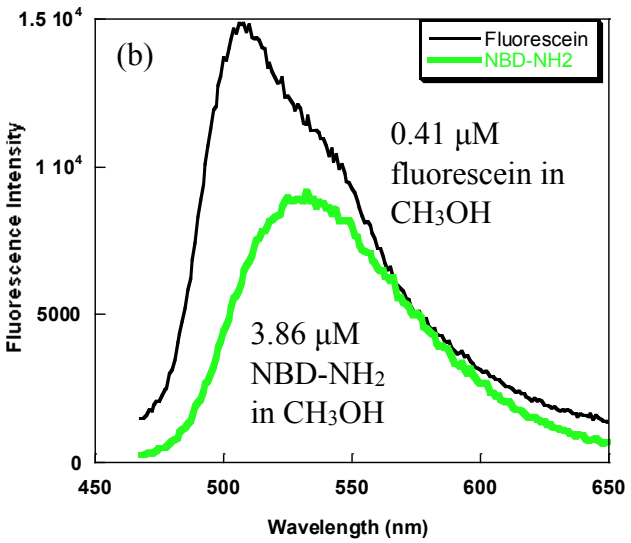
(b)
Fluorescein
NBD-NH2
0.41 µM
fluorescein in
CH3OH
3.86 µM
NBD-NH2
in CH3OH
Fluorescence Intensity
Wavelength (nm)
1.5 10^4
1 10^4
5000
0
450
500
550
600
650

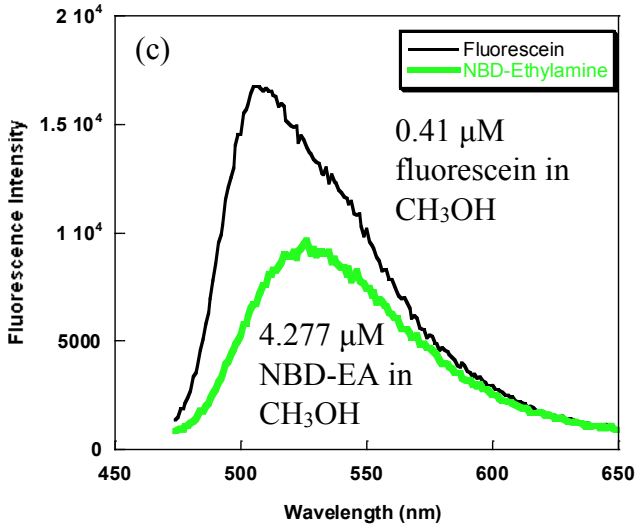
(c)
Fluorescein
NBD-Ethylamine
0.41 µM
fluorescein in
CH3OH
4.277 µM
NBD-EA in
CH3OH
Fluorescence Intensity
Wavelength (nm)
2 10^4
1.5 10^4
1 10^4
5000
0
450
500
550
600
650

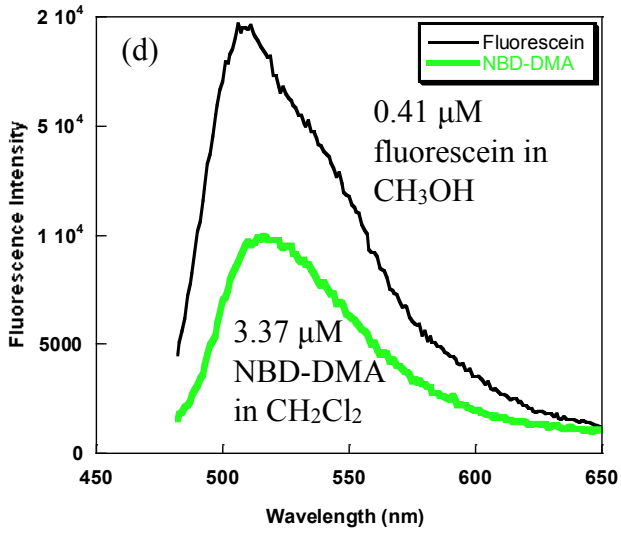
(d)
Fluorescein
NBD-DMA
0.41 µM
fluorescein in
CH3OH
3.37 µM
NBD-DMA
in CH2Cl2
Fluorescence Intensity
Wavelength (nm)
2 10^4
5 10^4
1 10^4
5000
0
450
500
550
600
650

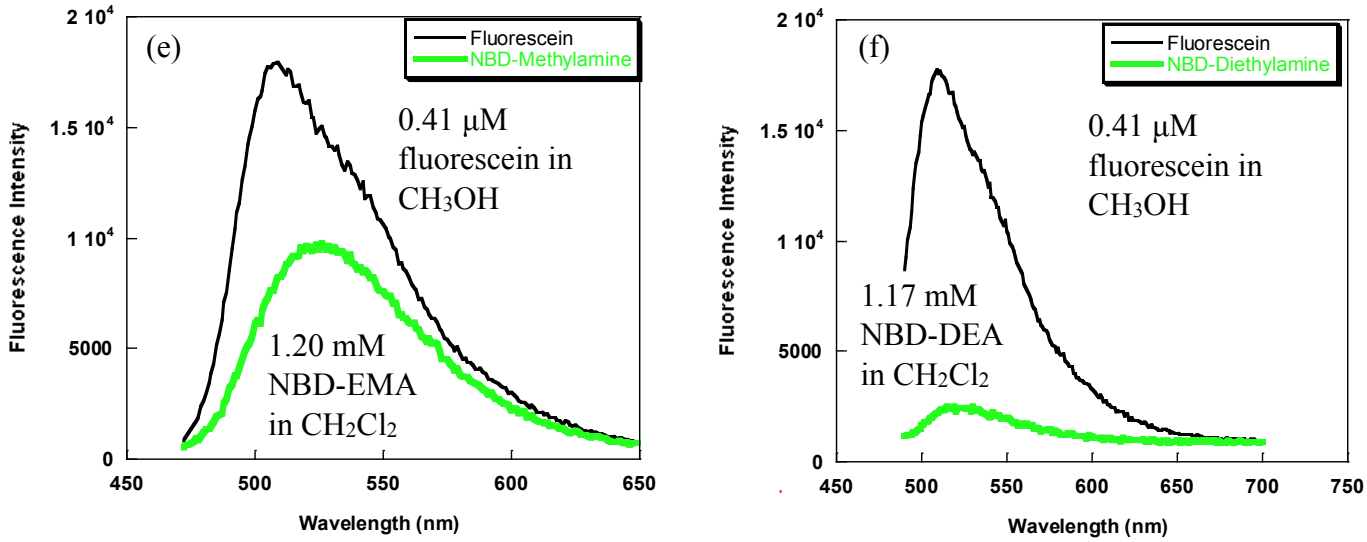

Figure 4.30. Fluorescence spectra of (a) 4.07 x 10^{-7} M fluorescein (black line) and 4.52 x 10^{-6} M NBD- methylamine (green line) in methanol, excitation wavelength, λ = 462 nm (b) 4.07 x 10^{-7} M fluorescein (black line) and 3.86 x 10^{-6} M NBD-NH_2 (green line) in methanol, excitation wavelength, λ = 458 nm. (c) 4.07 x 10^{-7} M fluorescein (black line) and 4.27 x10^{-6} M NBD-ethylamine (green line) in acetonitrile, excitation wavelength, λ = 464 nm. (d) 4.07 x 10^{-7} M fluorescein (black line) in methanol and 3.37 x10^{-6} M NBD-dimethylamine in dichloromethane, excitation wavelength, λ= 472 nm. (e) 4.07 x 10^{-7} M fluorescein (black line) in methanol and 1.20x10^{-4} M NBD-ethylmethylamine in dichloromethane (green line) in dichloromethane, excitation wavelength, λ = 475 nm. (f) 4.07 x 10^{-7} M fluorescein (black line) in methanol and 1.17 x 10^{-4} M NBD-diethylamine in dichloromethane, excitation wavelength, λ = 480 nm. (Note: for quantum yield determination, the standard and the unknown are usually excited with the same wavelength. The λ_{max} of absorption for the respective NBD- chromophore was chosen as the excitation wavelength.

Chapter 5: Conclusion

A summary of the results obtained from the investigation of two-photon excitation properties of the dipolar NBD-chromophores in solution and in zeolites has been provided in Table 5.1.

Table 5.1. Overall summary of the results obtained for different analogues of NBD-chromophores in solution and in zeolites.

Substitution Pattern of Amine	λ_{max} Absorbance (nm)	TPA Cross Section (σ)	Average 2P:1P (Solution)	Average 2P:1P (NaY)	Enhancement Factor
H-N-H	447	1.40	0.020	0.036	2
H-N-CH_3	460	1.20	0.033	0.12	3
H-N-C_2H_5	461	0.94	0.019	0.10	5
CH_3-N-CH_3	478	0.41	0.028	0.17	6
CH_3-N-C_2H_5	480	0.35	0.020	0.17	8
C_2H_5-N-C2H_5	484	0.23	0.045	0.22	5

The results obtained through this investigation show that the optical properties of the dipolar NBD-chromophores are sensitive to solvent polarity. In Table 4.1 and 4.5, it was shown that the λ_{max} for absorption and emission of the NBD- chromophores were red-shifted in more polar solvents. The red-shifting was attributed to the enhanced charge redistribution between the donor and the acceptor substituents upon excitation, a phenomenon that is considered to be of importance in terms of the ability of the organic chromophore to demonstrate superior TPA activity.[2,4,24,25] However, the results have also shown that enhanced charge redistribution between donor and acceptor substituents within the molecules does not necessarily result in superior TPA

properties as there are other factors that have to be considered, such as hydrogen bonding interactions, the substitution pattern and the substituents attached to the donor amine and the emission properties.

The SPEF and TPEF intensities of the NBD-chromophore were observed to be lower in Figure 4.2 and 4.10 in water, the most polar solvent. The relatively low intensities was attributed to a hydrogen bonding interactions between the lone pair of amine and water (Scheme 4.2), which restricts the charge redistribution between donor and acceptor and thus results in poor emission properties.[28] Interactions between methanol and ethanol and the chromophore have also been reported in the literature, which explains the lower SPEF and TPEF intensities observed in methanol and ethanol in compared to in dichloromethane, a less polar solvent.[17] Solvent polarity seemed to have a similar influence on the overall single-photon excitation and two-photon excitation properties of the NBD-chromophores, as similar 2P:1P ratios in the range of 0.01-0.03 were observed for NBD-DMA and NBD-NH_2 in solvents with varying polarity, Table 4.2 and Table 4.6.

A second factor that was observed to influence the photophysics of the NBD-derivatives was the substitution pattern of the donor amine. The λ_{max} for absorption was observed to be red-shifted as the donor amine of the NBD-derivative became more substituted. Likewise, NBD-derivatives with unsubstituted and *N*-alkylated amines emitted superior SPEF and TPEF intensities in solution and in zeolites, compared to the NBD-derivatives consisting of *N,N*-dialkylsubstituted amine.

The TPA cross-section (σ) determined for all six NBD-analogues was observed to decrease as the amine became more sterically substituted. The decrease in the TPA cross section (σ) was attributed to allylic 1,3- strain which may force the NBD derivatives with bulkier groups

to adopt a geometry that is not ideal for two-photon absorption.[28,29] As was the case with the solvent polarity, the nature of substitution seemed to have an equal overall effect on the SPE and TPE properties of the NBD-chromophores in solution as a similar 2P:1P ratio in the range of 0.02-0.04 was observed.

In contrast to solution, the 2P:1P ratio for NBD-chromophores was observed to vary in Y zeolites, with the ratio getting bigger as the donor amine of the NBD-chromophore became more substituted. As a result, the enhancement factor, or the degree to which the zeolite enhanced two-photon absorption, tended to increase with increasing substitution on the nitrogen of the amine, starting at 2 for NBD-NH_2 and peaking at 8 for NBD-EMA. The increase in the enhancement factor in zeolites was also consistent with the red-shifting of the λ_{max} of absorption for the NBD-analogues, which suggests that factors that cause red-shifting in absorption maxima also play a role in determining the effectiveness by which the zeolite can enhance two-photon absorption.[28,29] Overall TPEF enhancement is observed for NBD-chromophores in Y zeolites and despite emitting modest SPEF and TPEF intensity, a larger 2P:1P ratio and greater TPEF enhancement is observed for the NBD-derivatives consisting of *N,N*-dialkylsubstituted amine.

Overall, the main goal of the work was to investigate whether the polar and restrictive environment of the zeolite influenced the two-photon excitation efficiency of the dipolar NBD-chromophores. From the results obtained, it can be concluded that analogues of dipolar NBD-chromophore undergo significant TPEF enhancement relative to solution within the Y zeolite framework.

References

1. Göppert-Mayer, M. *Ann. Phys*. **1931**, *401*, 273-294.

2. Pawlicki, M.; Collins, H.A.; Dennings, R.G.; Anderson, H. L. *Angew. Chem. Int. Ed*. **2009**, *48*, 3244-3266.

3. So, P. T. C.; Dong, C. Y.; Masters, B. R.; Berland, K. M. *Annu. Rev. Biomed. Eng*. **2000**, *02*, 399-429.

4. Franken, P. A.; Hill, A. E.; Peters, C. W.; Weinrich, G. *Phys. Rev. Lett*. **1961**, *7*, 118-119.

5. Kaiser, W.; Garrett, C. G. B. *Phys. Rev. Lett*. **1961**, *7*, 229-231.

6. Zipfel, W. R.; Williams, R. M.; Webb, W. W. *Nat. Biotechnol*. **2003**, *21*, 1369-1377.

7. Helmchen, F.; Denk, W. *Nat. Methods*. **2005**, *2*, 932-940.

8. Kawata, S.; Kawata, Y. *Chem. Rev*. **2000**, *100*, 1777-1788.

9. LaFratta, C. N.; Fourkas, J. T.; Baldacchini, T.; Farrer, R. A. *Angew. Chem. Int. Ed*. **2007**, *46*, 6238-6258.

10. Fisher, W. G.; Partridge Jr, W. P.; Dees, C.; Wachter, E. A. *Photochem. Photobiol*. **1997**, *66*, 141-155.

11. Rohati-Mukherjee, K. K. In *Fundamentals of Photochemistry*; Wiley Eastern Limited.: New Delhi, **1978**; pp 3-13.

12. Berezin, M. Y.; Achifelu, S. *Chem. Rev*. **2010**, *110*, 2641-2684.

13. Rohati-Mukherjee, K. K. In *Fundamentals of Photochemistry*: Wiley Eastern Limited.: New Delhi, **1978**; pp 137-140.

14. He, S.; Tan, L-S.; Zheng, Q.; Prasad, P. N. *Chem. Rev*. **2008**, *108*, 1245-1330.

15. Sheik-Bahae, M.; Said, A. A.; Wei, T.-H.; Hagan, D. J.; Van Stryland, E.W. *IEEEJ. Quantum Electron*. **1990**, *26*, 760-769.

16. Kim, G. Y.; Kwak, C. H. In *Simple Optical Methods for Measuring Optical Nonlinearities and Rotational Viscosity in Nematic Liquid Crystals*. Available from: http://www.intechopen.com/books/new-developments-in-liquid-crystals/simple-optical-methods-for-measuring-optical-nonlinearities-and-rotational-viscosity-in-nematic-liquid. (Retrieved December 2015).

17. Wang, H.; Zhang, Qio,; Zhang, J.; Li, L.; Zhang, Q.; Li, S.; Zhang, S.; Wu, J.; Tian, Y. *Dyes and Pigments*. **2014**, *102*, 263-272.

18. Corrêa, D. S.; Oliviera, S. L.; Boni, L. D.; Misoguti, L.; Zilio, S. C.; Mendonça, C. R. *Appl. Phys. Lett*. **2006**, *8*, 021911.

19. Xu, C.; Webb, W. W. *J. Opt. Soc. Am*. **1996**, *13*, 481-491.

20. Markarov, N. S.; Drobizhev, M.; Rebane, A. *Opt. Exp.* **2008**, *16*, 4029-4047.

21. Bort, G.; Gallavardin, T.; Ogden, D.; Dalko, P. I. *Angew. Chem. Int. Ed*. **2013**, *52*, 4526-4537.

22. Terenziani, F.; Katan, C.; Badaeva, E.; Tretiak, S.; Blanchard-Desce, M. *Adv. Mater*. **2008**, *20*, 4641-4678.

23. Ki, H. M.; Jung, C.; Kim, B.R.; Jung, S-Y.; Hong, J. H.; Ko, Y-G.; Lee. K. J.; Cho, B. R. *Angew. Chem. Int. Ed*. **2007**, *46*, 3460-3463.

24. Ehrlich, J. E.; Wu, X. L.; Lee, I.-Y. S.; Hu, Y.; Röckel, H.; Marder, S.R.; Perry, J. W. *Opt. Letter*. **1997**, *22*, 1843-1845.

25. Albota, M.; Beljonee, D.; Brédas, J.-L.: Ehrlich, J. E.; Fu, J.-Y.; Heikal, A. A.; Hess, S. E.; Kogej, T.; Levin, M. D.; Marder, S. R.; McCord-Maughon, D.; Perry, J. W.; Röckel, H.; Rumi, M.; Subramaniam, G.; Webb, W. W.; Wu, X.-L.; Xu, C. *Science*. **1998**, *281*, 1653.

26. Pond, S. J. K.; Rumi, M.; Levin, M. D.; Parker, T. C.; Beljonne, D.; Day, M. W.; Brédas, J.-L.; Marder, S. R.; Perry, J. W. *J. Phys. Chem. A*. **2002**, *106*, 11470-11480.

27. Reinhardt, B. A.; Brott, L. L.; Clarson, S. J.; Dillard, A. G.; Bhatt, J. C.; Kannan, R.; Yuan, L.; He, S. G.; Prasad, P. N. *Chem. Mater*. **1998**, *10*, 1863-1874.

28. Singha, S.; Kim, D.; Roy. B.; Sambasivan, S.; Moon, H.; Rao, A. S.; Kim, J. Y.; Joo, J.; Park, J. W.; Rhee, Y. M.; Wang, J.; Kim, K. H.; Shin, Y. H.; Jung, J.; Ahn, K. H. *Chem. Sci*. **2015**, *6*, 4335-4342.

29. Peng, T.; Yang, D. *Org. Lett*. **2010**, *12*, 496-499.

30. Peng, L. W.; Dantus, M.; Zewail,A. H.; Kemnitz, K.; Hicks, J. M.; Eisenthal, K. B. *J. Phys. Chem*. **1987**, *91*, 6162-6167.

31. Cazeau-Dubroca, C.; Lyazidi, S. A.; Cambou, P.; Peirigua, A.; Cazeau, P.; Pesquer, M. *J. Phys. Chem*. **1989**, *93*, 2347-2358.

32. Hoffman, R. W. *Chem. Rev*. **1989**, *89*, 1841-1860.

33. Grabowski, Z. R.; Rotkiewicz, K.; Rettig, W. *Chem. Rev*. **2003**, *103*, 3899-4031.

34. Luo, Y.; Norman, P.; Macak, P.; Ågren, H. *J. Phys. Chem. A*. **2000**, *104*, 4718-4722.

35. Wang, C. K.; Zhao, K.; Su, Y.; Yan, R.; Zhao, X.; Luo, Y. *J. Chem. Phys*. **2003**, *119*, 1208-1213.

36. Zhao, K.; Ferrighi, L.; Frediani, L.; Wang, C.-K.; Luo, Y. *J. Chem. Phys*. **2007**, *126*, 204509.

37. Virtra, R. Geotimes. Mineral Resource of the Month: Natural and Synthetic Zeolites. http://www.geotimes.org/june08/article.html?id=nn_zeolites.html#links. (Accessed December 11, 2015).

38. KMI Zeolite. http://www.kmizeolite.com/History.html. (Accessed December 15, 2015).

39. Davis, M. E. *Ind. Eng. Chem. Res*. **1991**, *30*, 1675-1683.

40. U. S. Geological Survey. http://minerals.usgs.gov/minerals/pubs/commodity/zeolites/. (Accessed December 11, 2015).

41. Davis, M. E.; Lobo, R. F. *Chem. Mater*. **1992**, *4*, 756-768.

42. Lobo, R. F. Introduction to the Structural Chemistry of Zeolites. In *Handbook of Zeolite Science and Technology*; Aurebach, S. M.; Carrado, K. A.; Dutta, P. K., Eds: Marcel Dekker Inc.: New York, 2003; pp 65-89.

43. Klinowski, J. *Chem. Rev*. **1991**, *91*, 1459-1479.

44. Yoon, K. B.; Huh, T. J.; Kochi, J. K. *J. Phys. Chem*. **1995**, *99*, 7042-7053.

45. Breck, D. W. *J. Chem. Educ*. **1964**, *41*, 678-689.

46. Loewenstein, W. *Amer. Mineral*. **1954**, *39*, 92.

47. Hashimoto, S. *J. Photochem. Photobiol. C.; Photochem. Rev*. **2003**, *4*, 19-49.

48. Sivaguru, J.; Natarajan, A.; Kaanumalle, L. S.; Shailaja, J.; Uppili, S.; Joy, A.; Ramamurthy, V. *Acc. Chem. Res*. **2003**, *36*, 509-521.

49. Ramamurthy, V.; Turro, N. J. *J. Inclus. Phenom. Mol*. **1995**, *21*, 239-282.

50. Hunger, M.; Brunner, E. *Mol. Sieves*. **2004**, *4*, 201-293.

51. Uppili, S.; Thomas, K. J.; Crompton, E. M.; Ramamurthy, V. *Langmuir.* **2000**, *16*, 265-274.

52. Ramamurthy, V.; Eaton, D. F.; Caspar, J. V. *Acc. Chem. Res*. **1992**, *37*, 299-307.

53. Yoon, K. B. *Chem. Rev*. **1993**, *93*, 321-339.

54. Thomas, K. J.; Ramamurthy, V. *Langmuir.* **1998**, *14*, 6687-6692.

55. Li, C.; Wu, Zii. Microporous Materials Characterized by Vibrational Spectroscopies. In *Handbook of Zeolite Science and Technology*; Aurebach, S. M.; Carrado, K. A.; Dutta, P. K., Eds: Marcel Dekker Inc.: New York, 2003; pp 423-513.

56. García, H. G.; Roth, H. D.; *Chem. Rev*. **2002**, *102*, 3947-4007.

57. Shailaja, J.; Lakshminarasimhan, P. H.; Pradhan, A. R.; Sunoj, R. B.; Jockusch, S.; Karthikeyan, S.; Uppili, S.; Chandrasekhar, J.; Turro, N. J.; Ramamurthy, V. J. *Phys. Chem. A*. **2003**, *107*, 3187-3198.

58. Kirschhok, C.; Fuess, H. *Zeolites*. **1996**, *17*, 381-388.

59. Fitch, A. N.; Jobic, H.; Renouprez, A. *J. Chem. Soc., Chem. Commun*. **1985**, *5*, 284-286.

60. Ma, J.; Dougherty, D. *Chem. Rev*. **1997**, *97*, 1303-1324.

61. Taft, R. W.; Anvia, F.; Gal, J.-F.; Walsh, S.; Capon, M.; Holmes, M. C.; Hosn, K.; Oloumi, G.; Vasanwala, R.; Yazdani, S. *Pure Appl. Chem*. **1990**, *62*, 17-23.

62. Gapeev, A.; Dunbar, R. C. *J. Am. Chem. Soc*. **2001**, *123*, 8360-8365.

63. Sivaguru, J.; Shailaja, J.; Ramamurthy, V. Organic Photochemistry within Zeolites: Selectivity through Confinement. In *Handbook of Zeolite Science and Technology*; Aurebach, S. M.; Carrado, K. A.; Dutta, P. K., Eds: Marcel Dekker Inc.: New York, 2003; pp 515-589.

64. Ramamurthy, V.; Sanderson, D. R.; Eaton, D. F. *J. Phys. Chem*. **1993**, *97*, 13380-13386.

65. Diffuse Reflectance, Theory and Applications. http://www.piketech.com/files/pdfs/DiffuseAN611.pdf. (Accessed March 20, 2016).

66. Alvaro, M.; Garcia, H.; Garcia, S.; Marquez, F.; Scaiano, J. C. *J. Phys. Chem. B*. **1997**, *101*, 3043-3051.

67. Heberer, H.; Kersting, H.; Matschiner, H. *J. Prakt. Chem*. **1985**, *327*, 487-504.

68. Boiocchi, M.; Boca, L. D.; Esteban-Gómez, D.; Fabbrizzi, L.; Licchelli, M.; Monzani, E. *Chem. Eur. J.* **2005**, *11*, 3097-3104.

69. Boulton, A. J.; Ghosh, P. B.; Katritzky, A. R. *J. Chem. Soc. (B).* **1966**, *10*, 1004-1011.

70. Heyne, B.; Beddie, C.; Scaiano, J. C. *Org. Biomol.Chem*. **2007**, *5*, 1454-1458.

71. Jacobsen, N. E. Advanced NMR Theory: NOESY and DQF COSY. In *NMR Spectroscopy Explained, Simplified Theory, Applications and Examples for Organic Chemistry and Structural Biology*; John Wiley & Sons Inc.: New Jersey, 2007; pp 408-426.

72. Sternhell, S. Rotation About Single Bonds in Organic Molecules. In *Dynamic Nuclear Magnetic Resonance Spectroscopy*; Jackman, L. M.; Cotton, F. A., Eds: Academic Press Inc.: New York, 1975; pp 163-196.

73. Crampton, M. R.; Isanbor, C.; Willett, C. *J. Can. Chem*. **2005**, *83*, 1222-1227.

74. Ferry-Forgues, S.; Lavabre, D. *J. Chem. Educ.* **1999**, *76*, 1260-1264.

75. Heller, C. A.; Henry, R. A.; McLaughlin, B. A.; Bliss, D. E. *J. Chem. Eng. Data*. **1974**, *19*, 214-219.

76. Dielectric Chart, University of Washington. http://depts.washington.edu/eooptic/linkfiles/dielectric_chart%5B1%5D.pdf. (Accessed February 28, 2016).

77. Rurack, K.; Spieles, M. *Anal. Chem*. **2011**, *83*, 1232-1242.

78. Seko, T.; Ogura, K.; Kawakami, Y.; Sugino, H.; Toyotama, H.; Tanaka, *J. Chem. Phys. Lett*. **1998**, *291*, 438-444.

^{1}H-NMR SPECTRA OF THE NBD- CHROMOPHORES.

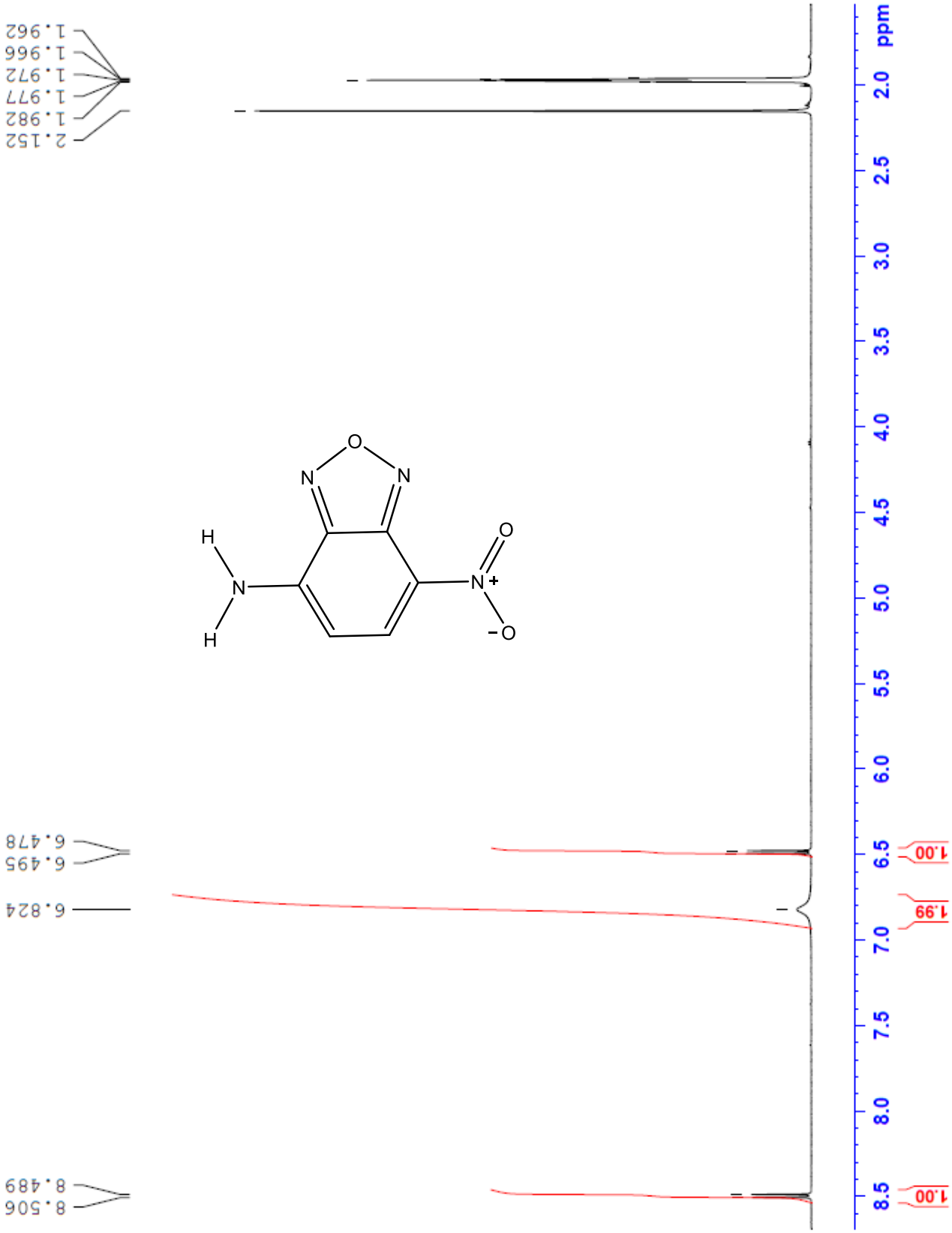
1.962
1.966
1.972
1.977
1.982
2.152
6.478
6.495
6.824
8.489
8.506
ppm
2.0
2.5
3.0
3.5
4.0
4.5
5.0
5.5
6.0
6.5
7.0
7.5
8.0
8.5
1.00
1.99
1.00
O
N
N
H
N
H
N+
O
-O

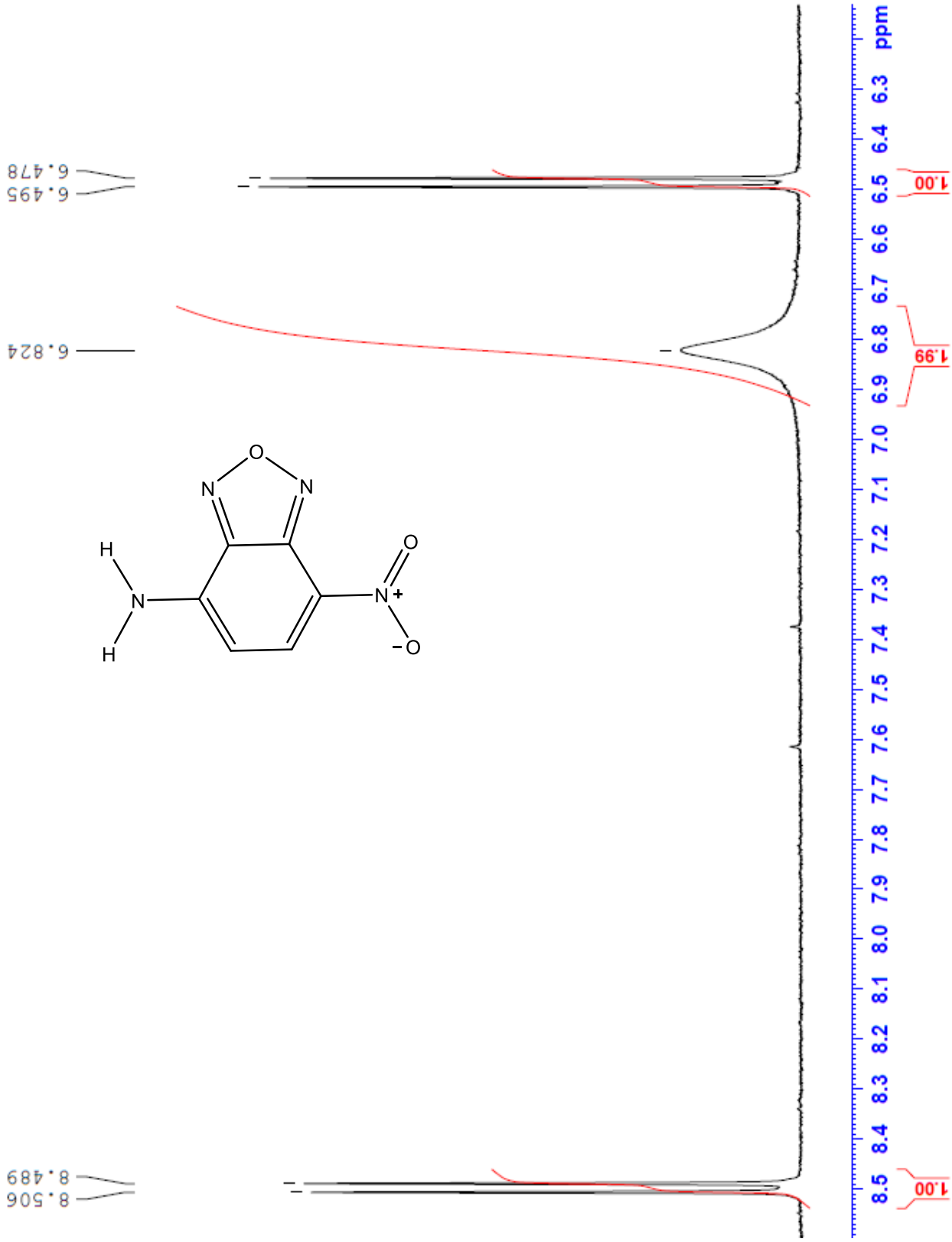
8.506
8.489
6.824
6.495
6.478
ppm
6.3
6.4
6.5
6.6
6.7
6.8
6.9
7.0
7.1
7.2
7.3
7.4
7.5
7.6
7.7
7.8
7.9
8.0
8.1
8.2
8.3
8.4
8.5
1.00
1.99
1.00
O
N
N
H
N
H
O
N+
O

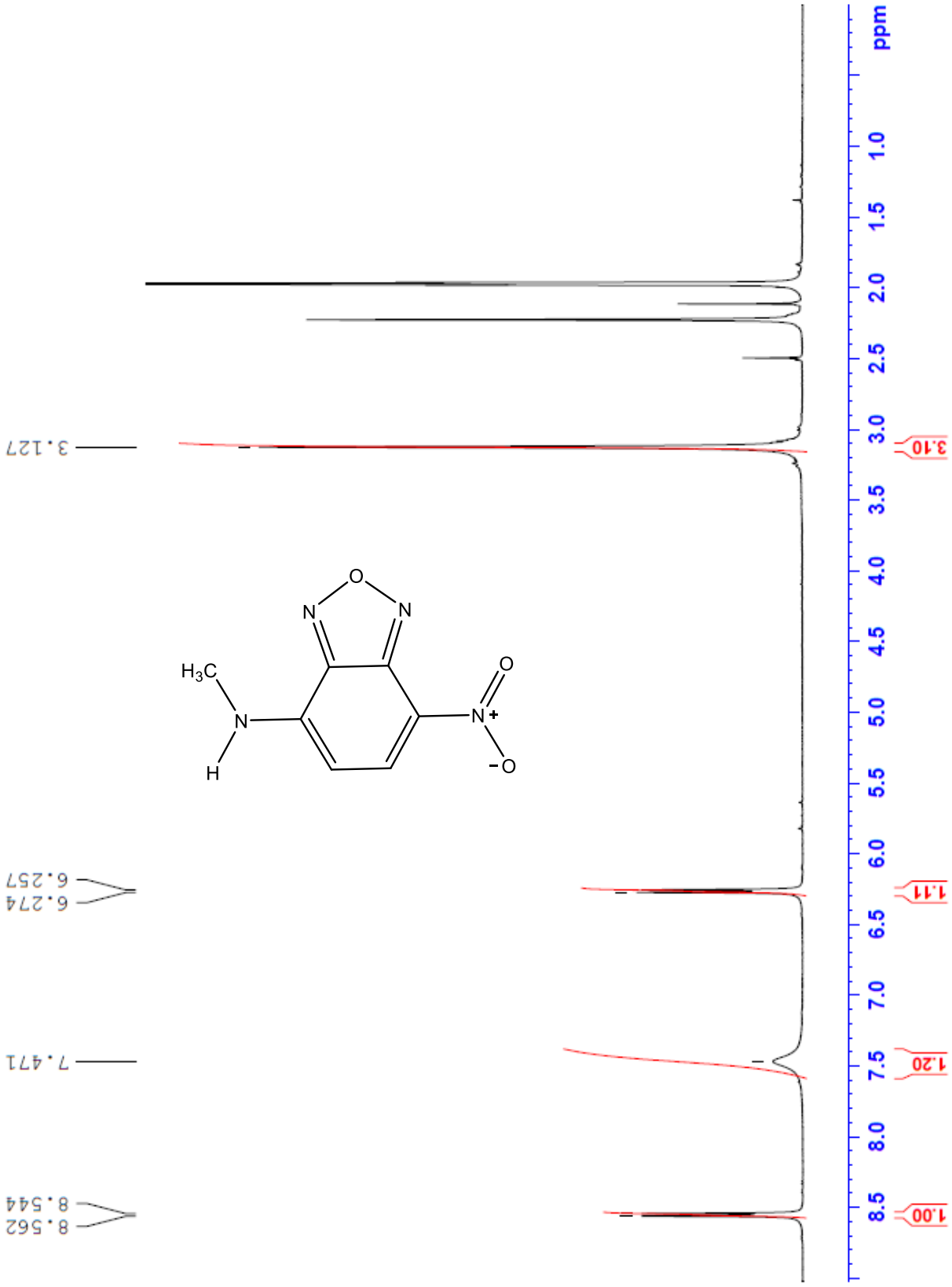
8.562
8.544
7.471
6.274
6.257
3.127
1.00
1.20
1.11
3.10
ppm
1.0
1.5
2.0
2.5
3.0
3.5
4.0
4.5
5.0
5.5
6.0
6.5
7.0
7.5
8.0
8.5
O
N
N
H3C
N
H
N+
O
-O

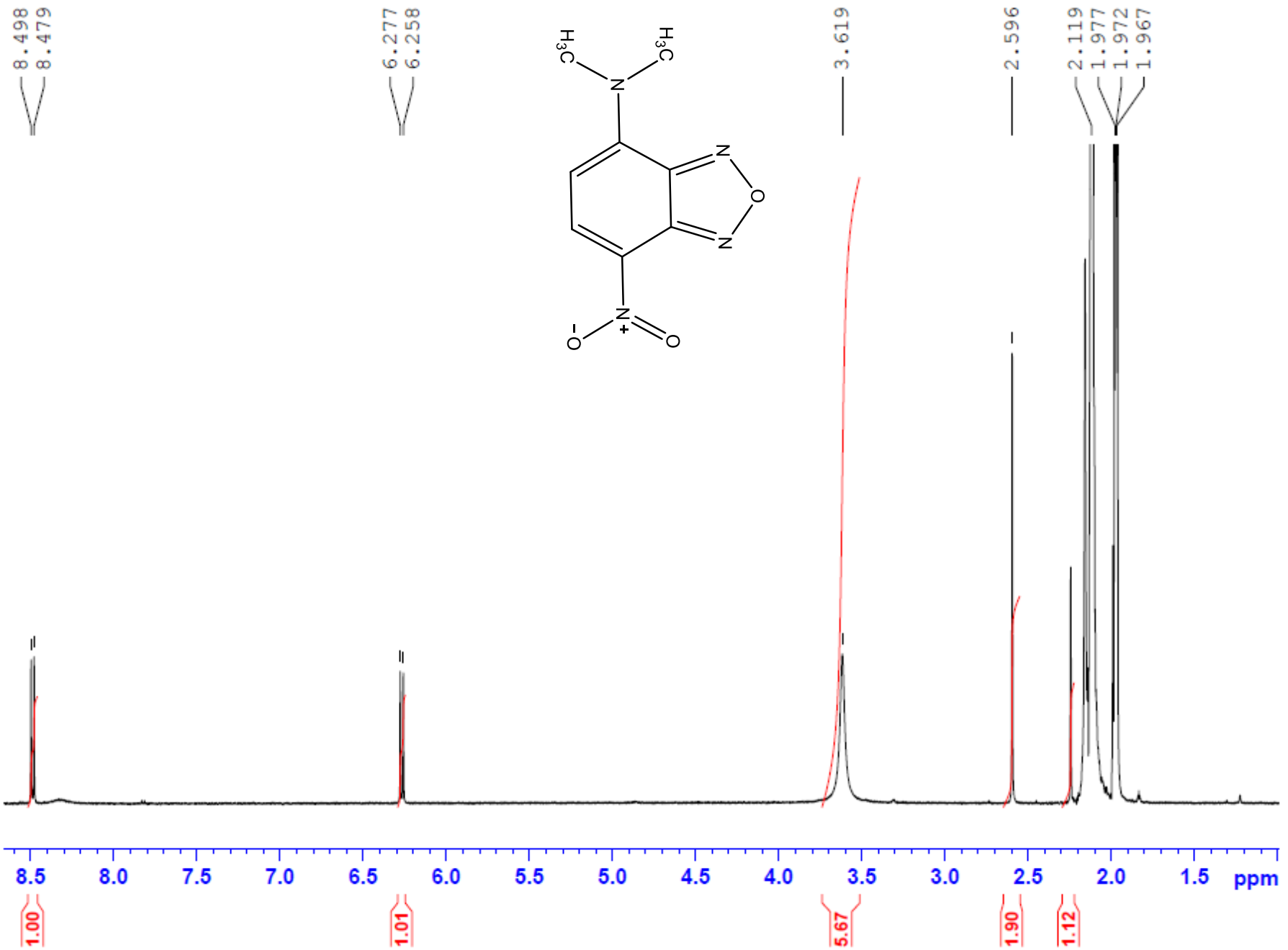
8.498
8.479
6.277
6.258
3.619
2.596
2.119
1.977
1.972
1.967
8.5
8.0
7.5
7.0
6.5
6.0
5.5
5.0
4.5
4.0
3.5
3.0
2.5
2.0
1.5
ppm
1.00
1.01
5.67
1.90
1.12

300 MHz Room temperature

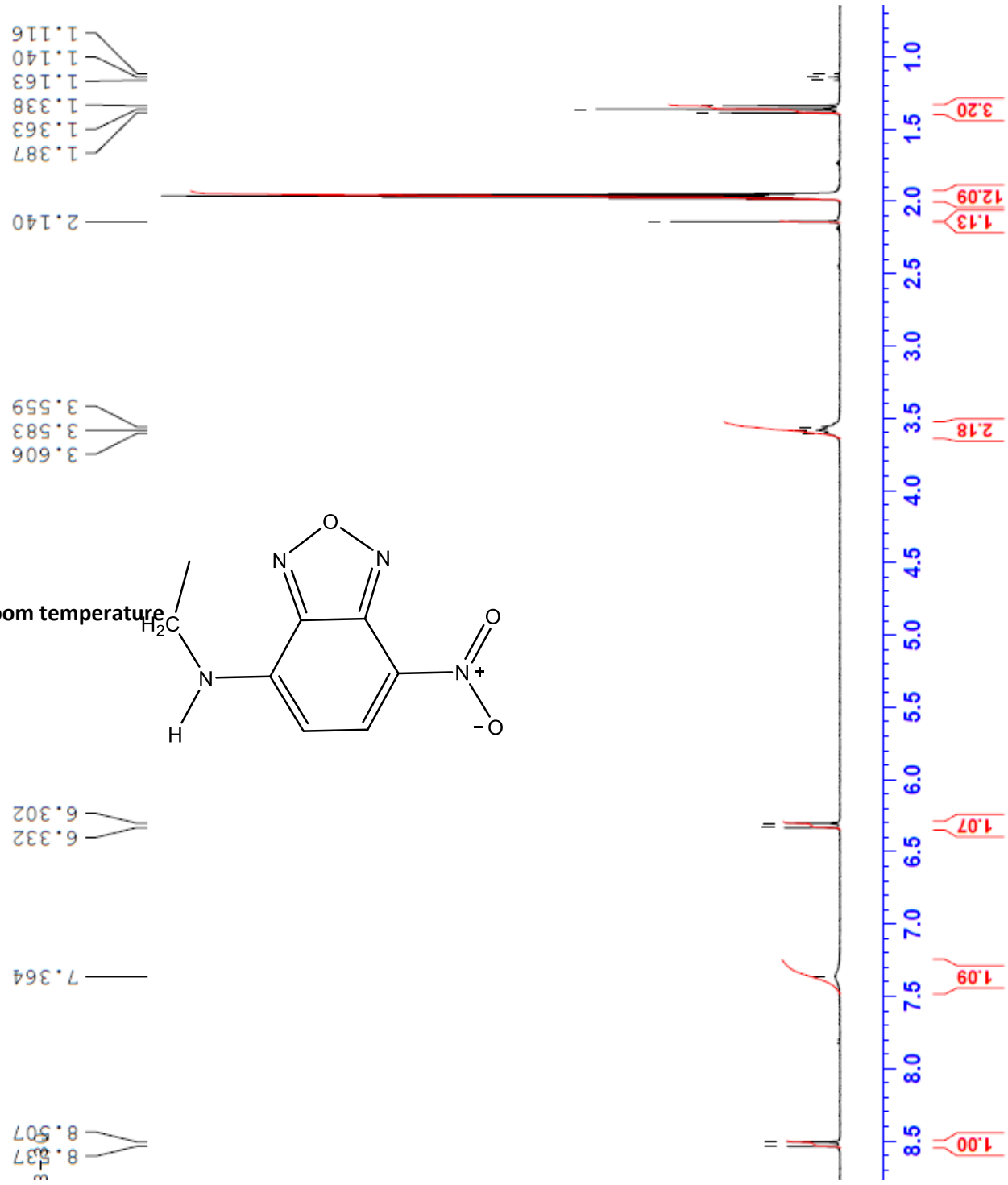

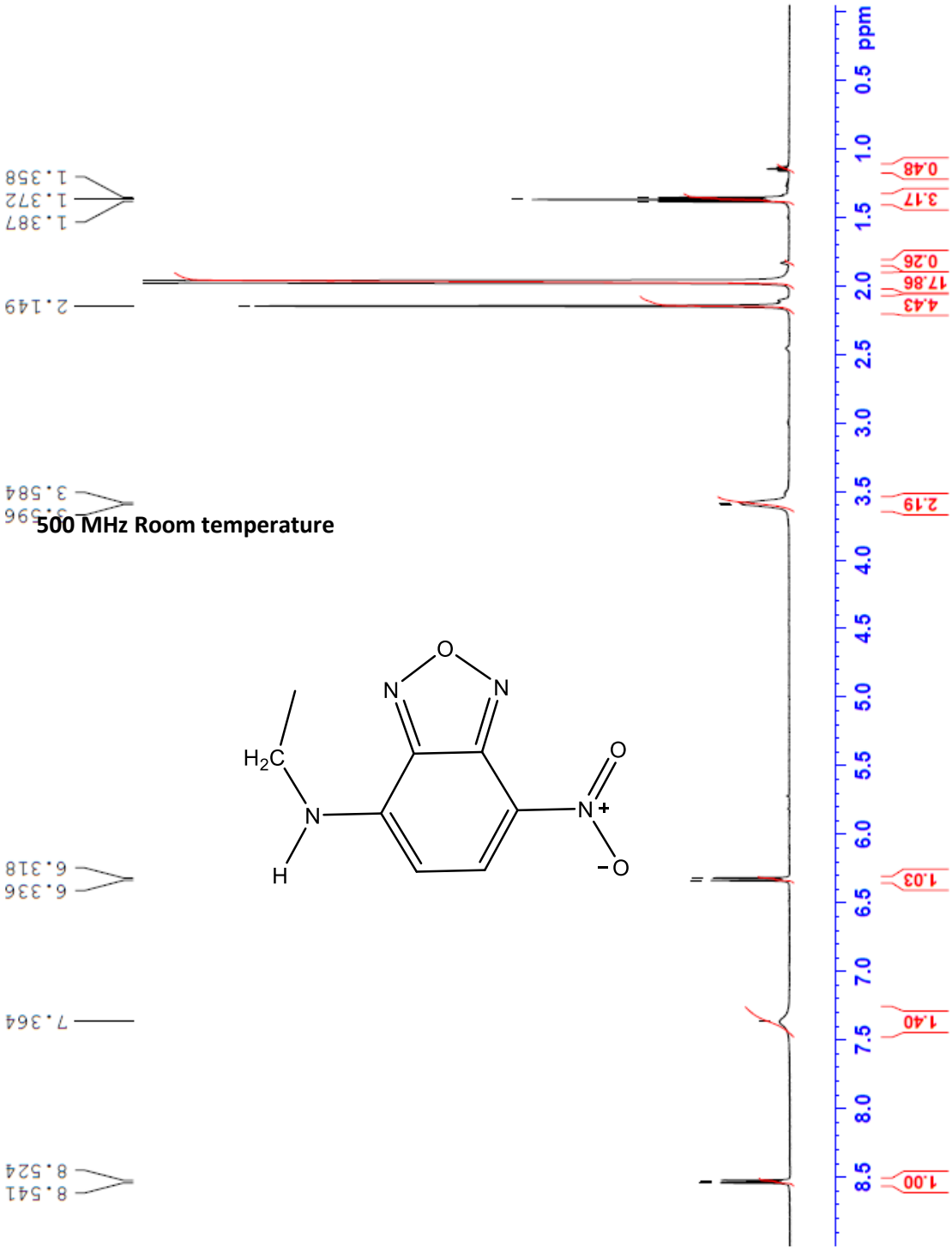

500 MHz Room temperature

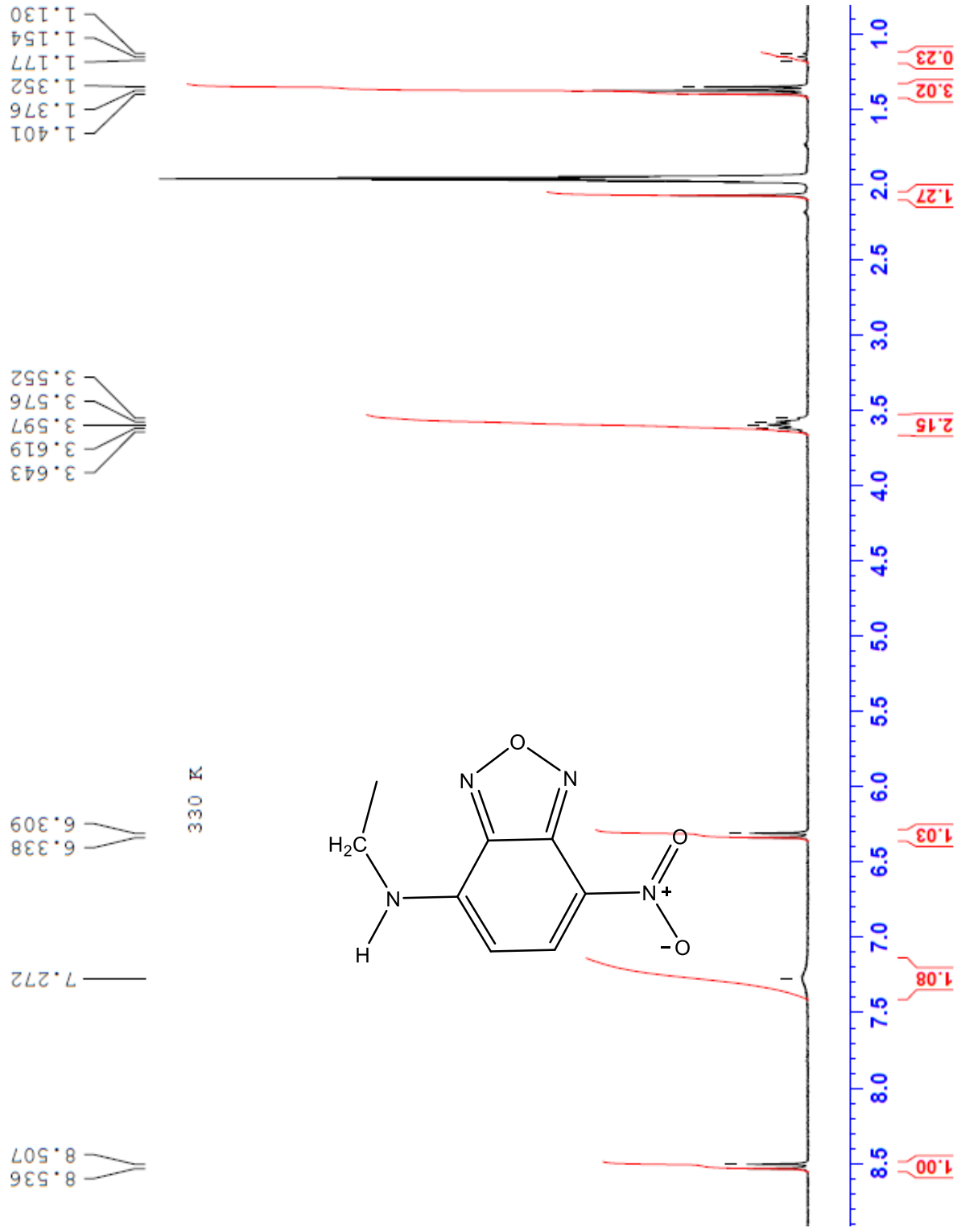
1.130
1.154
1.177
1.352
1.376
1.401
3.552
3.576
3.597
3.619
3.643
6.309
6.338
7.272
8.507
8.536
330 K
0.23
3.02
1.27
2.15
1.03
1.08
1.00
1.0
1.5
2.0
2.5
3.0
3.5
4.0
4.5
5.0
5.5
6.0
6.5
7.0
7.5
8.0
8.5
O
N
N
H2C
N
H
N+
O
-O

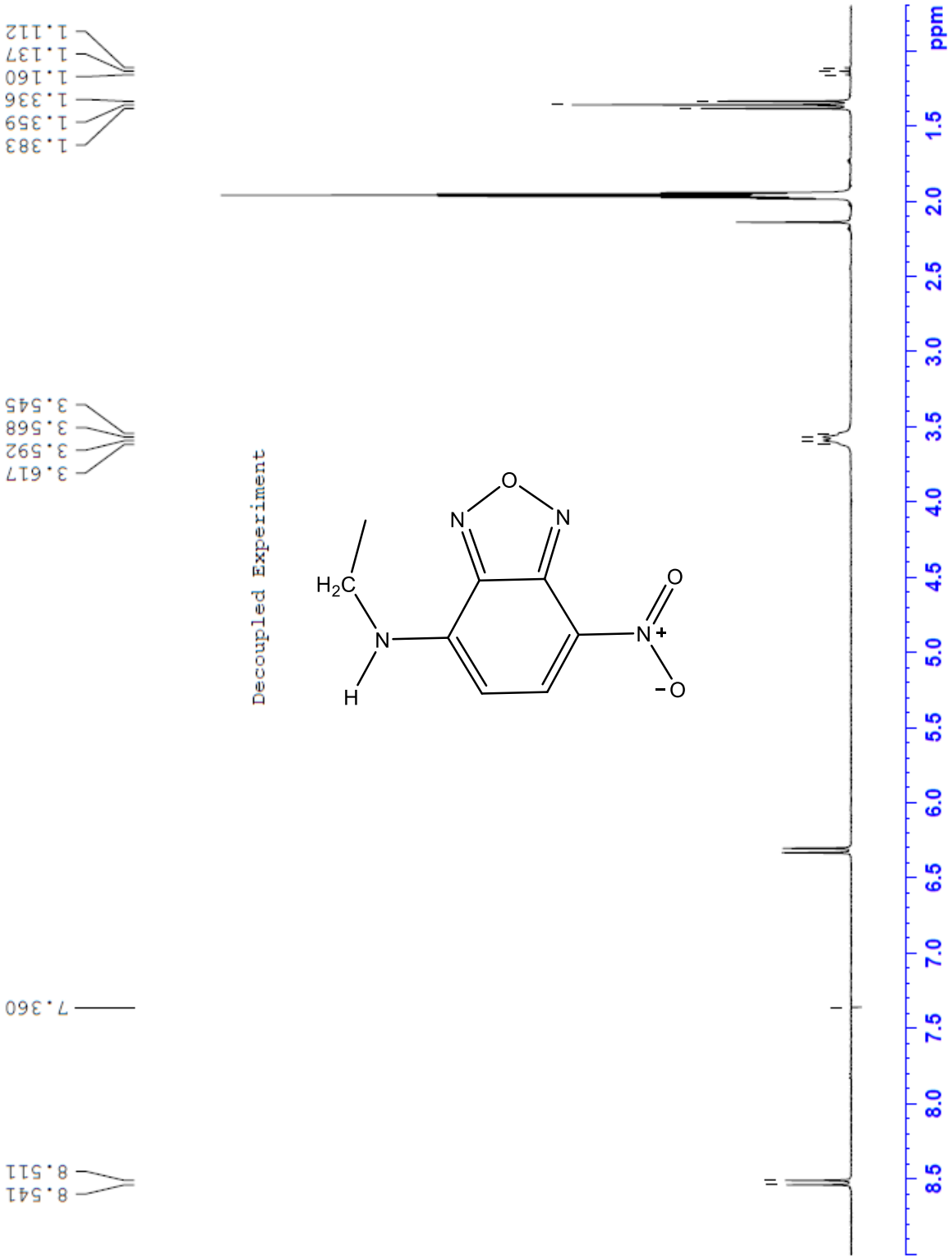
Decoupled Experiment
1.112
1.137
1.160
1.336
1.359
1.383
3.545
3.568
3.592
3.617
7.360
8.511
8.541
ppm
8.5
8.0
7.5
7.0
6.5
6.0
5.5
5.0
4.5
4.0
3.5
3.0
2.5
2.0
1.5
O
N
N
H2C
N
H
N+
O
-O

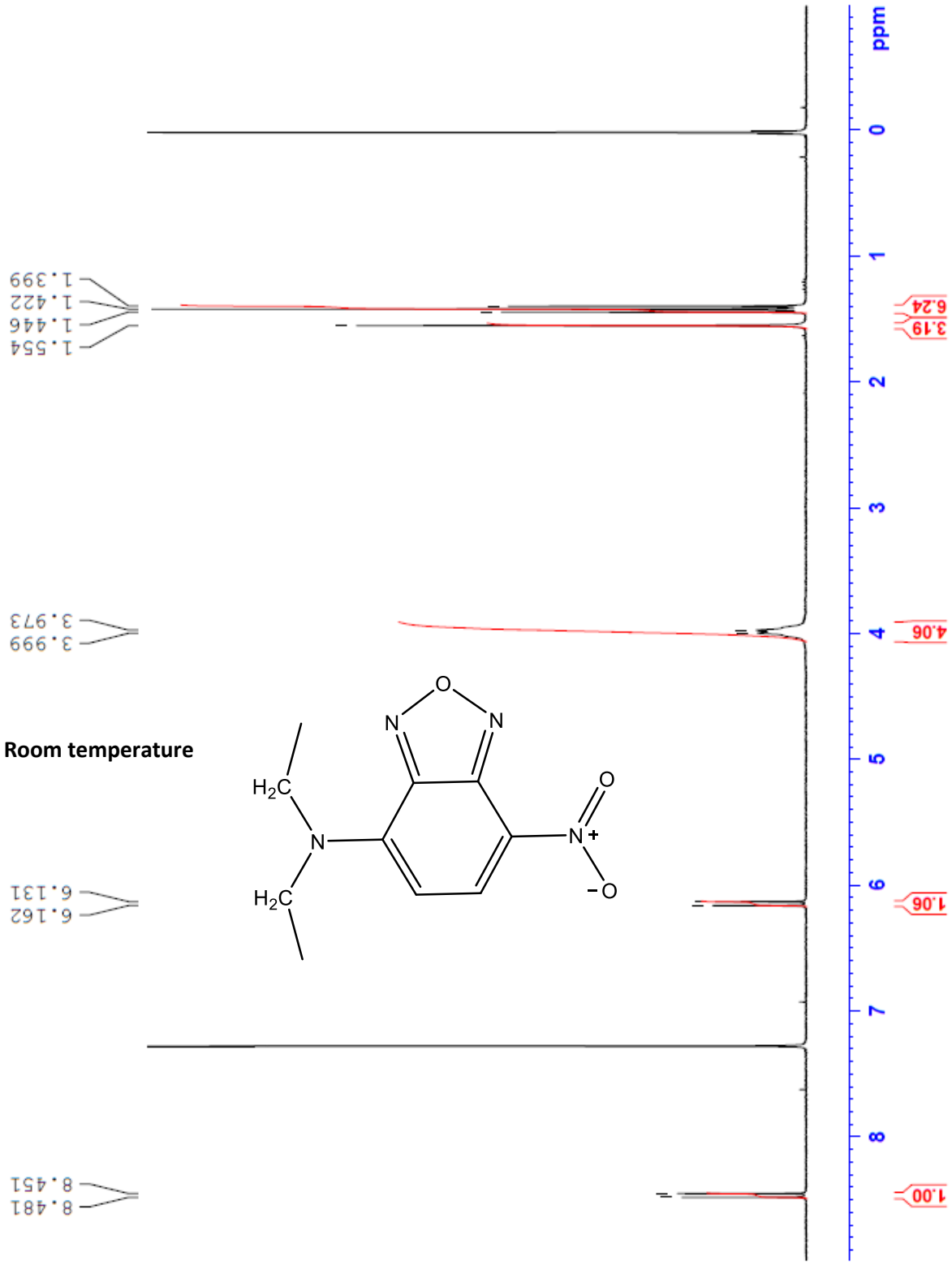
ppm
0
1
2
3
4
5
6
7
8
1.399
1.422
1.446
1.554
3.973
3.999
6.131
6.162
8.451
8.481
6.24
3.19
4.06
1.06
1.00
Room temperature
O
N
N
H2C
N
H2C
N+
O
O-

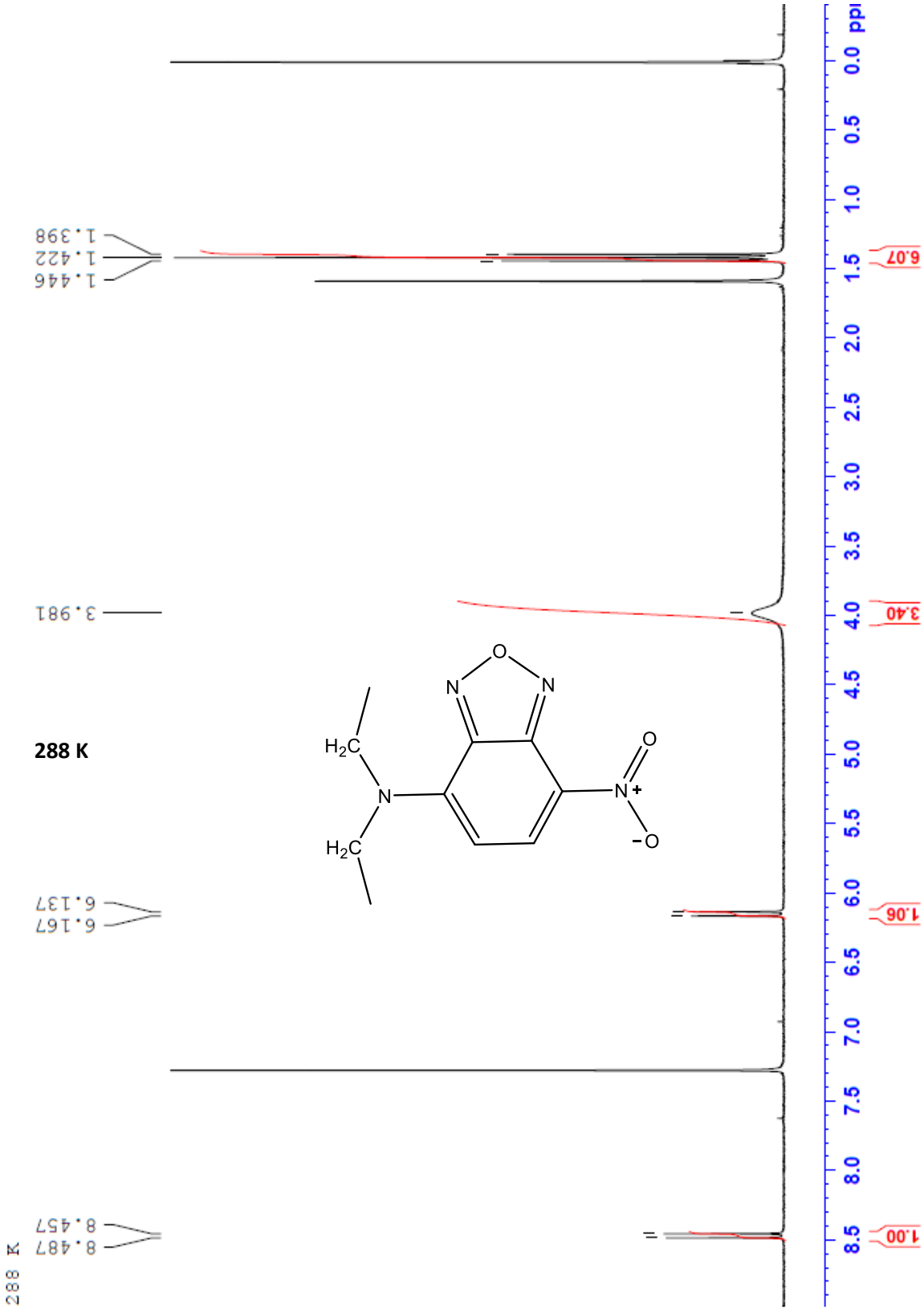
288 K
1.398
1.422
1.446
3.981
6.167
6.137
8.487
8.457
6.07
3.40
1.06
1.00
ppm
0.0
0.5
1.0
1.5
2.0
2.5
3.0
3.5
4.0
4.5
5.0
5.5
6.0
6.5
7.0
7.5
8.0
8.5
O
N
N
H2C
N
H2C
N+
O
-O

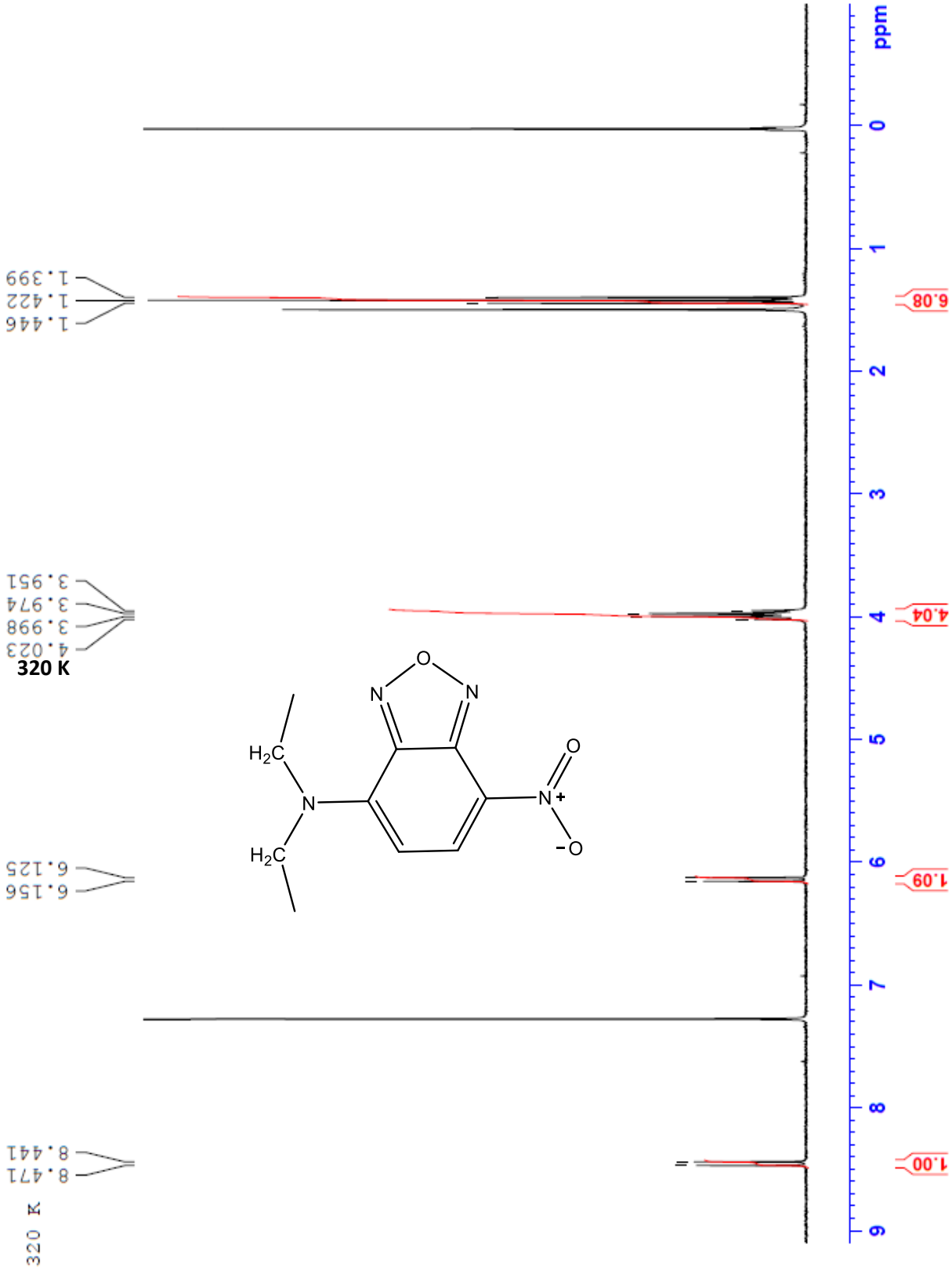
1.399
1.422
1.446
3.951
3.974
3.998
4.023
320 K
6.125
6.156
8.441
8.471
320 K
ppm
0
1
2
3
4
5
6
7
8
9
6.08
4.04
1.09
1.00
H2C
N
H2C
O
N
N
N+
O
-O

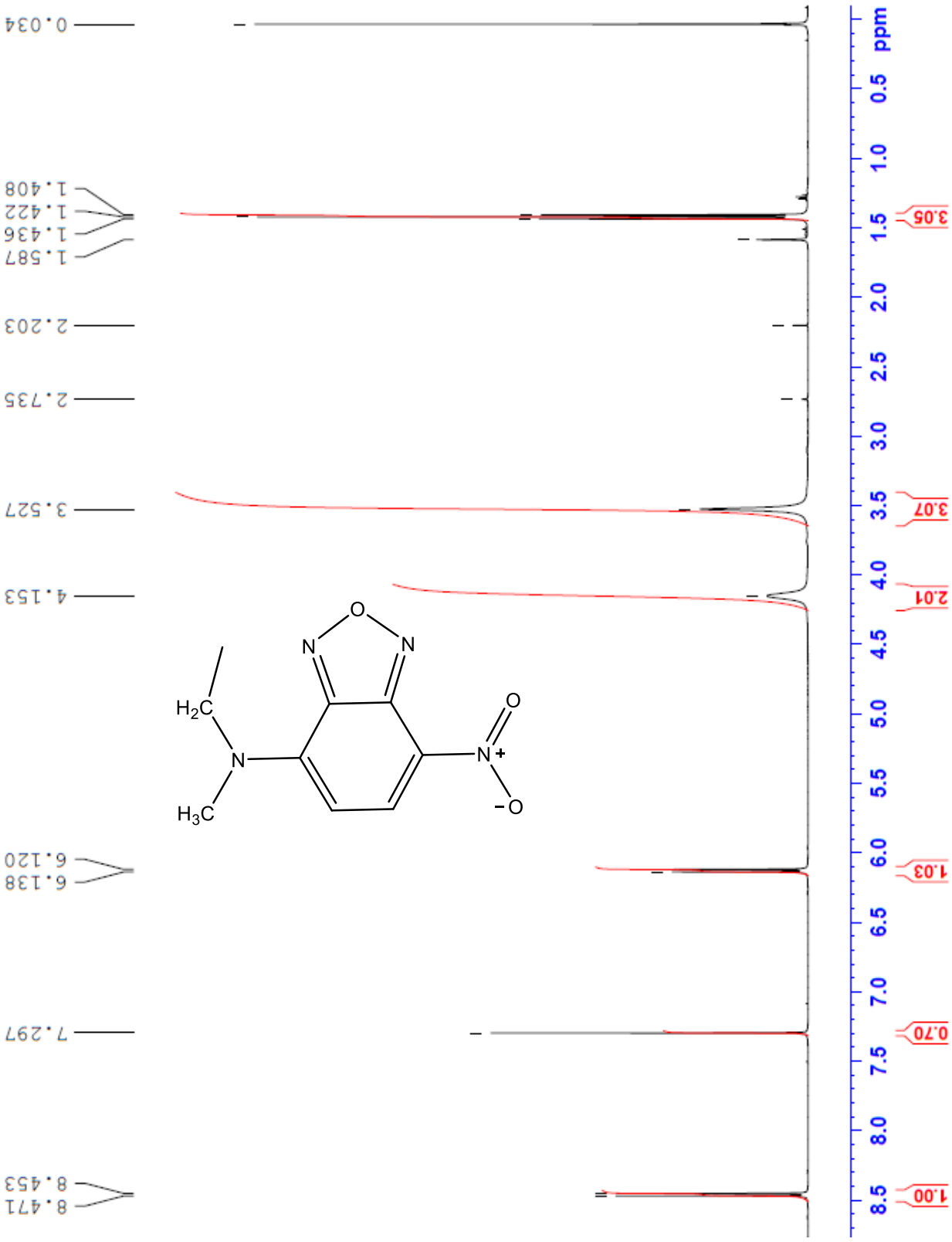
0.034
1.408
1.422
1.436
1.587
2.203
2.735
3.527
4.153
6.120
6.138
7.297
8.453
8.471
3.05
3.07
2.01
1.03
0.70
1.00
ppm
0.5
1.0
1.5
2.0
2.5
3.0
3.5
4.0
4.5
5.0
5.5
6.0
6.5
7.0
7.5
8.0
8.5
O
N
N
H2C
N
H3C
O
N+
-O

Appendix and supporting data for NBD-NH_2

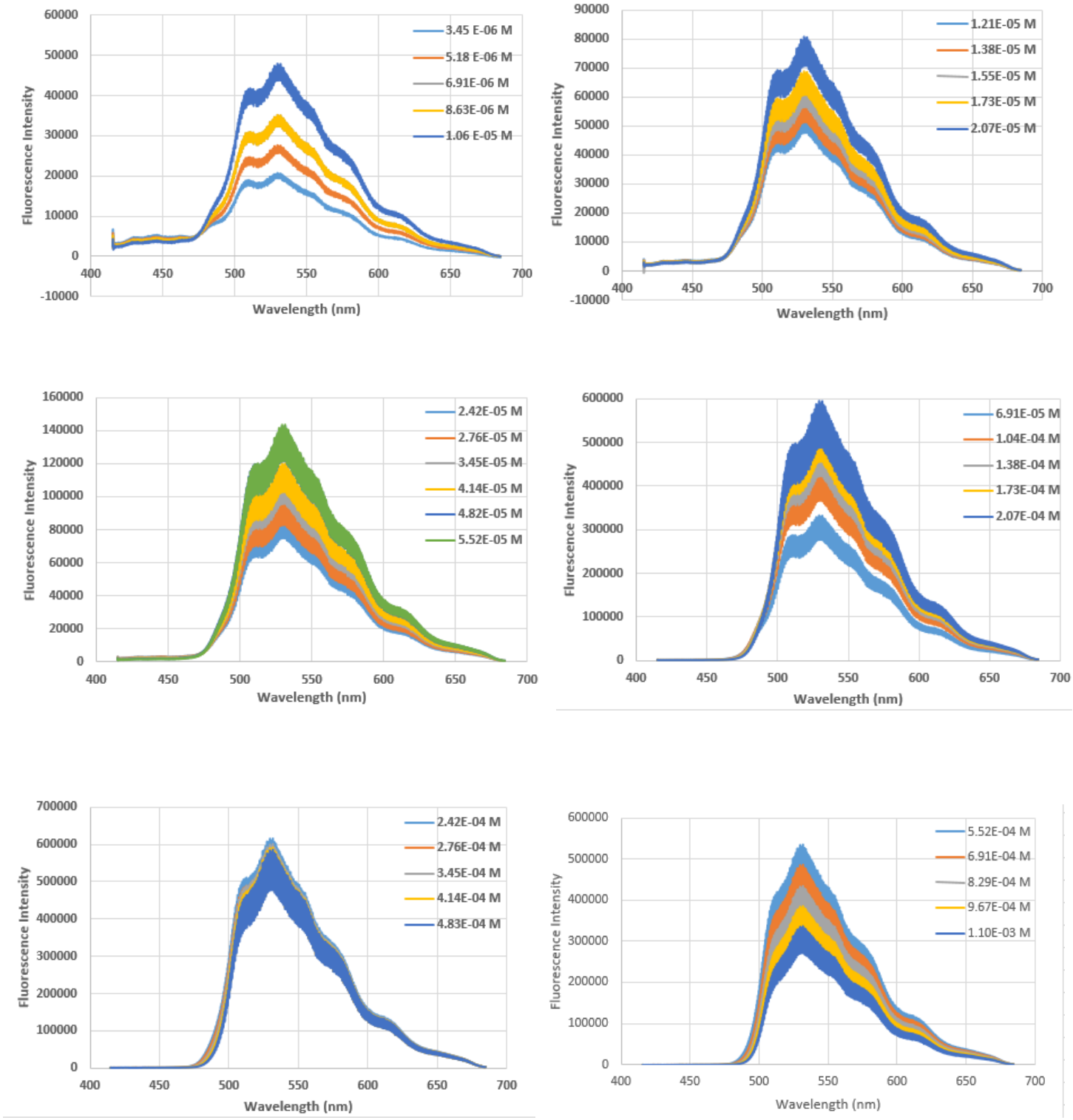

Figure A1.1. Single-Photon excited fluorescence (SPEF) spectra of NBD-NH_2 ranging from the concentration of 3.45 x 10^{-6} M to 1.10 x 10^{-3} M in 100% dichloromethane.

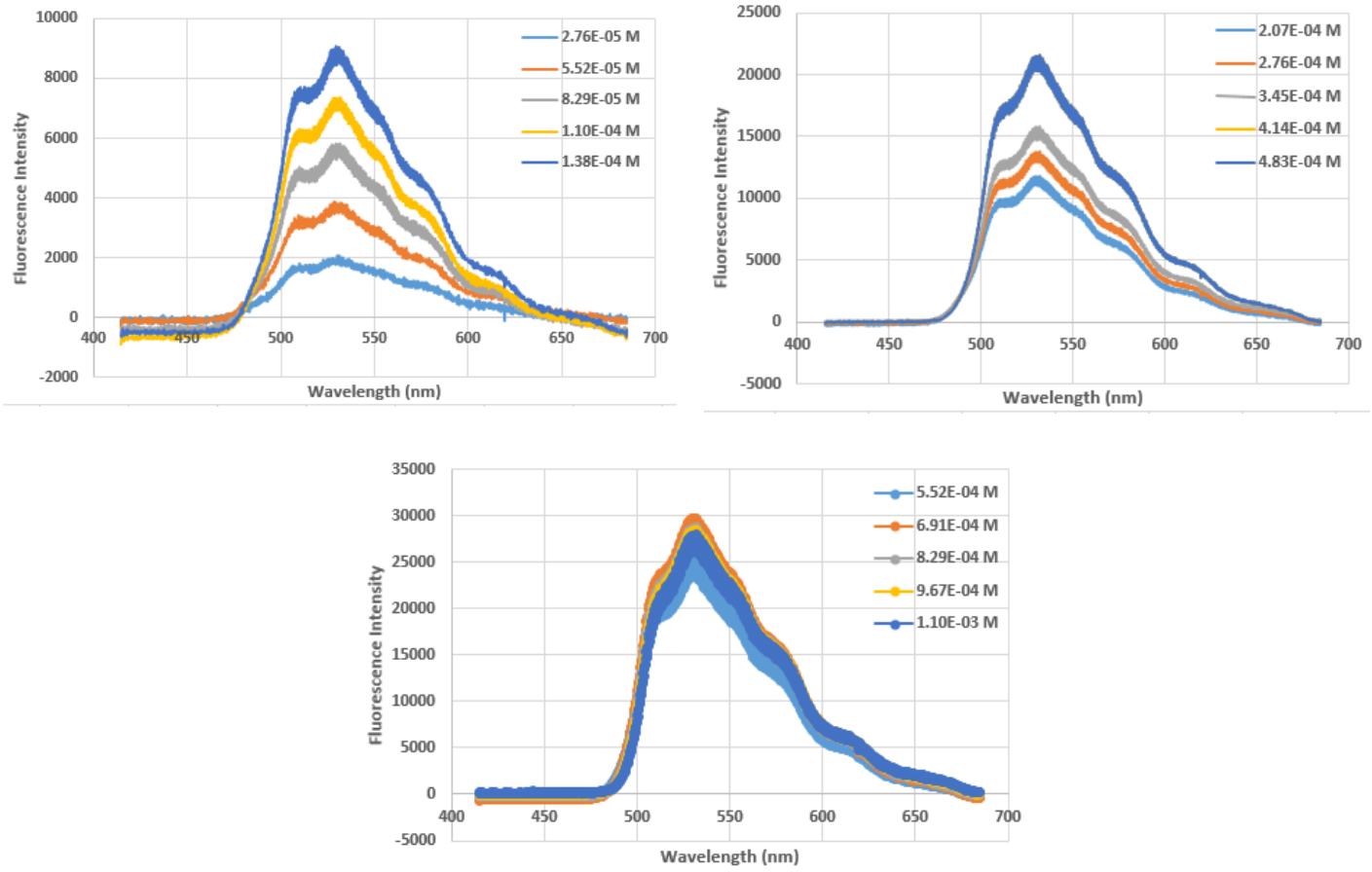

Figure A1.2. Two-Photon excited fluorescence (TPEF) spectra of NBD-NH_2 ranging from the concentration of 2.76 x 10^{-5} M to 1.10 x 10^{-3} M in 100% dichloromethane.

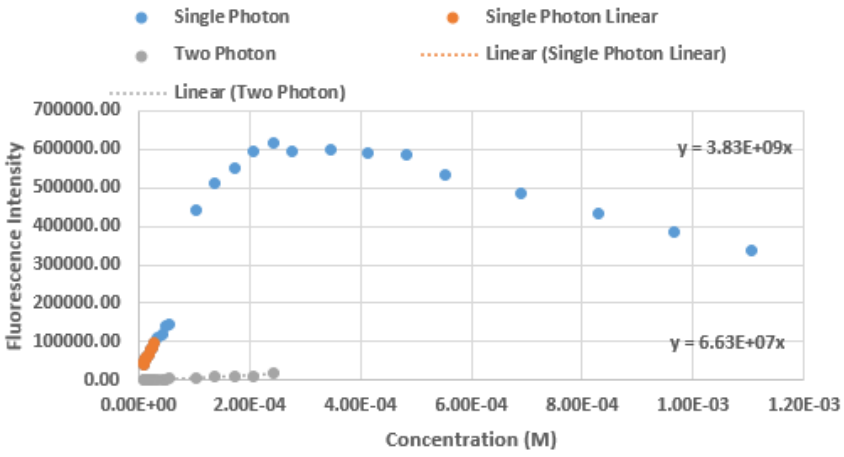

Figure A1.3.Relationship between SPEF (blue circle) and TPEF intensities (grey circle) and concentration of NBD-NH_2 in dichloromethane.

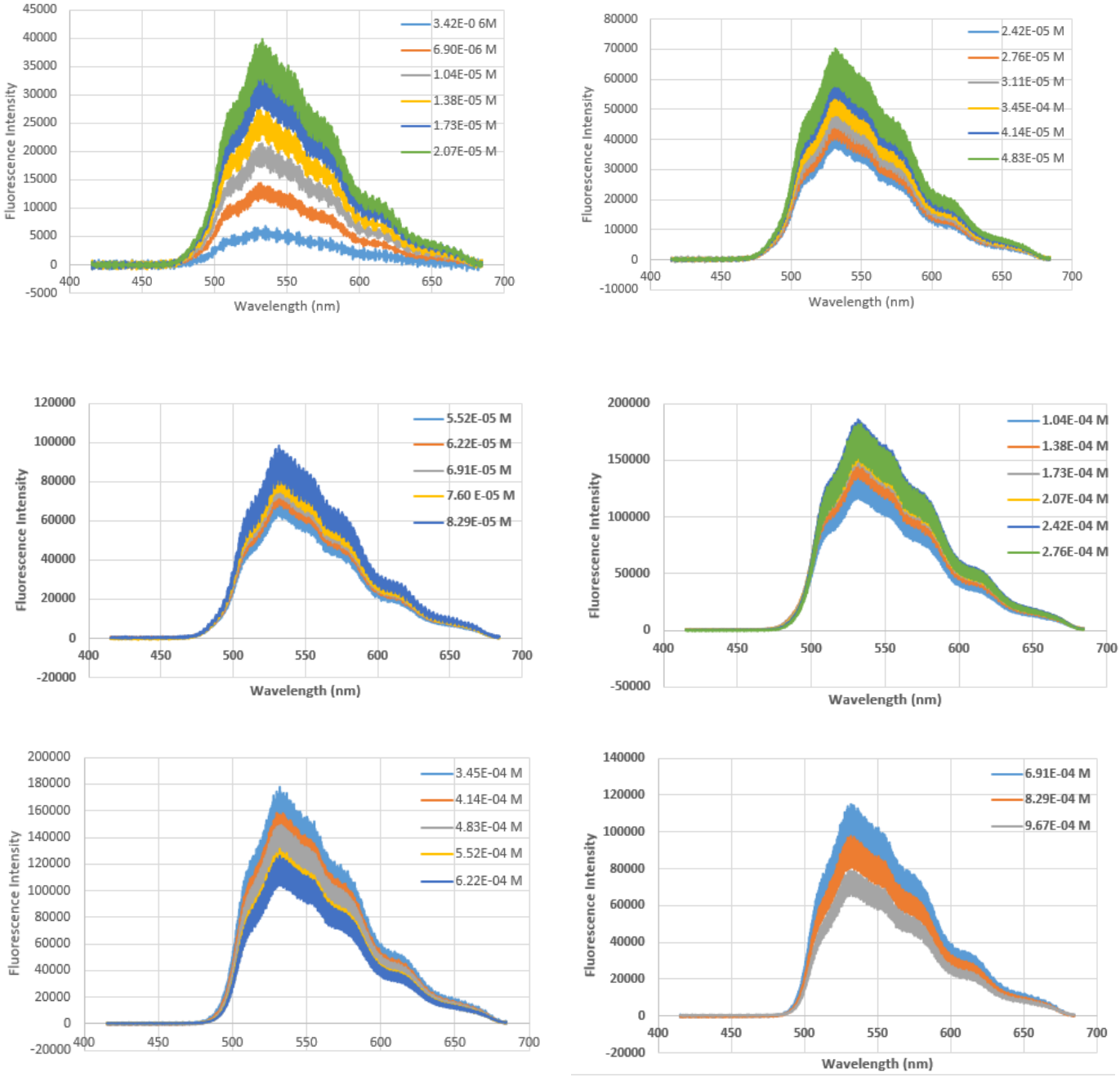

Figure A1.4. SPEF spectra of NBD-NH_2 in acetonitrile ranging from a concentration of 3.42 x 10^{-6} M to 9.67 x 10^{-4} M.

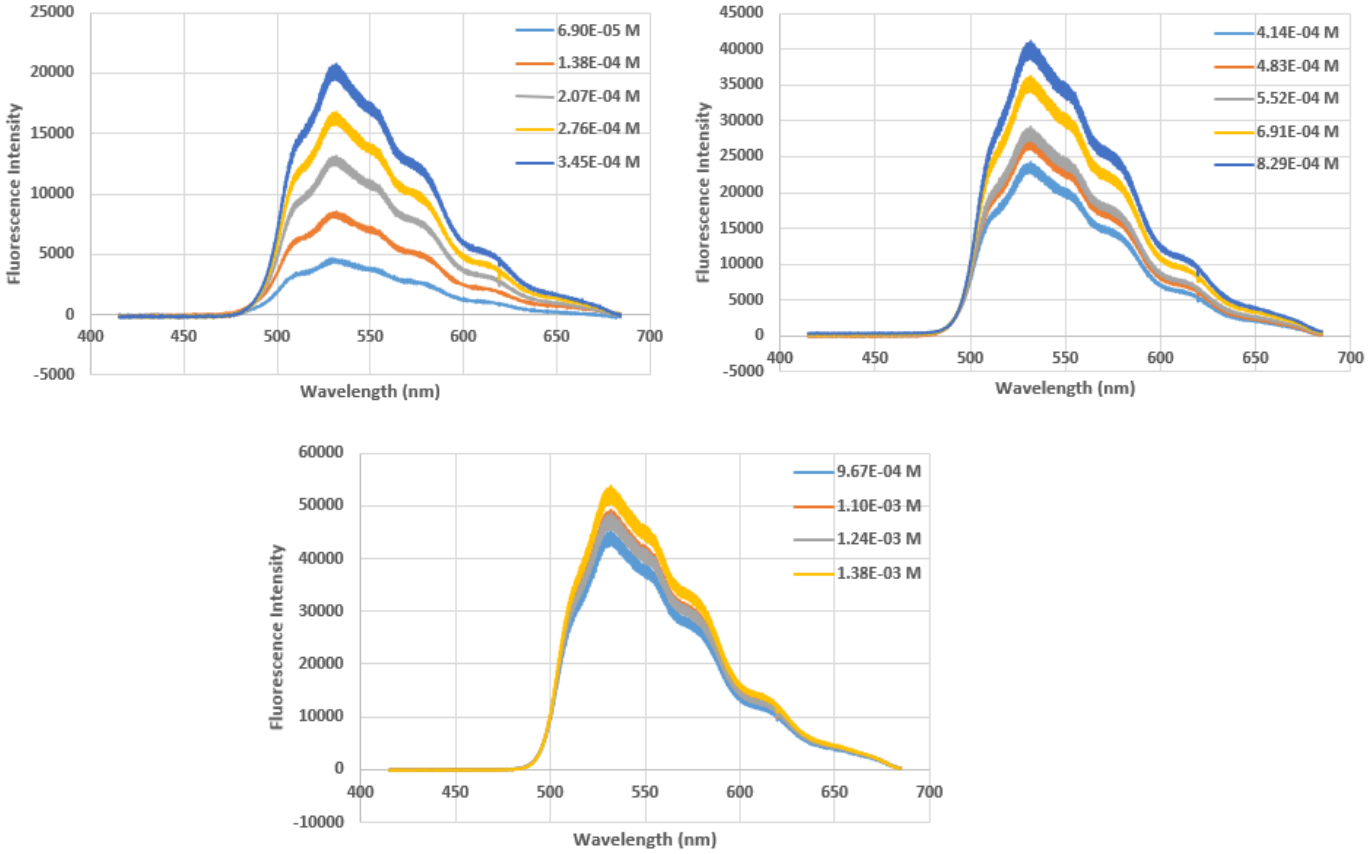

Figure A1.5. TPEF spectra of NBD-NH_2 in 100% acetonitrile ranging from a concentration of 6.90 x 10^{-5} M to 1.38 x10^{-3} M.

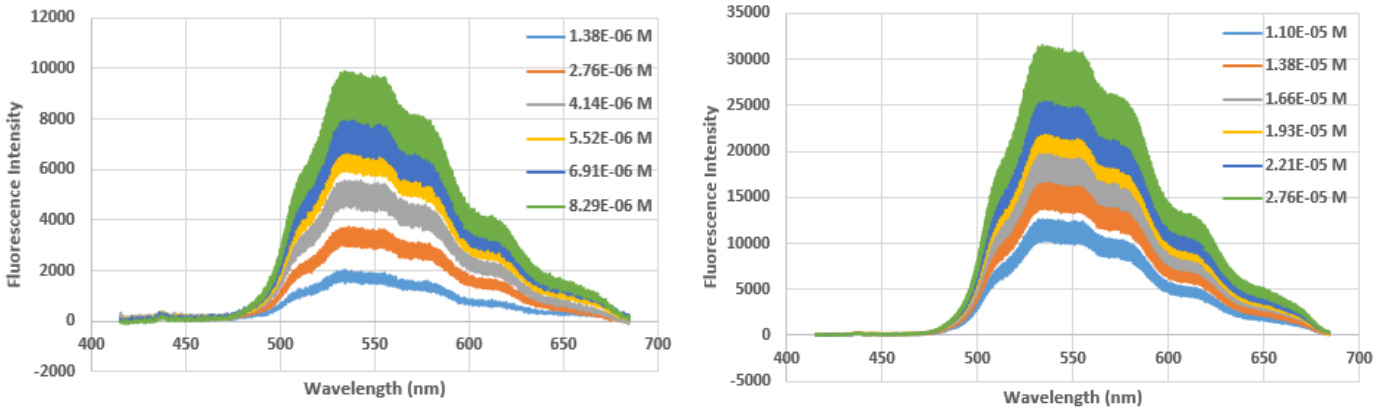

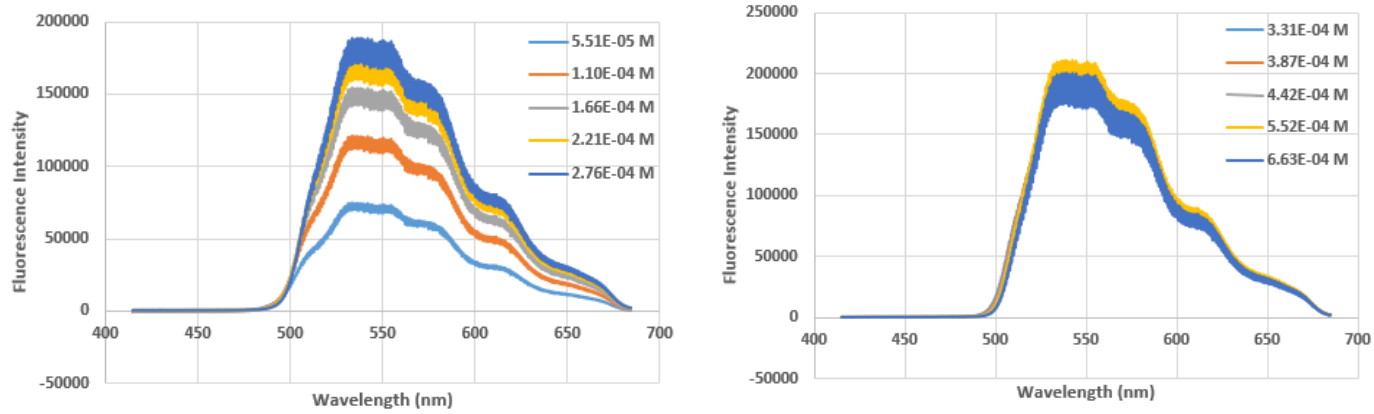

Figure A1.6. SPEF spectra of NBD-NH_2 ranging from a concentration of 1.38 x 10^{-6} M to 6.63 x 10^{-4} M in 100% Methanol.

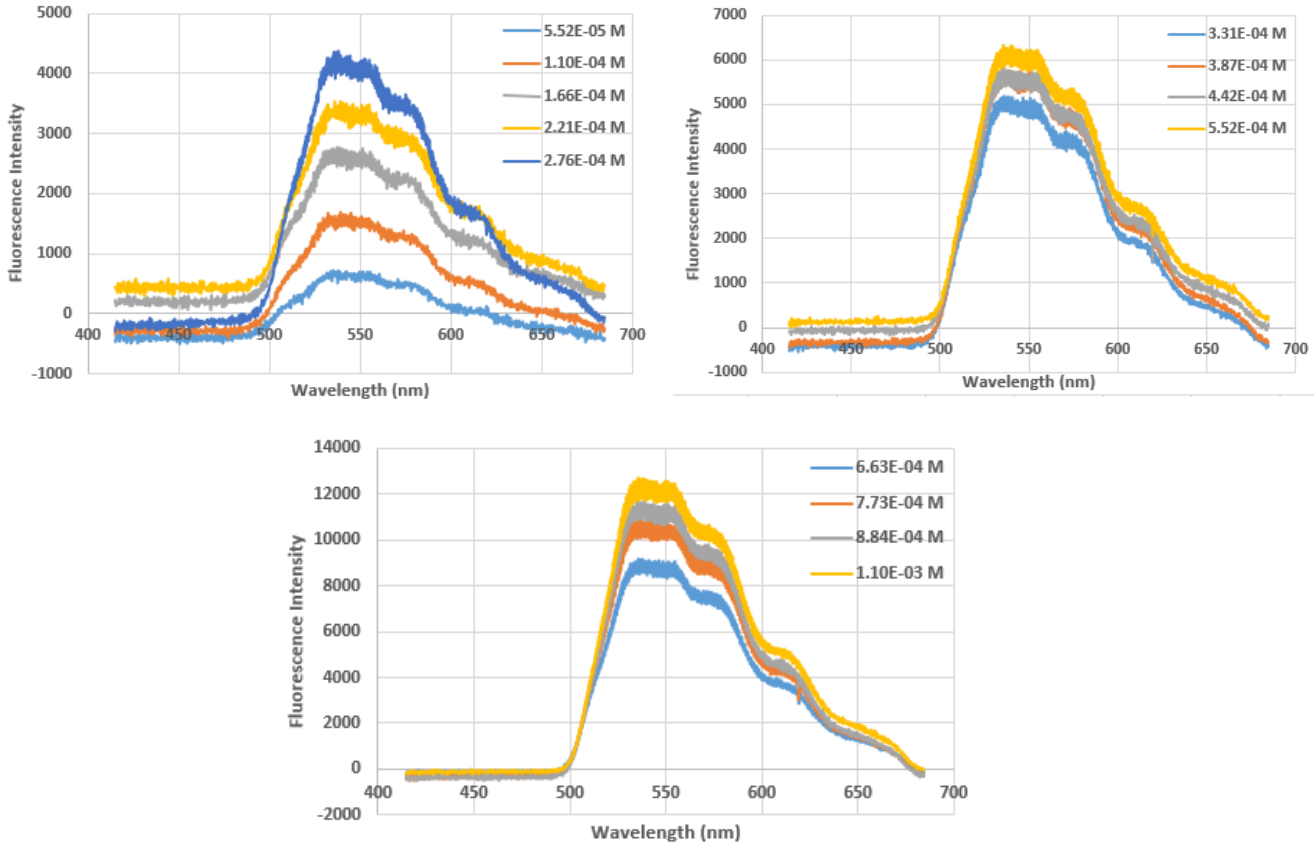

Figure A1.7. TPEF spectrum of NBD-NH_2 ranging from 5.52 x 10^{-5} M to 1.10 x 10^{-3} M in 100% Methanol.

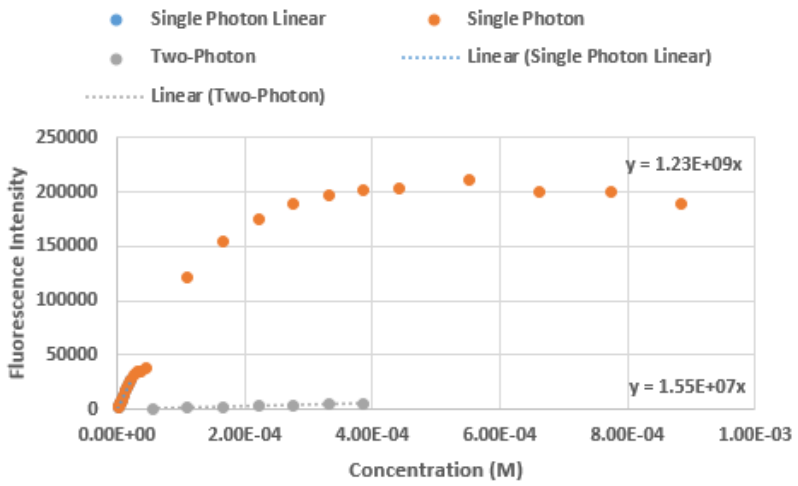

Figure A1.8. Relationship between SPEF (orange circles) and TPEF (grey circles) intensities and concentration of NBD-NH_2 in 100% Methanol.

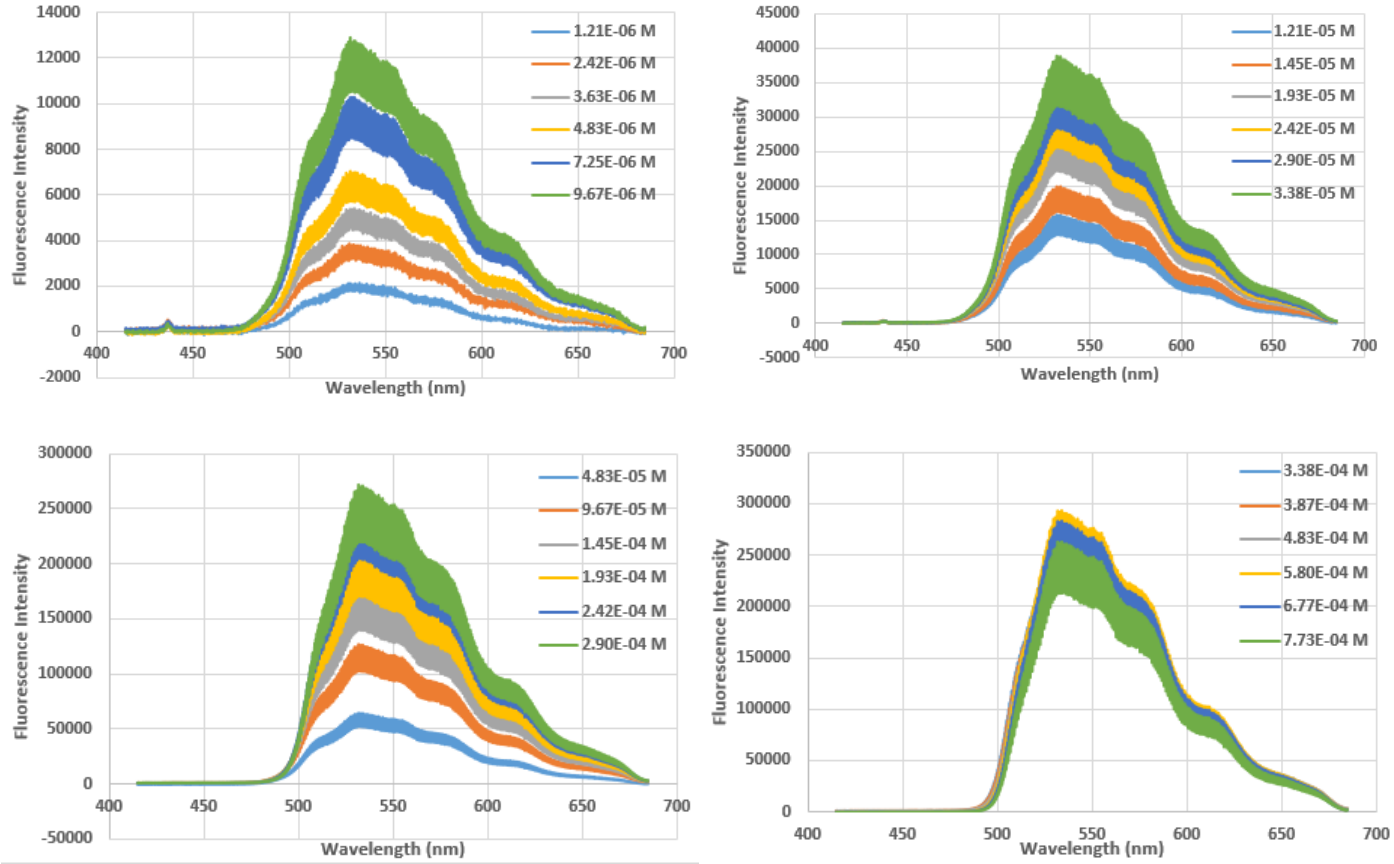

Figure A1.9. SPEF spectra of NBD-NH_2 in 100% ethanol ranging from a concentration of 1.21 x 10^{-6} M to 7.73 x 10^{-4} M.

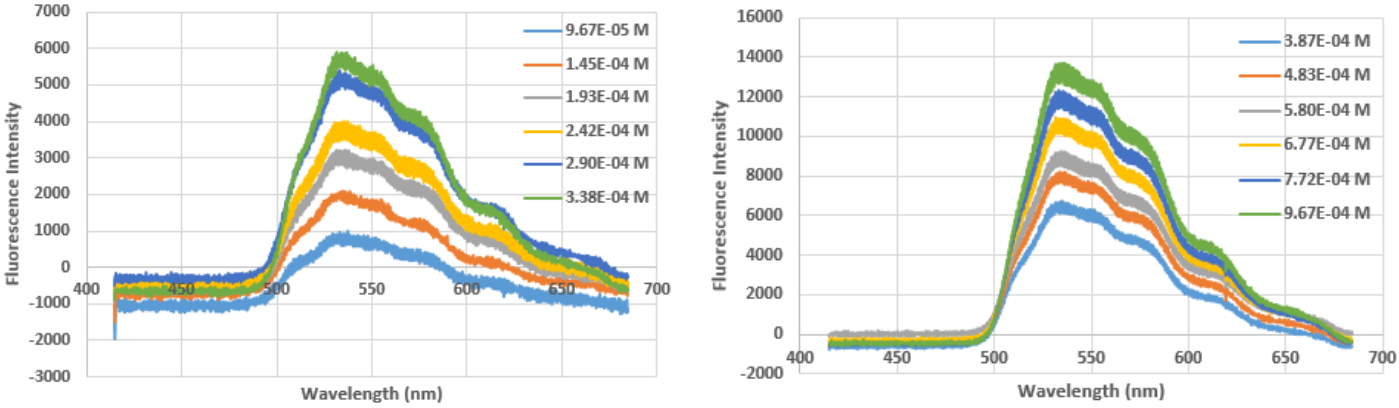

Figure A1.10 TPEF spectra of NBD-NH_2 in 100% ethanol ranging from a concentration of 9.67 x 10^{-5} M to 9.67 x 10^{-4} M.

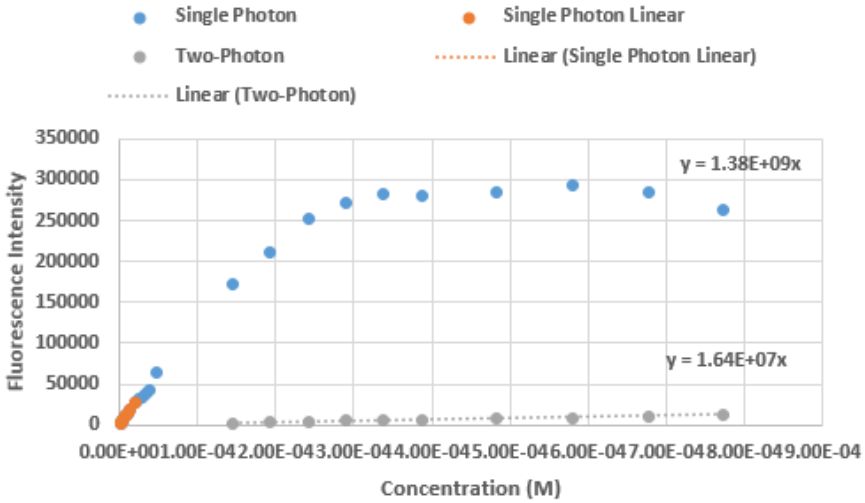

Figure A1.11 Relationship between SPEF (blue circle) and TPEF (grey circle) and concentration for NBD-NH_2 in 100% ethanol.

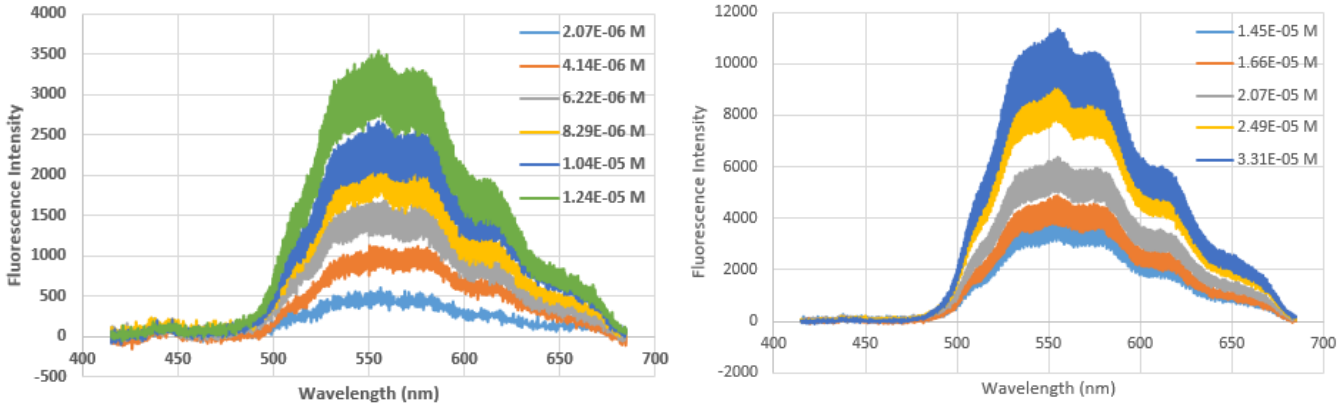

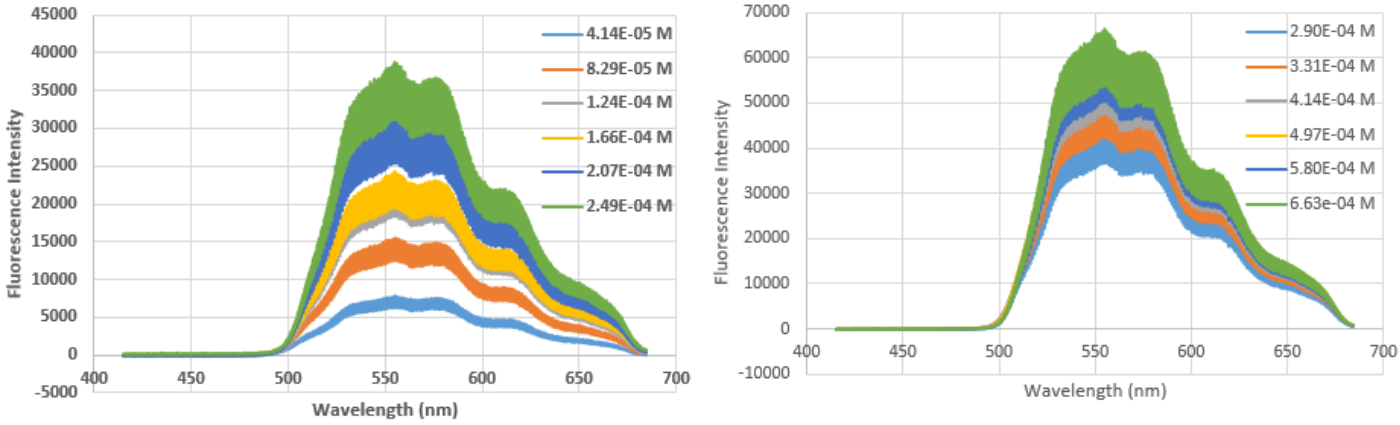

Figure A1.12. SPEF spectra of NBD-NH_2 in 50% Methanol 50% Water ranging from a concentration of 2.07 x 10^{-6} M to 6.63 x 10^{-4} M.

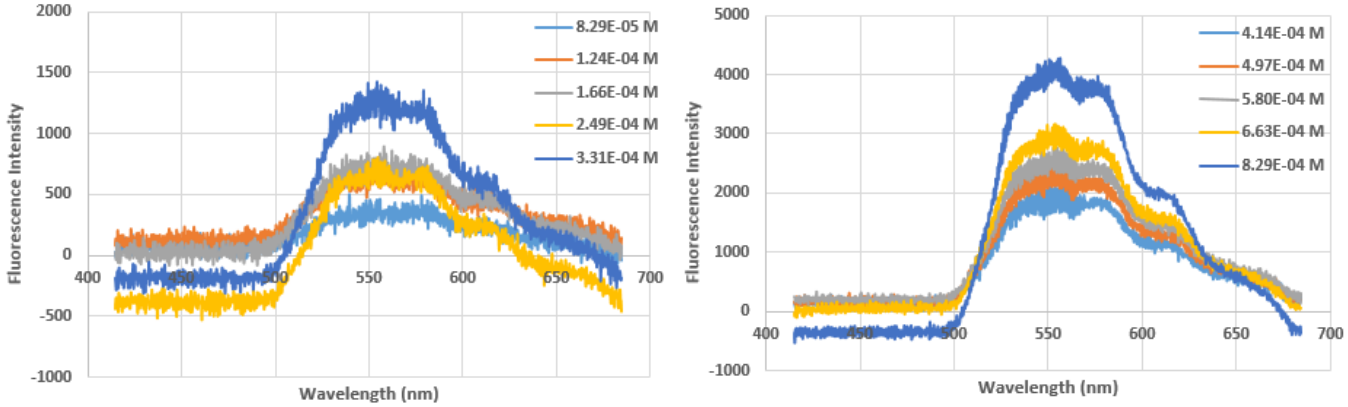

Figure A1.13. TPEF spectra of NBD-NH_2 in 50% Methanol 50% Water ranging from a concentration of 8.29 x 10^{-5} M to 8.29 x 10^{-4} M.

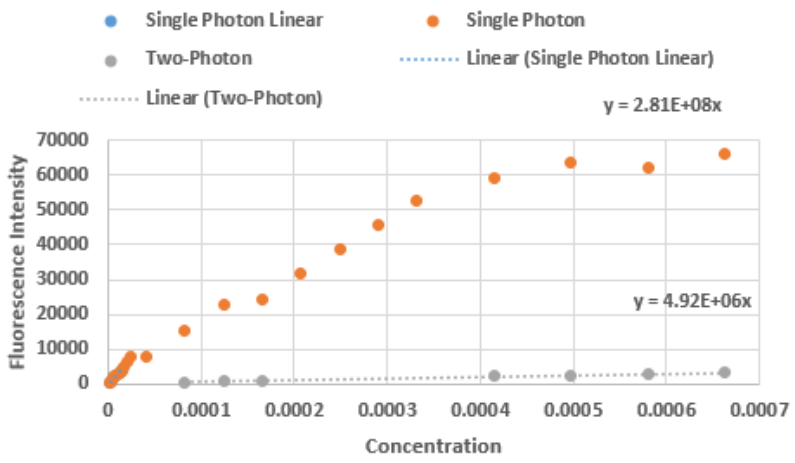

Figure A1.14. Relationship between SPEF (blue circles) and TPEF (grey circles) intensities and concentration of NBD-NH_2 in 50% Methanol 50% Water.

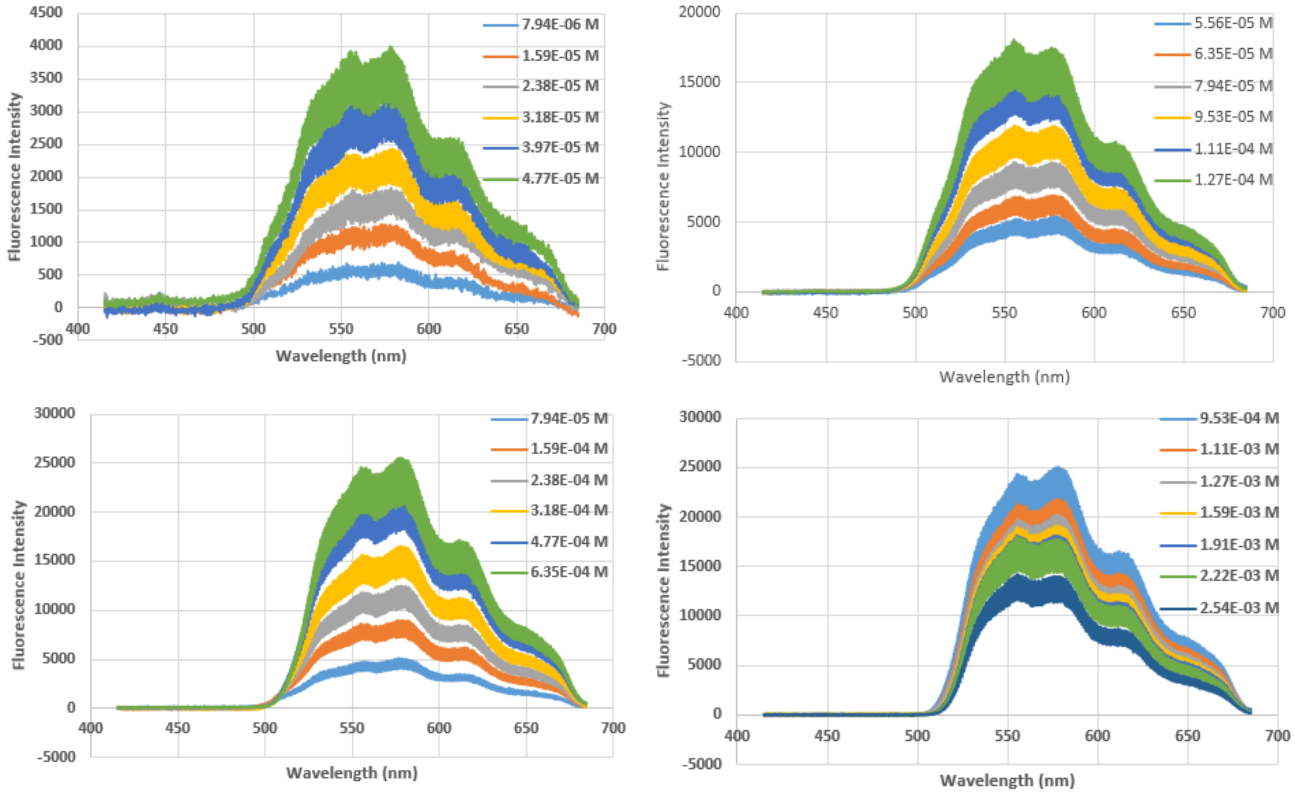

Figure A1.15. SPEF spectra of NBD-NH_2 in 100% H_2O ranging from a concentration of 7.94 x 10^{-6} M to 2.54 x 10^{-3} M.

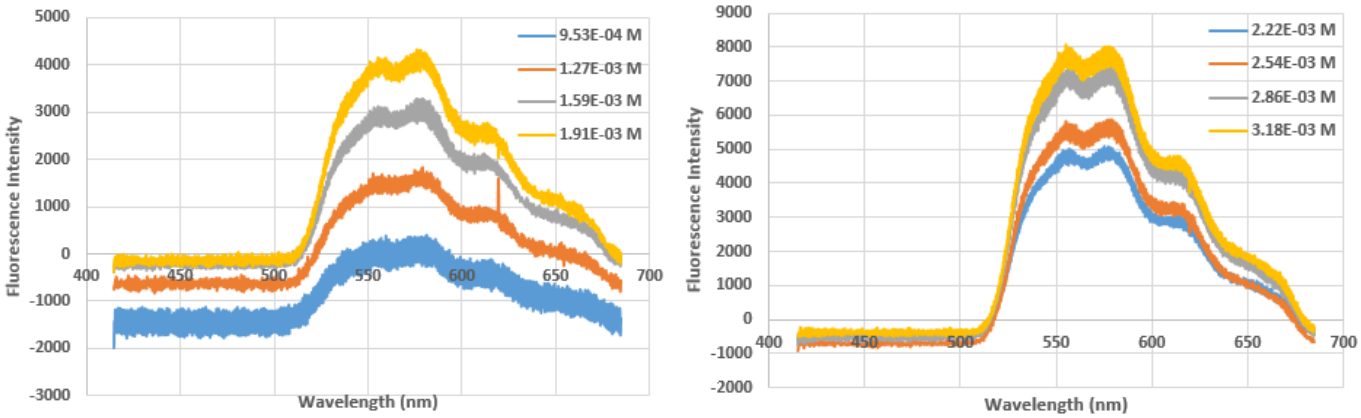

Figure A1.16. TPEF spectra of NBD-NH_2 in 100% H_2O ranging from a concentration of 9.53 x 10^{-4} M to 3.18 x 10^{-3} M.

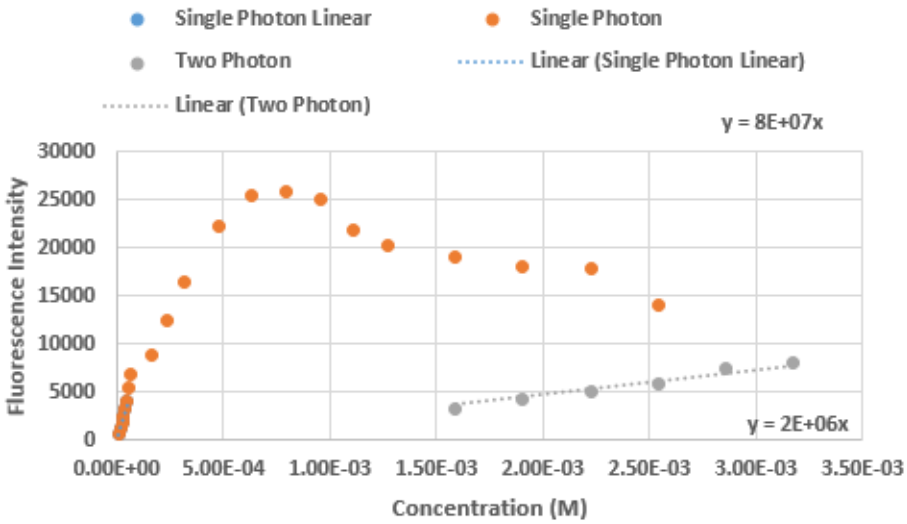

Figure A1.17. Relationship between SPEF (orange circles) and TPEF (grey circles) intensities and concentration of NBD-NH_2 in 100% Water.

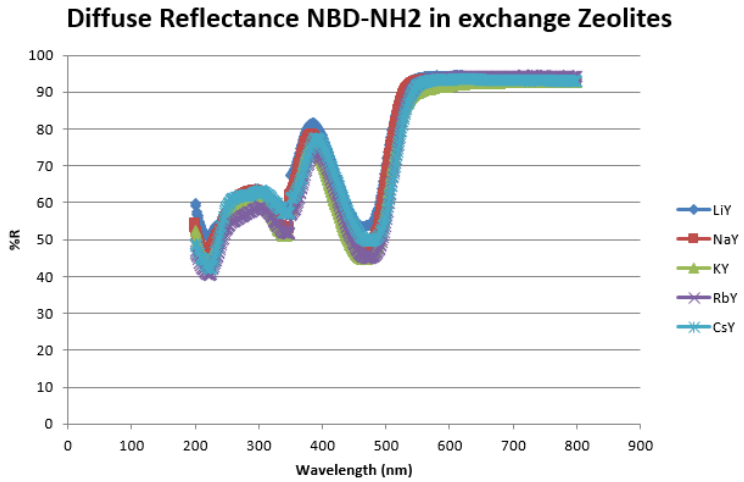

Figure A1.18 Diffuse Reflectance Spectra of NBD-NH_2 in alkali cation exchanged zeolites, %Reflectance as a function of wavelength.

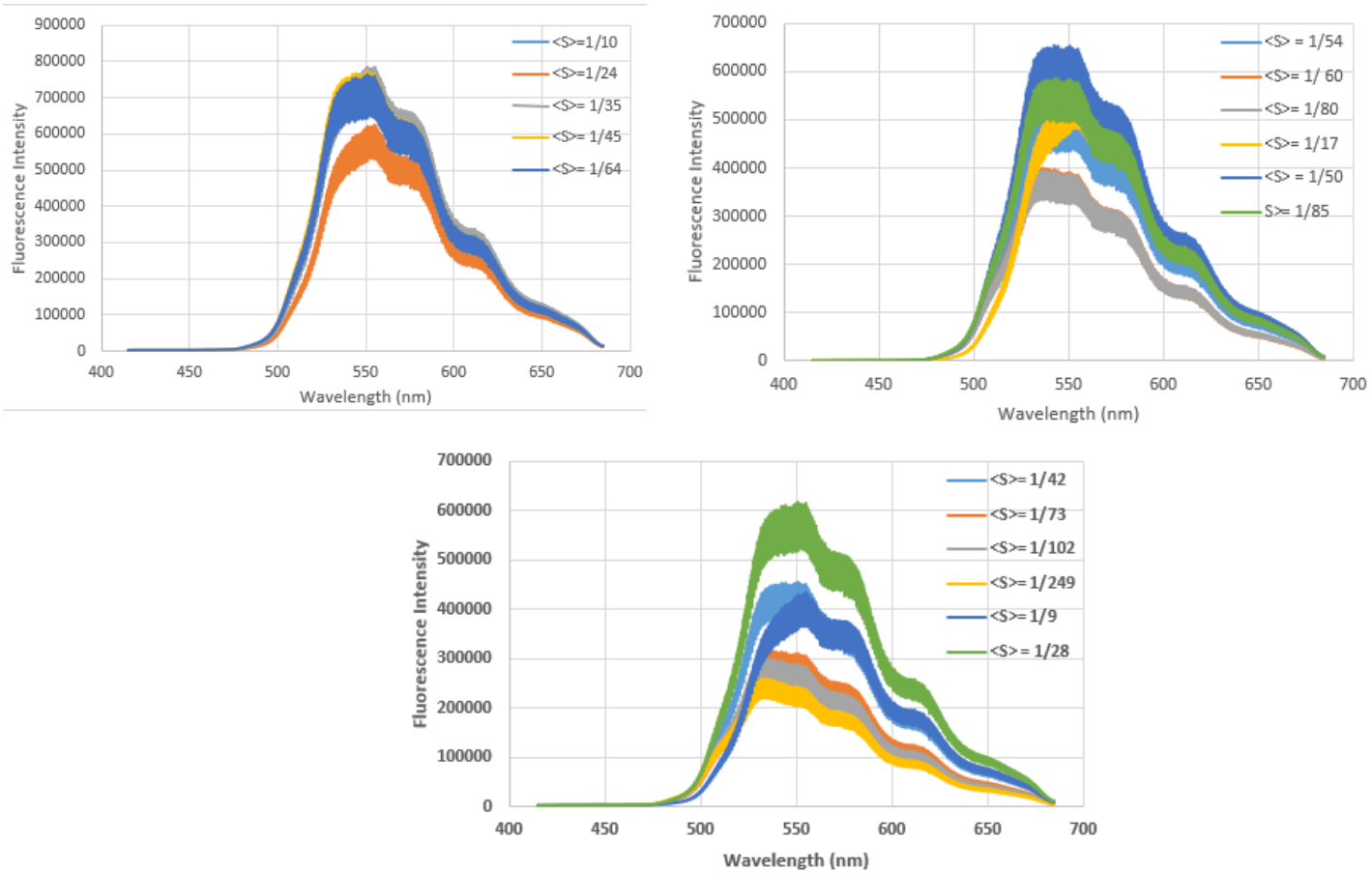

Figure A1.19. SPEF spectra of NBD-NH_2 incorporated in NaY at various different loading level <S>.

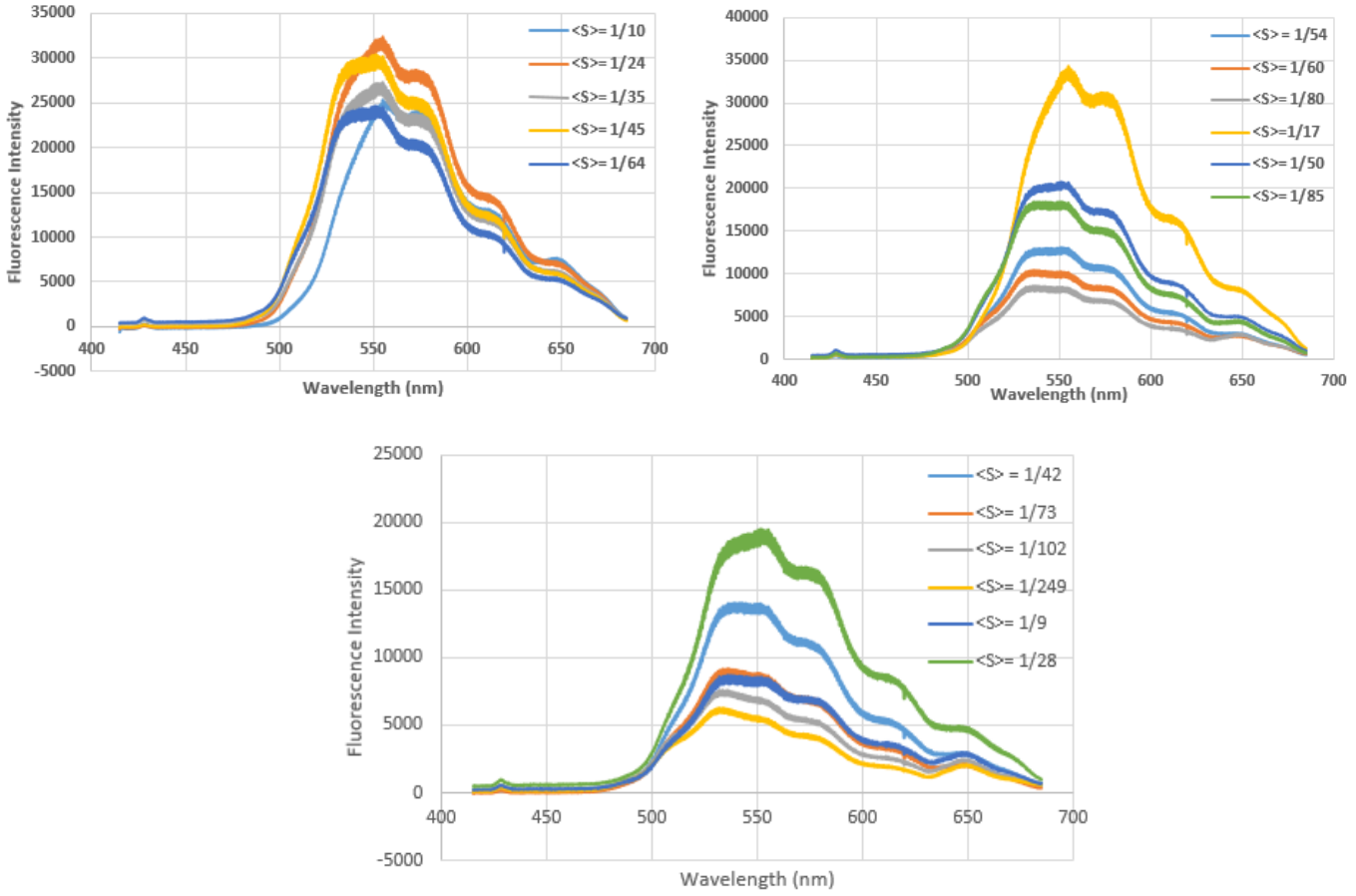

Figure A1.20. TPEF spectra of NBD-NH_2 incorporated in NaY at various different loading level <S>.

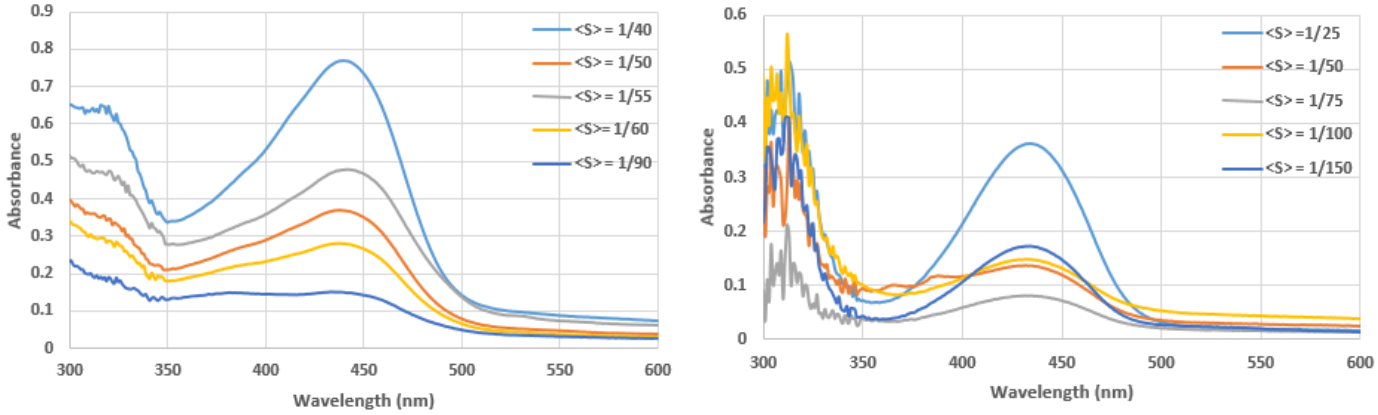

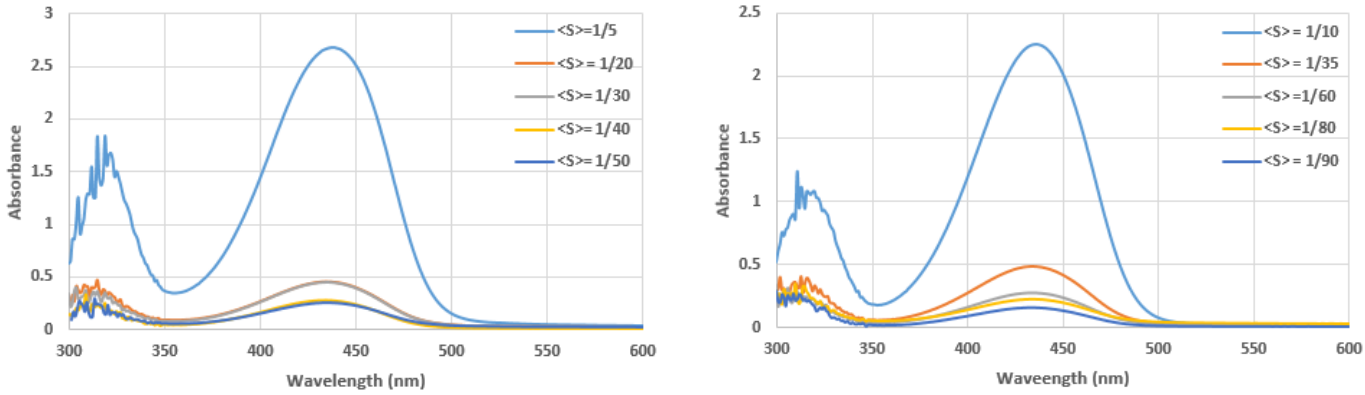

Figure A1.21. UV-vis spectra of the decanted dichloromethane used to incorporate NBD-NH_2 in NaY, for some loading level both the decanted solvent showed characteristic absorption, whereas for some loading level only the first decanted solvent showed characteristic absorption properties.

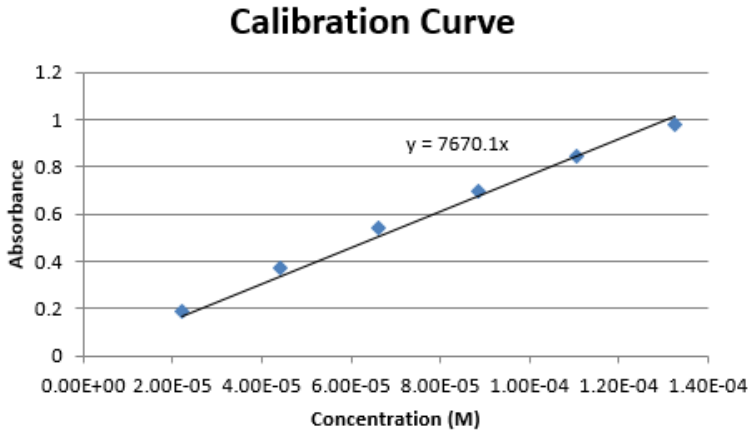

Figure A1.21. Calibration curve used to determine to exact loading level of NBD-NH_2 in Y zeolites.

Sample Calculation,

For a loading level of <S> = 1/20, a 0.004 M stock solution was prepared and 0.3348 g of NaY weighted,

The required volume, using Equation 3.2 and 3.3

$$0.05 = \frac{(0.3348 * 8)}{17321} * ncompound = 1750\ uL$$

Absorbance from (40 mL+ 1.750 mL of stock solution) = 0.460 and using the equation of calibration curve,

$$0.4640 = 7670.1x$$

$$x = (6.00 * 10^{-5})$$

$$mol\ out = (6.00 * 10^{-5}) * (41.750 * 10^{-3}) = 2.51 *\ 10^{-6}$$

$$mol\ in = (0.400 * 1750 * 10^{-6}) = 7.73 * 10^{-6}$$

$$Actual\ mol\ in = (7.73 * 10^{-6}) - (2.51 * 10^{-6}) = 5.23 * 10^{-6}$$

$$actual\ loading\ level < S > = \frac{5.23 * 10^{-6}}{\frac{(0.3348 * 8)}{17321}} = 1/29$$

Table A1.1. Summary of SPEF and TPEF intensities obtained from the respective spectra of NBD-NH_2 incorporated in NaY at various different loading level <S>

Experimental Loading Level <S>	**Actual Loading Level <S>**	**One Photon**	**Two Photon**	**1PA:2PA**	**2PA:1PA**
1/5	1/9	4.35 x 10^5	2.79 x 10^4	15.58	0.064
1/6	1/10	5.18 x 10^5	2.53 x 10^4	20.42	0.049
1/10	1/17	5.71 x 10^5	3.43 x 10^4	16.65	0.060
1/15	1/24	6.25 x 10^5	3.24 x 10^4	19.27	0.052
1/20	1/28	6.16 x 10^5	1.94 x 10^4	31.67	0.032
1/22	1/35	7.84 x 10^5	2.73 x 10^4	28.75	0.035
1/25	1/42	4.56 x 10^5	1.41 x 10^4	32.41	0.031
1/28	1/45	7.73 x 10^5	3.03 x 10^4	25.49	0.039
1/30	1/54	5.18 x 10^5	1.31 x 10^4	39.64	0.025
1/35	1/50	6.54 x 10^5	2.08 x 10^4	31.38	0.032
1/38	1/64	7.65 x 10^5	2.46 x 10^4	31.05	0.032
1/40	1/60	4.01 x 10^5	1.05 x 10^4	38.18	0.026
1/50	1/73	3.15 x 10^5	9.12 x 10^3	34.52	0.029
1/50	1/80	3.94 x 10^5	8.64 x 10^3	45.64	0.022
1/60	1/85	5.84 x 10^5	1.84 x 10^4	31.78	0.031
1/75	1/102	2.99 x 10^5	7.58 x 10^3	39.39	0.025
1/100	1/249	2.61 x 10^5	6.24 x 10^3	41.75	0.024
				Average	0.034

Appendix and supporting data for NBD-DMA

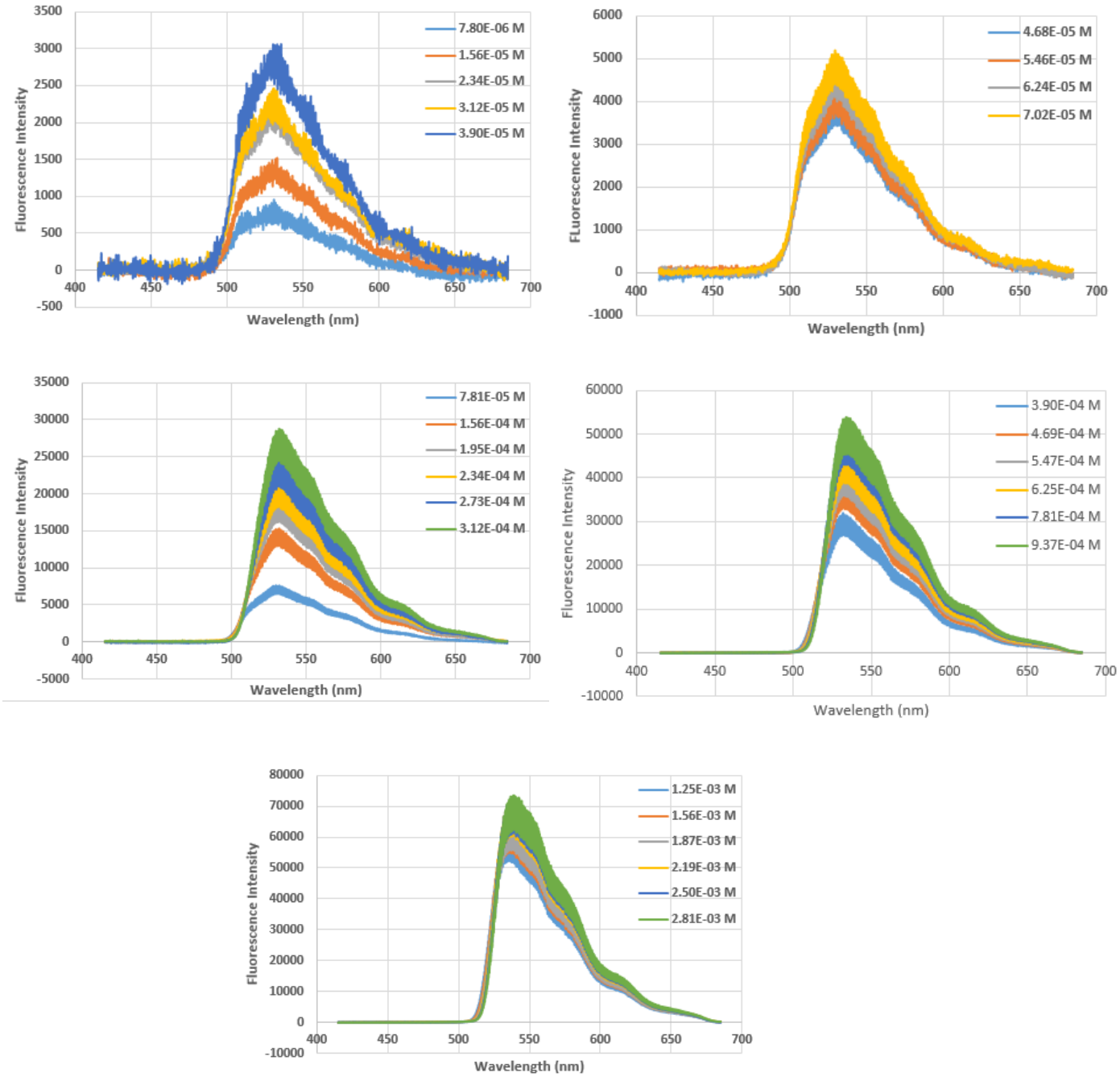

Figure A2.1. SPEF spectra of NBD-DMA in 100% dichloromethane ranging from a concentration of 7.80 x 10^{-6} M to 2.81 x 10^{-3} M.

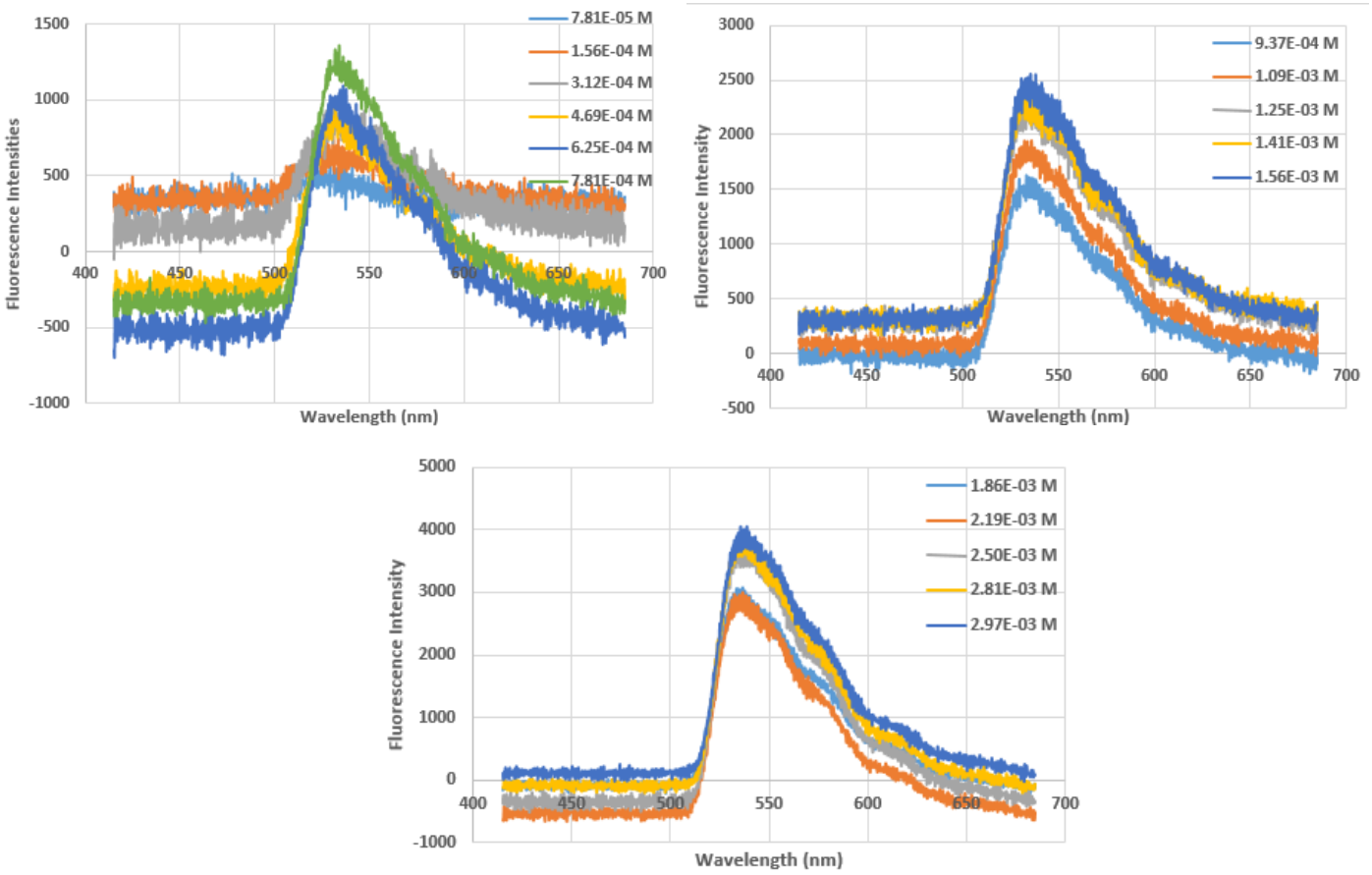

Figure A2.2. TPEF spectra of NBD-DMA in 100% dichloromethane ranging from a concentration of 7.81 x 10^{-5} M to 2.97 x 10^{-3} M.

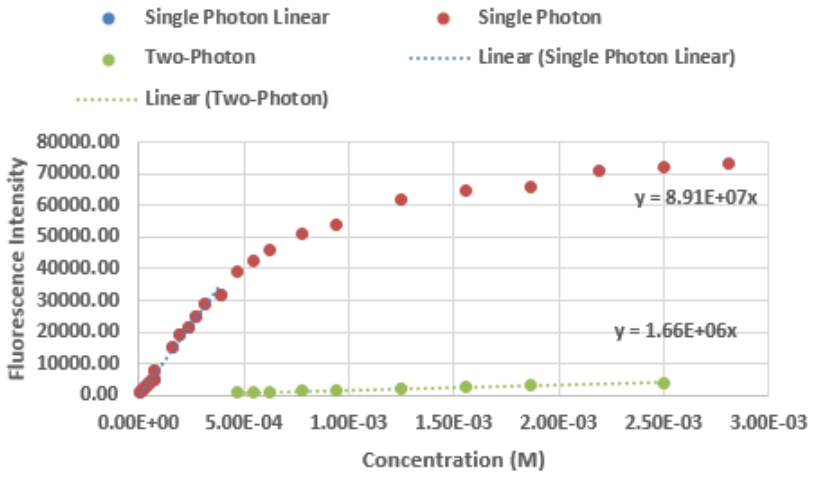

Figure A2.3. Relationship between SPEF (brown circles), TPEF intensities (green circles) and concentration of NBD-DMA in 100% dichloromethane.

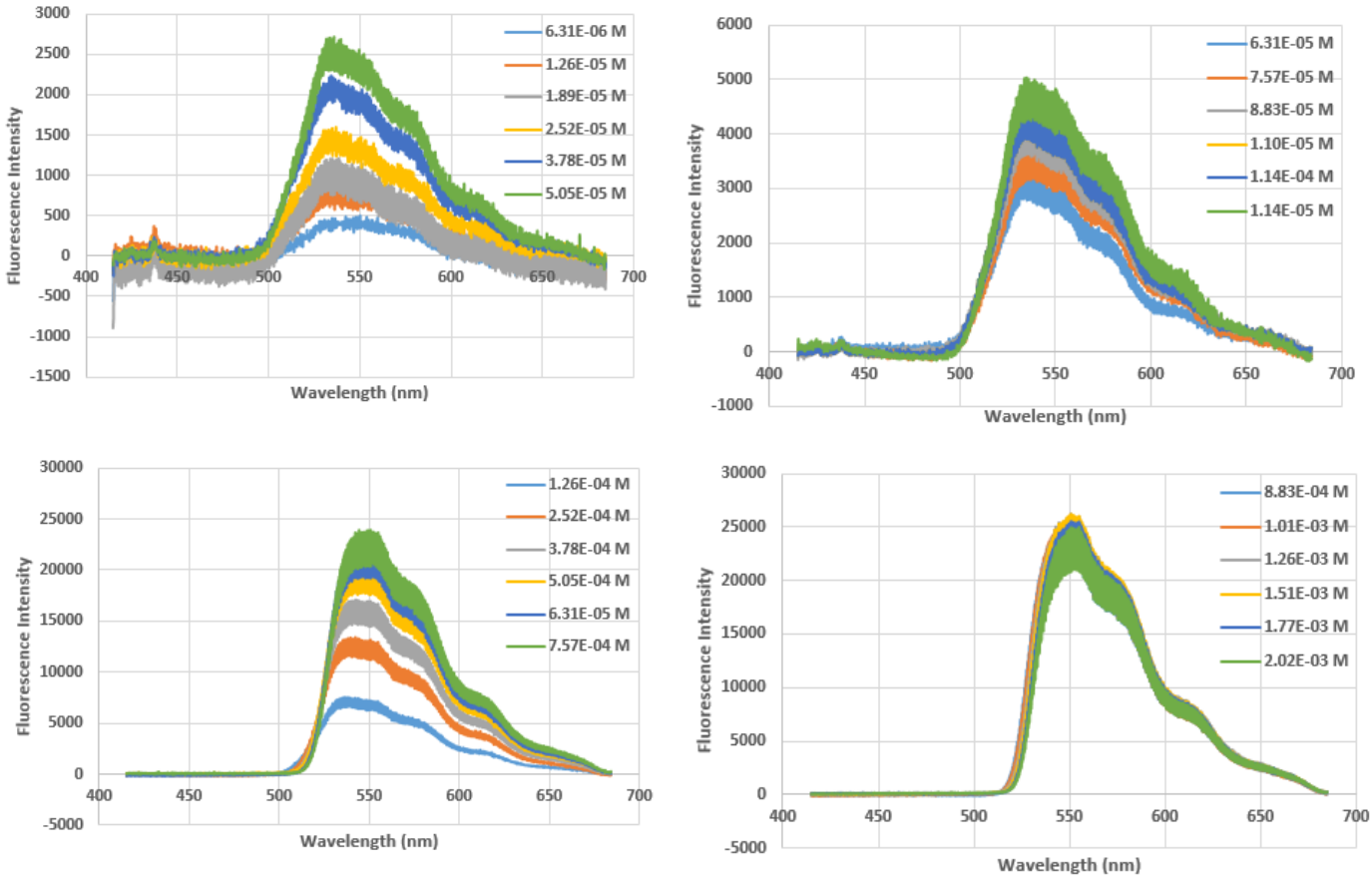

Figure A2.4. SPEF spectra of NBD-DMA in 100% acetonitrile ranging from a concentration of 6.31 x 10^{-6} M to 2.02 x 10^{-6} M.

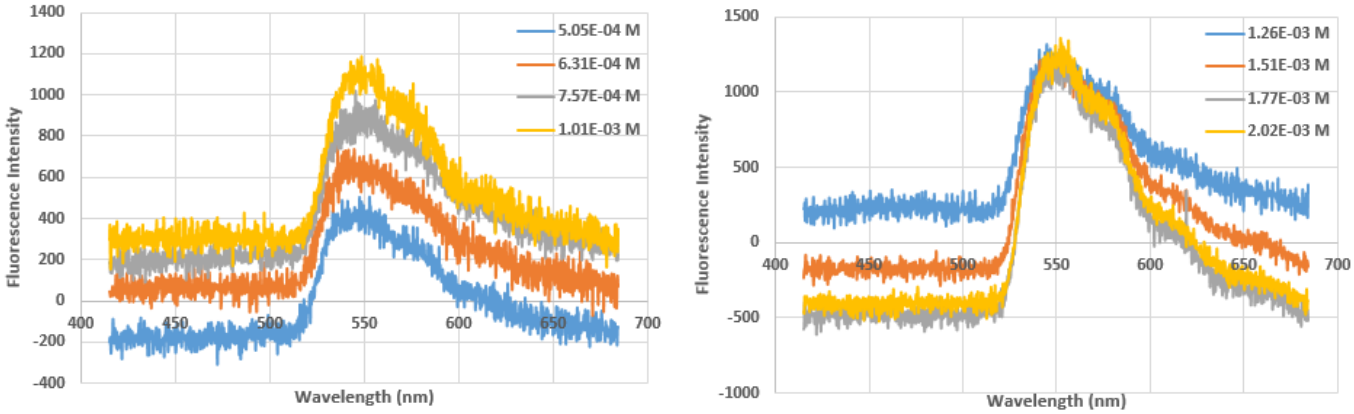

Figure A2.5. TPEF spectrum of NBD-DMA in 100% acetonitrile ranging from a concentration of 5.05 x 10^{-4} M to 2.02 x 10^{-3} M.

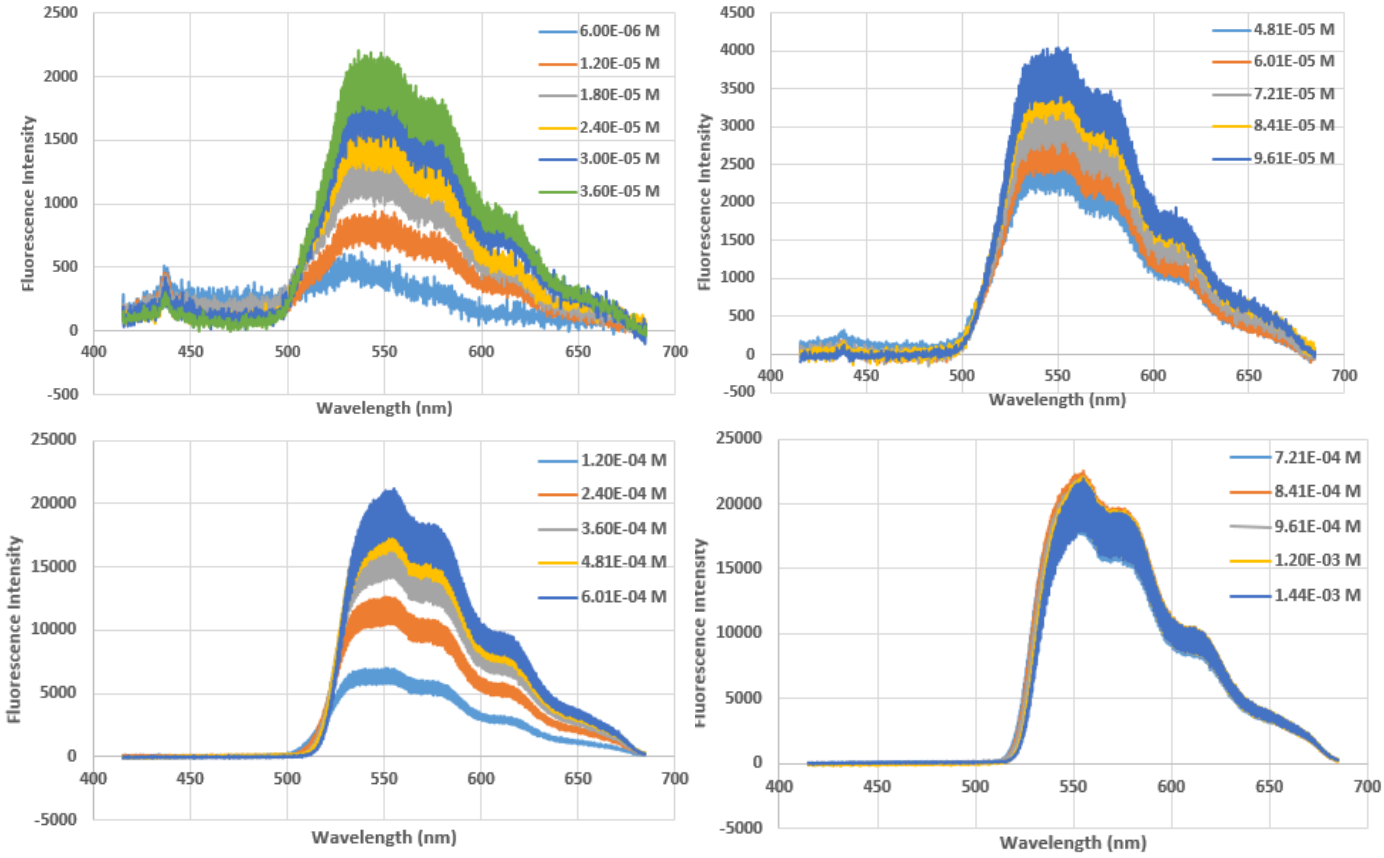

Figure A2.6. SPEF spectra of NBD-DMA in 100% Methanol ranging from a concentration of 6.00 x 10^{-6} M to 1.44 x 10^{-3} M.

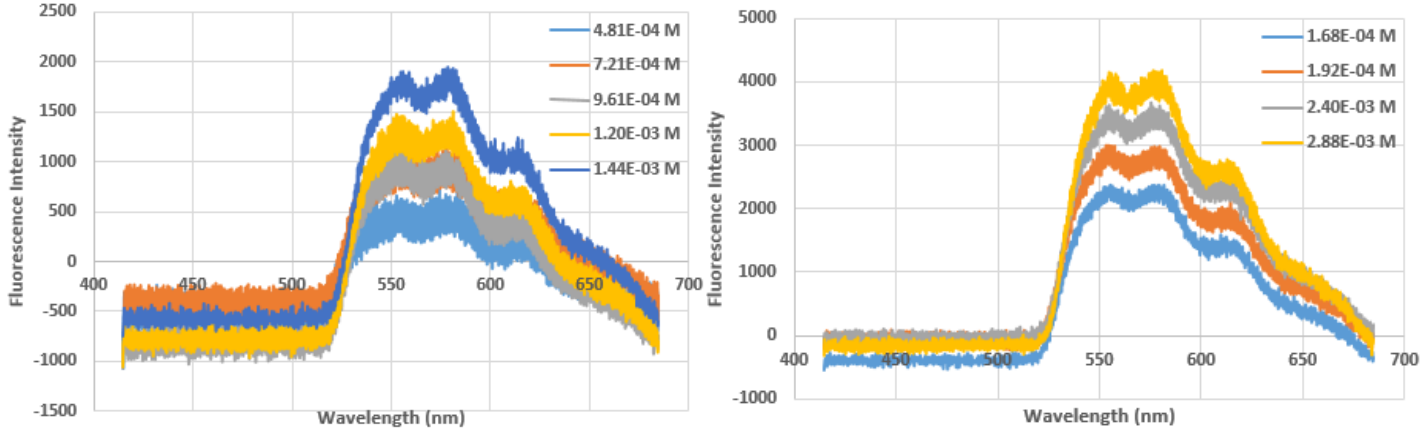

Figure A2.7. TPEF spectra of NBD-DMA in 100% Methanol ranging from a concentration of 4.81 x 10^{-4} M to 2.88 x 10^{-3} M.

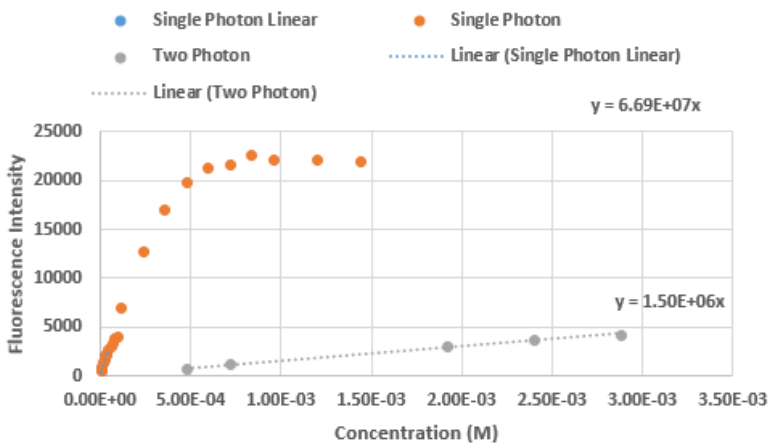

Figure A2.8. Relationship between SPEF (orange circles), TPEF intensities (grey circles) and concentration of NBD-DMA in 100% methanol.

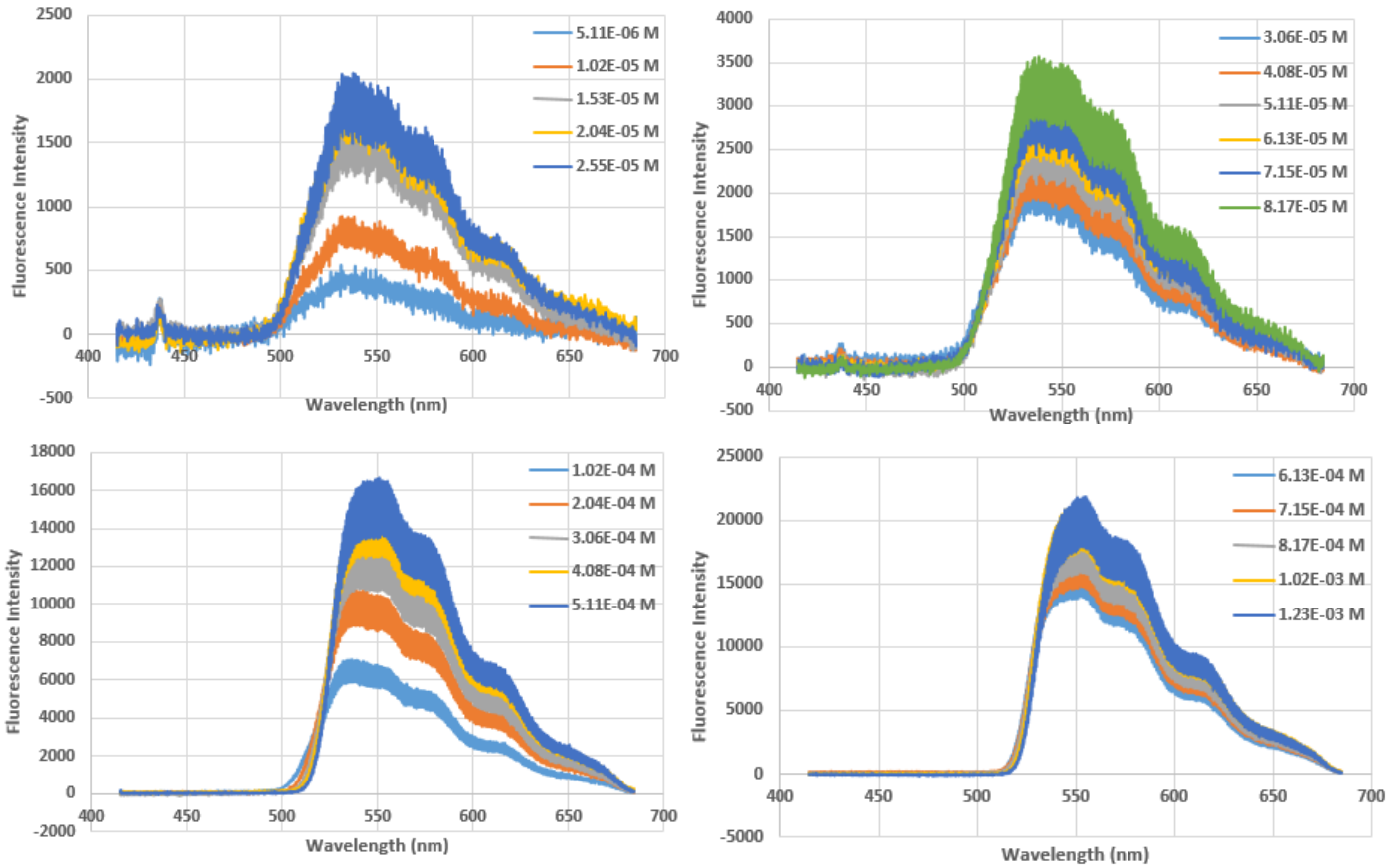

Figure A2.9. SPEF spectra of NBD-DMA in 100% ethanol ranging from a concentration of 5.11 x 10^{-6} M to 1.23 x 10^{-3} M.

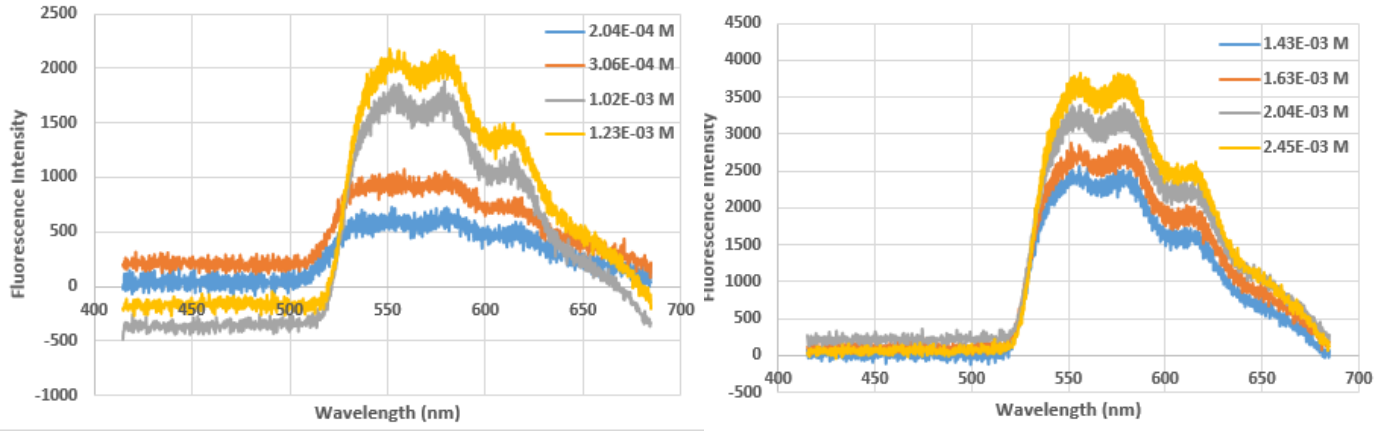

Figure A2.10. TPEF spectra of NBD-DMA in 100% ethanol ranging from a concentration of 2.04 x 10^{-4} M to 2.45 x 10^{-3} M.

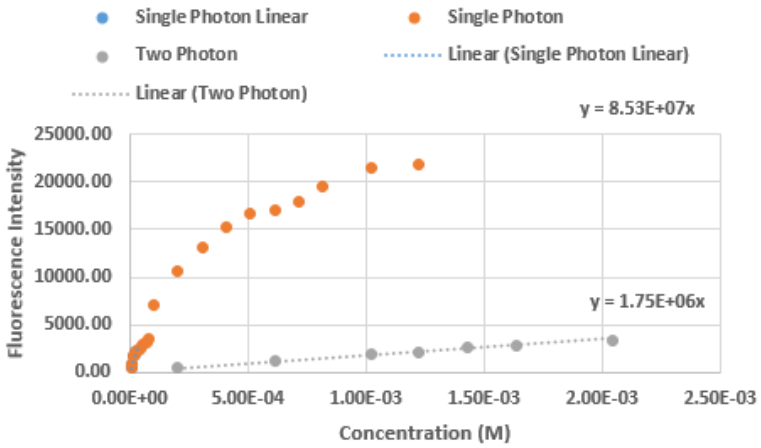

Figure A2.11. Relationship between SPEF (orange circles), TPEF (grey circles) and concentration of NBD-DMA in 100% ethanol.

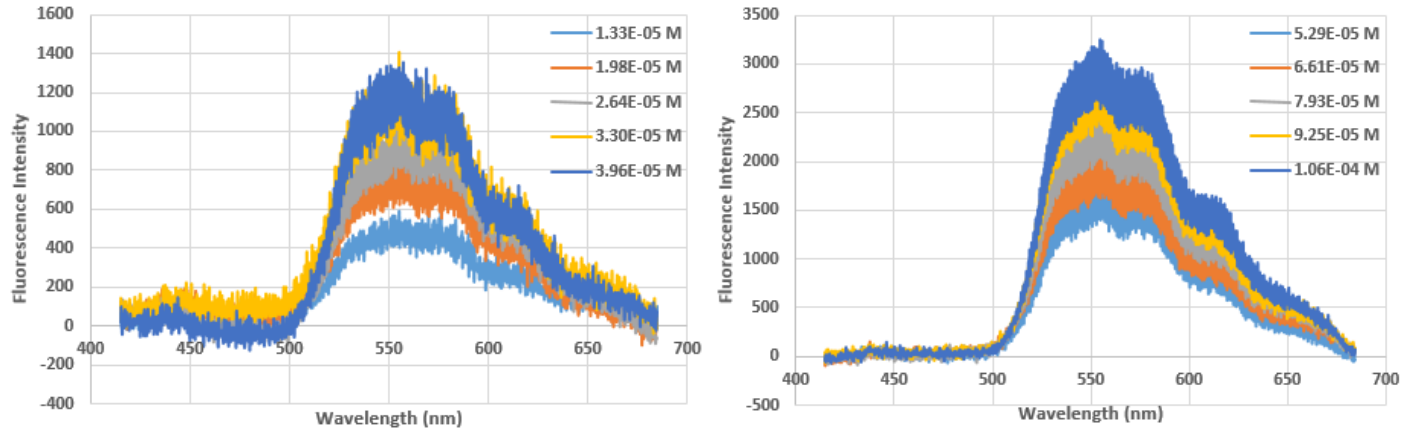

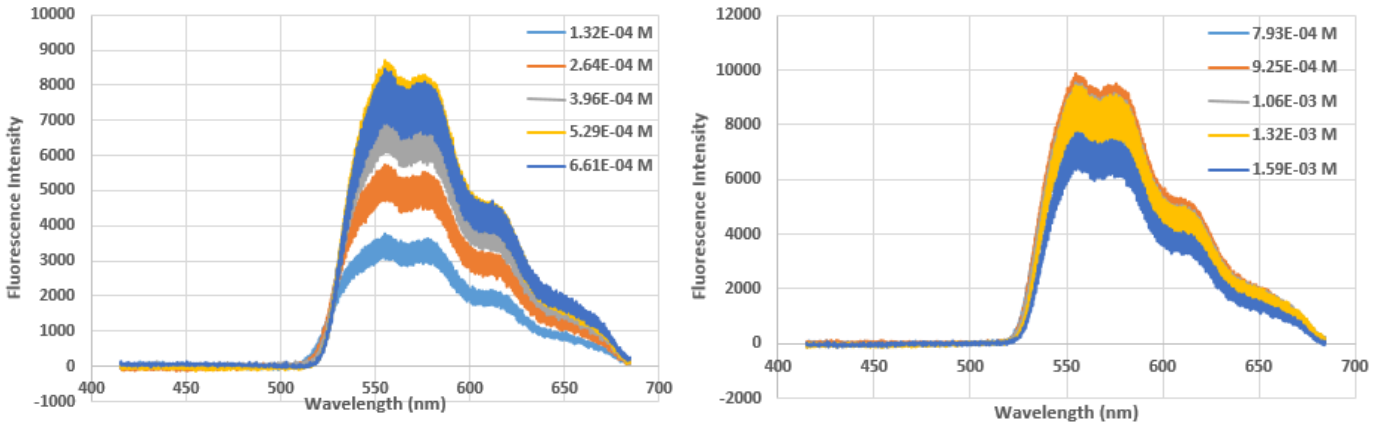

Figure A2.12. SPEF spectra of NBD-DMA in 50% water 50% methanol ranging from a concentration of 1.33 x 10^{-5} M to 1.59 x 10^{-3} M.

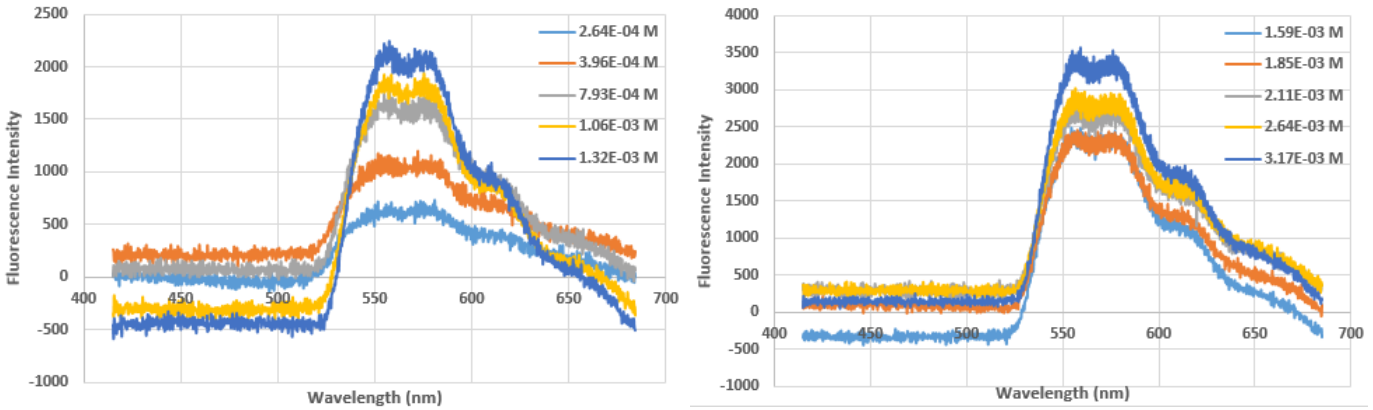

Figure A2.13. TPEF spectra of NBD-DMA in 50% water 50% methanol ranging from a concentration of 2.64 x 10^{-4} M to 3.17 x 10^{-3} M.

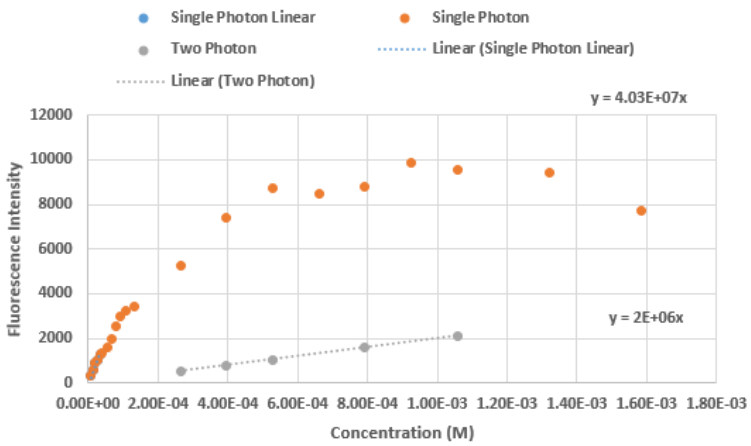

Figure A2.14. Relationship between SPEF (orange circles), TPEF (grey circles) intensities and concentration of NBD-DMA in 50% MeOH 50% H_2O.

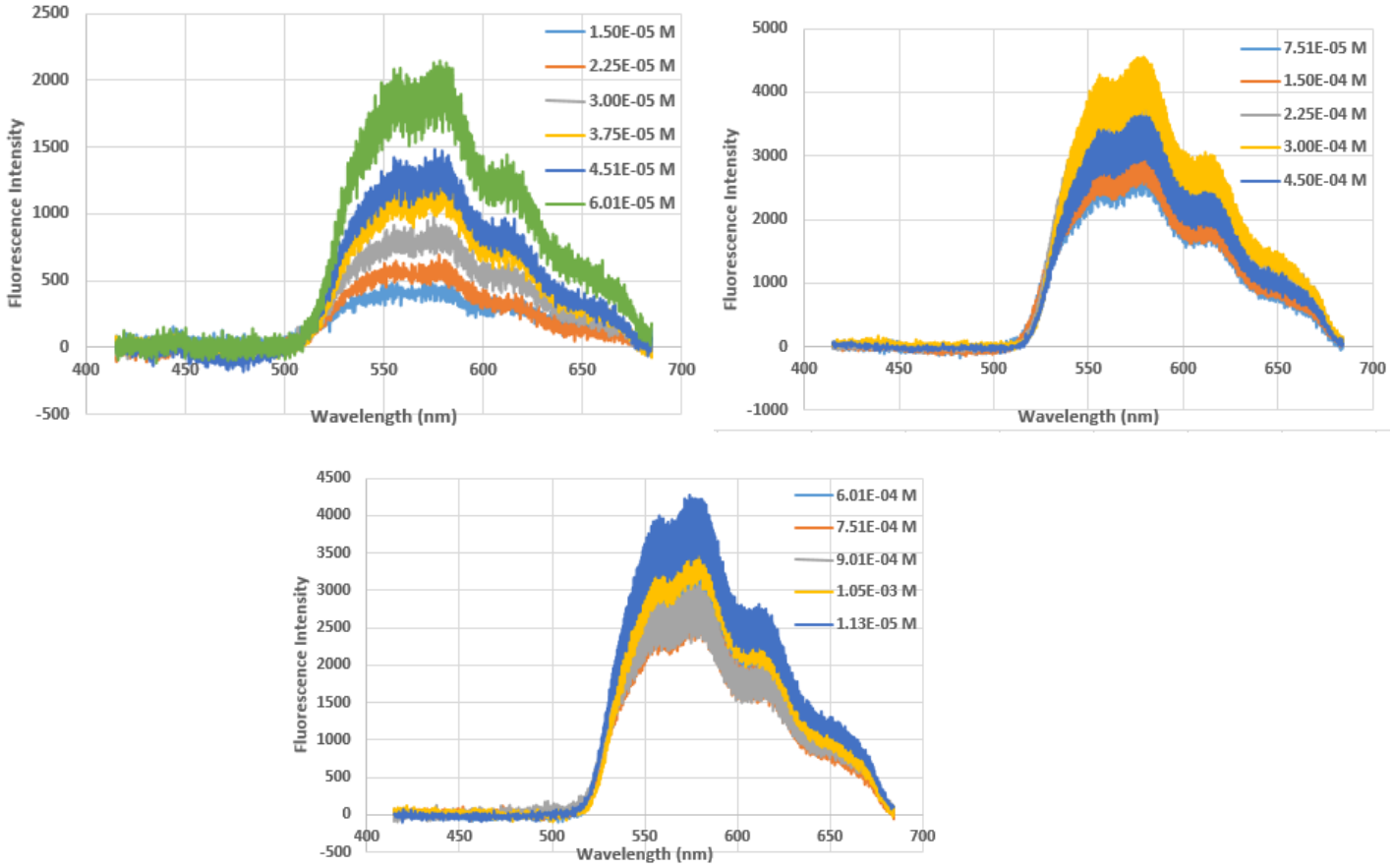

Figure A2.15. SPEF spectra of NBD-DMA in 100% water ranging from a concentration of1.05 x10^{-5} M to 1.13 x 10^{-3} M.

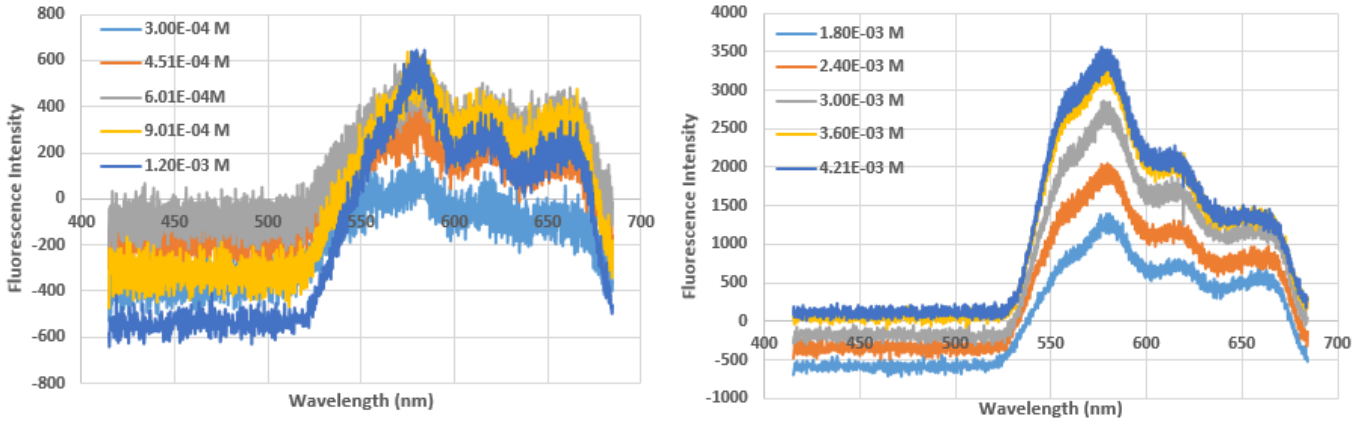

Figure A2.16. TPEF spectra of NBD-DMA in 100% water ranging from a concentration of 3.00 x 10^{-4} to 4.21 x 10^{-3} M.

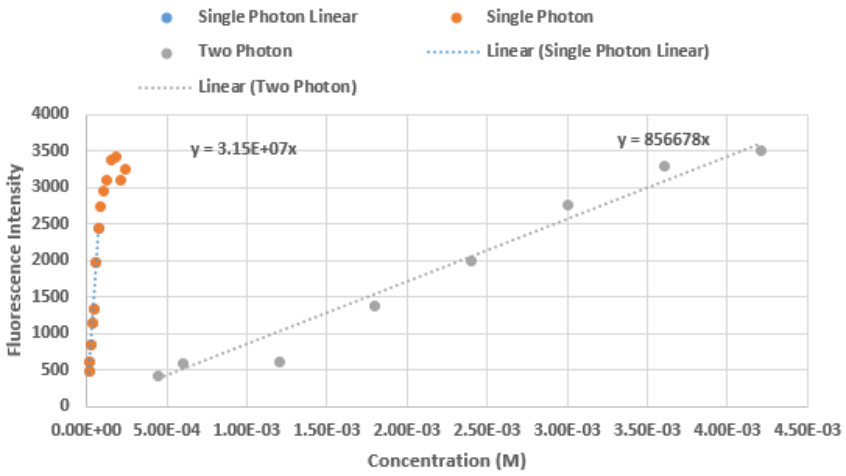

Figure A2.17. Relationship between SPEF (orange circles) and TPEF (grey circles) intensities and concentration of NBD-DMA in 100% H_2O.

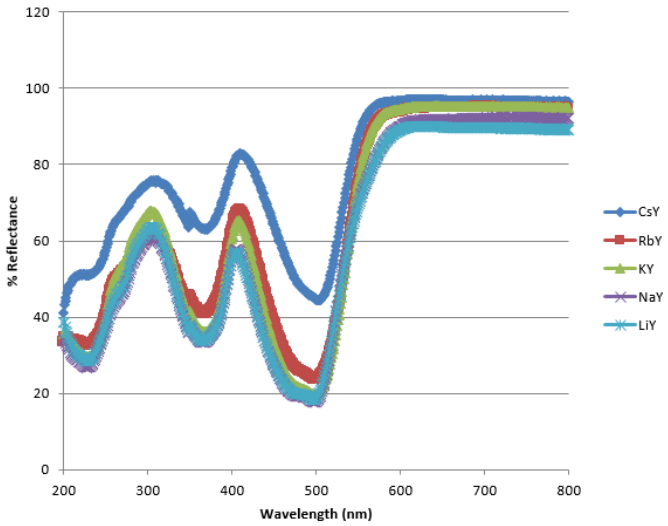

Figure A2.18. Diffuse Reflectance spectrum of NBD-DMA incorporated in alkali cation zeolites at an experimental loading level of <S> = 1/20.

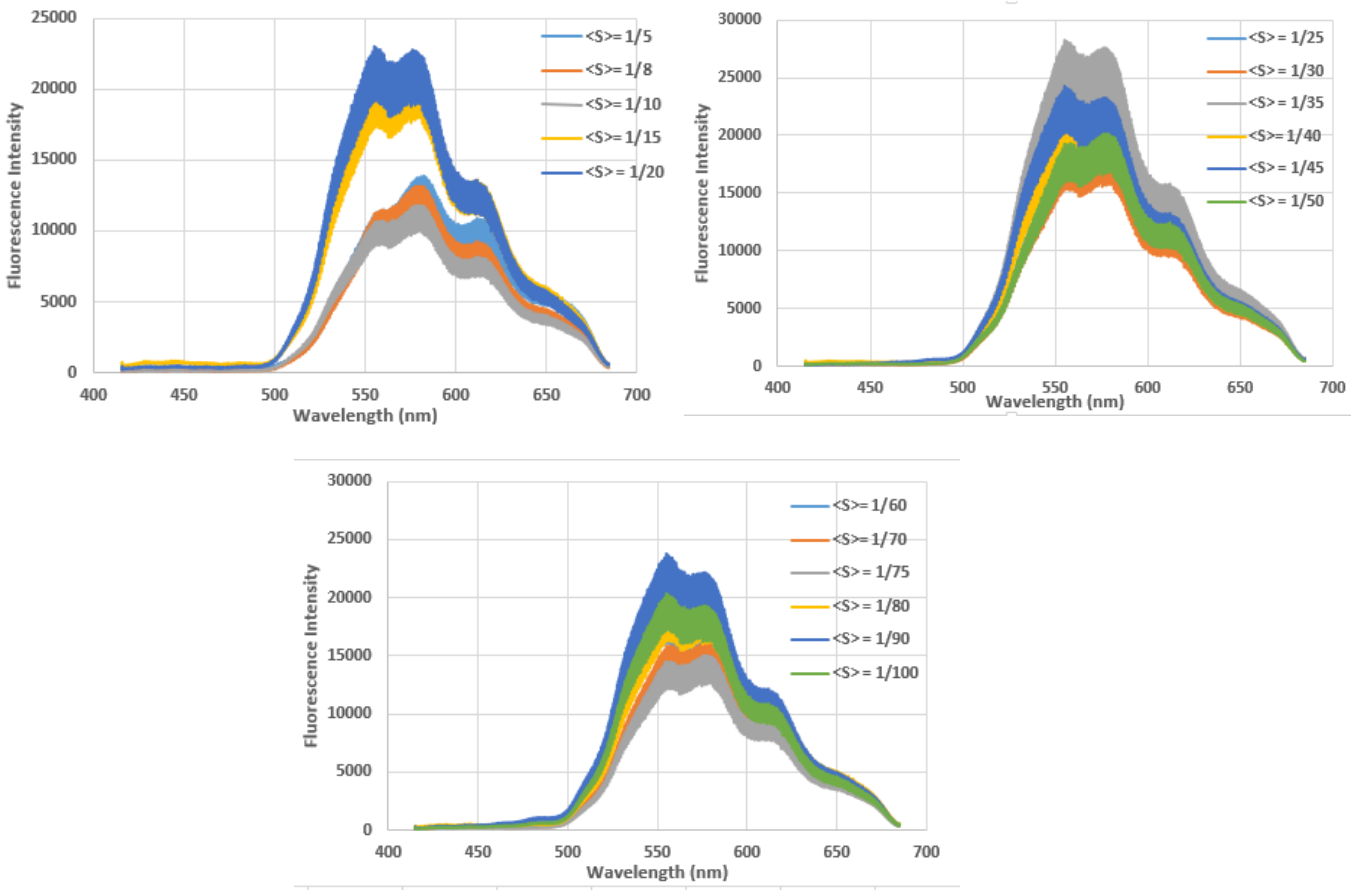

Figure A2.20. SPEF spectra of NBD-DMA incorporated in NaY at various different loading level <S>.

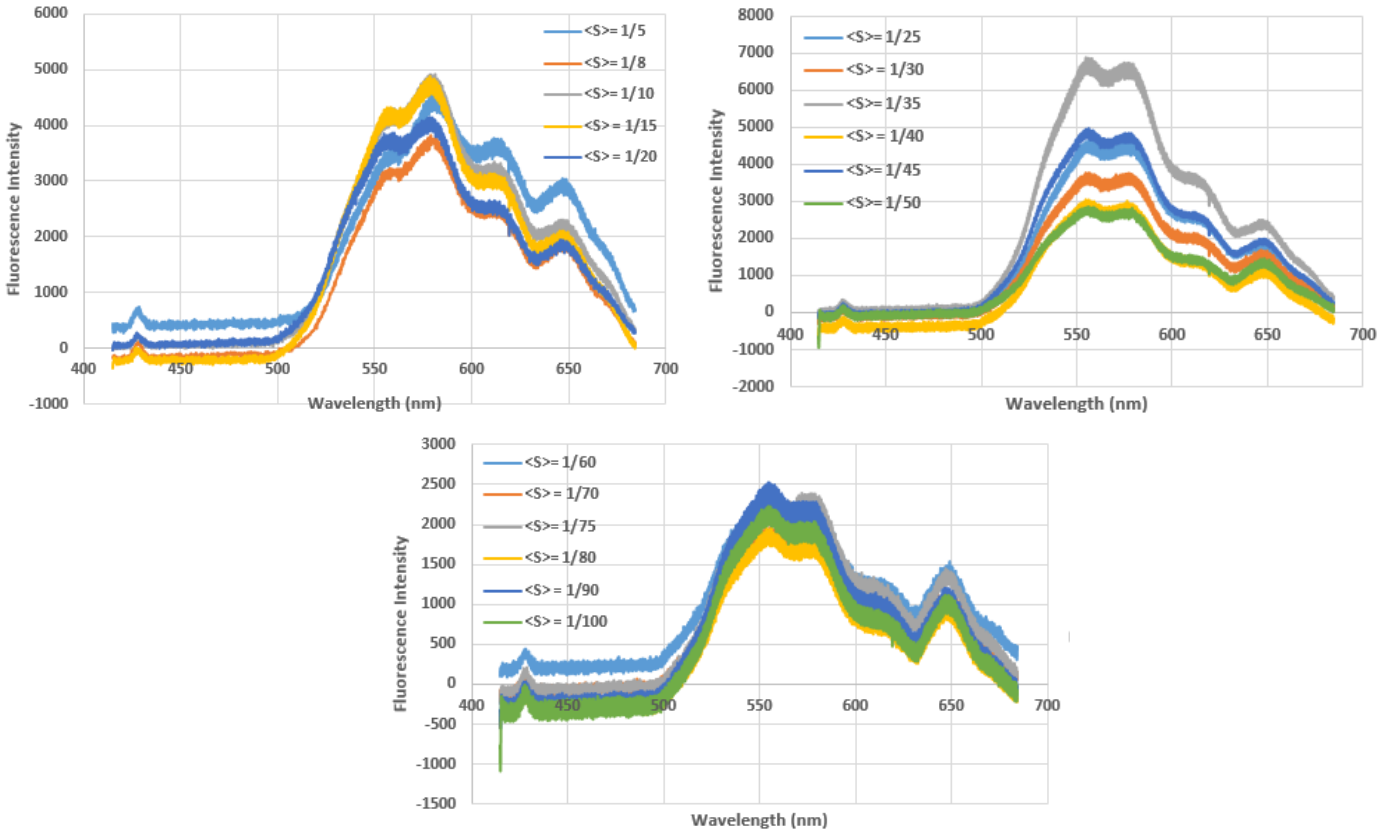

Figure A2.21. TPEF spectra of NBD-DMA incorporated in NaY at various different loading level <S>.

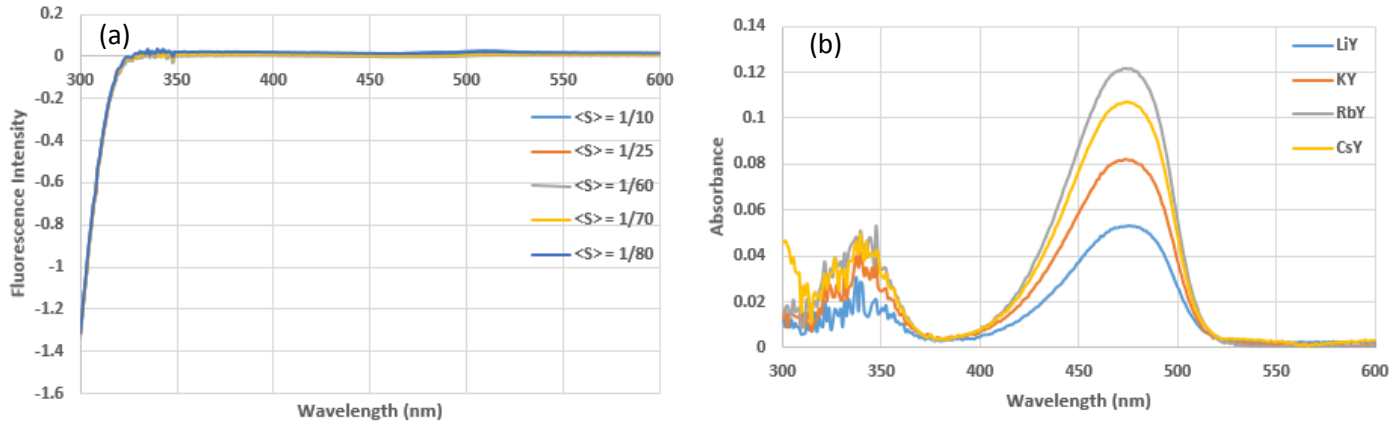

Figure A2.22 Typical UV-vis spectrua of the two combined decanted dichloromethane used to incorporate NBD-DMA in (a) NaY at various different loading level <S> and (b) alkali metal cation exchanged zeolites.

Table A2.1. Summary of SPEF and TPEF intensities from the respective SPEF and TPEF spectra of NBD-DMA incorporated in NaY at various different loading level <S>.

Loading Level <S>	SPEF	TPEF	1P:2P	2P:1P
1/5	1.39×10^4	4.58×10^3	3.04	0.33
1/8	1.32×10^4	3.83×10^3	3.44	0.29
1/10	1.17×10^4	4.92×10^3	2.38	0.42
1/15	2.16×10^4	4.88×10^3	4.43	0.23
1/20	2.30×10^4	4.14×10^3	5.56	0.18
1/25	2.42×10^4	4.64×10^3	5.22	0.19
1/30	1.88×10^4	3.77×10^3	4.99	0.20
1/35	2.82×10^4	6.87×10^3	4.11	0.24
1/40	2.16×10^4	3.03×10^3	7.12	0.14
1/45	2.42×10^4	4.99×10^3	4.86	0.21
1/50	1.94×10^4	2.40×10^3	8.08	0.12
1/60	1.94×10^4	2.39×10^3	8.10	0.12
1/70	1.62×10^4	1.97×10^3	8.20	0.12
1/75	1.50×10^4	2.43×10^3	6.17	0.16
1/80	1.94×10^4	1.97×10^3	9.88	0.10
1/90	2.38×10^4	2.53×10^3	9.41	0.11
1/100	2.03×10^4	2.24×10^3	9.09	0.11
			Average	0.16

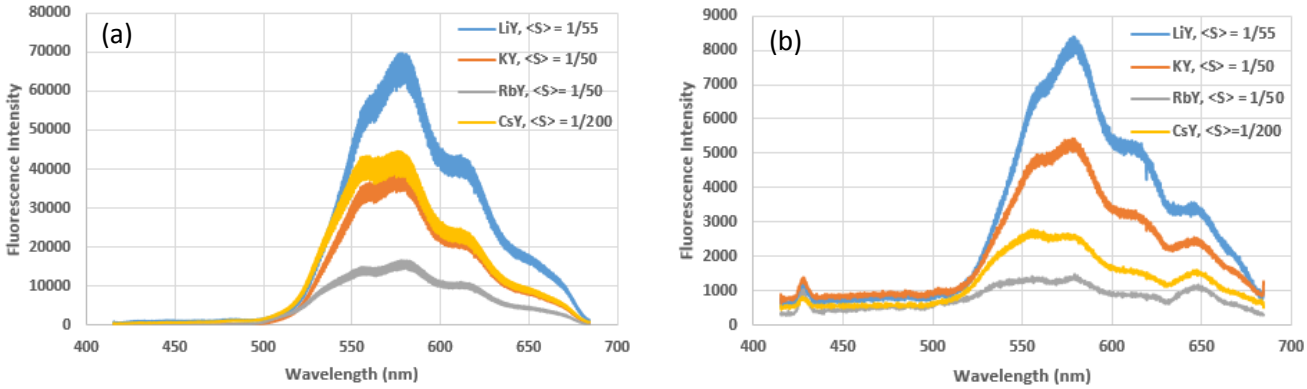

Figure A2.23. (a) SPEF (b) TPEF spectra of NBD-DMA incorporated in various different alkali metal cation exchanged zeolites. LiY (blue line, <S> = 1/55), KY (red line, <S> = 1/50), RbY (grey line, <S> = 1/50) and CsY (yellow line, <S> = 1/200

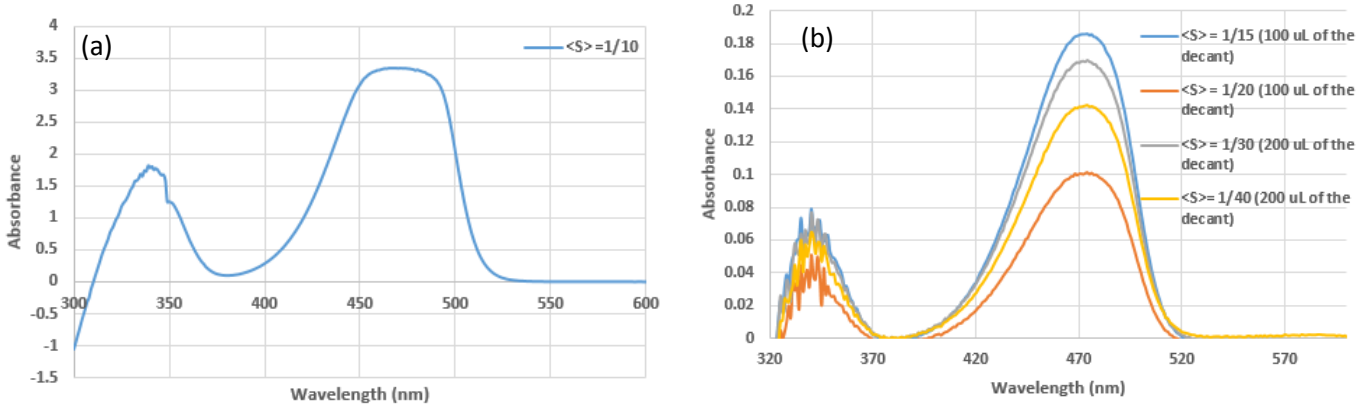

Figure A.2.24. UV-vis spectra of (a) the combined decanted dichloromethane used to incorporated NBD-DMA in a non-heated and hydrated NaY sample. (b) Diluted decanted dichloromethane used to incorporate NBD-DMA in a hydrated NaY at various different experimental loading level <S>. (Note: the decanted dichloromethane had to be diluted because all the sample showed absorption bands like (a) which means the decant is too concentrated and the value of absorption is unreliable in terms of determining the actual loading level.

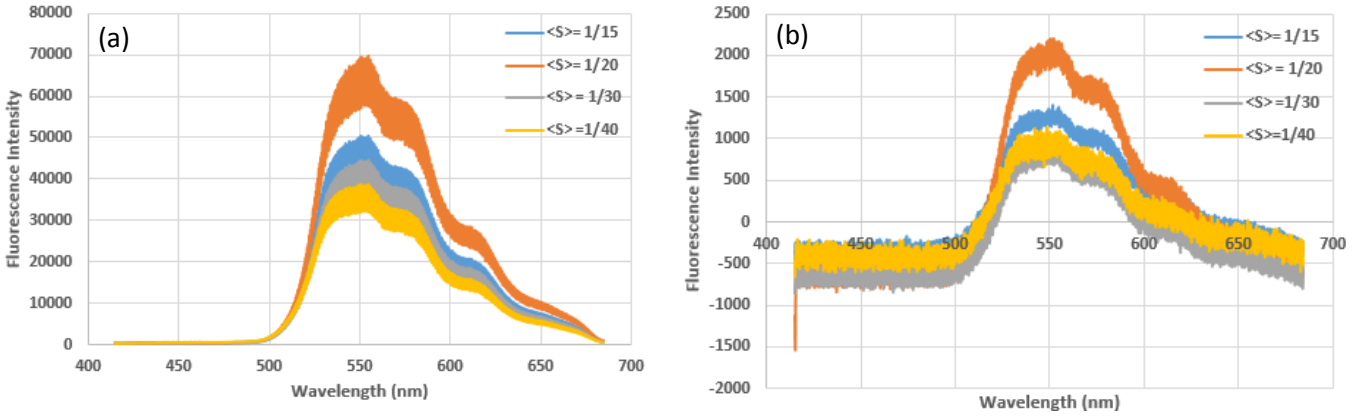

Figure A2.25 (a) SPEF (b) TPEF spectra of NBD-DMA incorporated in a non-heated/hydrated NaY at various different loading level <S>. NaY wasn't heated at 450°C prior to incorporation, actual loading level <S> unknown.

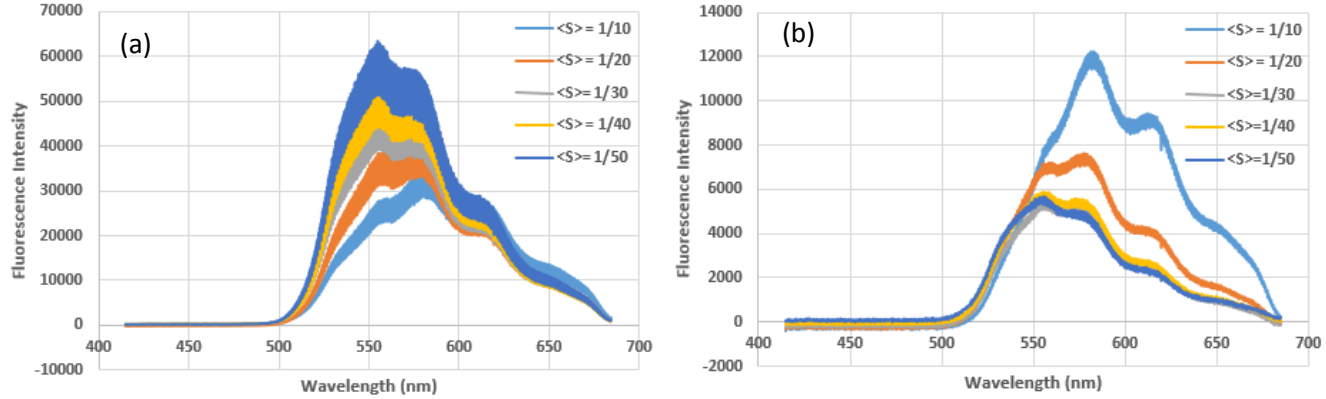

Figure A2.26. (a) SPEF (b) TPEF spectra of NBD-DMA incorporated in a dehydrated NaY at various different loading level <S>. NaY heated prior to incorporation and as a result, 100% incorporation observed. The zeolites were transferred directly to the laser cell in open atmosphere.

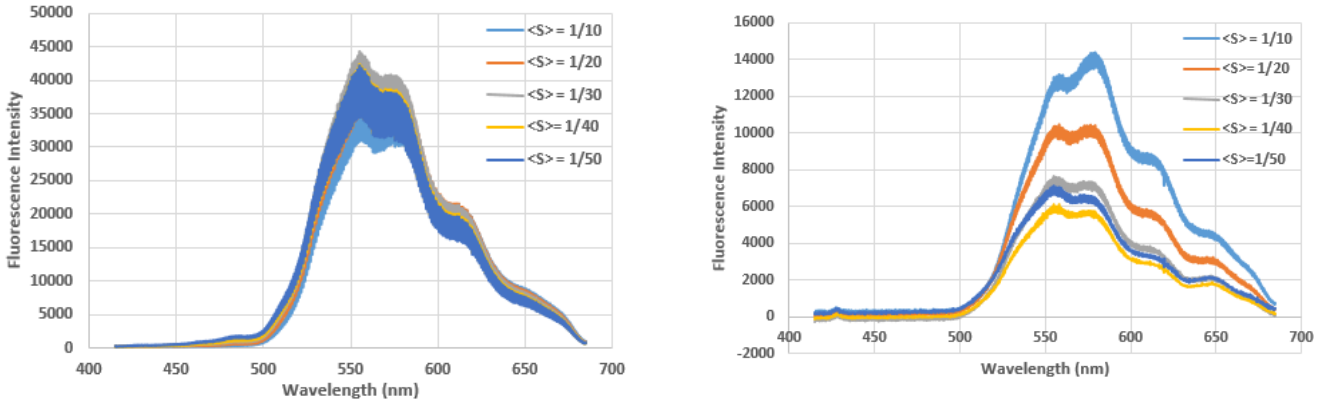

Figure A2.27. (a) SPEF (b) TPEF spectra NBD-DMA incorporated in a hydrated NaY at various different loading level. Same sample as Figure A2.26 but dried in a desiccator under vacuum to remove the dichloromethane present.

Appendix and supporting data for NBD-Methylamine

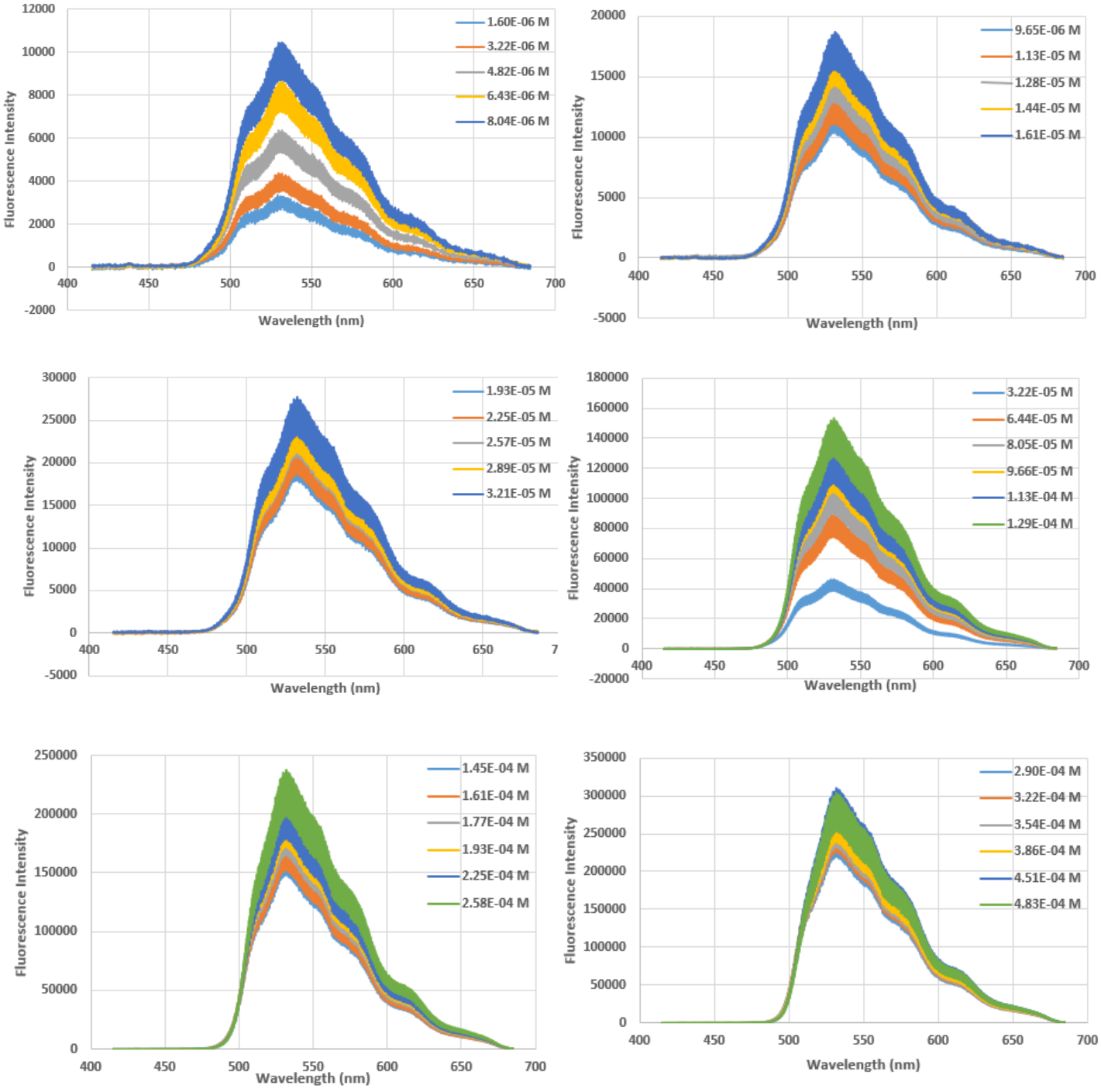

Figure A3.1. Single photon excitation fluorescence (SPEF) spectra of NBD-methylamine in 100% acetonitrile ranging from a concentration of 1.60 x 10^{-6} M to 4.83 x 10^{-4} M.

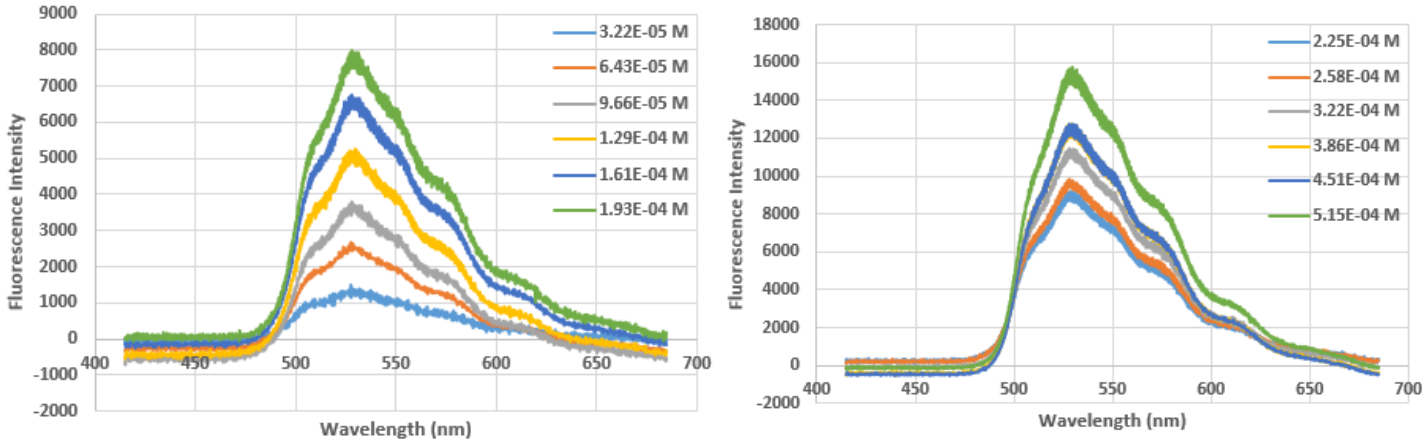

Figure A3.2. Two-Photon excitation fluorescence (TPEF) spectra of NBD-methylamine in 100% acetonitrile ranging from a concentration of 3.22 x 10^{-5} M to 5.15 x 10^{-4} M.

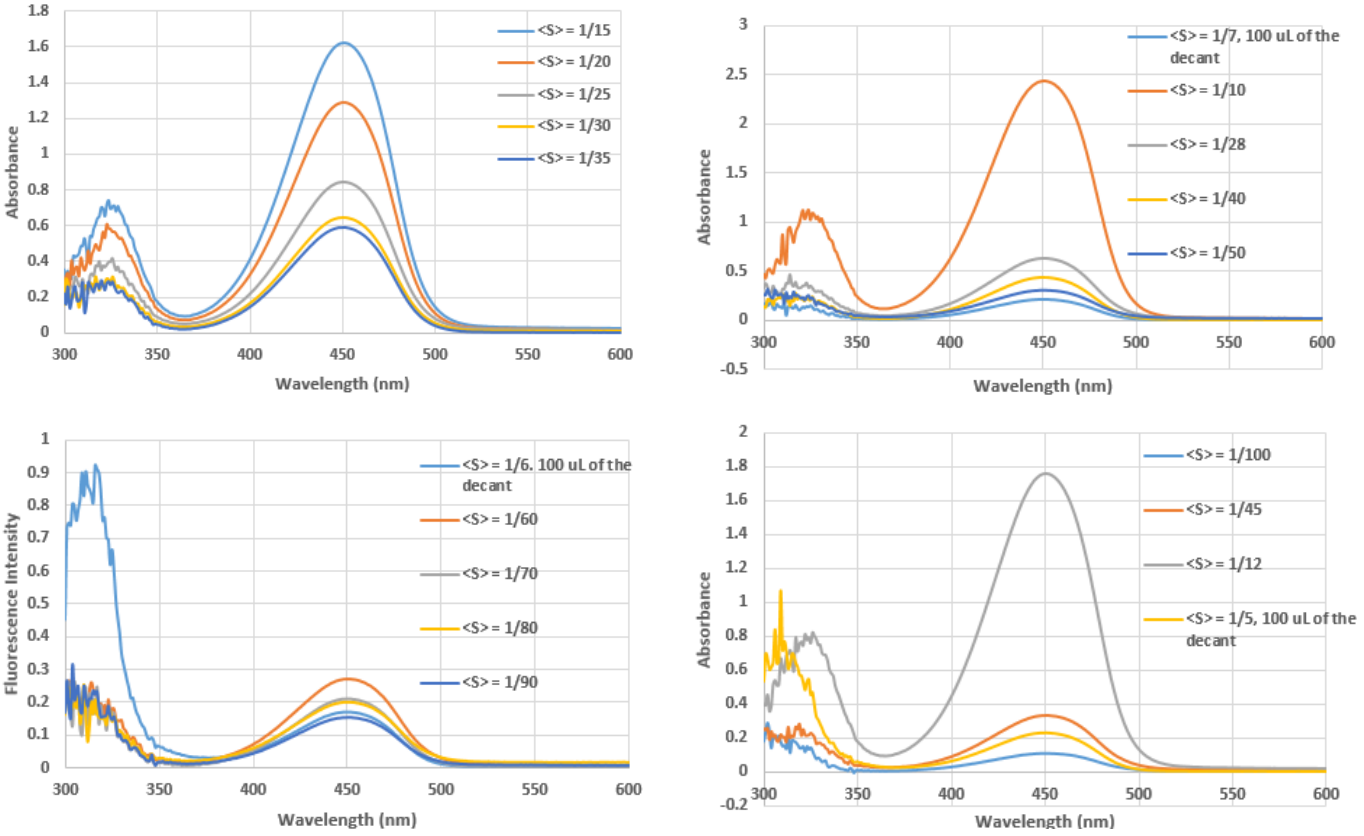

Figure A3.3. UV-vis spectra of the combined decanted dichloromethane used to incorporate NBD-methylamine in NaY at various different loading level <S>.

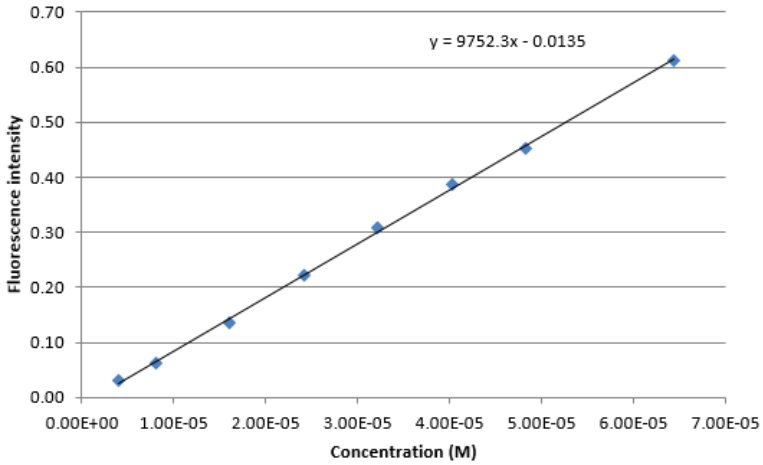

Figure A 3.4. Calibration Curve of NBD-methylamine used to determine the actual loading level <S> in Y zeolites.

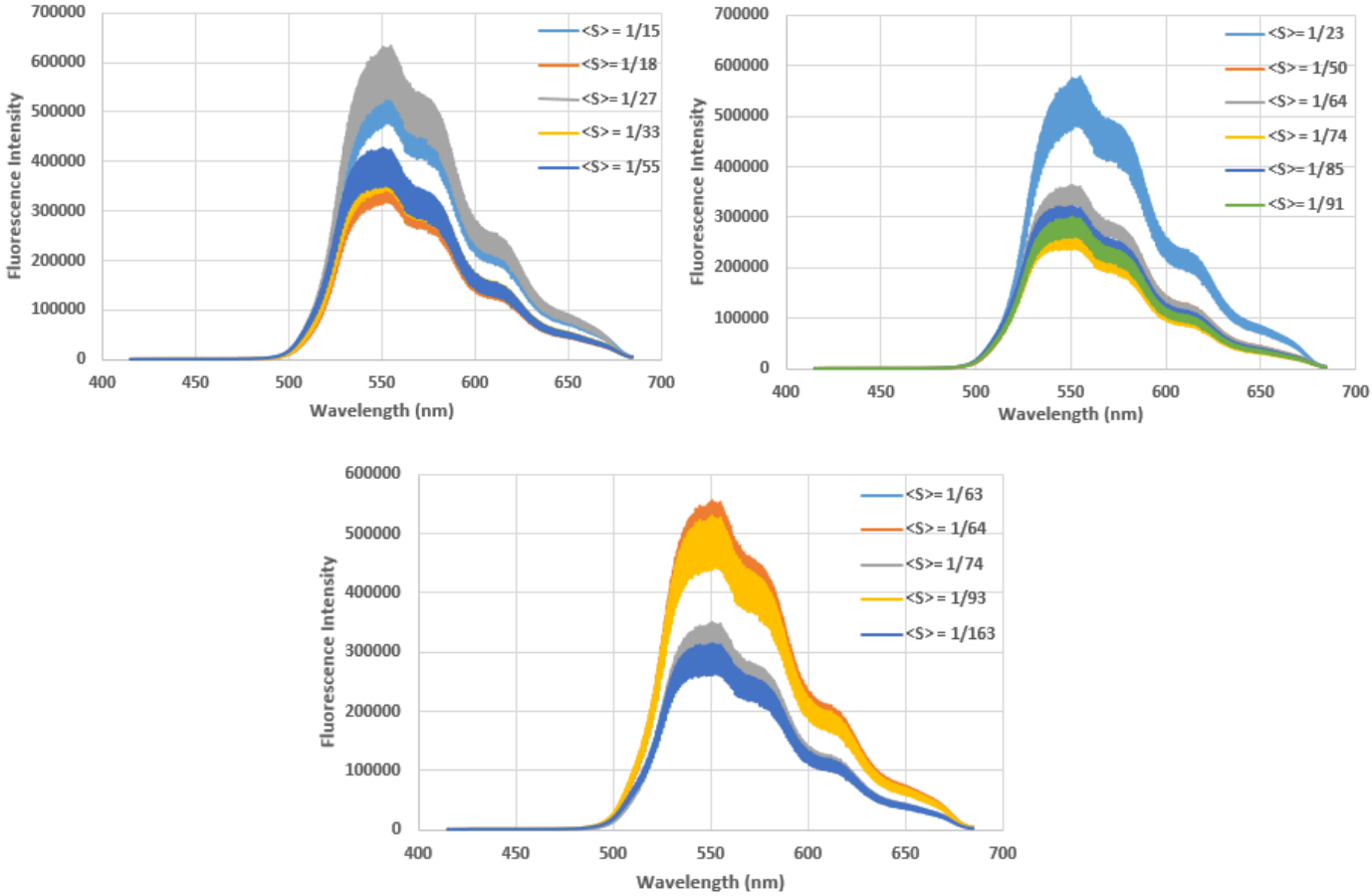

Figure A 3.5. SPEF spectra of NBD-methylamine incorporated in NaY at various different loading level <S>.

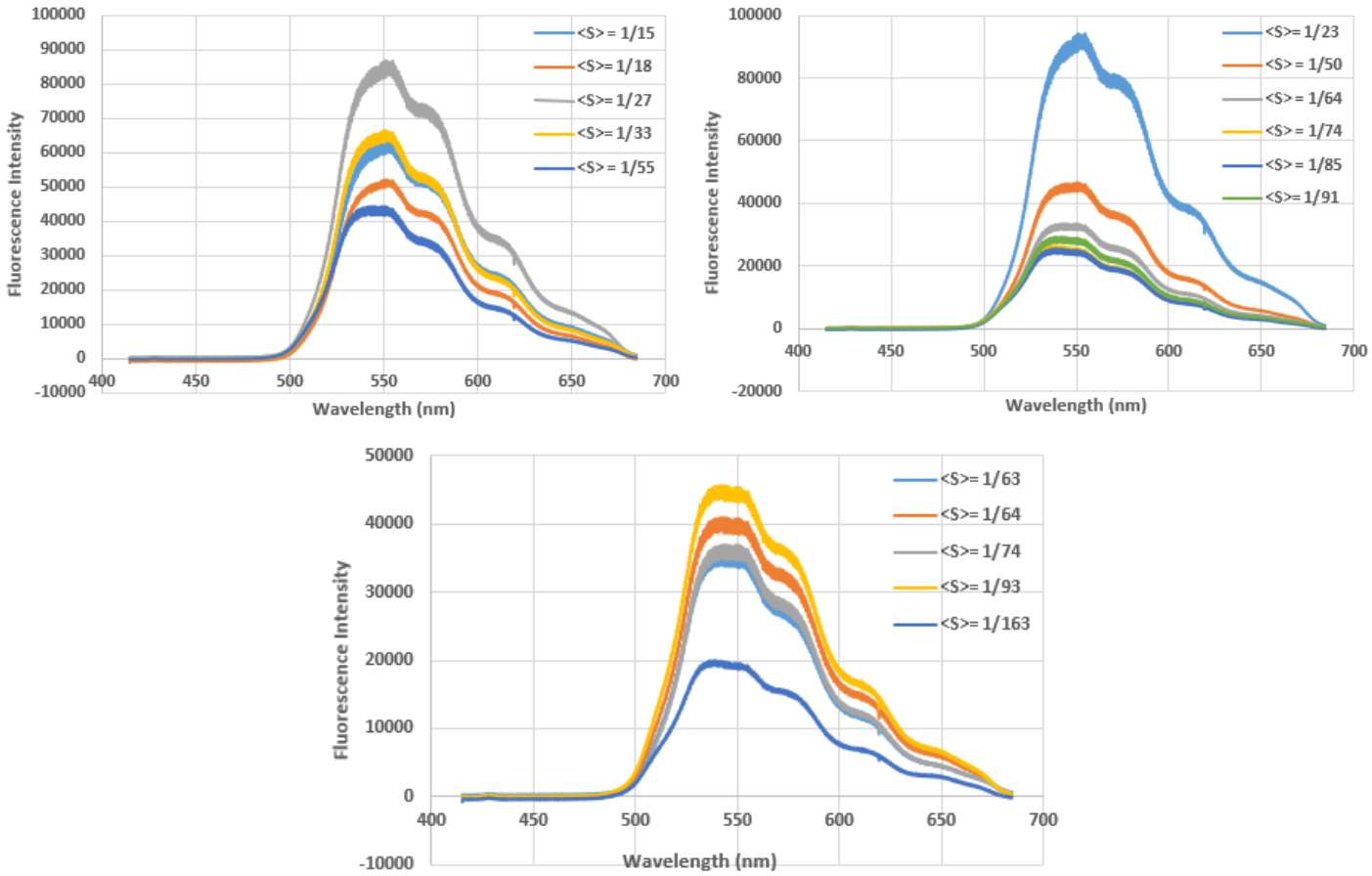

Figure A 3.6. TPEF spectra of NBD-methylamine incorporated in NaY at various different loading level <S>.

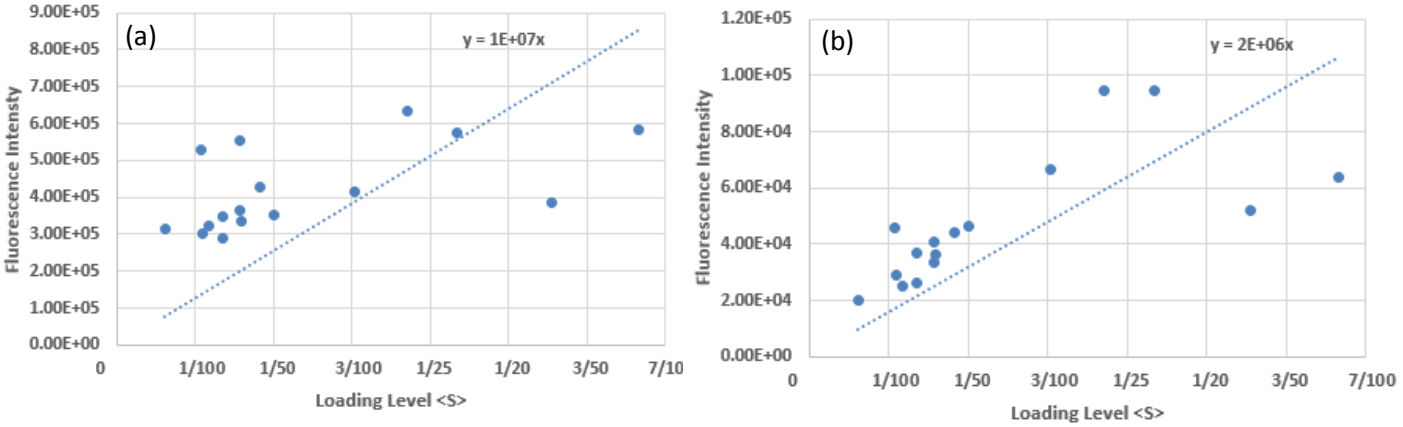

Figure A3.7. Relationship between (a) SPEF (b) TPEF intensities of NBD-methylamine and Loading level <S>.

Table A1.1 Summary of SPEF and TPEF intensities of the respective spectra of the NBD-methylamine incorporated in NaY at various different loading level <S>.

Experimental Loading Level <S>	Actual Loading Level <S>	One Photon	Two Photon	1PA:2PA	2PA:1PA
1/6	1/15	5.82×10^5	6.38×10^4	9.13	0.11
1/7	1/18	3.85×10^5	5.19×10^4	7.41	0.14
1/8	1/23	5.77×10^5	9.45×10^4	6.11	0.16
1/10	1/33	4.15×10^5	6.64×10^4	6.25	0.16
1/12	1/27	6.32×10^5	9.45×10^4	6.69	0.15
1/15	1/50	3.52×10^5	4.66×10^4	7.55	0.13
1/20	1/74	3.50×10^5	3.70×10^4	9.45	0.11
1/25	1/64	3.64×10^5	3.37×10^4	10.80	0.093
1/28	1/55	4.28×10^5	4.43×10^4	9.65	0.10
1/30	1/63	3.35×10^5	3.60×10^4	9.29	0.11
1/35	1/91	3.00×10^5	2.91×10^4	10.33	0.097
1/40	1/74	2.90×10^5	2.64×10^4	10.97	0.091
1/45	1/64	5.56×10^5	4.08×10^4	13.61	0.073
1/50	1/85	3.23×10^5	2.53×10^4	12.76	0.078
1/55	1/93	5.31×10^5	4.56×10^4	11.63	0.086
1/100	1/163	3.13×10^5	1.99×10^4	15.72	0.064
				Average	0.11

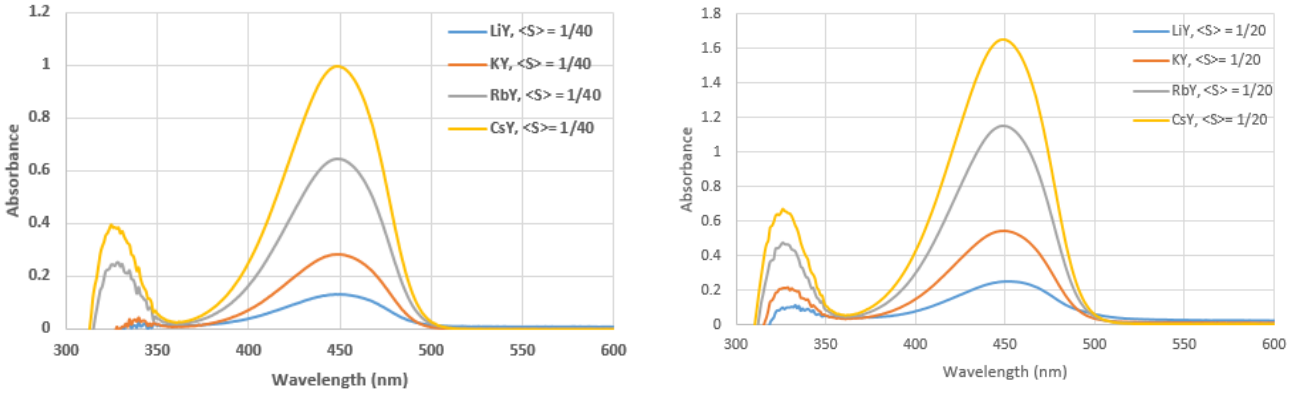

Figure A 3.8. UV-vis spectra of the combined decanted dichloromethane used to incorporate NBD-methylamine in alkali metal cation exchanged zeolites at various different loading level <S>.

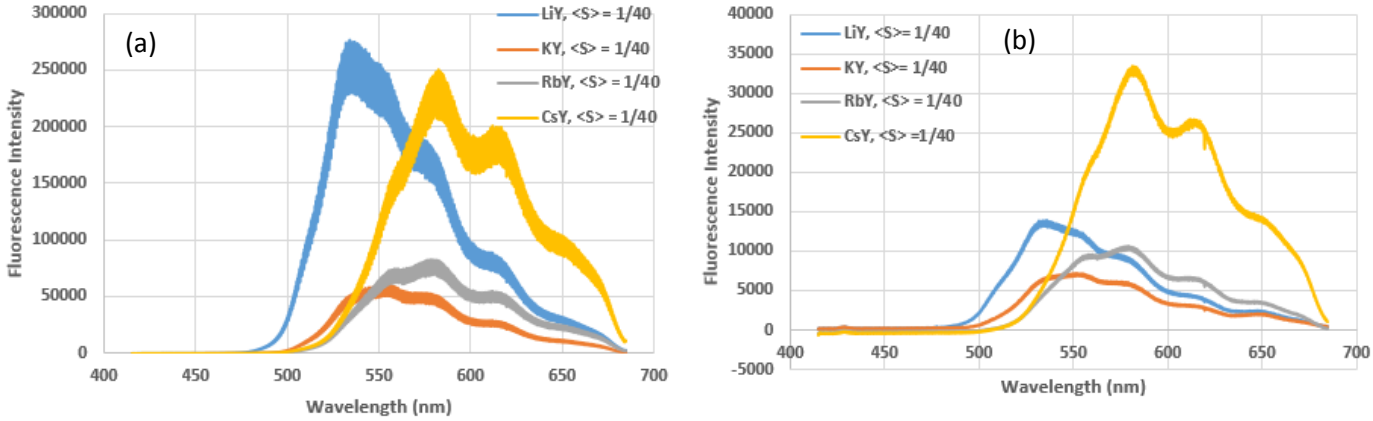

Figure A 3.9. (a) SPEF (b) TPEF spectra of NBD-methylamine incorporated in various different alkali metal cation exchanged zeolites at an experimental loading level of <S> = 1/40.

Appendix and supporting data for NBD-Ethylamine

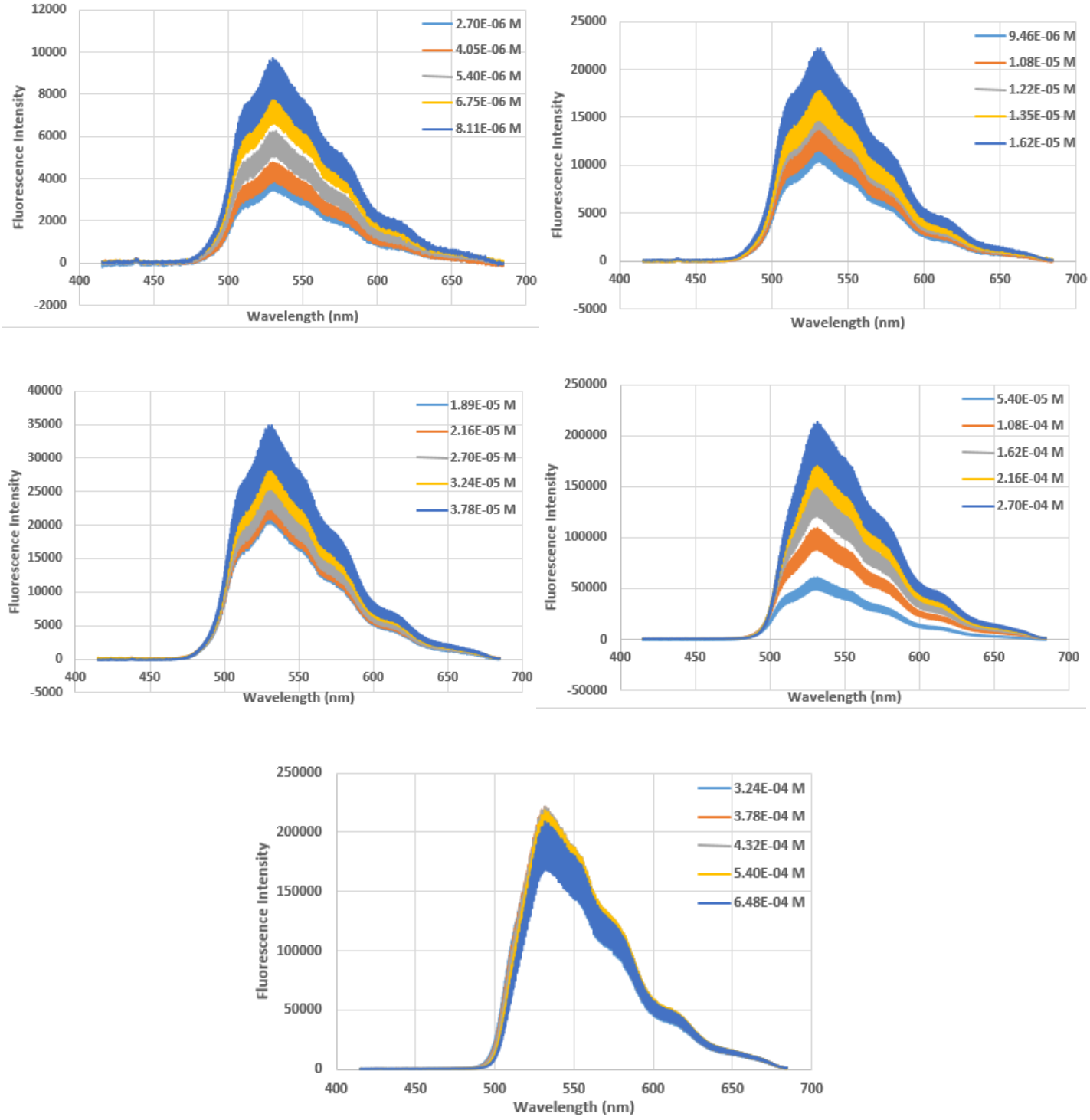

Figure A4.1. SPEF spectra of NBD-Ethylamine in 100% acetonitrile ranging from a concentration of 2.70 x 10^{-6} M to 6.48 x 10^{-4} M.

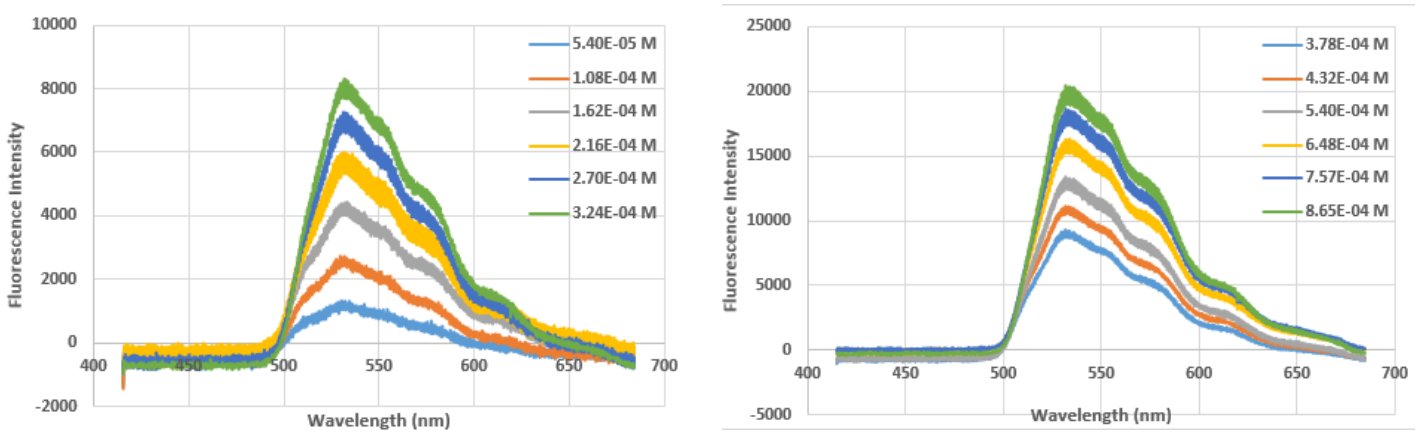

Figure A4.2. TPEF spectra of NBD-Ethylamine in 100% acetonitrile ranging from a concentration of 5.40 x 10^{-5} M to 8.65 x 10^{-4} M.

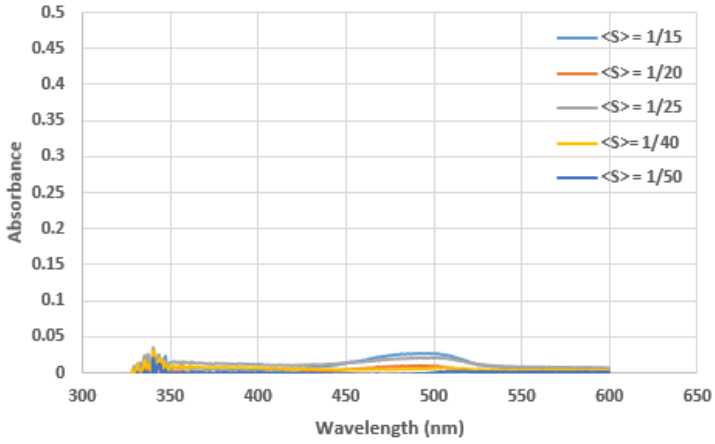

Figure A 4.3. Typical UV-vis spectrum of the two combined decanted dichloromethane used to incorporate NBD-ethylamine in metal cation exchanged zeolites. A 100% incorporation usually observed and as a result, experimental loading level <S> = actual loading level <S>.

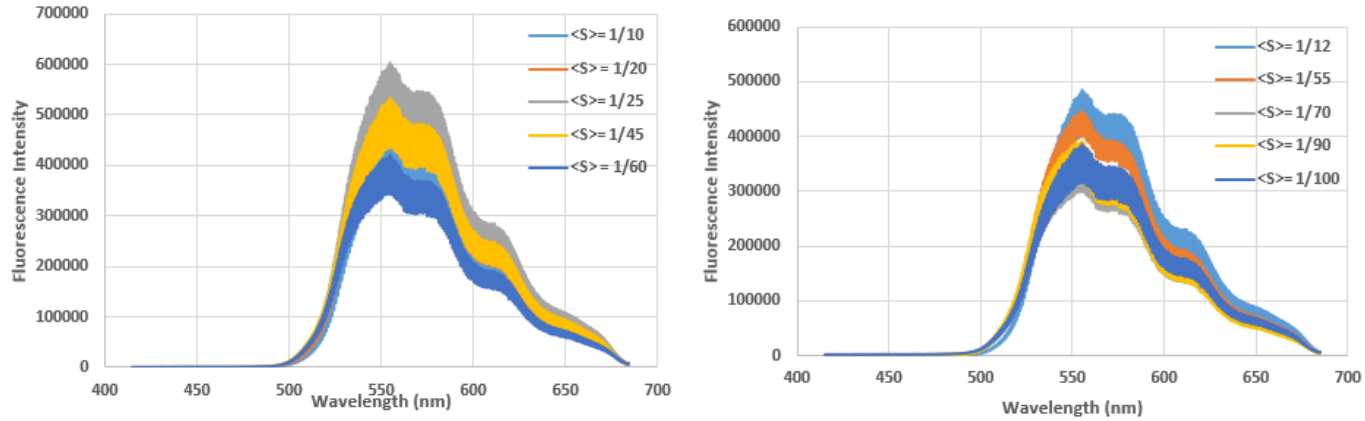

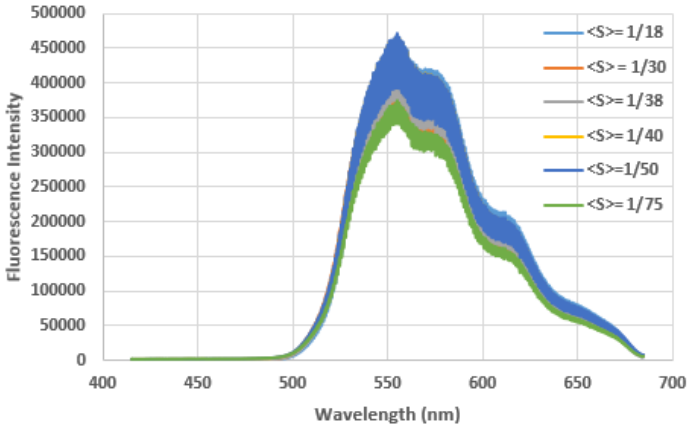

Figure A4.4. SPEF spectra of NBD-Ethylamine incorporated in NaY at various different loading level <S>.

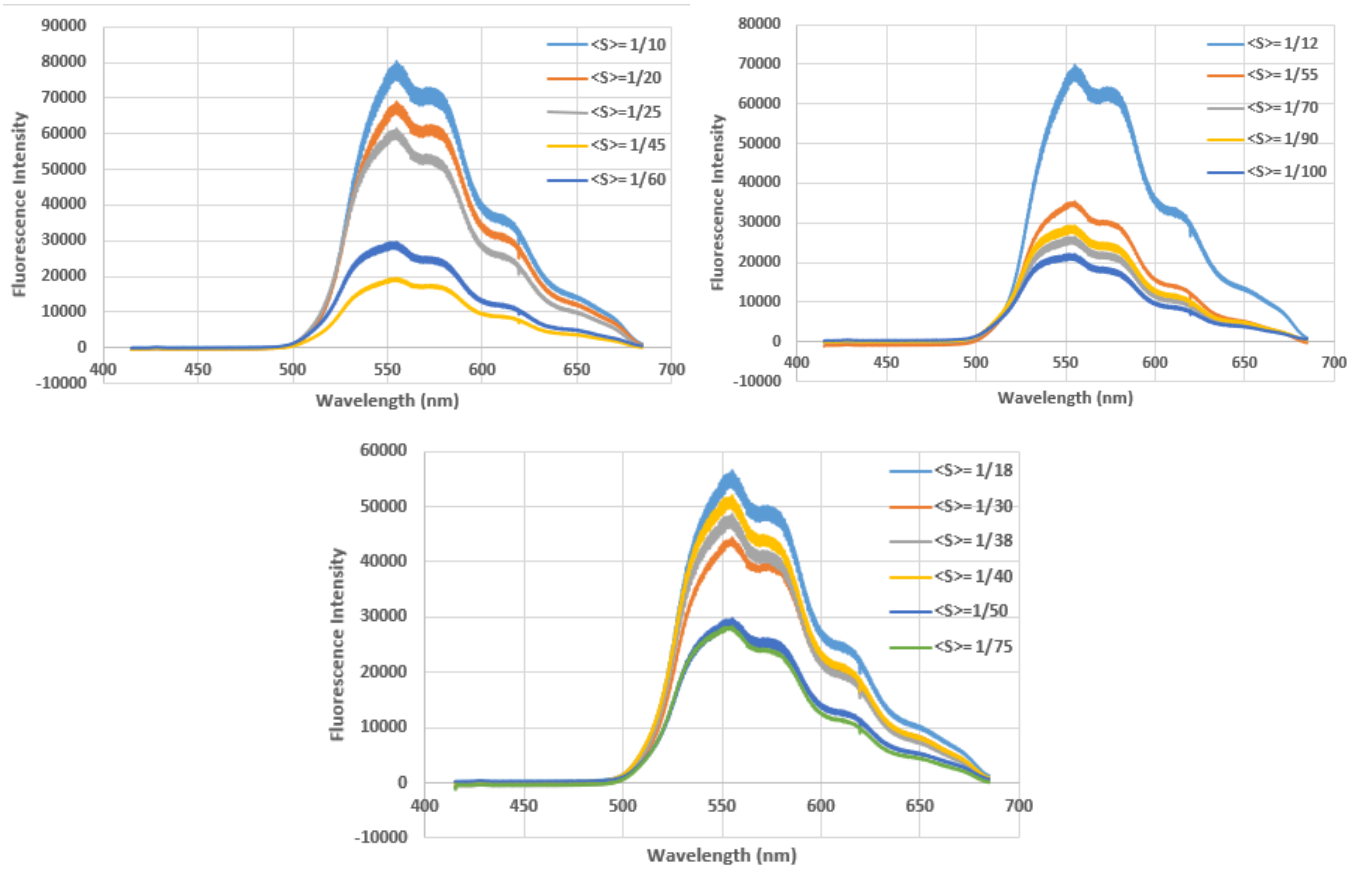

Figure A4.5. TPEF spectra of NBD-Ethylamine incorporated in NaY at various different loading level <S>.

Table A4.1. Summary of SPEF and TPEF intensities of the respective spectra of NBD-ethylamine in NaY at various different loading level <S>.

Loading Level <S>	SPEF	TPEF	1P:2P	2P:1P
1/10	4.80×10^5	8.05×10^4	5.97	0.17
1/12	4.85×10^5	7.00×10^4	6.93	0.14
1/18	4.69×10^5	5.66×10^4	8.29	0.12
1/20	5.24×10^5	6.90×10^4	7.60	0.13
1/25	6.03×10^5	6.13×10^4	9.85	0.10
1/30	4.46×10^5	4.44×10^4	10.04	0.10
1/38	4.69×10^5	5.66×10^4	8.29	0.12
1/40	4.69×10^5	5.20×10^4	9.02	0.11
1/45	5.34×10^5	4.65×10^4	11.47	0.087
1/50	4.72×10^5	2.96×10^4	15.93	0.063
1/55	4.46×10^5	3.54×10^4	12.61	0.079
1/60	4.20×10^5	2.96×10^4	14.20	0.070
1/70	3.66×10^5	2.64×10^4	13.86	0.072
1/75	3.75×10^5	2.84×10^4	13.20	0.076
1/90	3.91×10^5	2.94×10^4	13.33	0.075
1/100	3.87×10^5	2.20×10^4	17.59	0.057
			Average	0.10

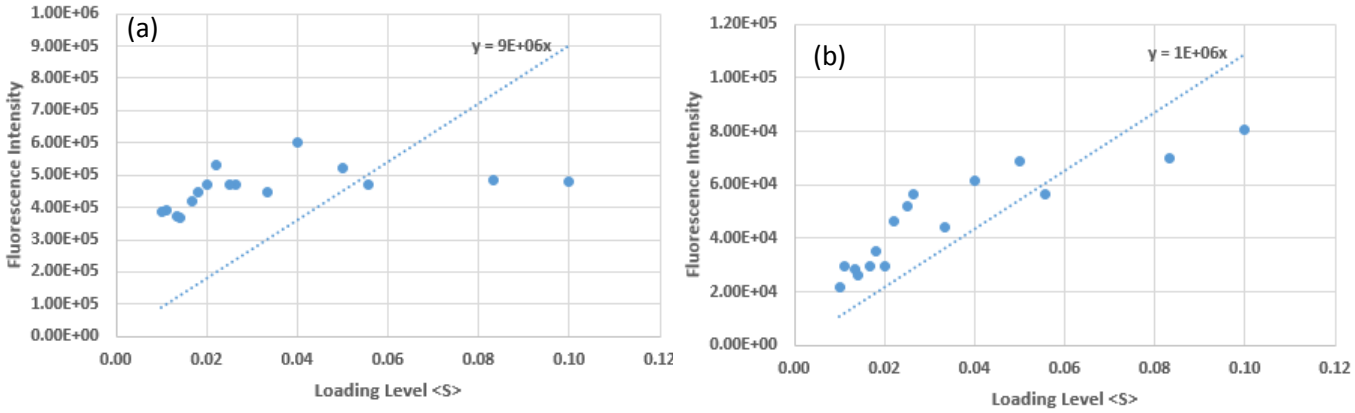

Figure A4.6. Relationship between (a) SPEF (b) TPEF intensities of NBD-Ethylamine and different loading levels <S>.

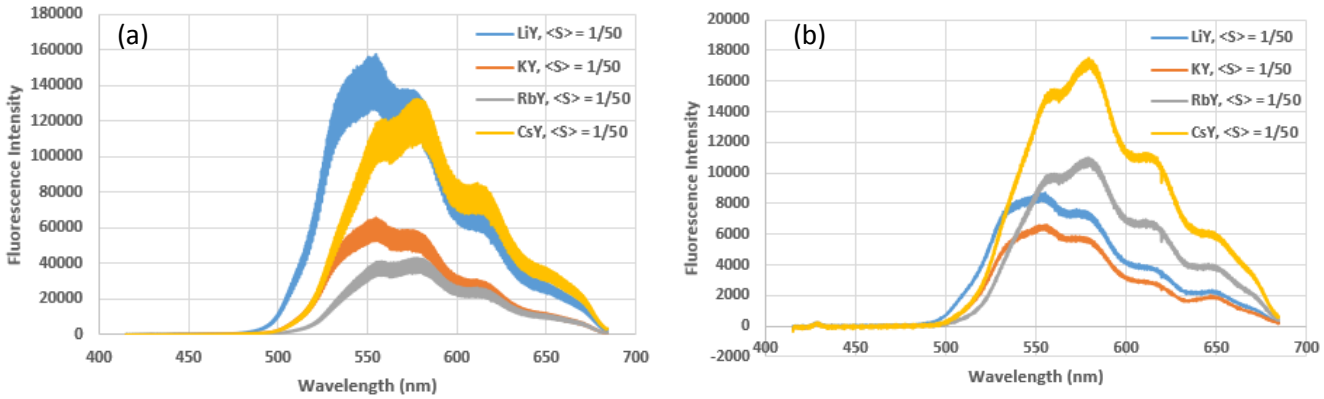

Figure 4A.7. (a) SPEF (b) TPEF spectra of NBD-ethylamine incorporated in various different alkali metal cation exchanged zeolites at an experimental loading level <S> = 1/50.

Appendix and supporting data for NBD-Ethylmethylamine

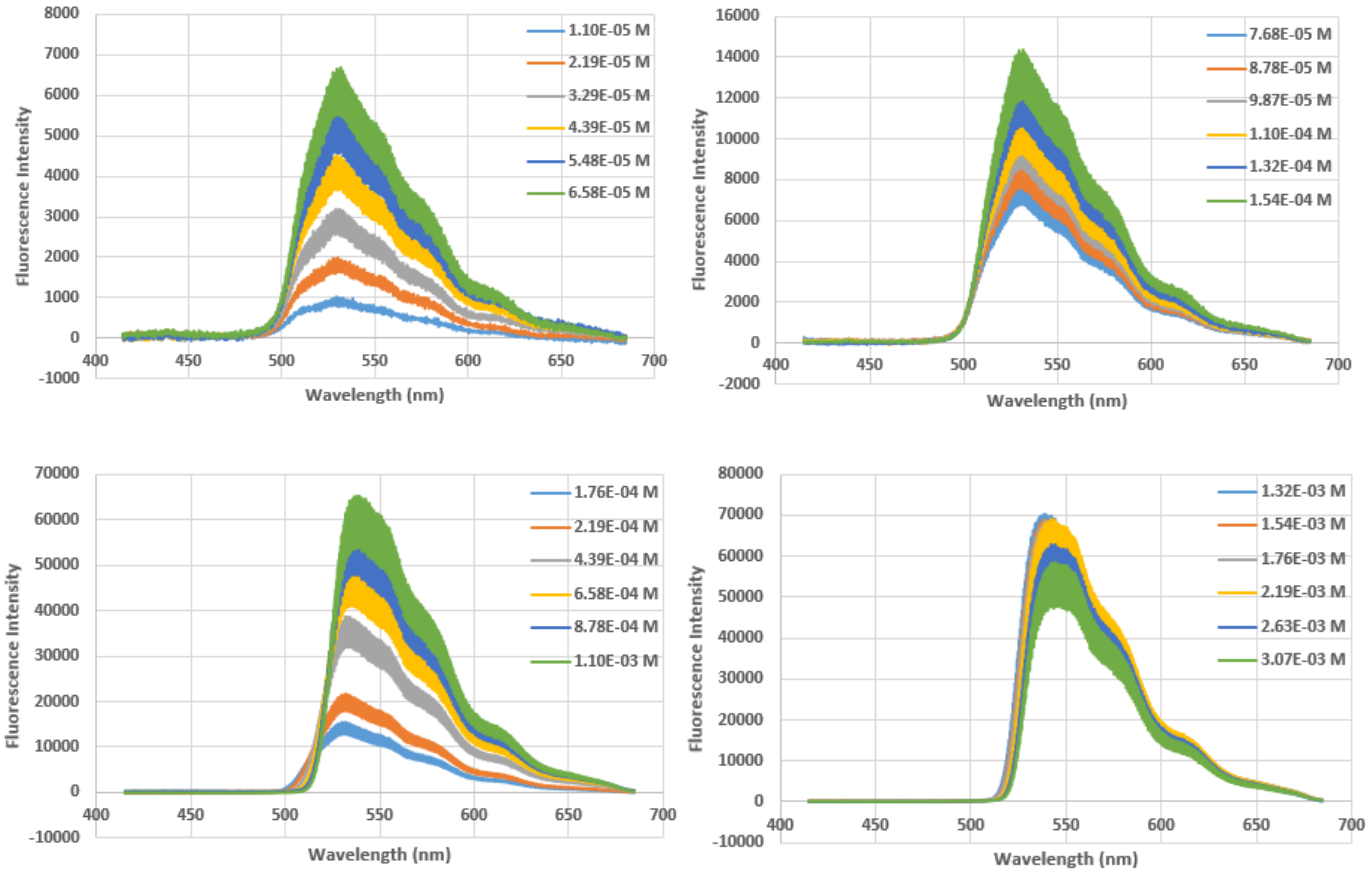

Figure A5.1. SPEF spectra of NBD-ethylmethylamine in 100% dichloromethane ranging from a concentration of 1.10 x 10^{-5} M to 3.07 x 10^{-3} M.

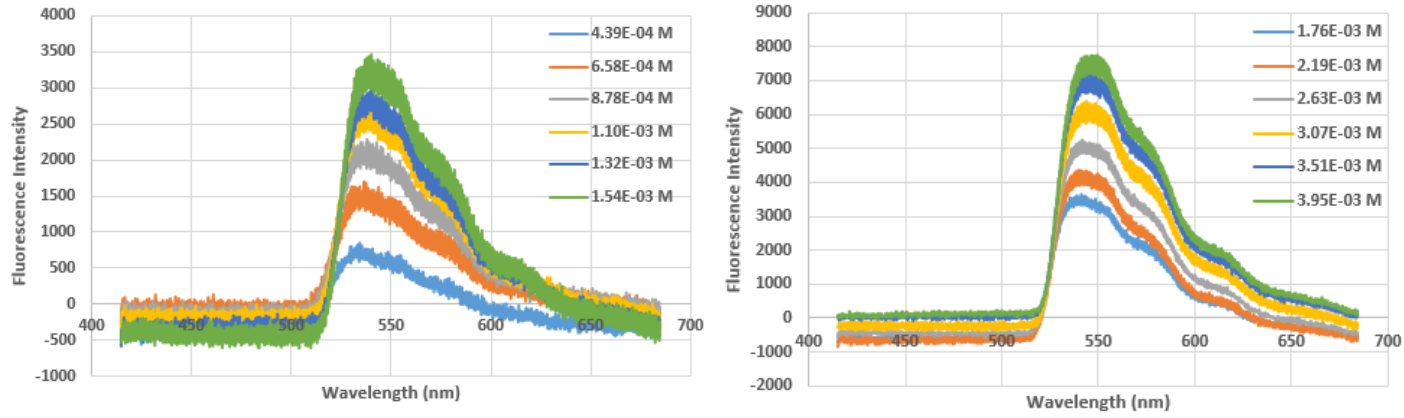

Figure A5.2. TPEF spectra of NBD-ethylmethylamine in 100% dichloromethane ranging from a concentration of 4.39 x 10^{-4} M to 3.95 x 10^{-3} M.

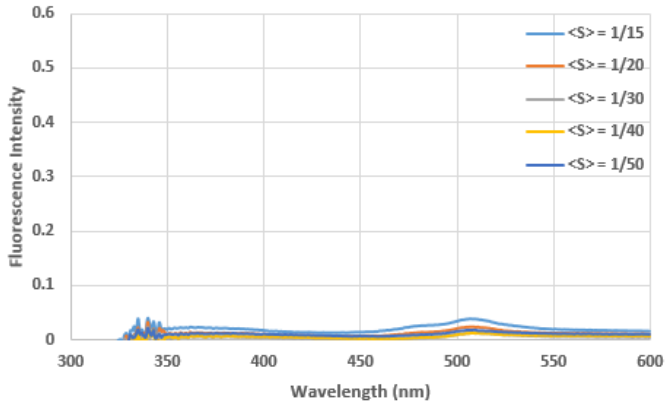

Figure A5.3. Typical UV-vis spectrum of the combined decanted dichloromethane used to incorporate NBD-ethylmethylamine in NaY. For most part, experimental loading level <S> = actual loading level <S>.

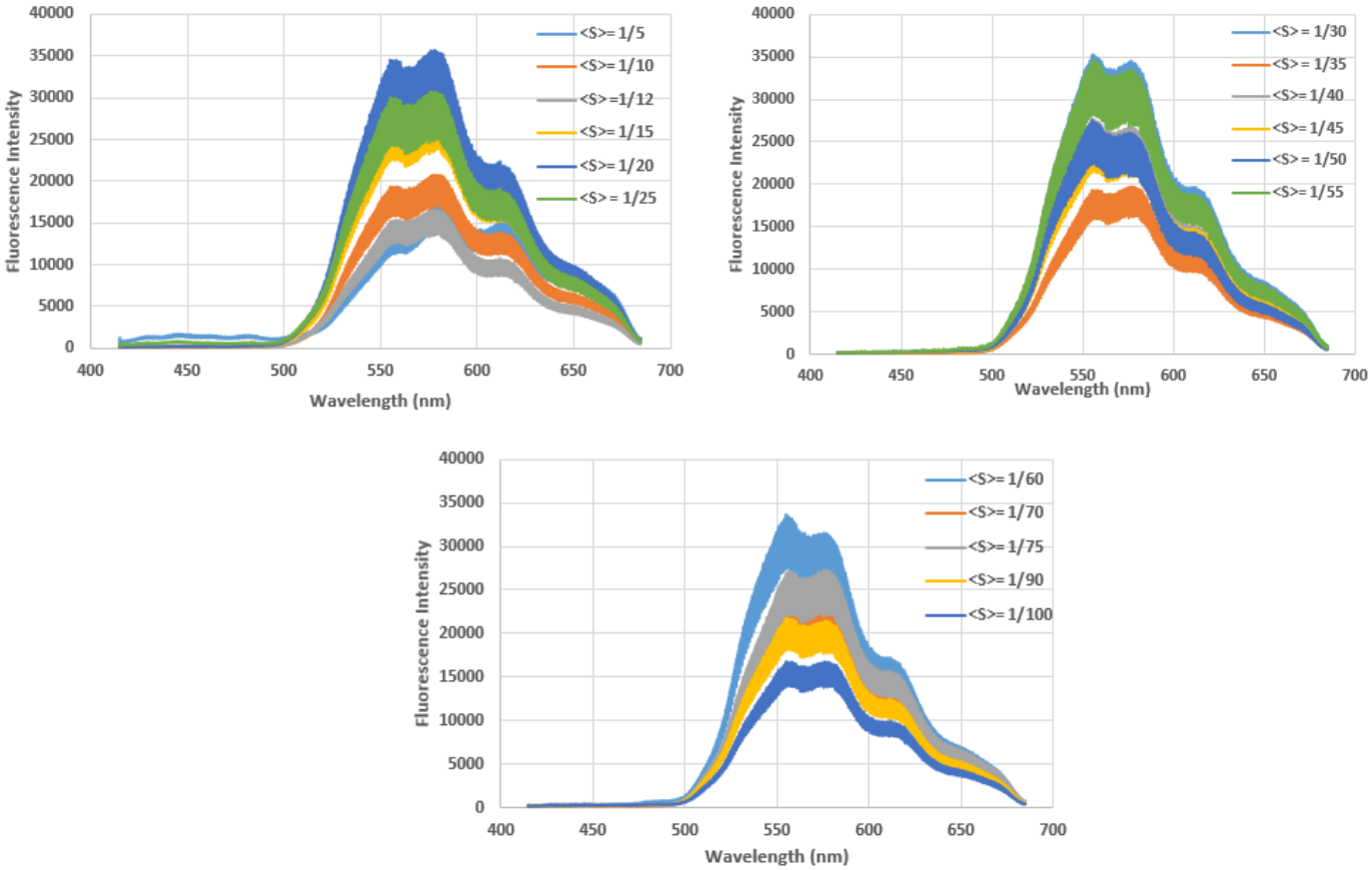

Figure A5.4. SPEF spectra of NBD-Ethylmethylamine incorporated in NaY at various different loading level <S>.

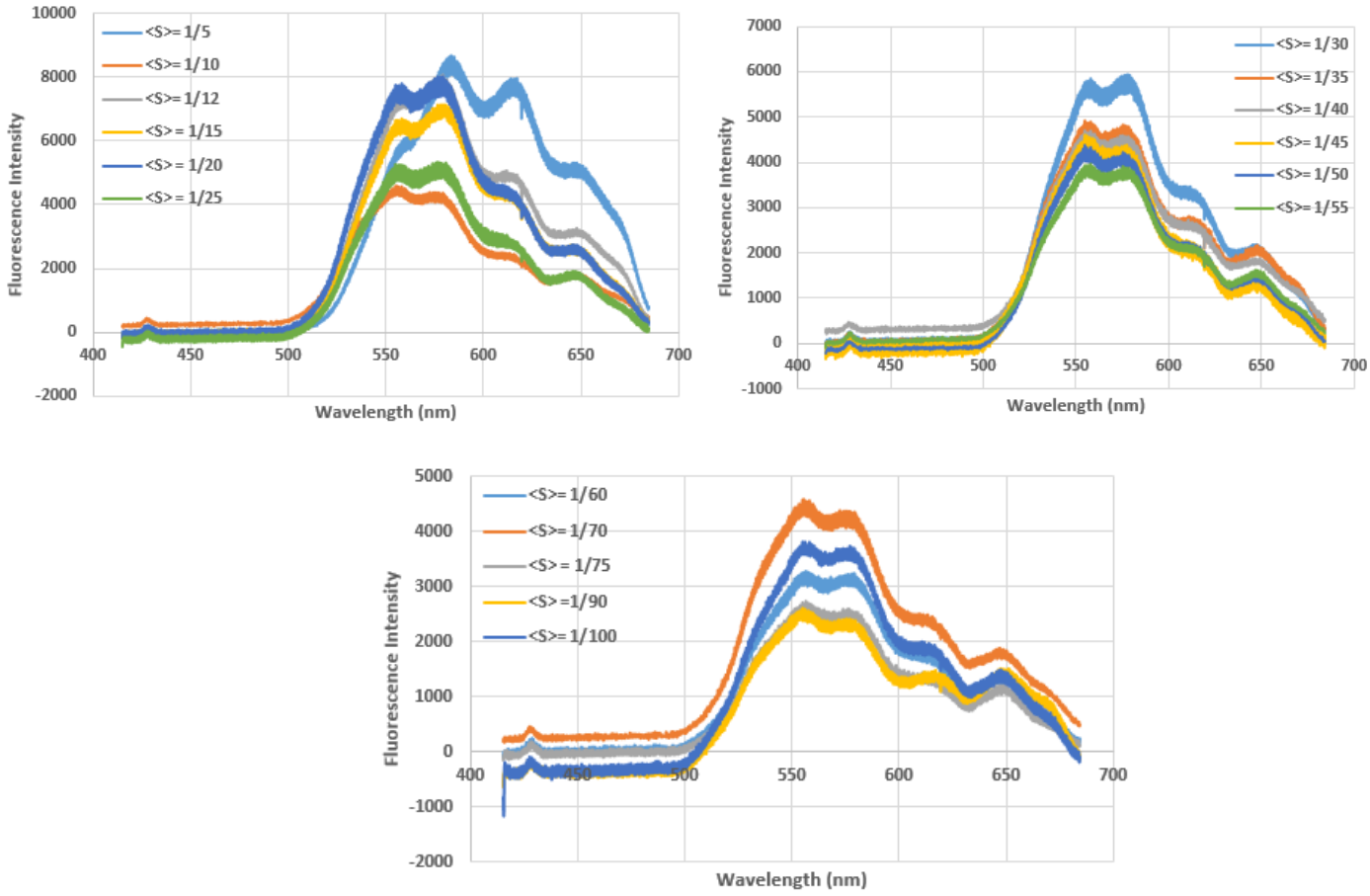

Figure A5.5. TPEF spectra of NBD-Ethylmethylamine incorporated in NaY at various different loading level <S>.

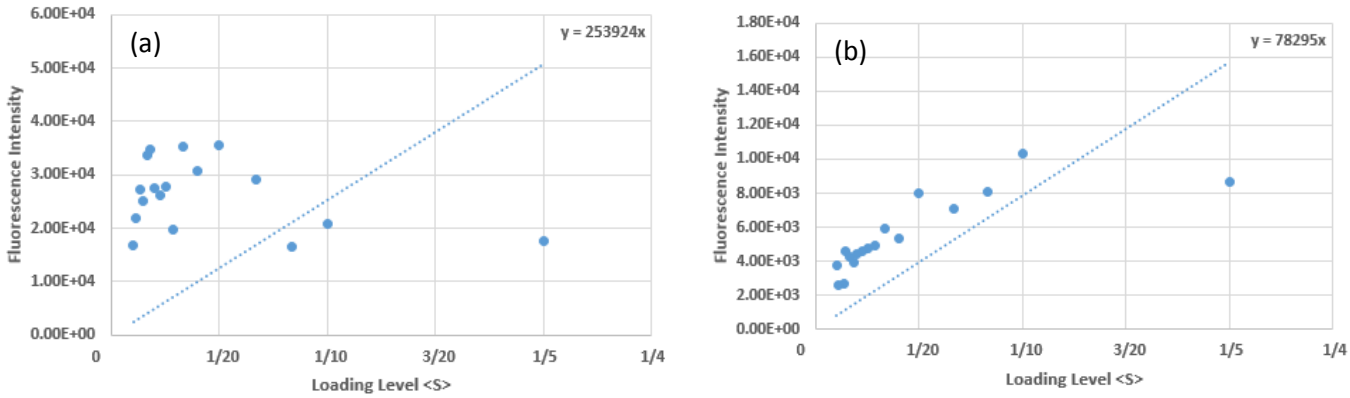

Figure A5.6. Relationship between (a) SPEF (b) TPEF intensities of NBD-ethylmethylamine and various different loading level <S>.

Table A5.1. Summary of SPEF and TPEF intensities using the respective spectra of NBD-ethylmethylamine incorporated in NaY at various different loading level <S>.

Loading Level <S>	SPEF	TPEF	1P:2P	2P:1P
1/5	1.77×10^4	8.67×10^3	2.04	0.49
1/10	2.07×10^4	1.04×10^4	2.00	0.50
1/12	1.65×10^4	8.09×10^3	2.05	0.49
1/15	2.90×10^4	7.13×10^3	4.07	0.25
1/20	3.56×10^4	8.03×10^3	4.43	0.23
1/25	3.07×10^4	5.33×10^3	5.76	0.17
1/30	3.53×10^4	5.95×10^3	5.93	0.17
1/35	1.97×10^4	4.91×10^3	4.01	0.25
1/40	2.78×10^4	4.72×10^3	5.88	0.17
1/45	2.61×10^4	4.59×10^3	5.67	0.18
1/50	2.75×10^4	4.40×10^3	6.25	0.16
1/55	3.46×10^4	3.95×10^3	8.78	0.11
1/60	3.37×10^4	4.28×10^3	7.87	0.13
1/70	2.50×10^4	4.59×10^3	5.45	0.18
1/75	2.73×10^4	2.72×10^3	10.02	0.10
1/90	2.18×10^4	2.59×10^3	8.42	0.12
1/100	1.67×10^4	3.80×10^3	4.41	0.23
			Average	0.21

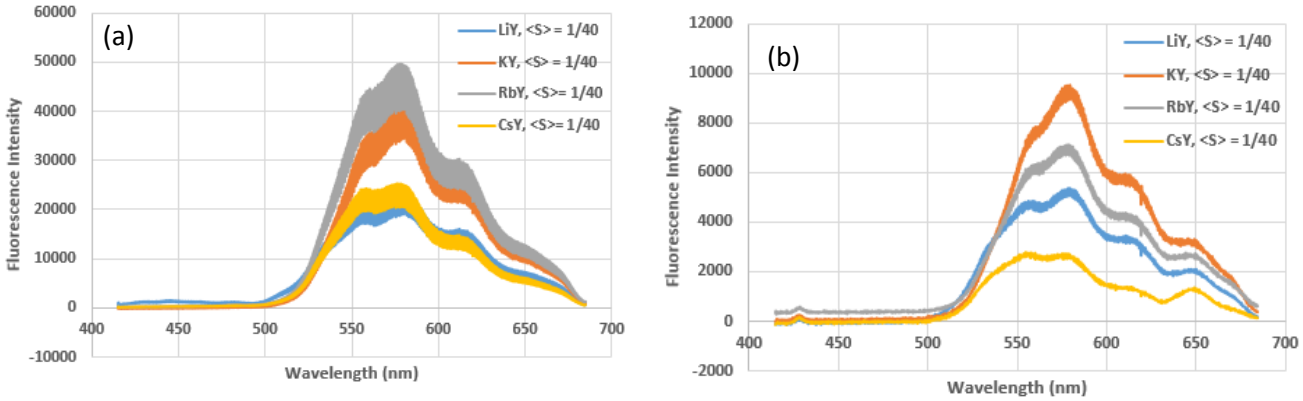

Figure A5.7 (a) SPEF (b) TPEF spectra of NBD-ethylmethylamine incorporated in alkali metal cation exchanged zeolites at a loading level of <S> = 1/40.

Appendix and supporting data for NBD-Diethylamine

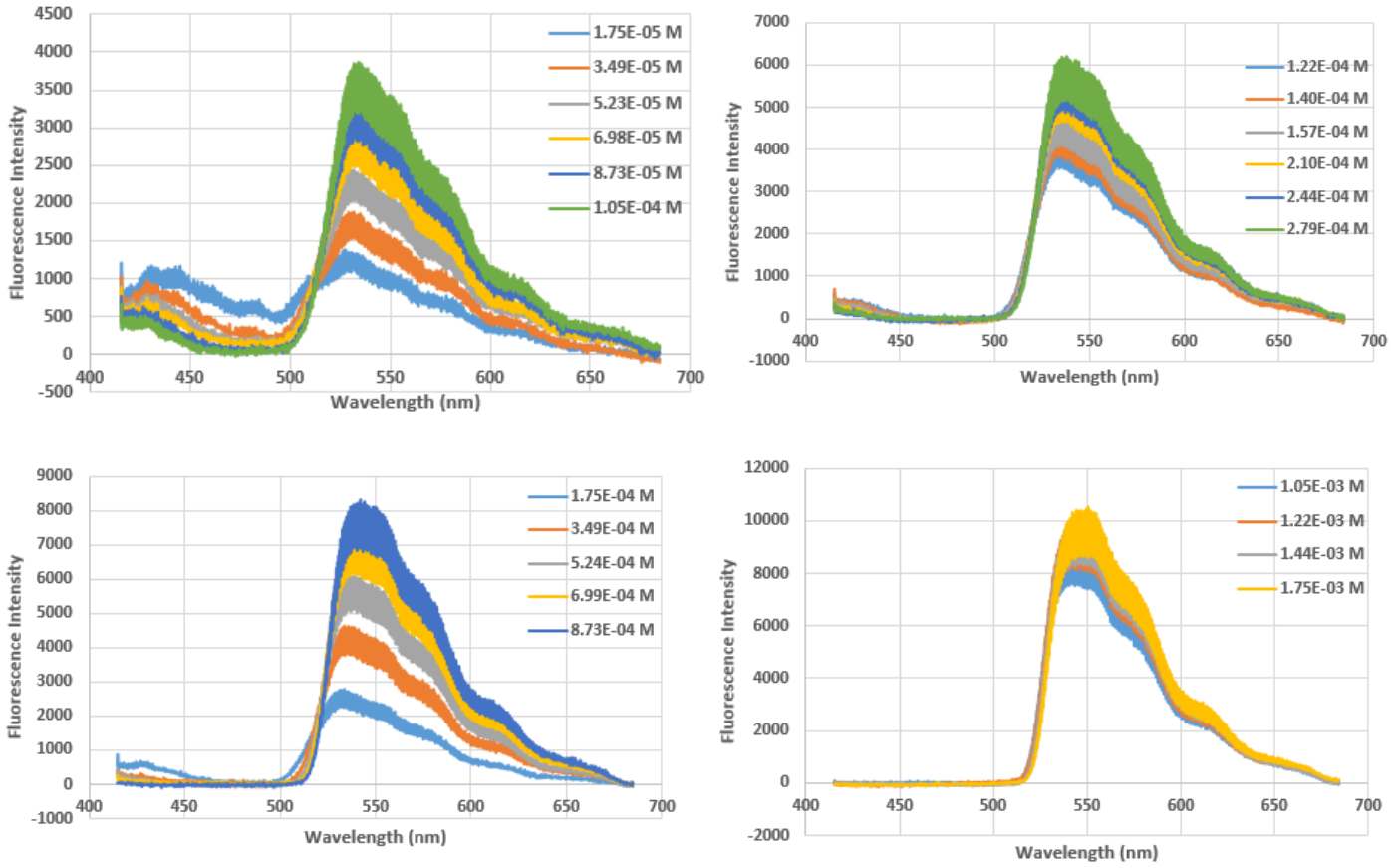

Figure A6.1. SPEF spectra of NBD-diethylamine in 100% dichloromethane ranging from a concentration of 1.75 x 10^{-5} M to 1.75 x 10^{-3} M.

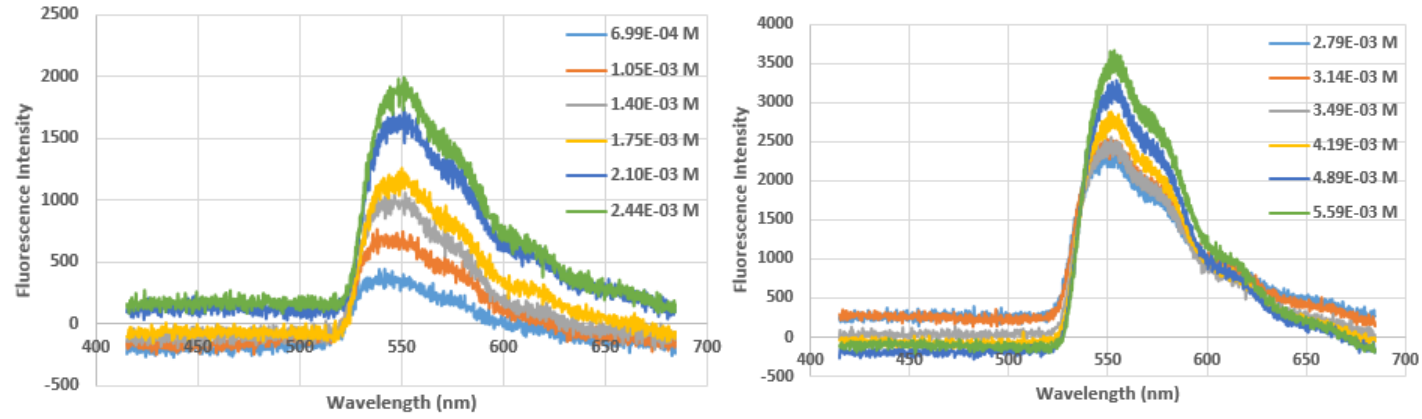

Figure A6.2. TPEF spectra of NBD-Diethylamine in 100% dichloromethane ranging from a concentration of 6.99 x 10^{-4} M to 5.59 x 10^{-3} M.

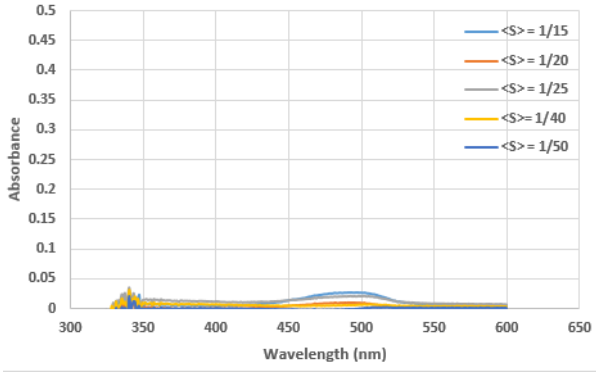

Figure A 6.3. Typical UV-vis spectra of the combined decanted dichloromethane used to incorporate NBD-diethylamine in NaY at various different loading level. Experimental loading level <S> = actual loading level <S>.

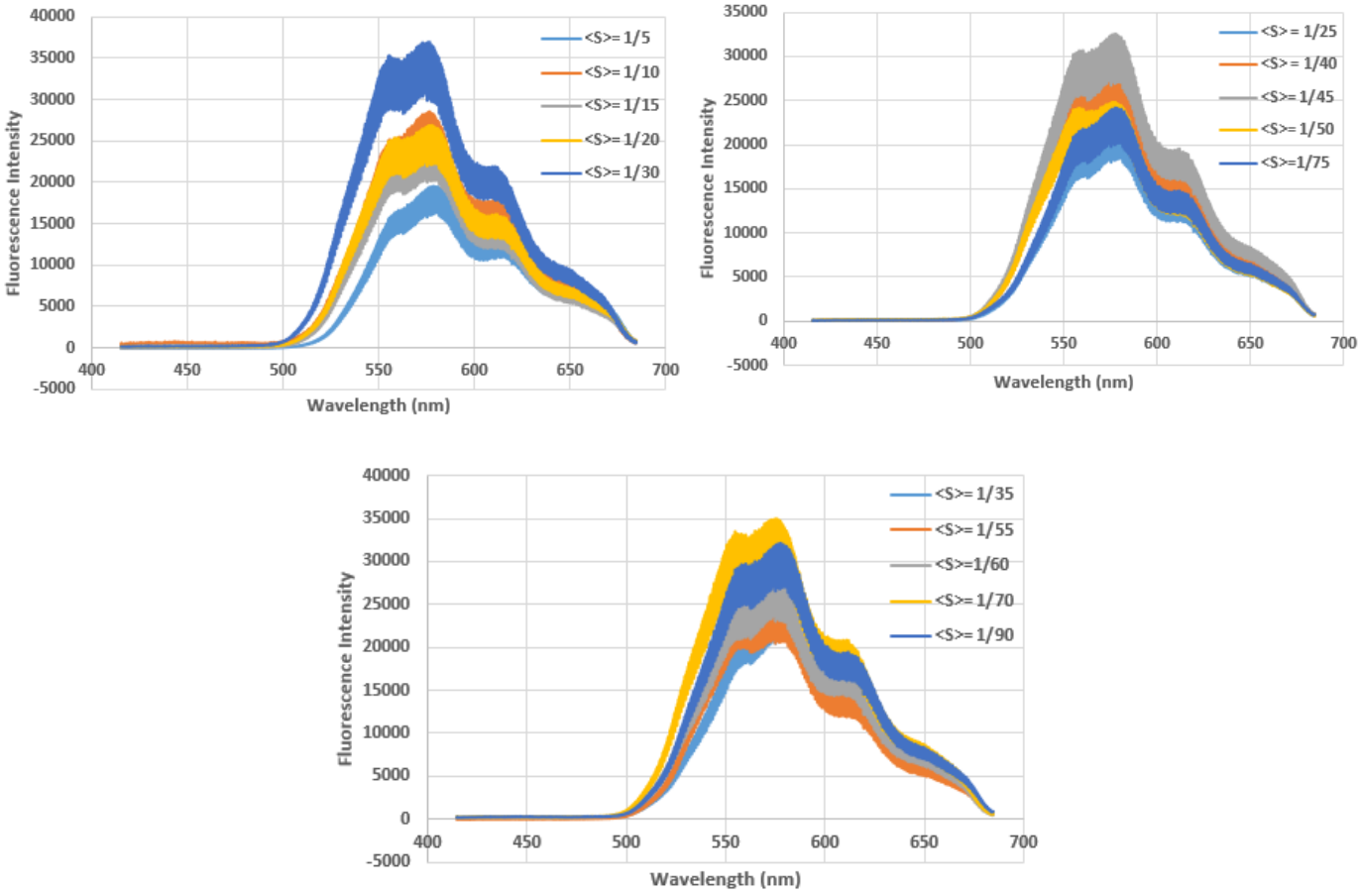

Figure A6.5. SPEF spectra of NBD-diethylamine incorporated in NaY at various different loading level <S>.

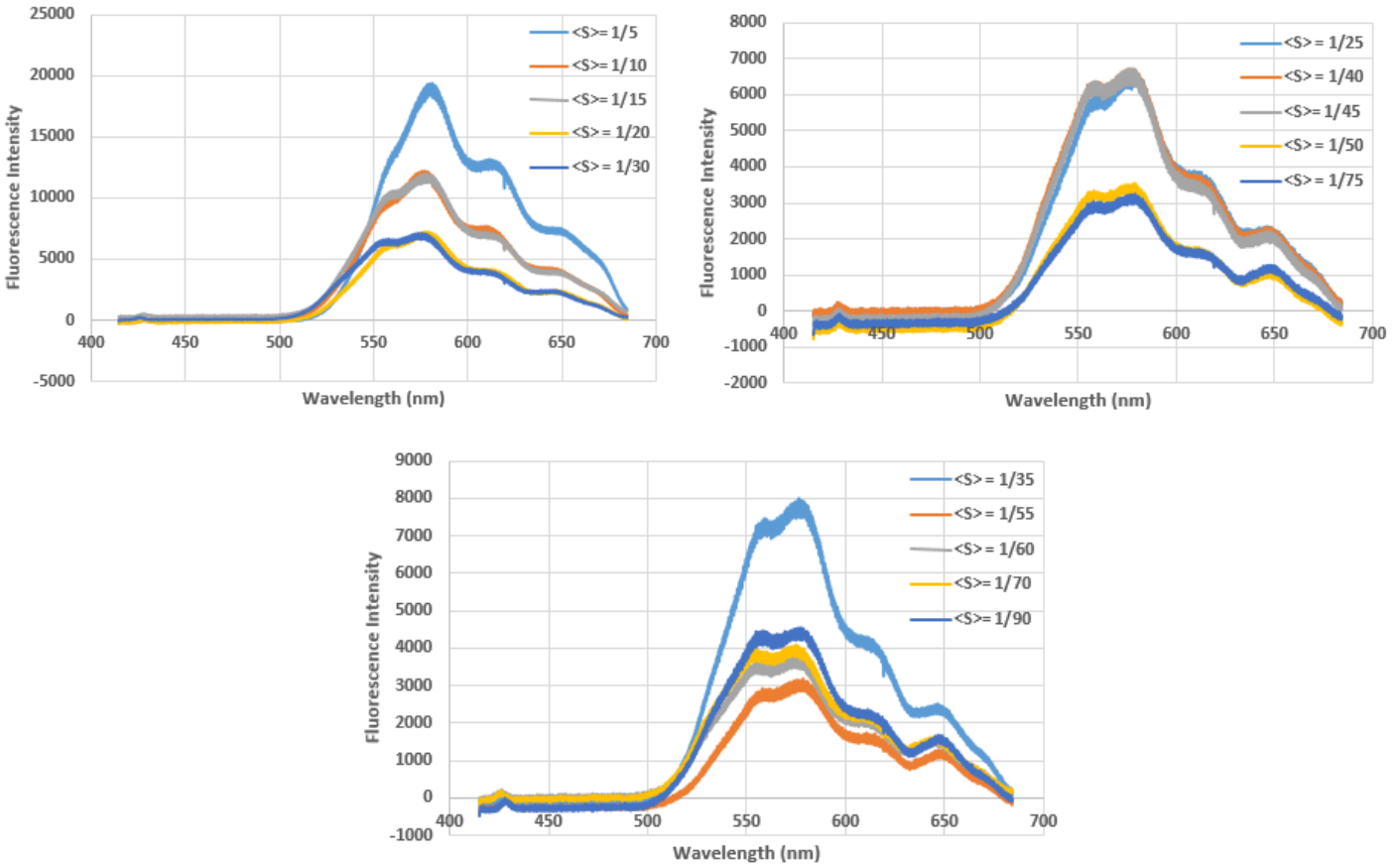

Figure A6.6. TPEF spectra of NBD-Diethylamine incorporated in NaY at various different loading level <S>.

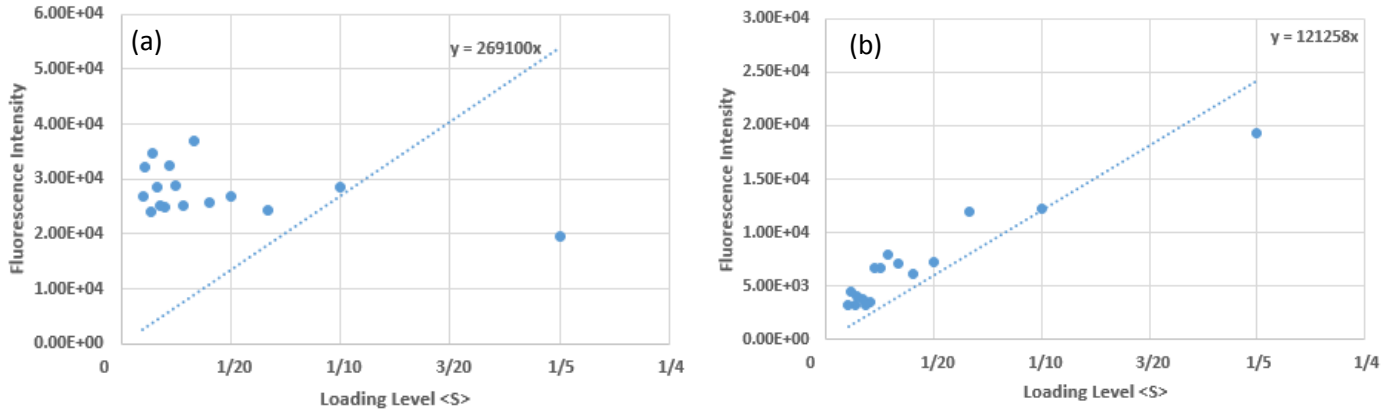

Figure A6.7. Trends for (a) SPEF (b) TPEF intensities of NBD-Diethylamine incorporated in NaY at various different loading level <S>.

Table A6.1. Summary of the SPEF and TPEF intensities of the respective spectra of NBD-DEA incorporated in NaY at various different loading level <S>.

Loading Level <S>	**1PEF**	**2PEF**	**1P:2P**	**2P:1P**
1/5	1.95×10^4	1.94×10^4	1.01	0.99
1/10	2.86×10^4	1.22×10^4	2.34	0.43
1/15	2.43×10^4	1.20×10^4	2.02	0.49
1/20	2.68×10^4	7.24×10^3	3.71	0.27
1/25	2.56×10^4	6.14×10^3	4.17	0.24
1/30	3.70×10^4	7.15×10^3	5.18	0.19
1/35	2.53×10^4	8.01×10^3	3.16	0.32
1/40	2.89×10^4	6.73×10^3	4.29	0.23
1/45	3.26×10^4	6.75×10^3	4.83	0.21
1/50	2.48×10^4	3.56×10^3	6.95	0.14
1/55	2.51×10^4	3.20×10^3	7.86	0.13
1/60	2.84×10^4	3.75×10^3	7.58	0.13
1/70	3.48×10^4	4.11×10^3	8.47	0.12
1/75	2.42×10^4	3.26×10^3	7.41	0.13
1/90	3.21×10^4	4.55×10^3	7.06	0.14
1/100	2.70×10^4	3.20×10^3	8.42	0.12
		Average		**0.22**

Appendix and supporting data for TPA Cross Section (σ) determination of the NBD- Chromophores.

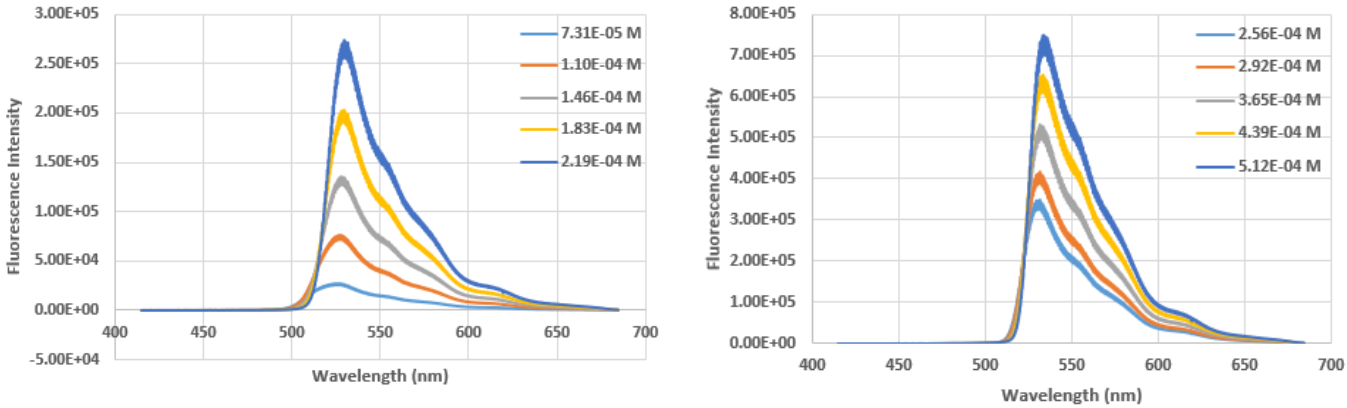

Figure A7.1. TPEF spectra of fluorescein in methanol ranging from a concentration of 7.31 x 10^{-5} to 5.12 x 10^{-4} M.

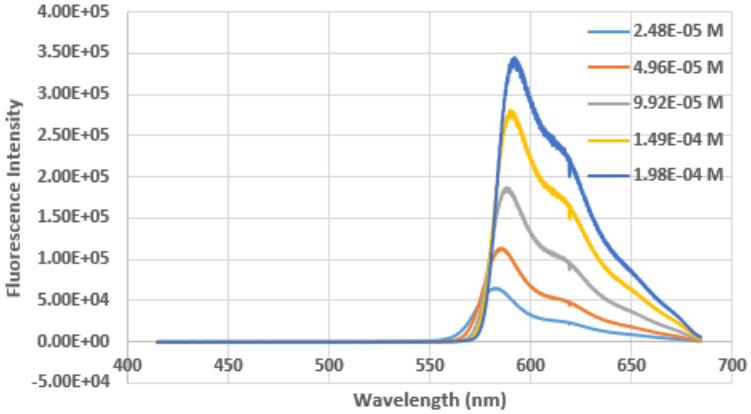

Figure A7.2. TPEF spectra of rhodamine B in methanol ranging from a concentration of 2.48 x 10^{-5} to 1.98 x 10^{-4} M.

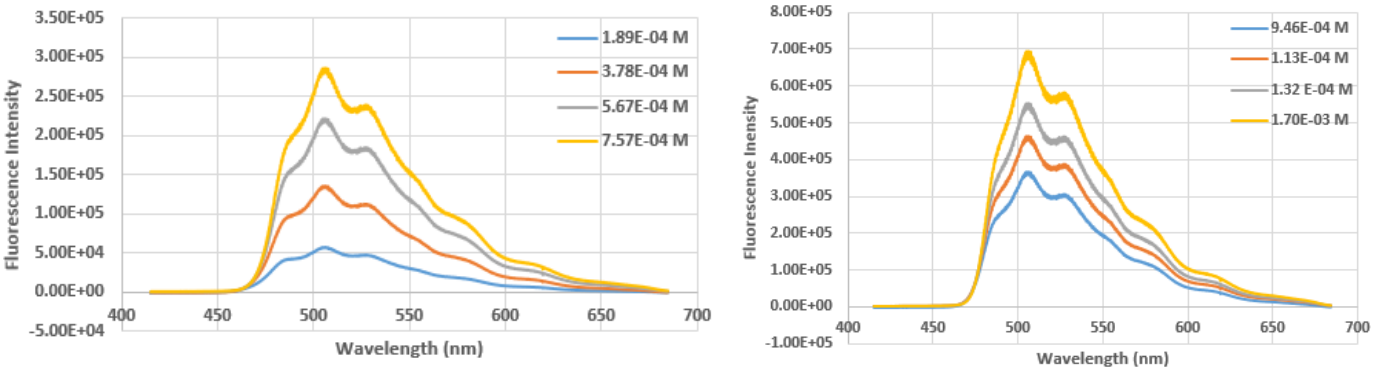

Figure A7.3. TPEF spectra of coumarin in methanol ranging from a concentration of 1.89 x 10^{-4} M to 1.70 x 10^{-3} M .

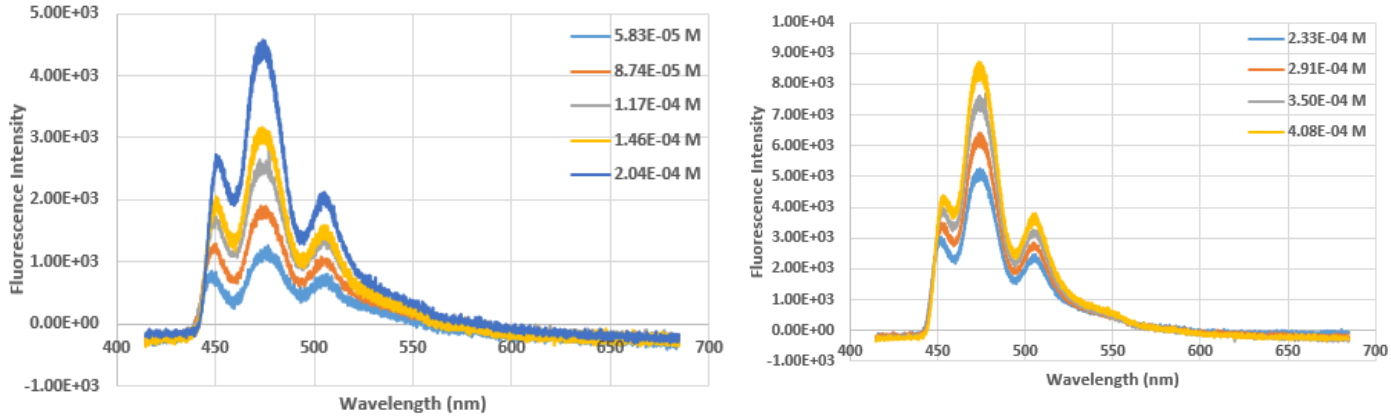

Figure A7.4. TPEF spectra of perylene in methanol ranging from a concentration of 5.83 x 10^{-5} to 4.08 x 10^{-4} M.

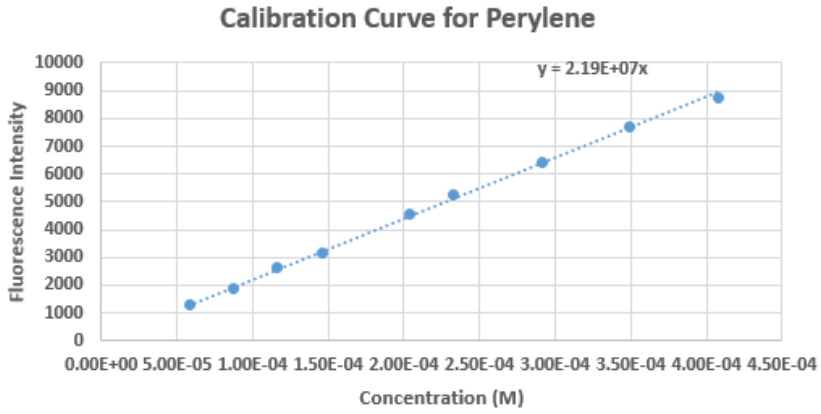

Figure A7.5. Calibration plot showing relationship between TPEF intensities and concentration of perylene in dichloromethane.

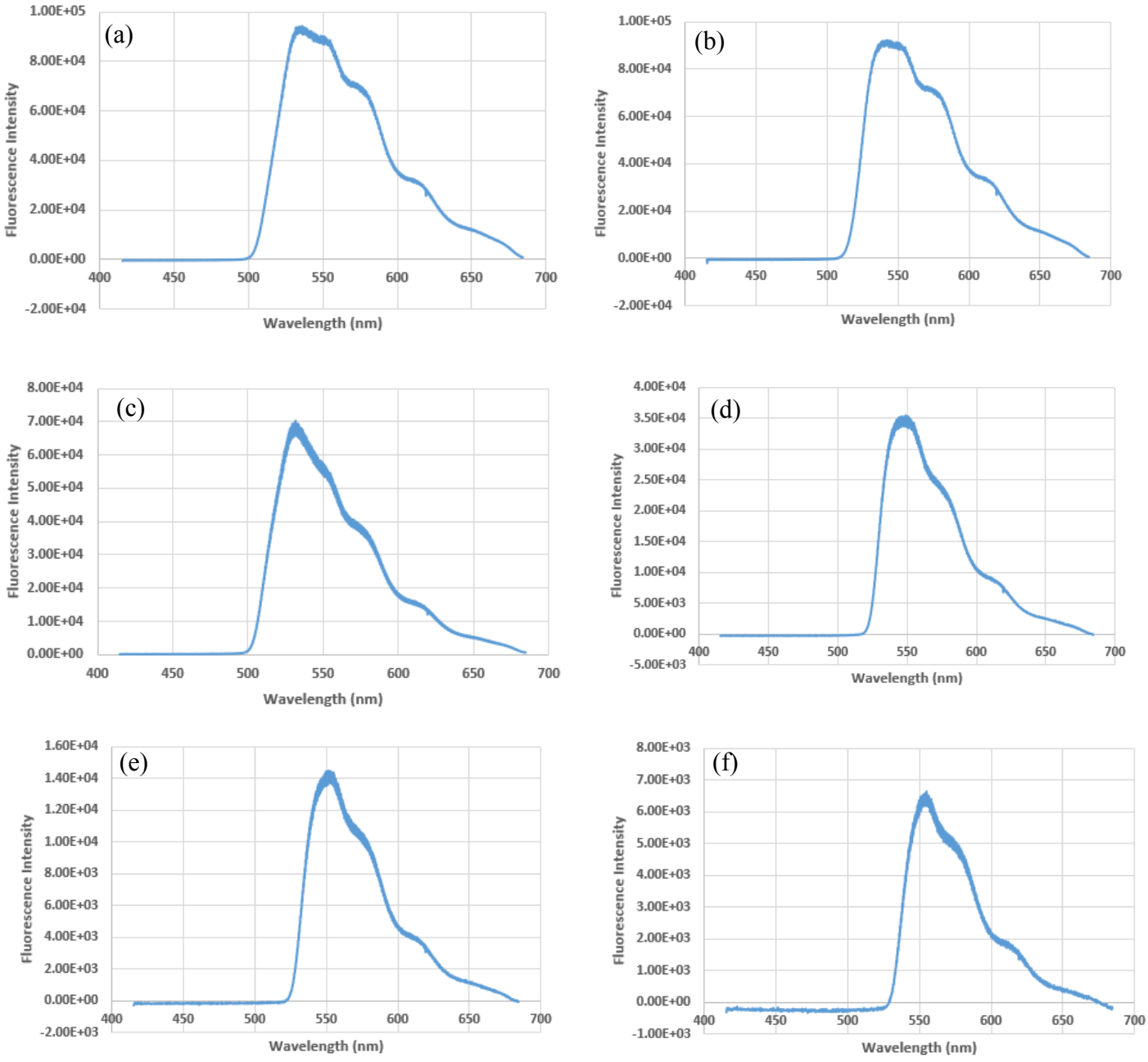

Figure A7.6. TPEF spectra of (a) 0.006 M NBD-NH_2 (b) 0.006 M NBD-methylamine in acetonitrile as the solvent. (c) 0.006 M NBD-ethylamine (d) 0.006 M NBD-dimethylamine (e) 0.006 NBD-ethylmethylamine (f) 0.006 M NBD-diethylamine in dichloromethane as the solvent. The spectra are used to determine the TPA cross-section (σ) of the respective chromophore.